Construction and analysis of spectral signatures for defects in complex media

Fabien Pourre

INSTITUT POLYTECHNIQUE DE PARIS

NNT : 2024IPPAE024

Thèse de doctorat

ENSTA

Construction and analysis of spectral signatures for defects in complex media

Thèse de doctorat de l'Institut Polytechnique de Paris
préparée à l'École nationale supérieure de techniques avancées

École doctorale n°574 École doctorale de mathématiques Hadamard (EDMH)
Spécialité de doctorat : Mathématiques appliquées

Thèse présentée et soutenue à Palaiseau, le 2 Décembre 2024, par

FABIEN POURRE

Composition du Jury :

Philippe Moireau Professeur, Ecole polytechnique	Président
Roland Griesmaier Professeur, Karlsruhe Institute of Technology	Rapporteur
Michael Vogelius Professeur, Rutgers University	Rapporteur
Fioralba Cakoni Professeure, Rutgers University	Examinatrice
Laure Giovangigli Enseignante chercheuse, ENSTA Paris	Examinatrice
Rainer Kress Professeur, University of Göttingen	Examinateur
Houssem Haddar Directeur de Recherche, Inria	Directeur de thèse
Lorenzo Audibert Ingénieur de recherche, EDF R&D	Co-directeur de thèse

Contents

Introduction

State of the art

From the deep understanding of our physical world to some medical and military applications, the study of wave phenomena has captivated throughout the twentieth century. While its primary applications are industrial or found in applied mathematics, scattering theory has also challenged the mathematical analysis community, leading to the development of a sophisticated mathematical framework. This theory focuses on the effects that occur when a wave encounters an obstacle or an inhomogeneity in a complex medium. Such interactions between an incident field and an object produce a scattered field, with the total field being the sum of both. There are various approaches to model this complex phenomenon. In this manuscript, we focus on the harmonic acoustic waves governed by the Helmholtz equation. This equation describes the propagation of acoustic waves in space and has also a use in elasticity (describing the propagation of pressure and shear waves) as well as in electromagnetism. The objects within the complex medium may be impenetrable obstacles, in which case they are represented by their geometry and their boundary condition, or inhomogeneities characterized by the physical parameters, such as the refractive index in acoustic isotropic media. A natural question would be how the scattered field field behaves based on the obstacles, or, conversely, determining which complex medium generated a given scattered field. This is why we discern two main axes in the scattering theory:

1) The *direct scattering problem* consists in the determination of the scattered field, generated by a known incident field, from the partial differential equation that governs it (with the knowledge of the complex medium in which it propagates, including the defects and inhomogeneities).

2) The *inverse scattering problem* aims at recovering information about the medium (nature of the obstacles, physical parameters in the wave equation, ...) by sending a family (possibly infinite) of known incident fields and collecting the associated scattered fields.

These two aspects, although closely related, have different approaches and have both been studied simultaneously throughout the past hundred years. The direct scattering problem was crucial to understand wave propagation, especially in seismology or telecommunications. It has experienced a major development in the late 80s to generate multiple numerically computed data to put to the test the numerous inverse algorithms, because no analytical

solution is available in general. Although the existence of a solution was achieved in the middle of the last century through integral equations and boundary integral equations, one of the main issues was to assure its uniqueness, which was proved thanks to the work of Sommerfeld, Rellich and Vekua ([64, 60, 67]). Having settled this problematic, the community turned to the numerical generation of a solution of such equation through boundary element methods or finite element methods for instance, depending on the nature of the defects, its geometry...

Before focusing into the technical part of *inverse scattering problem*, it is crucial to define which part of the scattered field is accessible and will be exploited. To replicate the real life scenarios, the data is constituted of the measurements of the wave field on either a boundary of the domain (near field) or, when taken far from the object of study, the far field pattern. The far field pattern, which is the distance-independent coefficient in the first order term of the asymptotic behavior of the scattered field at infinity, offers a robust mathematical framework, closed to the physical reality, to investigate the inverse scattering theory. When considering plane waves as the incident field, the far field pattern depends on two parameters: the direction of incidence of the plane wave and the direction of observation. The primary goal of the inverse problem will be to recover any information about the complex medium from the far field pattern for all directions of incidence and all directions of observation. The data can be encapsulated in an operator F known as the far field operator. This operator plays an essential role in many of the mathematical analysis of the inverse problem and some of its properties are discussed in [15, 24, 26].
In contrast to the direct scattering problem, the mathematical aspect of the inverse scattering problem encountered initial difficulties due to two main issues: the problem is non linear (the scattered field depends nonlinearly on the physical parameters or the boundary condition on the obstacle) and is ill-posed (neither the existence of a unique solution nor the continuous dependence on the initial condition is always guaranteed). For non-penetrable scatterers, the existence of a solution at a fixed frequency was solved in the early 1940s by Vekua and Weyl [67, 69] and the uniqueness was established in the generalized case a decade later [47]: if two obstacles with two boundary conditions have the same far field operator, then they are identical. The isotropic acoustic case was also resolved by Nachman [56] in the late 80s. A mathematical curiosity and challenge was to ensure the uniqueness result with only a single (or a finite number of) incident plane wave. The answer holds true under some geometric assumptions on the obstacle (see [29, 51]).

The ill-posedness, consequence of the compactness of the far field operator, can lead to a very different solution in case of small errors in the data or, in some cases, to the absence of a solution. As D. Colton and R. Kress explain in [27], it is wrong to question the existence of a solution to the inverse problem. Instead, the attention should be on the design of stable methods for finding an approximation of ∂D (the scatterer) from the perturbed data. A well-known approach to handle both ill-posedness and non linearity separately is through decomposition methods. While these methods have shown promising results, they require some a priori information and may be time consuming. Notable examples include the work of Imbriale and Mittra ([39]) or [42] by Kirsch and Kress in 1986 followed by the point

source method [58] a decade later. A more popular approach is iterative methods. They use optimization techniques to approximate step by step the unknown defect. Despite their high accuracy with limited data, these methods have three main drawbacks: 1) Each optimization step necessitates solving the forward problem; making an efficient forward solver essential, 2) Reliable a priori information about the obstacle is crucial to achieve convergence of the algorithm, 3) Most of the convergence results remain unresolved and have not yet been established. We refer to [61, 33, 36, 45, 55] for various examples, to [40, 48, 46] that exploits boundary integral equations in the optimization method and to [30, 63, 9] for applications of level set methods. The substantial numerical cost of the forward solver and the importance of a good initialization guess make implementing these methods in industry challenging.

As a result, a new category of techniques known as sampling methods, emerged in the last two decades of the XXth century. They contrast with the iterative methods because they do not require prior knowledge of the geometry or on the boundary condition, nor do they necessitate any type of forward solver. This approach reduces computation time and is valid only for a large number of incident fields. Essentially, sampling methods provide an indicator function that determines whether or not a point on the probed domain is part of a defect. The term "sampling" refers to the evaluation of this indicator function across a grid of points. The outcome result is an image that visually distinguishes the regions with scatterers from those without. The leading method in this field is the Linear Sampling Method (LSM), first presented in 1996 by A. Kirsch and D. Colton ([24]). Other notable methods in this category include the Singular Source Method [59], the Probe Method [38], the Dual Space Method [28] and the Factorization Method [41].

The LSM seeks to recover the geometry of the obstacles. For a given point z in the domain, the key question is whether we can design a combination of plane waves as the incident field such that the far field pattern generated by the unknown medium coincides with the far field pattern of a point source at z. This problem is equivalent to solving a highly ill-posed equation. There are no solutions if z lies outside a scatterer, as the scattered field would then possess the same regularity as a point source at z, which is absurd. While the existence of a solution when z is within a defect is not generally guaranteed, an approximation argument can be used by the denseness properties of the far field operator and the incident waves. Numerically, the equation is usually solved by Tikhonov regularization [65, 66] with the regularization parameter chosen according to Morozov's discrepancy principle [53, 54]. It is important to note that this approach does not account for the nature of the defect and is applicable to both obstacles and inhomogeneities. Although the LSM is quite effective as an initial approach, with convincing numerical results, the solution provided by Tikhonov regularization does not necessarily yield the exact predicted indicator function, especially in case of noisy data. The Factorization Method offers an alternative that addresses this mathematical gap, but it demands more restrictive assumptions [41]. A different approach, the Generalized Linear Sampling Method (GLSM) [8], was developed in 2013 by changing the penalization term in the Tikhonov regularization. It provides an alternative indicator function which correctly handles the noisy data. In conclusion, these

LSM based samplings methods have the following characteristics (compared to the iterative methods):

1) Simple to implement with faster computation time,

2) No prior information needed nor initial guess: can handle both penetrable and non penetrable obstacles with any number of components,

3) Posses a solid theoretical justification but is not flexible (designed for specific types of problems),

4) Require some more or less restrictive assumptions.

Item 4) includes knowledge of the far field pattern for a large number of incident plane waves and necessitates the exclusion of some specific wavenumbers called the Transmissions Eigenvalues (TE). TE play a critical role in the mathematical justification of the LSM. At these frequencies, it is possible to design an incident field that produces a trivial scattered field outside the defects (see Figure 1): the scatterers become invisible. It has

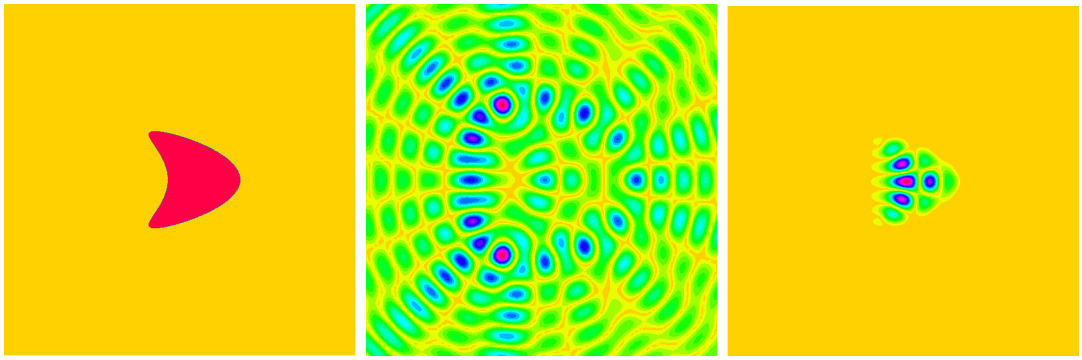

Figure 1: Illustration of the invisibility of the obstacle at a TE $k = 7.95$. Left: Penetrable inhomogeneity with kited form and refractive index $n = 2$ inside. Middle: Incident field. Right: Scattered field

been demonstrated that this set of wavenumbers is discrete ([25, 62]) and non empty ([28]). Initially regarded as undesirable to ensure the validity of the algorithms, the connection of the TE with the physical properties of the material (such as their monotonicity with respect to the refractive index [17]) has made them highly relevant for the inverse problem. It has been established that they can be determined from the far field operator (i.e. the available data) using two approaches ([14, 43]). This has inspired the development of an imaging algorithm that exploits a slightly modified version of TE and their monotonic dependence on the number of defects provides a quantitative indicator of crack density ([7]).

In practice, these Transmissions Eigenvalues and their properties have attracted significant interest from industries in the non-destructive material quality certification. This is a particularly critical assessing safety in constructions where concrete plays a crucial role. Concrete is omnipresent in the construction landscape, particularly in the reactor building

of nuclear power plants. As these structures age, it becomes essential to conduct a diagnostic to ensure the material's integrity: impermeability, handling high temperatures... Monitoring its evolution and identifying any defects that could compromise its proper functioning can be achieved through non destructive testing. Concrete is composed of a background of cement paste mixed with aggregates whose size is comparable to or smaller than the considered wavelength, along with metallic reinforcing bars and a microstructure that includes voids or water, referred to as pores. As a first approach, the reinforcing bars and the pores are omitted. Aggregates are therefore small obstacles that are typically present in large quantities and positioned very close together as presented in a picture of concrete in Figure 2. Modeling such a medium is a significant challenge. One approach is to represent the

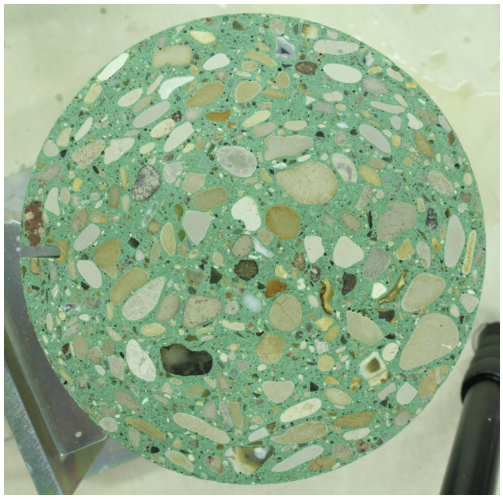

Figure 2: Example of a cylindrical cross-section of concrete.

aggregates as small penetrable inclusions. In this context, classical methods, such as the LSM, not only fail to provide quantitative results but also do not yield exploitable images. Consider for instance a union of small and close scatterers such as presented in the left part of Figure 3. The high density of the inclusions challenges the Linear Sampling Method (LSM) that tries to construct an indicator function for the geometry of the scatterers. We display in the right part of Figure 3 the indicator result provided by the LSM for a fixed frequency. We clearly observe that not only the method fails to recover the geometry, but also gives no information about their distribution. Indeed, this method illuminates the obstacles support, which represents almost the entire domain.

Objective of the thesis

The objective of this thesis is to build an imaging algorithm that can estimate the density of the aggregates and recover the local distribution of those small inhomogeneities.

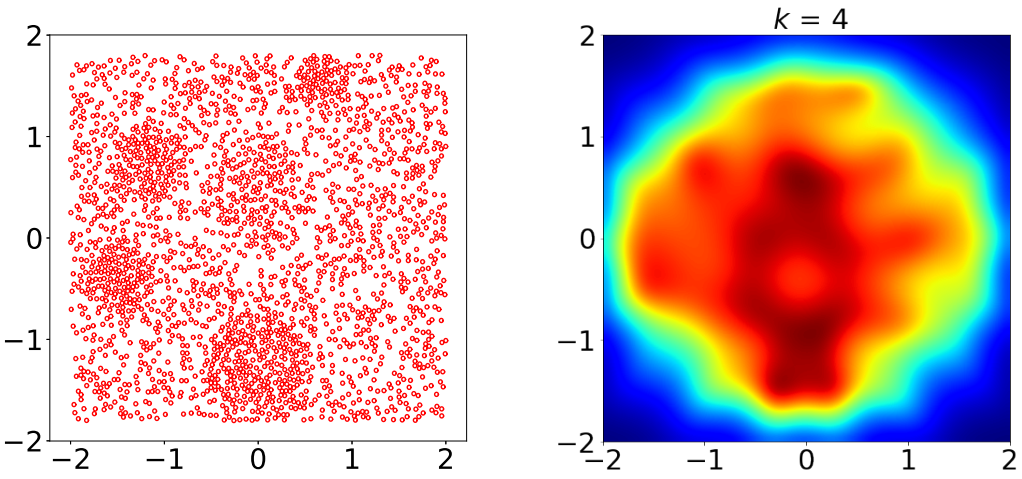

Figure 3: Left: the domain D constituted by 2250 small circles of radius 0.02 having a constant index of refraction $n = 2$. Right: indicator function provided by the LSM with 1% added noise to the far field operator F and for frequency $k = 4$ (the wavelength is roughly 80 times higher than the radius of the circles.)

Inspiration is drawn from the monotonicity property of the TE. The mathematical challenges of their study along with the need to possess data for a large range of frequencies has led to modify the concept of invisibility associated with TEs. Instead of comparing the scattered field to the vacuum, the new approach involves comparing it at a fixed wavenumber to a numerical scattering problem, referred to as the background. To highlight a resonance around the scatterers, the background includes a resonator with a specific boundary condition that depends on a parameter denoted μ. The use of artificial backgrounds for the construction of spectral signatures or for the design of imaging algorithms has been explored in many studies ([23, 22, 5, 34, 20, 1]). TE are generalized by the values of μ for which an incident wave exists such that the scattered field from the unknown complex medium coincides with the scattered field from the artificial background (instead of the vacuum as in TE). This is equivalent to the study of an eigenvalue problem within the resonator that involves the probed domain local properties. Consequently, the spectral signature μ only depends on the local physical properties. The challenge we would like to address in this work is to design appropriate boundary conditions to ensure that the spectral signature provides quantifiable information about the medium and can be used in a robust manner in an imaging algorithm. We expect new sampling methods that outperform in configurations as in Figure 3.

Outline of the thesis

Chapter 1 : Sampling methods and spectral signatures This chapter provides a motivation for using a particular class of spectral signatures in imaging algorithms. After

introducing some notations, the Linear Sampling Method (LSM) is presented with numerical examples to illustrate its effectiveness. Theoretically, this method encounters some issues at certain wavenumbers, known as Transmission eigenvalues, which are solution to an eigenvalue problem. The chapter then explores some of their main properties, namely their monotonicity and how they can be determined from the data. The final section focuses on a generalization of these eigenvalues that construct spectral signatures with properties similar to TE, while addressing their limitations.

Chapter 2: The averaged Steklov eigenvalue A fundamental aspect for imaging algorithm is the choice of the background model. The metamaterial background proposed in [4] provides a promising starting point due to its flexibility, the discrete nature of its eigenvalues, and their monotonicity with respect to the refractive index. For small values of the parameters, the eigenvalues become very close to each others, making it challenging to numerically recover them. Therefore, the largest eigenvalue would be the most natural choice for use in an inversion algorithm.
In this chapter, we demonstrate that, as the metamaterial parameter goes to infinity, the associated spectrum converges to a simplified spectrum containing only one non zero eigenvalue. This is very appealing from the numerical point of view, since it significantly simplifies the identification of the non zero eigenvalue from measured data. This allows for a better quantitative interpretation of the indicator function. This chapter is adapted from [12] and includes an additional section that slightly generalizes this spectral parameter to a family of spectral parameters sharing similar properties.

Chapter 3: An indicator function for the refractive index We develop in this chapter a method to recover some macroscopic information on the refractive index n from the far field operator F. This method is inspired by the one introduced in [7] and exploit the monotonicity property of the modified transmission eigenvalue of the spectral problem introduced in Chapter 2 with respect to the refractive index. The first step is to explain how one can identify the modified transmission eigenvalue from F^μ [16, 4, 22]. We employ the framework of the Generalized Linear Sampling Method [8] (GLSM) to prove this result in a constructive way. The proposed algorithm for a quantitative indicator function associated with the refractive index is then as follows: 1) choose a disc of given radius that we shall sweep over some sampling positions in the probed domain; 2) for each sampling position, identify the eigenvalue from far field data using the GLSM approach; 3) assign to the sampling position the difference between this eigenvalue and the eigenvalue associated with an index of refraction equals to one. The obtained indicator function would then be monotonically dependent with respect to the values of the true refractive index intersecting the disc. We shall explain the details of this procedure in the numerical section and discuss the choice of the disc radius in terms of the used frequency. We then show how the resulting indicator function gives superior results to those given by qualitative approaches such as the Linear Sampling Method [24]. Moreover, the sign of the indicator function would give an indication on how the mean value of the refractive index compares with respect to 1. This is also discussed and illustrated through some numerical tests in 2D.

Chapter 4: Averaged Steklov Eigenvalues, Inside Outside Duality and Application to Inverse Scattering This chapter is structured as follows. Section 4.2 is dedicated to the definition of an artificial background with an abstract formulation of the associated impedance boundary conditions that encompass the specific cases of Chapter 2. We then define the associated averaged Steklov eigenvalues (referred to as $\mathcal{B}-$eigenvalues). In Section 4.3 we introduce the inverse problem for inhomogeneous media and define a modified far field operator relative to the artificial background. A key factorization of this far field operator in then given. Section 4.4 contains the main theoretical result of this work, which is the characterization of the $\mathcal{B}-$eigenvalues using the Inside-outside Duality Method. In Section 4.5 we propose some validating numerical tests against analytical expressions obtained for circular domains. We then propose an algorithm implementing the Inside-outside Duality Method that can be used in the imaging algorithm proposed in [10]. We conclude with some validating numerical examples where we reconstruct the average value of refractive index of the probed medium from noisy far field data. Some technical results are given in an appendix.

Chapter 5: The Inside-outside duality with artificial background with a non penetrable resonator The previous chapter introduced the inside-outside duality method for recovering a specific class of eigenvalues. These eigenvalues arise from an artificial background problem with a non-penetrable obstacle. This chapter extends of this work by addressing the recovery of two different classes of eigenvalues. The first part of this chapter revisits the inside-outside duality method using the same artificial background as in Chapter 4, but with the wavenumber playing the role of the spectral parameter. The second part explores the inside-outside duality method for a new class of eigenvalues, derived from an artificial background problem with a non-penetrable obstacle but under different boundary conditions. This class notably includes the Steklov eigenvalues. We conclude with numerical illustrations of the algorithm for a quantitative indicator function associated with the refractive index presented in Chapter 3, adapted to these new eigenvalues.

Chapter 1

Sampling methods and spectral signatures

Contents

1.1 Introduction

This chapter provides a motivation for using a particular class of spectral signatures in imaging algorithms. After introducing some notations, the Linear Sampling Method (LSM) is presented with numerical examples to illustrate its effectiveness. Theoretically, this method encounters some issues at certain wavenumbers, known as Transmission eigenvalues, which are solution to an eigenvalue problem. The chapter then explores some of their main properties, namely their monotonicity and how they can be determined from the data. The final section focuses on a generalization of these eigenvalues that construct spectral signatures with properties similar to TE, while addressing their limitations.

For a more comprehensive and detailed aspects of the material presented in this introductory chapter, we refer the reader to the monographs [26, 15].

1.2 Notation and statement of the inverse problem

Let D be a bounded domain in $\mathbb{R}^m, m = 2, 3$ with piecewise smooth boundary ∂D and connected complement. We denote by ν the outward normal field on ∂D. We shall consider the following scattering problem, with inhomogeneity supported in D. For $k > 0$ the wavenumber, let $u \in H^1_{loc}(\mathbb{R}^m)$ be the total field and u^s be the scattered field solutions of:

$$\begin{cases} \Delta u + k^2 n u = 0 \text{ in } \mathbb{R}^m, \\ u = u^s + u^i \\ \lim\limits_{r\to+\infty} \int_{|x|=r} |\frac{\partial u^s}{\partial r} - iku^s|^2 = 0, \end{cases} \tag{1.1}$$

where the incident field $u^i = e^{ikx\cdot d}$, denoted $u^i(., d)$ for $d \in \mathbb{S} = \{x \in \mathbb{R}^m, |x| = 1\}$ the unit sphere. We extend this notation to $u^s(., d)$ and $u(., d)$. The real refractive index $n \in L^\infty(\mathbb{R}^m)$ is such that $n > 0$ in D and $n = 1$ in $\mathbb{R}^m \backslash \overline{D}$. It is known that problem (1.1) is well posed for any $n \in L^\infty(\mathbb{R}^m)$ satisfying $\Im m(n) \geq 0$ in $\mathbb{R}^m$.
The Helmholtz equation (1.1) can also be written for the scattered field as:

$$\begin{cases} \Delta u^s + k^2 n u^s = k^2(1-n)u^i \text{ in } \mathbb{R}^m, \\ \lim\limits_{r\to+\infty} \int_{|x|=r} |\frac{\partial u^s}{\partial r} - iku^s|^2 = 0, \end{cases} \tag{1.2}$$

Setting $\hat{x} := x/|x|$, the scattered field u^s has the following expansion for all $\hat{x} \in \mathbb{S}$ as $|x| \to +\infty$:

$$u^s(x, d) = \frac{e^{ik|x|}}{|x|^{\frac{m-1}{2}}} u^\infty(\hat{x}, d) + O\left(\frac{1}{|x|^{\frac{m+1}{2}}}\right) \tag{1.3}$$

with $u^\infty(., d)$ being the so called far field pattern of the scattered field. We define the far field operator $F : L^2(\mathbb{S}) \to L^2(\mathbb{S})$ by

$$(Fg)(\hat{x}) := \int_{\mathbb{S}} g(d) u^\infty(\hat{x}, d) ds(d), \quad \hat{x} \in \mathbb{S}. \tag{1.4}$$

By linearity of equation (1.1), we remark that $u^\infty_g := Fg$ is the far field pattern of the scattered field u^s_g, solution of (1.1) with $u^i = v_g$ the Herglotz wave function defined for $g \in L^2(\mathbb{S})$ by

$$v_g(x) := \int_{\mathbb{S}} e^{ikxd} g(d) ds(d). \tag{1.5}$$

For mathematical purposes and further use, we define, for a given $\psi \in L^2(D)$, the unique function $w^s \in H^2_{loc}(\mathbb{R}^m)$ satisfying

$$\begin{cases} \Delta w^s + k^2 n w^s = k^2(1-n)\psi \text{ in } \mathbb{R}^m, \\ \lim\limits_{r\to+\infty} \int_{|x|=r} |\frac{\partial w^s}{\partial r} - ikw^s|^2 = 0. \end{cases} \tag{1.6}$$

Observe that if $\psi = v_g$, then $w^s = u^s_g$. Introduce the far field constant γ such that

$$\gamma := \begin{cases} 4\pi \text{ if } m = 3, \\ e^{-i\frac{\pi}{4}}\sqrt{8\pi k} \text{ if } m = 2. \end{cases} \tag{1.7}$$

We define the L^2-adjoint of H by

$$H^*(\psi) := \int_D \psi(y) e^{-ik\hat{x}\cdot y} dy. \tag{1.8}$$

In that case, the far field operator F has the following factorization [41, 8]

$$F = H^* T H, \tag{1.9}$$

where $T : L^2(D) \to L^2(D)$ is defined by

$$\gamma T(\psi) = -k^2(1-n)(\psi + w^s), \tag{1.10}$$

with w^s the solution of (1.6). The scattering operator $S : L^2(\mathbb{S}) \to L^2(\mathbb{S})$, associated with the far field operator, is defined by:

$$S := I + \frac{2ik}{\overline{\gamma}} F. \tag{1.11}$$

This operator is unitary and the operator F is normal if n is real valued [26, 41].

Statement of the inverse problem The inverse problem we would like to address is to retrieve information about the geometry of D and the refractive index n from the knowledge of the far field operator F.

1.3 The Linear sampling method (LSM)

The LSM seeks to accurately reconstruct the shape of D by considering an indicator function to determine whether a sampling point $z \in \mathbb{R}^m$ lies within D. For $z \in \mathbb{R}^m$, we set $\phi(., z) \in L^2_{loc}(\mathbb{R}^m)$, the radiating fundamental solution to the equation $\Delta\phi(., z) + k^2\phi(., z) = -\delta_z$ in $\mathbb{R}^m$ and denote by ϕ_z^∞ its far field pattern. It is well-known that:

$$\phi(x, z) := \begin{cases} \frac{e^{ik|x-z|}}{4\pi|x-z|} \text{ in } \mathbb{R}^3, \\ \\ \frac{i}{4} H_0^{(1)}(k|x-z|) \text{ in } \mathbb{R}^2, \end{cases} \tag{1.12}$$

where $H_0^{(1)}$ denotes the Hankel function of the first kind of order zero.
First presented in [24], this method relies on the resolution of $Fg = \phi_z^\infty$. In simple terms, this equation connects the position of the sampling point z (whether $z \in D$ or not) with whether the norm of the Herglotz wave $\|v_g\|_{L^2(D)}$ is bounded or unbounded. A natural imaging algorithm is to plot this norm for a set of sampling points z to reveal the shape of the obstacles. More rigorously it exploits a factorization of the far field operator and in particular the range of the operators at stake.
We introduce the operator $H : L^2(\mathbb{S}) \to L^2(D)$ defined by

$$Hg := v_g|_D, \tag{1.13}$$

along with $G : \overline{\mathcal{R}(H)} \to L^2(\mathbb{S})$:

$$G\psi = w^\infty, \tag{1.14}$$

where w^∞ is the far field pattern associated with w^s solution of (1.6) with source ψ. $\overline{\mathcal{R}(H)}$ denotes the closure of the range of H and by showing that the L^2-adjoint of H is injective, one can prove that:

$$\overline{\mathcal{R}(H)} = \{v \in L^2(D), \Delta v + k^2 v = 0 \text{ in } D\}. \tag{1.15}$$

The far field operator F has the following factorization

$$F = GH. \tag{1.16}$$

The range characterization of D can be expressed as:

$$z \in D \text{ if and only if } \phi_z^\infty \in \mathcal{R}(G).$$

This assertion is not true for all value of k. We outline the proof of the first implication which illustrates the necessity of excluding a specific set of wavenumbers.
Assume that $z \in D$. The objective is to construct an incident field $v \in \overline{\mathcal{R}(H)}$ such that $Gv = \phi_z^\infty$. If such v exists, the equality implies that $w^s = \phi_z$ in $\mathbb{R}^m \backslash D$. The regularity of w^s imposes that $w^s = \phi_z$ and $\partial_\nu w^s = \partial_\nu \phi_z$ on ∂D. Hence one obtains that $w^s|_D \in H^2(D)$ and $v \in L^2(D)$ verify:

(1.17) It is thus possible to construct such an incident field v and establish the first implication, provided that the previous equation (1.3) has a solution. This holds true if a specific set of wavenumbers called the Transmission eigenvalues (TE) is excluded. We refer to [15, Theorem 2.3] for a complete proof of this result.

Definition 1. *$k \in \mathbb{C}$ is a transmission eigenvalue (TE) if there exists $(u, v) \in L^2(D) \times L^2(D)$ non trivial with $u - v \in H_0^2(D)$ such that:*

$$\begin{cases} \Delta u + k^2 n u = 0 \text{ in } D, \\ \Delta v + k^2 v = 0 \text{ in } D, \\ u - v = 0 \text{ on } \partial D, \\ \partial_\nu (u - v) = 0 \text{ on } \partial D. \end{cases} \tag{1.18}$$

This problem is referred to as the transmission eigenvalue problem.

In addition, the TE correspond to the values k for which the operator G is not injective. For v in the kernel of G, by Rellich's lemma, the associated scattered field u^s vanishes in $\mathbb{R}^m \backslash D$. As a result, the total field $u = u^s + v$ and v satisfy (1.18). This offers an equivalent definition of the TE. Transmission eigenvalues correspond to the values of k for which there exists a non trivial incident field in $L^2(D)$ such that $u^s = 0$ in $\mathbb{R}^m \backslash D$. We refer to Figure 1 for an illustration of the phenomena.
It should be mentioned that if such a v is a Herglotz wave (which is generally not the case), then the far field operator F is also not injective. In this specific scenario, k is referred to

as a non-scattering wavenumber [18, 68]. It has been recently demonstrated that, under some appropriate conditions on the inhomogeneity, the set of non-scattering wavenumbers is empty [19].
We can state the main theorem of the noiseless LSM [24].

Theorem 1. *Assume that k is not a Transmission eigenvalue. Then,*

1. *for $z \in D$ and for all $\varepsilon > 0$, there exists $g_z^\varepsilon \in L^2(\mathbb{S})$ such that:*

$$\|Fg_z^\varepsilon - \phi_z^\infty\|_{L^2(\mathbb{S})} < \varepsilon \quad \text{and} \quad \lim_{\varepsilon \to 0} \|v_{g_z^\varepsilon}\|_{L^2(D)} < \infty. \tag{1.19}$$

2. *for $z \notin D$ and for all $\varepsilon > 0$, every $g_z^\varepsilon \in L^2(\mathbb{S})$ such that $\|Fg_z^\varepsilon - \phi_z^\infty\|_{L^2(\mathbb{S})} < \varepsilon$, we have:*

$$\lim_{\varepsilon \to 0} \|v_{g_z^\varepsilon}\|_{L^2(D)} = \infty. \tag{1.20}$$

The inverse of the $L^2(D)$ norm of the Herglotz wave provides an indicator of the shape of D: the values approaching 0 correspond to the points outside the obstacle. However, since D is unknown, this norm is not computable. In numerical implementation, $\|v_{g_z^\varepsilon}\|_{L^2(D)}$ is substituted by $\|g_z^\varepsilon\|_{L^2(\mathbb{S})}$. The LSM imaging algorithm consists then in finding, for a fixed ε, the corresponding g_z^ε for each sampling points $z \in \mathbb{R}^m$ and displaying the inverse of its norm. Theorem 1 does not indicate how to construct such g_z^ε. In practice, although it is not clear which solution is obtained, g_z^ε is determined using Tikhonov regularization combined with the Morozov's discrepancy principle as it yields good results. Figure 1.1 (left) illustrates the LSM imaging algorithm in $\mathbb{R}^2$ for a centered circular scatterer of radius 1 and a constant refractive index $n = 3$ inside for $k = 6$ on a 90×90 uniformed grid of $[-2.1, 2.1] \times [-2.1, 2.1]$.

Figures 1.2, 1.3, 1.4 and 1.5 present the LSM for various configuration (shown on the left side of each figure) with wavenumbers $k = 3$ or $k = 4$. In these figures, areas with defects in the medium are represented by colored zones in the LSM imaging results. Despite these visual indications, the results are unsatisfactory for closely spaced scatterers. In particular, Figure 1.6 shows the indicator function for a cluttered medium. In this figure, more intensely colored regions appear to indicate areas of higher density, suggesting that the LSM may capture variations of the refractive index. However, Theorem 1 does not provide any quantitative results and there is no theoretical foundation within the LSM to exploit the numerical values of the density indicator. Consequently, while the visual representations may carry some information, we lack theoretical basis to interpret it.

1.4 Transmission eigenvalues and the Generalized Linear Sampling Method (GLSM)

We begin this section by emphasising the impact of the transmission eigenvalues on the resulting reconstruction provided by the LSM. In the configuration of Figure 1.1, for D

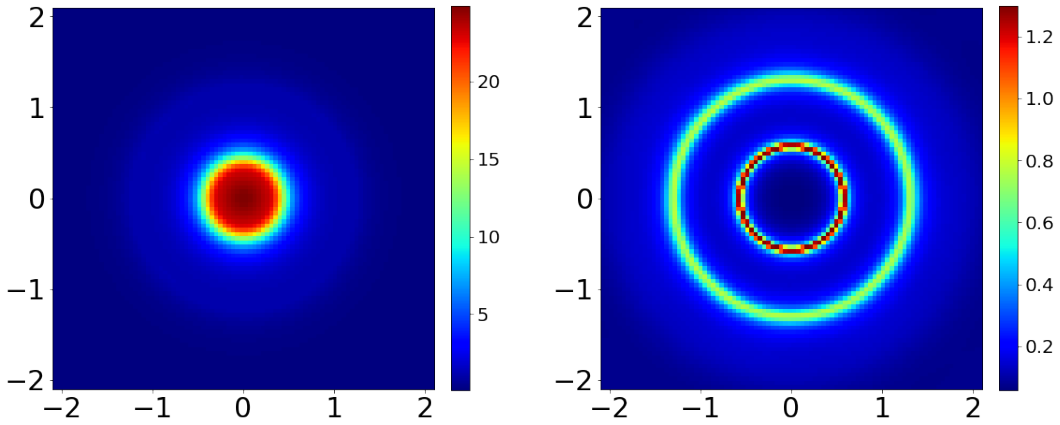

Figure 1.1: Indicator function provided by the LSM for a centered at the origin circular obstacle D of radius 1 and a constant refractive index $n|_D = 3$ on a 90×90 uniformed grid of $[-2.1, 2.1] \times [-2.1, 2.1]$. Left: for a wavenumber $k = 6$. Right: for a wavenumber $k = 4.16$.

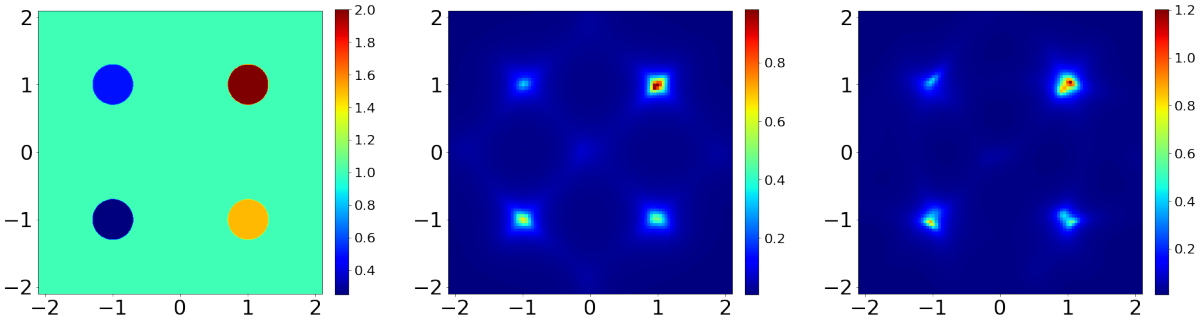

Figure 1.2: Left: Four diffracting discs of radius 0.3 associated with four different values of the refractive index $n = 0.25$ (bottom left), $n = 0.5$ (top left), $n = 1.5$ (bottom right) and $n = 2$ (upper right). Indicator function provided by the LSM on a 100×100 uniformed grid of $[-2.1, 2.1] \times [-2.1, 2.1]$ with 1% of added noise. Middle: for $k = 3$. Right: for $k = 4$.

a centered at the origin circular scatterer of radius $\rho = 1$, the solutions of equation (1.3) $(u := w^s + v, v)$ assume an analytical expression:

$$\begin{cases} u = \sum_{q\in\mathbb{Z}} \alpha_q J_q(kr\sqrt{n})e^{iq\theta}, \\ v = \sum_{q\in\mathbb{Z}} \beta_q J_q(kr)e^{iq\theta}, \end{cases} \tag{1.21}$$

where J_q denotes the Bessel function of first kind of order q. By enforcing the boundary conditions, we deduce that k is a transmission eigenvalue if there exists $q \in \mathbb{Z}$ such that the

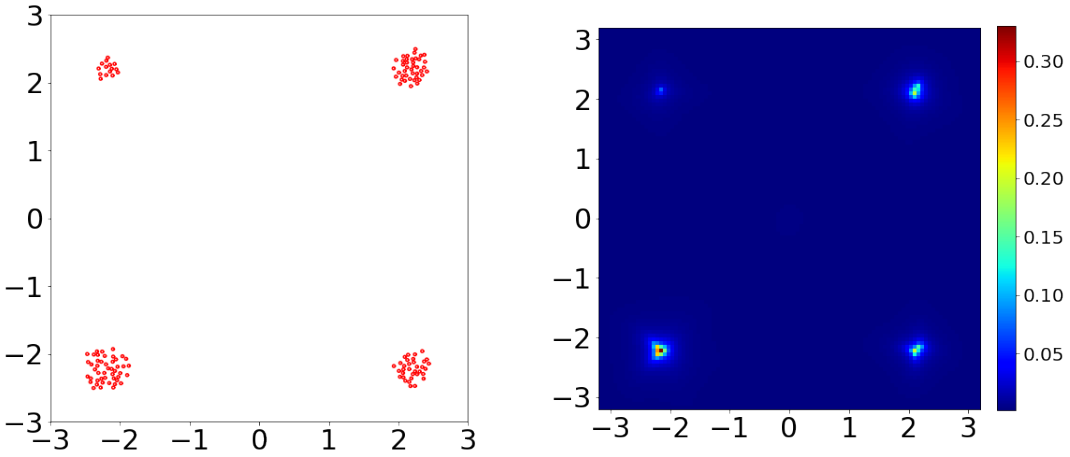

Figure 1.3: Left: the domain D constituted by small circles located at the four corners with refractive index $n|_D = 2$. Right: Indicator function provided by the LSM on a 100×100 uniformed grid of $[-3.2, 3.2] \times [-3.2, 3.2]$ for a wavenumber $k = 3$ with 1% of added noise.

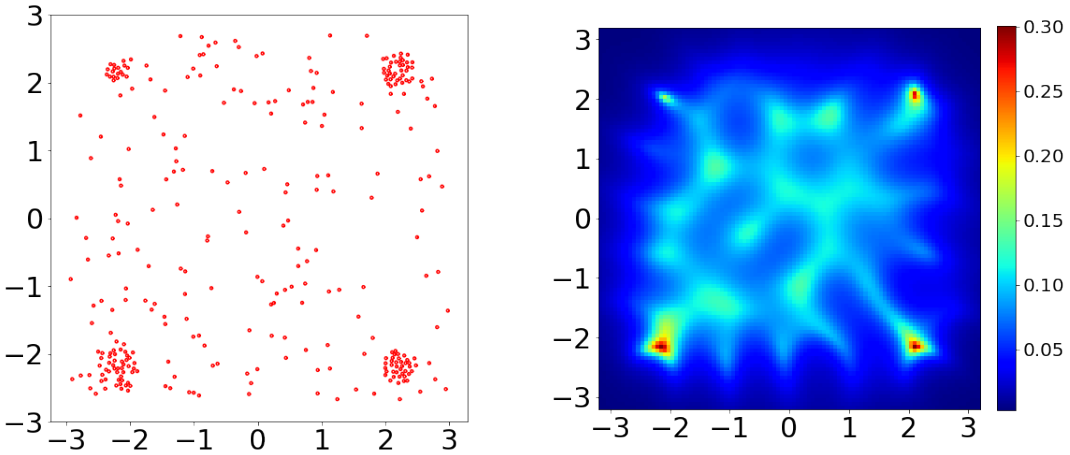

Figure 1.4: Left: the domain D constituted by small circles with refractive index $n|_D = 2$ and some additional obstacles in between the corner. Right: Indicator function provided by the LSM on a 100×100 uniformed grid of $[-3.2, 3.2] \times [-3.2, 3.2]$ for a wavenumber $k = 3$ with 1% of added noise.

following determinant vanishes:

$$\begin{vmatrix} J_q(k\rho\sqrt{n}) & -J_q(k\rho) \\ \sqrt{n}J_q'(k\rho\sqrt{n}) & -J_q'(k\rho) \end{vmatrix} = 0. \tag{1.22}$$

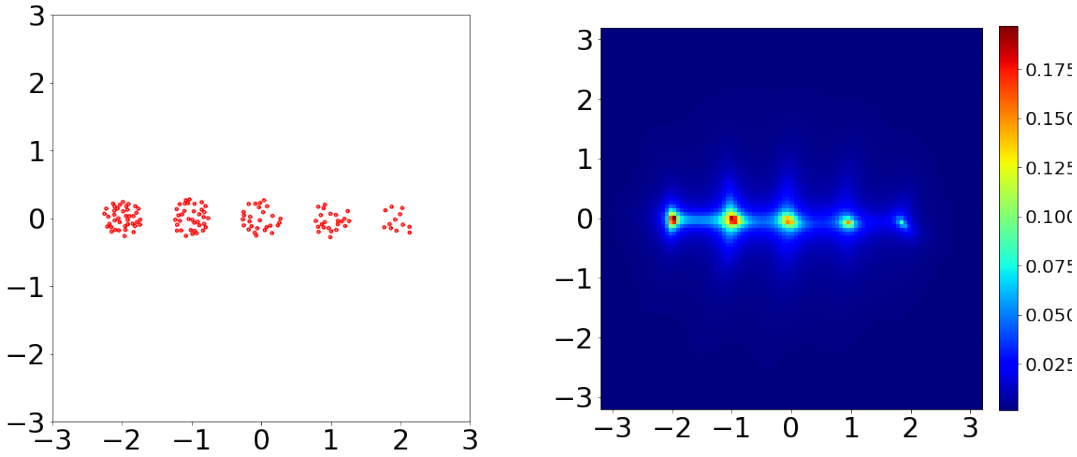

Figure 1.5: Left: the domain D constituted by small circles concentrated i in four aligned areas with refractive index $n|_D = 2$. Right: Indicator function provided by the LSM on a 100×100 uniformed grid of $[-3.2, 3.2] \times [-3.2, 3.2]$ for a wavenumber $k = 3$ with 1% of added noise.

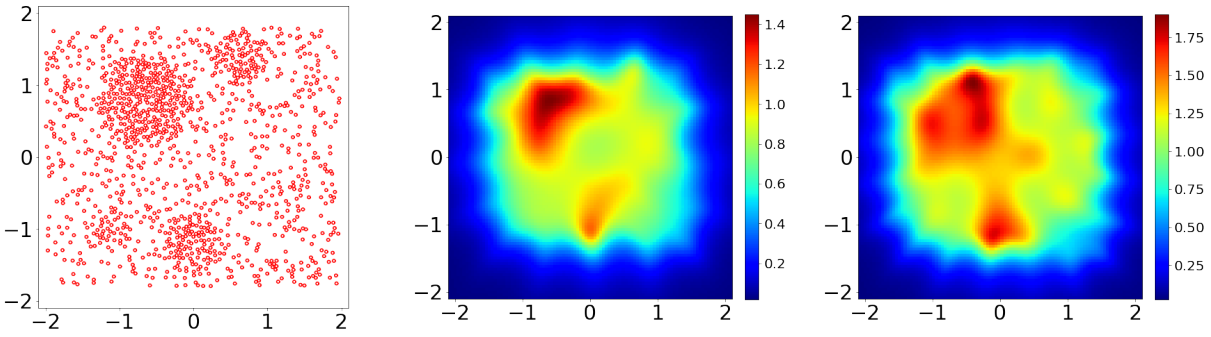

Figure 1.6: Left: the domain D constituted by 1257 small circles of radius 0.02 having a constant index of refraction $n|_D = 2$. Indicator function provided by the LSM on a 100×100 uniformed grid of $[-2.1, 2.1] \times [-2.1, 2.1]$ with 1% of added noise. Middle: for $k = 3$. Right: for $k = 4$.

We display in Figure 1.1 (right) the LSM result for k being the first transmission eigenvalue (around ~ 4.16) for $n|_D = 3$. It is clear that it does not provide the same level of accuracy as in Figure 1.1 (left). This is an illustration of why the transmissions eigenvalues are frequencies to avoid for the LSM. However, these wavenumbers have a strong connection with the properties of the refractive index n and may play a valuable role in reconstruction algorithms.

The analysis and study of problem (1.18) falls outside the classical variational framework

for second order PDE. Indeed, multiplying both equations by test functions $u', v' \in H^1(D)$ such that $u'|_{\partial D} = v'|_{\partial D}$, the following variational formulation is obtained:

$$\int_D \nabla u \nabla \overline{u'} dx - \int_D \nabla v \nabla \overline{v'} dx - k^2 \int_D (nu\overline{u'} + v\overline{v'}) dx = 0. \tag{1.23}$$

The negative sign in front of the second term prevents this formulation from being of Fredholm type. The standard tools used to analyse eigenvalue problems for self-adjoint operators (for instance Dirichlet or Neumann eigenvalues) are not applicable in this context. If $n \neq 1$, a bilaplacian formulation can be established for $w := u - v \in H_0^2(D)$. This reformulation allows the problem to be expressed as a quadratic eigenvalue problem. We refer to [15, Chapter 3 and 4] for a more detailed proof. We now state a theorem recasting known results on TEs [17]:

Theorem 2. *Assume that $n - 1$ is of constant sign with $\sup_D n < 1$ or $\inf_D n > 1$. Then, there exists an infinite set of real transmission eigenvalues with $+\infty$ as the only accumulation point.*
In addition, for n_1, n_2 two refractive indices, the $j-$th transmission eigenvalues k_j satisfies the following monotonicity relation:

$$\begin{cases} k_j(n_2) < k_j(n_1), & \text{if } n_1 < n_2, \\ k_j(n_1) < k_j(n_2), & \text{if } n_2 < n_1, \end{cases} \tag{1.24}$$

Monotonicity relation (1.24) is an important observation that may be exploited for imaging algorithms as we shall mention later.
Next, we address the way to determine those Transmission eigenvalues from far field data. In this section, we introduce a method based on the Generalized Linear Sampling Method. This method overcomes the limitations of the LSM at the cost of a greater computational cost. We present its analytical framework, referring to [8] for more details.

Let X and Y be two Hilbert spaces. We consider a bounded linear operator $F : X \to X$ that has dense range and can be factorized as $F = GH$ where $H : X \to Y$ and $G : \overline{\mathcal{R}(H)} \subset Y \to X$ are bounded linear operators with $\overline{\mathcal{R}(H)}$ being the closure of the range of H in Y. In addition let $B : X \to \mathbb{R}^+$ be a continuous functional that satisfies the following assumption.

Assumption 3. *Given a sequence $\{g_n\} \in X$, the sequence $\{B(g_n)\}$ is bounded if and only if the sequence $\{\|Hg_n\|_Y\}$ is bounded.*

For a given parameter $\alpha > 0$ and $\phi \in X$, we consider the following cost functional

$$J_\alpha(g, \phi) := \alpha B(g) + \|Fg - \phi\|_X^2 \tag{1.25}$$

This cost functional has no minimizer in general, however its positivity implies that we can define $j_\alpha(\phi) := \inf_{g \in X} J_\alpha(g, \phi)$.
The central theorem of the GLSM is the following characterization of the range of G in terms of F and B.

Theorem 4. *In addition to Assumption 3 we assume that F has dense range. Let $C > 0$ be a given constant independant of α and consider a minimizing sequence $\{g_\alpha\}$ of J_α such that:*

$$J_\alpha(\phi, g_\alpha) \leq j_\alpha(\phi) + C\alpha \tag{1.26}$$

Then $\phi \in \mathcal{R}(G)$ if and only if the sequence $B(g_\alpha)$ is bounded as $\alpha \to 0$.

The application of this theorem to the far field operators F and $B(g) := \|Hg\|_{L^2(D)}$ with $\phi := \phi_z^\infty$ for $z \in \mathbb{R}^m$ can offer a method for recovering transmission eigenvalues.

Theorem 5. *Assume that D is simply connected. Then, a real number $k > 0$ is a transmission eigenvalue if and only if for any ball $B_l \subset D$,the set of point z such that $B(g_\alpha^z)$ is bounded and $\|Fg_\alpha^z - \phi_z^\infty\|_{L^2(\mathbb{S})} \to 0$ as $\alpha \to 0$ is nowhere dense in B_l.*

A proof is provided in [15, Chapter 5, Section 5.1]. Theorem 5 provides an indicator function for the transmission eigenvalues which presents a peak (numerically corresponding to an unbounded term) at those values. This allows to numerically recover the real TE. These TE are of particular interest due to their monotonical dependence with respect to the refractive index, the discreteness of their set and the possibility to determine them from the knowledge of the far fields. However, several drawbacks exist:

1) Since only the far fields F for a real wavenumber k are available, only the real transmission eigenvalues can be recovered, whose existence is not guaranteed for a complex refractive index.

2) Their determination requires the knowledge of the far field operator F over a wide range of frequencies k.

3) Their mathematical analysis is challenging and varies depending on the nature of the obstacle (penetrable, void, ...)

4) The monotonocity property (1.24) provides only global information about the medium.

To handle these issues, the concept of the transmission eigenvalue has been extended as follows.

1.5 Modified transmission eigenvalues

1.5.1 An extension of the Transmission eigenvalues

The idea that has been exploited in many related works [5, 6] is to gain a degree of freedom by considering in (1.18) $\Delta v + k^2 n_b v = 0$ instead of the homogeneous Helmholtz equation, where n_b will play the role of a fictive refractive index such that $n_b = 1$ outside a regular bounded simply connected domain D_b. Such modified eigenvalue problem can be obtained by considering $v = v_b$ solution of the forward scattering problem:

$$\begin{cases} \Delta v_b + k^2 n_b v_b = 0 \text{ in } \mathbb{R}^m, \\ v_b = v_b^s + u^i \\ \lim\limits_{r \to +\infty} \int_{|x|=r} |\frac{\partial v_b^s}{\partial r} - ikv_b^s|^2 = 0, \end{cases} \tag{1.27}$$

where u^i is the incident field as in (1.1). We denote by F_b its associated far field operator. Assume that $D \subset D_b$. The application of the Linear Sampling Method to the modified far field operator $\mathcal{F} := F - F_b$ necessitates the exclusion of the wavenumbers k that solve the following eigenvalue problem:

$$\begin{cases} \Delta u + k^2 n u = 0 \text{ in } D_b, \\ \Delta v + k^2 n_b v = 0 \text{ in } D_b, \\ u - v = 0 \text{ on } \partial D_b, \\ \partial_\nu (u - v) = 0 \text{ on } \partial D_b. \end{cases} \tag{1.28}$$

These modified transmission eigenvalues, that depend on the choice of n_b, can provide meaningful information on D . The scattering problem (1.27) is often referred as scattering problem for "artificial background medium". Artificial because it is specifically designed to suit the needs of the problem, does not depend on any unknown parameters and can thus be computed numerically beforehand. When applying the sampling method to $\mathcal{F}$, the unknown medium associated with F is compared to the background medium associated to F_b. In particular, when $F_b = 0$ or $n_b = 1$ in $\mathbb{R}^m$, it is compared to the vacuum (which corresponds to the LSM presented in Theorem 1).

The introduction of a background problem revealed the possibility of working with a parameter other than the frequency. Problem (1.27) can be adapted to yield an interior transmission problem that is simpler to analyse. We introduce a spectral parameter $\lambda \in \mathbb{R}$ that appears in the equation either inside or on the boundary of D_b. There are many possible choices for this approach, and they remain largely unexplored. We present a variation of problem (1.27) that explicitly solves the sign issue of the variational form (1.23).

1.5.2 Modified transmission eigenvalues associated with metamaterial background

This new set of modified transmission eigenvalues was introduced for the first time in [4] through the use of a well chosen metamaterial background.
Let $D_b \subset \mathbb{R}^m$ be a regular bounded simply connected domain. Let $u_b \in H^1_{loc}(\mathbb{R}^m)$ be the total field and u_b^s be the scattered field solutions of

$$\begin{cases} \operatorname{div}(a_b \nabla u_b) + k^2 n_b(\lambda) u_b = 0 \text{ in } \mathbb{R}^m, \\ u_b = u^i + u_b^s, \\ \lim\limits_{r \to +\infty} \int_{|x|=r} |\frac{\partial u_b^s}{\partial r} - iku_b^s|^2 = 0, \end{cases} \tag{1.29}$$

for some incident field u^i. The coefficients $a_b, n_b(\lambda) \in L^\infty(\mathbb{R}^m)$ are such that

$$a_b = \begin{cases} 1 \text{ in } \mathbb{R}^m \backslash \overline{D_b}, \\ -a \text{ in } D_b, \end{cases} \quad \text{and} \quad n_b(\lambda) = \begin{cases} 1 \text{ in } \mathbb{R}^m \backslash \overline{D_b}, \\ \lambda \text{ in } D_b, \end{cases} \tag{1.30}$$

for $a > 0$ and $a \neq 1$ and $\lambda \in \mathbb{R}$ that will play the role of a spectral parameter. Similarly to the forward scattering problem, we use the notation $u_b(.,d), u_b^s(.,d)$,$u_b^\infty(.,d)$ for $u^i = u^i(.,d)$ and consider the far field operator $F_b^\lambda : L^2(\mathbb{S}) \to L^2(\mathbb{S})$

$$(F_b^\lambda g)(\hat{x}) := \int_{\mathbb{S}} g(d) u_b^\infty(\hat{x}, d) ds(d), \quad \hat{x} \in \mathbb{S}. \tag{1.31}$$

We then define the modified far field operator $\mathcal{F}^\lambda : L^2(\mathbb{S}) \to L^2(\mathbb{S})$

$$\mathcal{F}^\lambda g := Fg - F_b^\lambda g. \tag{1.32}$$

We remark that the spectral parameter λ does not appear in $D \backslash D_b$. Consequently, the assumption that $D \subset D_b$ is no longer necessary. Let Ω be an open domain such that $\overline{\Omega} = \overline{D} \cup \overline{D_b}$ and such that Ω has a connected complement.

Definition 2. *Modified transmission eigenvalues λ correspond to the values of λ such that there exists a non trivial incident field u^i in $L^2(\Omega) \cap H^1(D_b)$ solution of the Helmholtz equation in Ω such that, $u^s = u_b^s$ in $\mathbb{R}^m \backslash \Omega$. In particular, we obtain that for these values, there exists a non trivial solution $w := u|_\Omega$ and $v := u_b|_\Omega$ of the following problem*

$$\begin{cases} \Delta w + k^2 n w = 0 \text{ in } \Omega, \\ \operatorname{div}(a_b \nabla v) + k^2 n_b(\lambda) v = 0 \text{ in } \Omega, \\ v = w \text{ on } \partial\Omega, \\ a_b \partial_\nu v = \partial_\nu w \text{ on } \partial\Omega. \end{cases} \tag{1.33}$$

In the case where $u|_\Omega = w$ and $u_b|_\Omega = v$ respectively coincide with the solutions of (1.1) and (1.29) with $u^i = v_g$, we have $\mathcal{F}g = 0$. This means that for this particular Herglotz wave, the scattered wave produced by the original media and the background media are the same outside Ω.
Let us consider the interior transmission problem (1.33) where D does not intersect ∂D_b as presented in Figure 1.7. In this case, solving the spectral problem (1.33) is equivalent

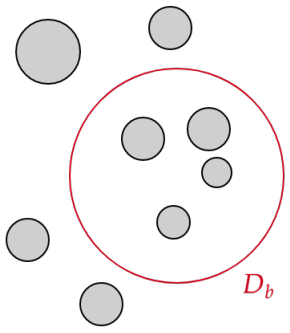

Figure 1.7: Configuration where $D \cap \partial D_b = \emptyset$

to solving the following one posed on D_b by setting $w = v = 0$ in $\Omega \backslash D_b$ (assuming that

k is not a transmission eigenvalue for classical interior transmission problem in D [15]): $w \in H^1(D_b), v \in H^1(D_b)$,

$$\begin{cases} \Delta w + k^2 n w = 0 \text{ in } D_b, \\ -a\Delta v + k^2 \lambda v = 0 \text{ in } D_b, \\ v = w \text{ on } \partial D_b, \\ -a\partial_\nu v = \partial_\nu w \text{ on } \partial D_b. \end{cases} \tag{1.34}$$

Let us denote by $\eta_0(n, D_b)$ the first Dirichlet eigenvalue of the problem:

$$\begin{cases} w \in H^1(D_b), \\ \Delta w + \eta n w = 0 \text{ in } D_b, \qquad w = 0 \text{ on } \partial D_b. \end{cases} \tag{1.35}$$

1.5.3 Main properties

We review the key properties of these eigenvalues and provide a more detailed proof of certain lemmas from [4].

Existence and Discreteness

Introduce the vector space $\mathbf{H}^1(D_b) := \{w, v \in H^1(D_b), w|_{\partial D_b} = v|_{\partial D_b}\}$. The eigenvalue problem (1.34) is equivalent to the variational formulation:

$$\int_{D_b} \nabla w \nabla \overline{w'} dx + a \int_{D_b} \nabla v \nabla \overline{v'} dx - k^2 \int_{D_b} n w \overline{w'} dx = -k^2 \lambda \int_{D_b} v \overline{v'} dx, \tag{1.36}$$

for all $(w', v') \in \mathbf{H}^1(D_b)$. For $\beta \in \mathbb{C}$, consider the selfadjoint operator $\mathbf{A}_\beta : \mathbf{H}^1(D_b) \to \mathbf{H}^1(D_b)$ defined as:

$$(\mathbf{A}_\beta(w, v), (w', v'))_{\mathbf{H}^1(D_b)} = \int_{D_b} \nabla w \nabla \overline{w'} dx + a \int_{D_b} \nabla v \nabla \overline{v'} dx - k^2 \int_{D_b} n w \overline{w'} dx + k^2 \beta \int_{D_b} v \overline{v'} dx. \tag{1.37}$$

The sign in front of a (a positive constant) ensures that this operator is of Fredholm type. Furthermore, it depends analytically on β. Let $\beta = i \in \mathbb{C}\backslash\mathbb{R}$. Consider $(w, v) \in \mathbf{H}^1(D_b)$ such that $\mathbf{A}_i(w, v) = 0$. By taking the imaginary part of (1.37) with $w' = \overline{w}$ and $v' = \overline{v}$, we find that $k^2 \int_{D_b} |v| dx = 0$. This implies that $v = 0$ in D_b and that $w \in H_0^1(D_b)$. From Green formula, we conclude that w is solution of:

$$\begin{cases} w \in H_0^1(D_b), \\ \Delta w + k^2 n w = 0 \text{ in } D_b, \\ \partial_\nu w = 0 \text{ on } \partial D_b, \end{cases} \tag{1.38}$$

which leads to $w = 0$ in D_b. This proves that $\mathbf{A}_i$ invertible. By analytic Fredholm theory, this demonstrates the existence of $\beta \in \mathbb{R}$ such that $\mathbf{A}_\beta$ is invertible and that the following problem is well posed:

$$\begin{cases} \Delta w + k^2 n w = 0 \text{ in } D_b, \\ -a\Delta v + k^2 \beta v = 0 \text{ in } D_b, \\ v = w \text{ on } \partial D_b, \\ -a\partial_\nu v = \partial_\nu w \text{ on } \partial D_b. \end{cases} \tag{1.39}$$

Lemma 6. *The spectrum of (1.34) is formed by a real sequence.*

Proof. Fix $\beta \in \mathbb{R}$ such that $\mathbf{A}_\beta$ is invertible. For $g \in L^2(D_b)$, set $(w_g, v_g) \in \mathbf{H}^1(D_b)$ the unique solution of:

$$\begin{cases} \Delta w_g + k^2 n w_g = 0 \text{ in } D_b, \\ -a\Delta v_g + k^2 \beta v_g = g \text{ in } D_b, \\ v_g = w_g \text{ on } \partial D_b, \\ -a\partial_\nu v_g = \partial_\nu w_g \text{ on } \partial D_b. \end{cases} \tag{1.40}$$

We now consider the compact and self adjoint operator $\mathbf{T} : L^2(D_b) \to L^2(D_b)$ such that:

$$\mathbf{T}g = v_g \in H^1(D_b). \tag{1.41}$$

The eigenvalue problem becomes:

$$-k^2(\lambda - \beta)\mathbf{T}g = g. \tag{1.42}$$

Standard results on the spectrum of compact and selfadjoint operators conclude the proof. □

Due to the compactness of the operator $\mathbf{T}$, the sequence $((\lambda_i - \beta)^{-1})_{i\in\mathbb{N}}$ converges to 0. Moreover, it can be shown by contradiction that there is at least one positive eigenvalue. In addition, provided that k^2 is not a Dirichlet eigenvalue of (1.35), the only accumulation point of this sequence is $-\infty$ [4, Theorem 5].

Monotonic dependence

With the existence and discreteness of the set of modified transmission eigenvalues established, the two main properties of the original transmission eigenvalues remain to be addressed. The monotonic dependence with respect to the refractive index n can also be demonstrated using a Courant-Fischer principle, as presented in the following Theorem [4, Theorem 6].

Theorem 7. *Assume that $k^2 < \eta_0(n, D_b)$, the first Dirichlet eigenvalue of (1.35). The largest positive eigenvalue of (1.34) $\lambda_0(n, D_b)$ satisfies:*

$$\lambda_0(n, D_b) = \sup_{(w,v)\in\mathbf{H}^1(D_b), v\neq 0} \frac{k^2 \int_{D_b} n|w|^2 dx - \int_{D_b} |\nabla w|^2 dx - a\int_{D_b} |\nabla v|^2 dx}{k^2 \int_{D_b} |v|^2 dx}. \tag{1.43}$$

Equation (1.43) is particularly relevant for an imaging algorithm. Unlike (1.24) where the monotonic dependence is global, the dependence of $\lambda_0(n, D_b)$ is local to D_b . A collection of those values for various position of D_b can provide enhanced information about the medium.

Inversion method

Analogous to the original TE, the modified transmission eigenvalues can be recovered using Theorem 4 (the GLSM Theorem). The proof details are similar to those in Chapter 3 and proceed as follows:

1) Factorize the modified far field operator in the form $\mathcal{F} = \mathcal{G}^\lambda \mathcal{H}^\lambda$ (see equation (3.3)).

2) Demonstrate that if λ is an eigenvalue of (1.34), then ϕ_z^∞ belongs to the range of $\mathcal{G}^\lambda$ (denoted $\mathcal{R}(\mathcal{G}^\lambda)$) for all $z \in D_b$ (see Lemma 20).

3) Prove that the set of points z for which $\phi_z^\infty \in \mathcal{R}(\mathcal{G}^\lambda)$ is nowhere dense in D_b if λ is not an eigenvalue of (1.34) (see Lemma 21).

4) Show that the operator $B(g) := |(Fg, g)_{L^2(\mathbb{S})}| + \|v_g\|^2_{H^1(D_b)}$ satisfies Assumption 3.

These steps are sufficient to establish the following theorem:

Theorem 8. *Assume that k is not a transmission eigenvalue associated with D and assume there exists $\beta > 0$ such that $n - 1 \geq \beta$ (or $1 - n \geq \beta$) in a neighborhood of ∂D.*
Consider the functional

$$J_\alpha(\phi_z^\infty, g) := \alpha B(g) + \|\mathcal{F}^\lambda g - \phi_z^\infty\|^2_{L^2(S)} \quad \text{and set} \quad j_\alpha(\phi_z^\infty) := \inf_{g \in L^2(\mathbb{S})} J_\alpha(\phi_z^\infty, g). \tag{1.44}$$

Let g_α^z be a minimizing sequence defined by

$$J_\alpha(\phi_z^\infty, g_\alpha^z) \leq j_\alpha(\phi_z^\infty) + C\alpha, \tag{1.45}$$

where $C > 0$ is a constant independent of α. Then a real number λ is not an eigenvalue of (1.34) if and only if the set of points z such that $B(g_\alpha^z)$ is bounded and $\|\mathcal{F}^\lambda g_\alpha^z - \phi_z^\infty\|_{L^2(\mathbb{S})} \to 0$ as $\alpha \to 0$ is nowhere dense in D_b.

This is just one of many examples of modified transmission eigenvalues. The challenge of designing a well chosen background to generate a new class of modified transmission eigenvalues remains an open problem. [4] also introduces the so-called Steklov eigenvalues, which share the same 3 main properties presented above and are derived from an artificial background with a non-penetrable obstacle. While these two examples show promising results, the next chapter is dedicated to the design of a new class of eigenvalues which addresses their potential numerical drawbacks.

Chapter 2

The averaged Steklov eigenvalue

Contents

2.1 Introduction

A fundamental aspect for imaging algorithm is the choice of the background model. The metamaterial background proposed in [4] provides a promising starting point due to its flexibility, the discrete nature of its eigenvalues, and their monotonicity with respect to the refractive index. For small values of the parameters, the eigenvalues become very close to each others, making it challenging to numerically recover them. Therefore, the largest eigenvalue would be the most natural choice for use in an inversion algorithm.
In this chapter, we demonstrate that, as the metamaterial parameter goes to infinity, the associated spectrum converges to a simplified spectrum containing only one non zero eigenvalue. This is very appealing from the numerical point of view, since it significantly simplifies the identification of the non zero eigenvalue from measured data. This allows for a better quantitative interpretation of the indicator function. This chapter is adapted from [12] and includes an additional section that slightly generalizes this spectral parameter to a family of spectral parameters sharing similar properties.

2.2 The new eigenvalue problem

2.2.1 The choice of the metamaterial parameter a

The set of eigenvalues of problem (1.34) can be recovered from the far field measurements using Theorem 8. However, the value of the parameter a greatly influences their location and proximity. How should this parameter be chosen to optimize the inversion algorithm? Consider, in dimension 2, the configuration depicted in Figure 2.1 (left) and let D_b (in green) be the ball of radius $\rho = 0.5$ centered at $(-0.5, 1)$. Figure 2.1 (right) shows the indicator function that depend on the spectral parameter λ which is derived from Theorem 8. Details of the numerical computation of this function can be found in Chapter 3 Section 3.4. We expect this function to present a peak at the eigenvalues of problem (1.34), which correspond numerically to a local maximum of the indicator function. However, distinguishing the small peaks from numerical errors becomes challenging. If an error occurs, an eigenvalue may be mistaken for the next or previous one, leading to the failure of any imaging reconstruction of the obstacles. This issue happens in particular with the negative eigenvalues. Since there

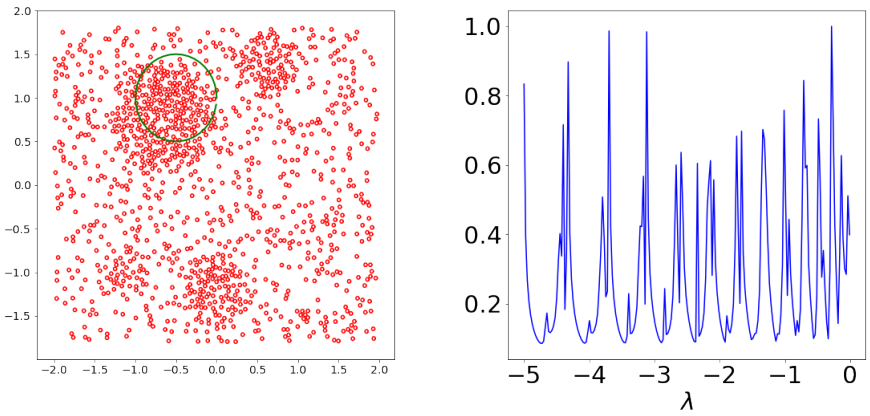

Figure 2.1: Left: The domain D (in red) and D_b, the ball of radius $\rho = 0.5$ centered at $(-0.5, 1)$ (in green). Right: The indicator function given by Theorem 8 with $k = 4$ and $a = 0.01$ with 1% of added noise.

are only a finite number of positive eigenvalues, the reconstruction algorithm appears to be more relevant with them. To avoid confusion with other eigenvalues, it is preferable to have only one positive eigenvalue. They can be computed analytically in the case of a ball and constant n as the zero of a determinant. Indeed, for $D = D_b$ a centered ball of radius ρ, the eigenvalues are solutions to:

$$\mathcal{P}_j(a, \lambda) = det \begin{pmatrix} J_j(k\rho\sqrt{n}) & -J_j(k\rho\sqrt{\frac{-\lambda}{a}}) \\ \sqrt{n}J_j'(k\rho\sqrt{n}) & a\sqrt{\frac{-\lambda}{a}}J_j'(k\rho\sqrt{\frac{-\lambda}{a}}) \end{pmatrix} = 0, \tag{2.1}$$

where $j \in \mathbb{Z}$ and J_j denotes the Bessel function of the first kind of order j.
Figure 2.2 shows that some simple configurations yield multiple positive eigenvalues. For

numerical efficiency, the parameter a in (1.33) should be chosen to simplify the structure of the spectrum (ie: only one positive eigenvalue) and maximize the sensitivity with respect to n. Figure 2.3 displays $\mathcal{P}_0(a,\lambda)^{-1}$ for various values of the metamaterial parameter a and

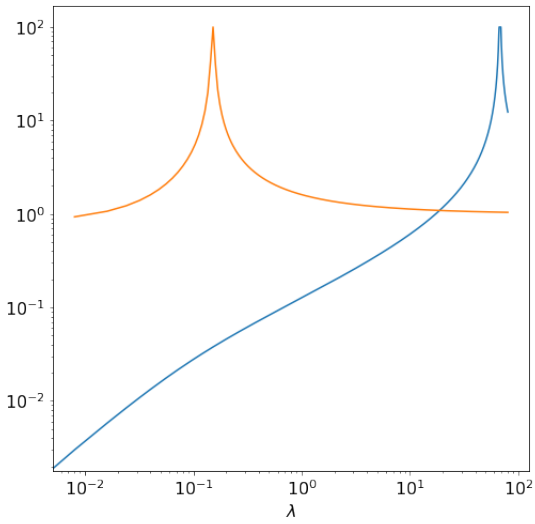

Figure 2.2: Values of $\mathcal{P}_0(a,\lambda)^{-1}$ (blue) and $\mathcal{P}_1(a,\lambda)^{-1}$ (orange) for constant $n|_{D_b} = 1$, $a = 0.1$ and product $k\rho = 2$. The peaks indicate where the function approaches 0.

λ. We observe that, as a goes to infinity, negative eigenvalues tend to $-\infty$ and the largest one converges to a unique positive value. To avoid adjusting the parameter a, it would be interesting to consider the spectral problem (1.33) as a goes to infinity. This limit is studied in the following section.

Remark 1. *Figure 2.3 also suggests that the largest eigenvalue converges to $+\infty$ as $a \to 0$. This can be shown via the Courant Fischer equality (1.43). For $a > 0$, take $w_a := K$, a constant and v_a a function in $H^1(D_b)$ such that $\int_{D_b} |v_a|^2 dx \leq a$ and $\int_{D_b} |\nabla v_a|^2 dx \geq \frac{1}{a}$ with the condition $v_a|_{\partial D_b} = K$. An idea to construct such v_a is to vanish it on an open set inside D_b and increase its value on a small zone around the border ∂D_b until it reaches K. In that case, one gets for λ_a the largest eigenvalue:*

$$\lambda_a \geq \frac{k^2K^2 \int_{D_b} n dx - a \int_{D_b} |\nabla v_a|^2 dx}{k^2 \int_{D_b} |v_a|^2 dx} \geq \frac{k^2K^2 \int_{D_b} n dx - 1}{k^2 a}, \tag{2.2}$$

which converges to $+\infty$ as a approaches 0^+ for K large enough.

2.2.2 The limit spectral problem as $a \to +\infty$

Theorem 9. *Assume that $k^2 < \eta_0(n, D_b)$. Let $(a_j)_j$ be an unbounded increasing sequence of positive numbers larger than 1. Let λ_j be the largest positive eigenvalue of*

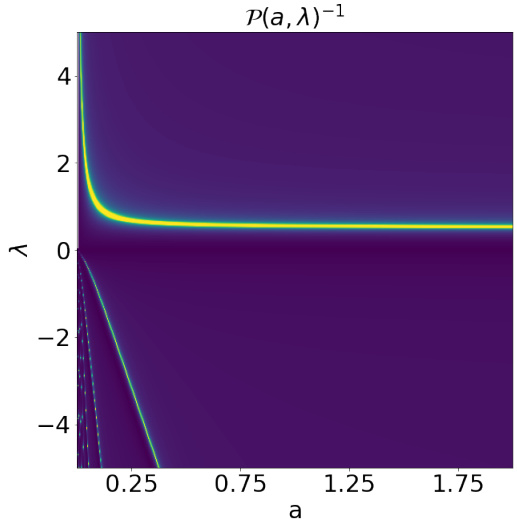

Figure 2.3: Values of $\mathcal{P}_0(a,\lambda)^{-1}$ for constant $n|_{D_b} = 1$ and product $k\rho = 1$. The bright regions indicate where the function approaches 0.

(1.34) for $a = a_j$ and $(w_j, v_j) \in H^1(D_b) \times H^1(D_b)$ be an associated eigenvector such that $\|w_j\|^2_{H^1(D_b)} + \|v_j\|^2_{H^1(D_b)} = 1$. Then, λ_j converges to some non negative value $\frac{\mu}{k^2|D_b|}$ and (up to a subsequence) w_j converges weakly in $H^1(D_b)$ and strongly in $L^2(D_b)$ to a non trivial function $w \in H^1(D_b)$ that satisfies

$$\begin{cases} \Delta w + k^2 n w = 0 \text{ in } D_b, \\ \mu w + \int_{\partial D_b} \partial_\nu w ds = 0 \text{ on } \partial D_b, \end{cases} \tag{2.3}$$

where $|D_b| := \int_{D_b} dx$. The corresponding sequence $(v_j)_j$ strongly converges to a constant in $H^1(D_b)$.

Proof. According to (1.43), the positive sequence (λ_j) is decreasing and therefore converges to some $\lambda \geq 0$. Moreover, since the sequence (w_j, v_j) is bounded in $H^1(D_b) \times H^1(D_b)$, up to a subsequence, we can assume that (w_j, v_j) converges to some (w, v) weakly in $H^1(D_b) \times H^1(D_b)$ and strongly in $L^2(D_b) \times L^2(D_b)$. Problem (1.34) is equivalent to the variational formulation:

$$\int_{D_b} \nabla w_j \nabla w' dx + a_j \int_{D_b} \nabla v_j \nabla v' dx - k^2 \int_{D_b} n w_j w' dx = -k^2 \lambda_j \int_{D_b} v_j v' dx, \tag{2.4}$$

for all $w', v' \in H^1(D_b), w' = v'$ on ∂D_b. Taking $v' = v_j$ and $w' = w_j$ in (2.4) shows that the sequence $a_j ||\nabla v_j||^2_{L^2(D_b)}$ is bounded. Therefore ∇v_j converges strongly to 0 in $L^2(D_b)$ which proves that $v = K$ a constant in D_b. We then infer that $w = K$ on ∂D_b. Taking $v' = 0$ in D_b and w' in $H^1_0(D_b)$ and passing to the limit as j goes to infinity in (2.9) shows that

$$\Delta w + k^2 n w = 0 \text{ in } D_b. \tag{2.5}$$

Since $-a_j\Delta v_j + k^2\lambda_j v_j = 0$ in D_b, we obtain, by integration over D_b, the Green formula and $-a_j\partial_\nu v_j = \partial_\nu w_j$ on ∂D_b,

$$\int_{\partial D_b} \partial_\nu w_j ds + \lambda_j k^2 \int_{D_b} v_j dx = 0,$$

where the first integral must be understood as $< H^{-\frac{1}{2}}(\partial D_b), H^{\frac{1}{2}}(\partial D_b) >$ duality pairing. This notation convention will be constantly used in the rest of the chapter. Passing to the limit in the previous equation leads to

$$\mu w + \int_{\partial D_b} \partial_\nu w ds = 0,$$

using the fact that $\partial_\nu w_j$ weakly converges to $\partial_\nu w$ in $H^{-\frac{1}{2}}(\partial D_b)$. This proves that w satisfies (2.3).
We now prove by contradiction that w is not a trivial function. Assume that $w = 0$. Then $K = 0$ and therefore $v = 0$. Taking $v' = v_j$ and $w' = w_j$ in (2.4) gives $\int_{D_b} |\nabla w_j|^2 dx + a_j \int_{D_b} |\nabla v_j|^2 dx \to 0$ as j goes to infinity. This proves that w_j converges strongly to 0 in $H^1(D_b)$ and we already have v_j converges to 0 strongly in $H^1(D_b)$. This contradicts $\|w_j\|^2_{H^1(D_b)} + \|v_j\|^2_{H^1(D_b)} = 1$. □

Remark 2. *In dimension* 2*, in the case where D_b is a disk of radius $\rho > 0$ and n is constant, one can compute explicitly the eigenvalue μ of problem (2.3). We get that $\mu = \mu_{\text{ref}}(n)$ where*

$$\mu_{\text{ref}}(n) := 2\pi\rho k\sqrt{n}\frac{J_1(k\rho\sqrt{n})}{J_0(k\rho\sqrt{n})}. \tag{2.6}$$

A similar expression can be derived in space dimension 3 *for balls.*

Theorem 9 suggests to replace the spectral problem (1.34) by (2.3) as a goes to infinity. As we shall demonstrate in the sequel, the eigenvalue problem (2.3) has a very simple spectrum constituted by at most one non zero eigenvalue. This is why it also constitutes a good candidate for the imaging algorithm and that will be the subject of Chapter 3, after introducing the associated direct scattering problem.

2.2.3 Analysis of the spectrum of (2.3)

This section is dedicated to the analysis of the spectral problem (2.3). This analysis requires to exclude values of k^2 that are eigenvalues of the following problem.

$$\begin{cases} w \in H^1_c(D_b), \\ \Delta w + k^2 n w = 0 \text{ in } D_b, \\ \int_{\partial D_b} \partial_\nu w ds = 0 \text{ on } \partial D_b, \end{cases} \tag{2.7}$$

where $H^1_c(D_b) := \{w \in H^1(D_b), w|_{\partial D_b} \text{ is constant}\}$. The eigenvalue problem (2.7) has a similar structure as Dirichlet or Neumann eigenvalue problems. It is equivalent to the

variational writing: $w \in H^1_c(D_b)$

$$\int_{D_b} \nabla w \nabla \overline{w'} dx - k^2 \int_{D_b} n w \overline{w'} dx = 0 \text{ for all } w' \in H^1_c(D_b). \tag{2.8}$$

It follows from standard results on the spectrum of self-adjoint compact operators that the spectrum of (2.7) is discrete and formed by a real sequence that accumulates at $+\infty$.

Proposition 10. *Assume that k^2 is not an eigenvalue of (2.7), then problem (2.3) has at most one eigenvalue. Moreover, this eigenvalue is non zero .*

Proof. Problem (2.3) is equivalent to the variational formulation: $w \in H^1_c(D_b)$

$$\int_{D_b} \nabla w \nabla \overline{w'} dx - k^2 \int_{D_b} n w \overline{w'} dx = -\frac{\mu}{|\partial D_b|} \int_{\partial D_b} w \overline{w'} ds \tag{2.9}$$

for all $w' \in H^1_c(D_b)$. Thanks to the Riesz representation theorem, we define two selfadjoint operators $\mathbb{A}$ and $\mathbb{T} : H^1_c(D_b) \to H^1_c(D_b)$ by:

$$\begin{aligned} (\mathbb{A}w, w')_{H^1(D_b)} &= \textstyle\int_{D_b} \nabla w \nabla \overline{w'} dx - k^2 \int_{D_b} n w \overline{w'} dx, \quad \forall w' \in H^1_c(D_b), \\ (\mathbb{T}w, w')_{H^1(D_b)} &= \textstyle\frac{1}{|\partial D_b|} \int_{\partial D_b} w \overline{w'} ds, \quad \forall w' \in H^1_c(D_b). \end{aligned} \tag{2.10}$$

The eigenvalue problem (2.3) is then equivalent to:

$$\mathbb{A}w = -\mu \mathbb{T}w, \text{ in } H^1_c(D_b). \tag{2.11}$$

Notice that since $w|_{\partial D_b}$ is constant,

$$(\mathbb{T}w, w')_{H^1(D_b)} = \frac{w|_{\partial D_b}}{|\partial D_b|} \int_{\partial D_b} \overline{w'} ds = w|_{\partial D_b} (\mathbb{T}w_1, w')_{H^1(D_b)},$$

where $w_1 := 1$ in D_b. Therefore, the range of $\mathbb{T}$ is of dimension 1.
Assume by contradiction that there exists two distinct eigenvalues μ_1, μ_2 associated with their eigenvector w_1, w_2. The hypothesis on k^2 shows that $\mathbb{A}$ is injective and therefore both eigenvalues are non zero. Since the range of $\mathbb{T}$ is a line, there exists $w_0 \in H^1_c(D_b)$ such that

$$w_0 = -\frac{1}{\mu_1 \alpha_1} \mathbb{A} w_1 = -\frac{1}{\mu_2 \alpha_2} \mathbb{A} w_2, \tag{2.12}$$

with $\alpha_1, \alpha_2 \in \mathbb{C}^*$. From the linearity of the operators, one obtains that $\mathbb{A}(w_1 - \frac{\mu_1 \alpha_1}{\mu_2 \alpha_2} w_2) = 0$. The injectivity of $\mathbb{A}$ gives a contradiction and therefore there exists at most one non zero eigenvalue of (2.11). □

Theorem 11. *The spectrum of problem (2.3) can be described as follows:*

1) Assume that k^2 is not an eigenvalue of (2.7).

a) If k^2 is not a Dirichlet eigenvalue of (1.35), then there exists an unique non zero eigenvalue μ to (2.3) and an associated eigenvector is $w_1 \in H^1(D_b)$ the unique solution of $\Delta w_1 + k^2 n w_1 = 0$ in D_b and $w_1 = 1$ on ∂D_b. In particular, we have $\mu = -\int_{\partial D_b} \partial_\nu w_1 ds = k^2 \int_{D_b} n w_1 dx$.

b) If k^2 is a Dirichlet eigenvalue of (1.35), then there are no eigenvalues to (2.3).

2) Assume that k^2 is an eigenvalue of (2.7). Then 0 is an eigenvalue of (2.3) and the associated eigenvectors are the eigenvectors of (2.7). If k^2 is not a Dirichlet eigenvalue, 0 is the unique eigenvalue.

Proof. We distinguish the various cases as in the Theorem.

1) Assume that k^2 is not an eigenvalue of (2.7). Then according the Proposition 10, we have at most one eigenvalue.

   a) If k^2 is not a Dirichlet eigenvalue of (1.35). Then the function w_1 as in item a) can be defined and one easily verifies that it is an eigenvector associated with $\mu = -\int_{\partial D_b} \partial_\nu w_1$.

   b) If k^2 is a Dirichlet eigenvalue of (1.35), assume by contradiction that there exists an eigenvalue μ of (2.3) associated with an eigenvector w. Since k^2 is not an eigenvalue of (2.7), $\mu \neq 0$ and $w|_{\partial D_b} \neq 0$. Let $w_0 \in H^1(D_b)$ the eigenvector verifying:

$$\begin{cases} \Delta w_0 + k^2 n w_0 = 0 \text{ in } D_b, \\ w_0 = 0 \text{ on } \partial D_b. \end{cases} \tag{2.13}$$

   Multiplying the previous equation by w_1, and integrating by part gives:

$$\int_{D_b} (\Delta w_0 + k^2 n w_0) w dx = \int_{\partial D_b} w \partial_\nu w_0 ds = w|_{\partial D_b} \int_{\partial D_b} \partial_\nu w_0 ds = 0. \tag{2.14}$$

   Therefore, w_0 is an eigenvector of (2.7) which is a contradiction .

2) Assume that k^2 is an eigenvalue of (2.7). One can easily verify that 0 is an eigenvalue of (2.3) by inserting $\mu = 0$ in equation (2.3). If k^2 is not a Dirichlet eigenvalue of (1.35), assume by contradiction that there exists a non zero eigenvalue μ of (2.3) and an associated eigenvector w_1. We denote by w_0 an eigenvector of (2.7). Notice that $w_0|_{\partial D_b} \neq 0$ and $w_1|_{\partial D_b} \neq 0$. We obtain a contradiction following a similar reasoning as in item 1-b.

□

We summarize the previous theorem in the following table.

The wavenumber k^2 is	a Dirichlet eigenvalue of (1.35)	not a Dirichlet eigenvalue of (1.35)
an eigenvalue of (2.7)	0 is an eigenvalue	0 is the unique eigenvalue
not an Eigenvalue of (2.7)	No eigenvalue	Unique eigenvalue $\mu = -\int_{\partial D_b} \partial_\nu w_1 ds$.

We have proved the existence of a unique eigenvalue of (2.3) under certain conditions on the wavenumber. The following theorem proves the monotonicity property of the eigenvalue with respect to the refractive index.

Theorem 12. *Assume that $0 < k^2 < \eta_0(n, D_b)$. Then k^2 is not an eigenvalue of (2.7). Let $\mu(k, n, D_b)$ be the unique eigenvalue of (2.3) as defined in Theorem 11 1-a. Then we also have*

$$\mu(k, n, D_b) = \sup_{w \in H^1_c(D_b), w|_{\partial D_b}=1} (k^2 \int_{D_b} n|w|^2 dx - \int_{D_b} |\nabla w|^2 dx). \tag{2.15}$$

This shows in particular that $\mu(k, n, D_b)$ is positive and is monotonically increasing with respect to n. Moreover, we have that $\mu(k, n, D_b) \to +\infty$ as $k^2 \to \eta_0(n, D_b)$.

Proof. We start by proving that k^2 is not an eigenvalue of (2.7). First of all, we notice that the first eigenvalue of (2.7) is 0 associated with the constant eigenvector 1. Then the second eigenvalue is given by:

$$k_1^2 = \inf_{E_2 \subset W_2} \sup_{w \in E_2, w \neq 0} \frac{\int_{D_b} |\nabla w|^2 dx}{\int_{D_b} n|w|^2 dx}, \tag{2.16}$$

where W_2 is the set of 2 dimensional subspaces of $H^1_c(D_b)$. For all $w \in H^1_0(D_b)$, there exists E_2 such that $w \in E_2$ since $H^1_0(D_b) \subset H^1_c(D_b)$. Reciprocally any $E_2 \subset W_2$ contains at least a non trivial element of $H^1_0(D_b)$, for instance $w = u_2|_{\partial D_b} u_1 - u_1|_{\partial D_b} u_2$ where u_1, u_2 are two linear independant vectors of E_2. Therefore:

$$k_1^2 \geq \inf_{w \in H^1_0(D_b)} \frac{\int_{D_b} |\nabla w|^2 dx}{\int_{D_b} n|w|^2 dx} = \eta_0(n, D_b). \tag{2.17}$$

Let $\Lambda > 0$ be such that the operator $\mathbb{A}'$ defined by

$$(\mathbb{A}' w, w')_{H^1(D_b)} = \int_{D_b} \nabla w \nabla \overline{w'} dx - k^2 \int_{D_b} n w \overline{w'} dx + \frac{\Lambda}{|\partial D_b|} \int_{\partial D_b} w \overline{w'} ds, \tag{2.18}$$

for all $w' \in H^1_c(D_b)$ is coercive. The existence of such Λ follows from Wirtinguer's type inequalities and the proof is given in section 2.5, Theorem 18. The eigenvalue problem (2.3) can be equivalently written as:

$$\mathbb{A}' w = -(\mu - \Lambda) \mathbb{T} w, \tag{2.19}$$

where $\mathbb{A}'$ is a selfadjoint coercive operator and $\mathbb{T}$ is a selfadjoint compact non negative operator. Identity (2.15) is then a direct consequence of the Courant-Fischer principle applied to the eigenvalue problem (2.19).
We now prove that $\mu(k, n, D_b) \to +\infty$ as $k^2 \to \eta_0(n, D_b)$. Let $j \in \mathbb{N}^*$ and denote by (k_j, w_j) the first eigenvalue and eigenvector with $||w_j||_{H^1(D_b)} = 1$ of the following spectral problem (j is fixed):

$$\begin{cases} w_j \in H^1_c(D_b), \\ \Delta w_j + k_j^2 n w_j = 0 \text{ in } D_b, \\ j w_j + \int_{\partial D_b} \partial_\nu w_j ds = 0 \text{ on } \partial D_b. \end{cases} \tag{2.20}$$

We obtain by the Courant-Fischer principle:

$$k_j^2 = \inf_{w\in H_c^1(D_b),w\neq 0} \frac{\frac{j}{|\partial D_b|}\int_{\partial D_b}|w|^2+\int_{D_b}|\nabla w|^2}{\int_{D_b} n|w|^2} \leq \inf_{w\in H_0^1(D_b),w\neq 0} \frac{\int_{D_b}|\nabla w|^2}{\int_{D_b} n|w|^2}. \tag{2.21}$$

Therefore, $(k_j^2)_j$ an increasing sequence and bounded by $\eta_0(n,D_b)$. This implies $k_j^2 \to \eta^*$ as j goes to infinity for some $\eta^* \leq \eta_0(n,D_b)$. The eigenvector w_j verifies:

$$\int_{D_b}|\nabla w_j|^2dx - k_j^2\int_{D_b} n|w_j|^2dx = -\frac{j}{|\partial D_b|}\int_{\partial D_b}|w_j|^2ds. \tag{2.22}$$

This equality proves that the right hand side remains bounded as j goes to infinity, which means that $w_j|_{\partial D_b} \to 0$. We then have that (up to a subsequence) $(w_j)_{j\in\mathbb{N}}$ converges weakly in $H^1(D_b)$ (and strongly in $L^2(D_b)$) to some w in $H_c^1(D_b)$ that verifies $\Delta w+\eta^* nw = 0$ in D_b and $w = 0$ on ∂D_b. Let us show that w is non trivial by using a contradiction argument. Suppose $w = 0$. From (2.22), we have:

$$\int_{D_b}|\nabla w_j|^2dx \leq k_j^2\int_{D_b} n|w_j|^2dx,$$

and therefore $\nabla w_j \to 0$ in $L^2(D_b)$. Consequently w_j strongly converges to 0 in $H^1(D_b)$. This contradicts $\|w_j\|_{H^1(D_b)} = 1$.
The fact that w is non trivial implies that η^* is a Dirichlet eigenvalue of (1.35) and therefore $\eta^* \geq \eta_0(n,D_b)$. We then have $\eta^* = \eta_0(n,D_b) = \lim_{j\to+\infty} k_j^2$. Observe that w_j is not in $H_0^1(D_b)$ thanks to (2.16). Using (2.15) and (2.22), we then get:

$$\mu(k_j,n,D_b) \geq \frac{k_j^2\int_{D_b} n|w_j|^2dx - \int_{D_b}|\nabla w_j|^2dx}{\int_{\partial D_b}|w_j|^2ds} = \frac{j}{|\partial D_b|}. \tag{2.23}$$

Thus, $\lim_{j\to+\infty}\mu(k_j,n,D_b) \geq \frac{j}{|\partial D_b|} \to_{j\to+\infty} +\infty$ □

Definition 3. *$\mu\in\mathbb{R}$ is an averaged Steklov eigenvalue if problem (2.3) admits a non trivial solution.*

2.3 An artificial background associated with (2.3)

The goal of this section is to introduce a scattering problem for which the spectral problem (2.3) would play the role of interior transmission problem similarly to the role played by (1.33) for (1.29). Let D_b and Ω be as in section 1.5.2. The new artificial scattering problem can be formulated as: the total field $u_b \in H^1_{loc}(\mathbb{R}^m)$ satisfies

$$\begin{cases} \Delta u_b + k^2 u_b = 0 \text{ in } \mathbb{R}^m\backslash\overline{D_b}, \\ \mu u_b + \int_{\partial D_b}\partial_\nu u_b ds = 0 \text{ on } \partial D_b, \\ u_b = u_b^s + u^i, \\ \lim_{r\to+\infty}\int_{|x|=r}|\frac{\partial u_b^s}{\partial r} - iku_b^s|^2 = 0, \end{cases} \tag{2.24}$$

for some incident field u^i and $\mu \in \mathbb{R}$ is the spectral parameter. The analysis of this scattering problem can be done using a standard technique, for instance a variational approach based on the introduction of the Dirichlet to Neumann operator. Let B_R (with boundary S_R) be a ball containing D_b for R large enough. We define the Dirichlet to Neumann map $\Lambda : H^{\frac{1}{2}}(S_R) \to H^{-\frac{1}{2}}(S_R)$ by $\Lambda\phi := \partial_\nu v|_{S_R}$, where v is the radiating solution to the Helmholtz equation in $\mathbb{R}^d \backslash B_R$ with $v = \phi$ on S_R, and where ν is the outward unit normal to S_R. Consider the following space

$$H^1_c(B_R \backslash D_b) := \{w \in H^1(B_R \backslash D_b), \quad w|_{\partial D_b} \text{ is constant } \}. \tag{2.25}$$

Then, solving the scattering problem (2.24) is equivalent to solving the following variational problem: $u \in H^1_c(B_R \backslash D_b)$ and for all $v \in H^1_c(B_R \backslash D_b)$,

$$\int_{B_R \backslash D_b} (\nabla u \nabla v - k^2 uv) dx - \int_{S_R} \Lambda uv ds - \frac{\mu}{|\partial D_b|} \int_{\partial D_b} uv ds = \ell(v) \tag{2.26}$$

where

$$\ell(v) := \int_{S_R} (\partial_\nu u^i - \Lambda u^i) v ds. \tag{2.27}$$

Theorem 13. *The scattering problem (2.24) is well posed for u^i such that $(\partial_\nu u^i - \Lambda u^i) \in H^{-\frac{1}{2}}(S_R)$.*

Proof. Using similar arguments as in [15], one can prove that this problem is well posed for $\mu \in \mathbb{R}$ (or more generally, for non zero complex value μ with $\Im(\mu) \geq 0$).
Equation (2.26) can be rewritten as:

$$(Fu, v) = l(v), \text{ for all } v \in H^1_c(B_R \backslash D_b), \tag{2.28}$$

where F can be decomposed as the sum of a coercive and a compact operator. The Fredholm alternative guaranties the well posedness of the problem if F is injective. Taking the imaginary part of equation (2.26) for $v = u$, one obtains that $\Im m(\int_{S_R} \Lambda uu ds) = 0$ which leads to $u = 0$ in $H^1_c(B_R \backslash D_b)$ in accordance with the corollary 1.7 of ([15]). □

Similarly to the forward scattering problem, we use the notation $u_b(., d)$, $u^s_b(., d)$, $u^\infty_b(., d)$ to respectively denote the total, scattered and far field when the incident field $u^i = u^i(., d)$ is the plane wave of direction $d \in \mathbb{S}$. Consider the far field operator $F^\mu_b : L^2(\mathbb{S}) \to L^2(\mathbb{S})$ defined by

$$(F^\mu_b g)(\hat{x}) := \int_{\mathbb{S}} g(d) u^\infty_b(\hat{x}, d) ds(d), \quad \hat{x} \in \mathbb{S}. \tag{2.29}$$

We then define the modified far field operator $\mathcal{F}^\mu : L^2(\mathbb{S}) \to L^2(\mathbb{S})$ as

$$\mathcal{F}^\mu g := Fg - F^\mu_b g. \tag{2.30}$$

For further use, especially in the proofs of Chapter 3, we notice that similarly to (1.6) the scattered field $u^s_b \in H^1_{loc}(\mathbb{R}^m \backslash D_b)$ satisfies:

$$\begin{cases} \Delta u^s_b + k^2 u^s_b = 0 \text{ in } \mathbb{R}^m \backslash D_b, \\ \mu u^s_b + \int_{\partial D_b} \partial_\nu u^s_b = -\mu u^i - \int_{\partial D_b} \partial_\nu u^i ds \text{ on } \partial D_b, \\ \lim\limits_{r \to +\infty} \int_{|x|=r} |\frac{\partial u^s_b}{\partial r} - iku^s_b|^2 = 0, \end{cases} \tag{2.31}$$

for u^i satisfying $\Delta u^i + k^2 u^i = 0$ in $\mathbb{R}^m$. We denote by $u^s_{b,g}$ the solution of (2.31) with $u^i = v_g$ defined in (1.5) and $u_{b,g} = u^s_{b,g} + v_g$ in $\mathbb{R}^m \backslash D_b$.

Remark 3. *The concept and properties of averaged Steklov eigenvalue can be extended to the scattering by an anisotropic inhomogeneity. Let A be a $m \times m$ symmetric matrix with $L^\infty(D)$ entries such that for all $x \in D$*

$$\overline{\xi} \cdot \Re e(A)\xi \geq \beta |\xi|^2 \quad \textit{and} \quad \overline{\xi} \cdot \Im m(A)\xi \leq 0 \quad \textit{for all} \quad \xi \in C^m, \tag{2.32}$$

for some constant $\beta > 0$. The problem (2.3) becomes

$$\begin{cases} \nabla \cdot A\nabla w + k^2 n w = 0 \text{ in } D_b, \\ \mu w + \int_{\partial D_b} \partial_{\nu_A} w ds = 0 \text{ on } \partial D_b, \end{cases} \tag{2.33}$$

where $\partial_{\nu_A} w := \nu \cdot A\nabla w$. Theorem 12 can be extended to this context. Let $\eta_0(n, A, D_b)$ denote the first Dirichlet eigenvalue of the problem: find $u \in H^1(D_b)$ non trivial such that $\nabla \cdot A\nabla u + k^2 n u = 0$ in D_b with $u = 0$ on ∂D_b.
For $0 < k^2 < \eta_0(n, A, D_b)$, there exits an unique eigenvalue $\mu(k, n, A, D_b)$ to problem (2.33) that satisfies:

$$\mu(k, n, A, D_b) = \sup_{w \in H^1_c(D_b), w|_{\partial D_b} = 1} (k^2 \int_{D_b} n|w|^2 dx - \int_{D_b} \overline{\nabla w} \cdot A\nabla dx). \tag{2.34}$$

The eigenvalue is thus monotically increasing with respect to n and monotically decreasing with respect to A.

2.4 Generalization

The previous eigenvalue problem was determined as a limit. However, a natural generalization of the boundary condition appears. For $f \in H^{\frac{1}{2}}(\partial D_b)$ non trivial, let $w \in H^1(D_b)$ be the solution of:

$$\begin{cases} \Delta w + k^2 n w = 0 \text{ in } D_b, \\ \mu w + f \int_{\partial D_b} \partial_\nu w \overline{f} ds = 0 \text{ on } \partial D_b. \end{cases} \tag{2.35}$$

We briefly adapt all the previous results and theorems to this new eigenvalue problem. Introduce the values of k^2, eigenvalues of:

$$\begin{cases} w \in H^1_f(D_b), \\ \Delta w + k^2 n w = 0 \text{ in } D_b, \\ \int_{\partial D_b} \partial_\nu w \overline{f} ds = 0 \text{ on } \partial D_b, \end{cases} \tag{2.36}$$

where $H^1_f(D_b) := \{w \in H^1(D_b), w|_{\partial D_b} \in Vect(f)\}$. It is equivalent to the variational writing: $w \in H^1_f(D_b)$

$$\int_{D_b} \nabla w \nabla \overline{w'} dx - k^2 \int_{D_b} n w \overline{w'} dx = 0 \text{ for all } w' \in H^1_f(D_b). \tag{2.37}$$

It follows from standard results on the spectrum of self-adjoint compact operators that the spectrum of (2.36) is discrete and formed by a real sequence that accumulates at $+\infty$.

Proposition 14. *Assume that k^2 is not an eigenvalue of (2.36), then problem (2.35) has at most one eigenvalue. Moreover, this eigenvalue is non zero .*

Proof. Problem (2.3) is equivalent to the variational formulation: $w \in H^1_f(D_b)$

$$\int_{D_b} \nabla w \nabla \overline{w'} dx - k^2 \int_{D_b} n w \overline{w'} dx = -\frac{\mu}{\int_{\partial D_b} |f|^2 ds} \int_{\partial D_b} w \overline{w'} ds \tag{2.38}$$

for all $w' \in H^1_f(D_b)$. Thanks to the Riesz representation theorem, we define two selfadjoint operators $\mathbb{A}_f$ and $\mathbb{T}_f : H^1_f(D_b) \to H^1_f(D_b)$ by:

$$\begin{aligned} (\mathbb{A}_f w, w')_{H^1(D_b)} &= \textstyle\int_{D_b} \nabla w \nabla \overline{w'} dx - k^2 \int_{D_b} n w \overline{w'} dx, \quad \forall w' \in H^1_f(D_b), \\ (\mathbb{T}_f w, w')_{H^1(D_b)} &= \textstyle\frac{1}{\int_{\partial D_b} |f|^2 ds} \int_{\partial D_b} w \overline{w'} ds, \quad \forall w' \in H^1_f(D_b). \end{aligned} \tag{2.39}$$

The eigenvalue problem (2.35) is then equivalent to:

$$\mathbb{A}_f w = -\mu \mathbb{T}_f w, \text{ in } H^1_f(D_b). \tag{2.40}$$

Notice that since $w|_{\partial D_b} = \alpha_w f$ with $\alpha_w \in \mathbb{C}$ a constant that depends on w,

$$(\mathbb{T}_f w, w')_{H^1(D_b)} = \frac{\alpha_w}{\int_{\partial D_b} |f|^2 ds} \int_{\partial D_b} f \overline{w'} ds = \alpha_w (\mathbb{T}_f w_1, w')_{H^1(D_b)},$$

where $w_1 = f$ on ∂D_b. Therefore, the range of $\mathbb{T}_f$ is of dimension 1. The hypothesis on k^2 shows that $\mathbb{A}_f$ is injective and therefore there exists at most one non zero eigenvalue of (2.40). □

Theorem 15. *The spectrum of problem (2.35) can be described as follows:*

1) *Assume that k^2 is not an eigenvalue of (2.36).*

   a) *If k^2 is not a Dirichlet eigenvalue of (1.35), then there exists an unique non zero eigenvalue μ to (2.35) and an associated eigenvector is $w_f \in H^1(D_b)$ the unique solution of $\Delta w_f + k^2 n w_f = 0$ in D_b and $w_f = f$ on ∂D_b. In particular, we have $\mu = -\int_{\partial D_b} \partial_\nu w_f \overline{f} ds$.*

   b) *If k^2 is a Dirichlet eigenvalue of (1.35), then there are no eigenvalues to (2.35).*

2) *Assume that k^2 is an eigenvalue of (2.36). Then 0 is an eigenvalue of (2.35) and the associated eigenvectors are the eigenvectors of (2.36). If k^2 is not a Dirichlet eigenvalue, 0 is the unique eigenvalue.*

The existence of such eigenvalues is summarised in the following table.

The wavenumber k^2 is	a Dirichlet eigenvalue of (1.35)	not a Dirichlet eigenvalue of (1.35)
an eigenvalue of (2.36)	0 is an eigenvalue	0 is the unique eigenvalue
not an Eigenvalue of (2.36)	No eigenvalue	Unique eigenvalue $\mu = -\int_{\partial D_b} \partial_\nu w_f \overline{f} ds$.

We have proved the existence of a unique eigenvalue of (2.35) under certain conditions on the wavenumber. The following theorem proves the monotonicity property of the eigenvalue with respect to the refractive index.

Theorem 16. *Assume that $0 < k^2 < \eta_0(n, D_b)$. Let $\mu(k, n, D_b, f)$ be the unique eigenvalue of (2.35). Then we also have*

$$\mu(k, n, D_b, f) = \sup_{w \in H^1_f(D_b), w|_{\partial D_b} = f} (k^2 \int_{D_b} n|w|^2 dx - \int_{D_b} |\nabla w|^2 dx). \tag{2.41}$$

This shows in particular that $\mu(k, n, D_b, f)$ is monotonically increasing with respect to n.

$\mu(k, n, D_b, f)$ is not necessary positive and can vanish as an eigenvalue of (2.36) may be smaller than $\eta_0(n, D_b)$.

Remark 4. *In dimension 2, in the case where D_b is a disk of radius $\rho > 0$, n is constant and $f = e^{iq\theta}$ for $q \in \mathbb{N}$, one can compute explicitly the eigenvalue μ of problem (2.35). We get that $\mu = \mu_{\text{ref,q}}(n)$ where*

$$\mu_{\text{ref,q}}(n) := -2\pi\rho k\sqrt{n} \frac{J_q'(k\rho\sqrt{n})}{J_q(k\rho\sqrt{n})}. \tag{2.42}$$

The function $g_0 : n \to \mu_{\text{ref,m}}(n)$ is injective if $\sqrt{n} \in]0, \frac{j_0}{k\rho}[$ where j_0 the first zero of J_0. Consequently, the constant refractive index n can be fully recovered from the knowledge of $\mu_{\text{ref,q}}(n)$ for any $q \in \mathbb{N}$.
We display in Figure 2.4 the behavior of $\mu_{\text{ref,q}}$ for various values of q. It is notable that the eigenvalue for $q = 0$ is more sensitive to variations of the refractive index n compared to the other ones. Assuming this behavior also holds for $n \in L^\infty(D_b)$, it suggests that setting $f = 1$ in (2.35) would give better imaging results.

Exactly like for $f = 1$, we formulate the artificial scattering problem as: the total field $u_b \in H^1_{loc}(\mathbb{R}^m)$ satisfies

$$\begin{cases} \Delta u_b + k^2 u_b = 0 \text{ in } \mathbb{R}^m \backslash \overline{D_b}, \\ \mu u_b + f \int_{\partial D_b} \partial_\nu u_b \overline{f} ds = 0 \text{ on } \partial D_b, \\ u_b = u_b^s + u^i, \\ \lim_{r \to +\infty} \int_{|x|=r} |\frac{\partial u_b^s}{\partial r} - iku_b^s|^2 = 0, \end{cases} \tag{2.43}$$

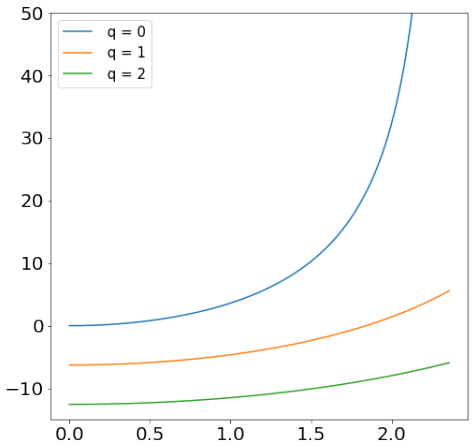

Figure 2.4: Plot of the function $-x\frac{J_q'(x)}{J_q(x)}$ for $q = 0, 1, 2$ on $[0, j_0[$ where j_0 is the first zero of J_0.

for some incident field u^i and $\mu \in \mathbb{R}$ is the spectral parameter.
Let B_R (with boundary S_R) be a ball containing D_b for R large enough. Consider the following space

$$H_f^1(B_R \backslash D_b) := \{w \in H^1(B_R \backslash D_b), \quad w|_{\partial D_b} \in Vect(f)\}. \tag{2.44}$$

Then, solving the scattering problem (2.43) is equivalent to solving the following variational problem: $u \in H_f^1(B_R \backslash D_b)$ and for all $v \in H_f^1(B_R \backslash D_b)$,

$$\int_{B_R \backslash D_b} (\nabla u \nabla v - k^2 uv)dx - \int_{S_R} \Lambda uv ds - \frac{\mu}{\int_{\partial D_b} |f|^2 ds} \int_{\partial D_b} uv ds = \ell(v) \tag{2.45}$$

where

$$\ell(v) := \int_{S_R} (\partial_\nu u^i - \Lambda u^i) v ds. \tag{2.46}$$

Theorem 17. *The scattering problem (2.43) is well posed for u^i such that $(\partial_\nu u^i - \Lambda u^i) \in H^{-\frac{1}{2}}(S_R)$.*

Proof. The proof can be done in the same way as for Theorem 13. □

Naturally, we can define the far field operator and the modified far field operator associated with this problem and, which will also be denoted as F_b and $\mathcal{F}_b^\mu$, respectively.

Definition 4. *$\mu \in \mathbb{R}$ is a $f-$averaged Steklov eigenvalue if problem (2.35) admits a non trivial solution.*

2.5 Complementary technical results

We first give a proof of a technical result used in Theorem 12.

Lemma 18. *If $k^2 < \eta_0(n, D_b)$, then there exists $\Lambda > 0$ such that*

$$\int_{D_b} |\nabla w|^2 dx - k^2 \int_{D_b} n|w|^2 dx + \Lambda \int_{\partial D_b} |w|^2 ds \geq c\|w\|^2_{H^1(D_b)}, \tag{2.47}$$

for all $w \in H^1_c(D_b)$ and for some constant $c > 0$.

Proof. Assume by contradiction there is no $\Lambda > 0$ such that the (2.47) holds for $k^2 < \eta_0(n, D_b)$.
Let $(\Lambda_j)_j$ an increasing unbounded sequence of positive constant. The contradiction argument ensures that for each Λ_j, there exists $w_j \in H^1_c(D_b)$ with $\|w_j\|_{H^1(D_b)} = 1$ such that

$$\int_{D_b} |\nabla w_j|^2 dx - k^2 \int_{D_b} n|w_j|^2 dx + \Lambda_j \int_{\partial D_b} |w_j|^2 ds \leq \frac{1}{j}. \tag{2.48}$$

This gives for instance

$$\int_{D_b} |\nabla w_j|^2 dx + \Lambda_j \int_{\partial D_b} |w_j|^2 ds \leq k^2 \int_{D_b} n|w_j|^2 dx + \frac{1}{j}. \tag{2.49}$$

One can assume that, up to a subsequence, w_j converges to some w, weakly in $H^1(D_b)$ and strongly in $L^2(D_b)$.
The term $\Lambda_j \int_{\partial D_b} |w_j|^2 ds$ must remain bounded, leading to $w = 0$ in ∂D_b. Hence $w \in H^1_0(D_b)$. Since the norm is weakly lower semi continuous, we have

$$\|\nabla w\|^2_{L^2(D_b)} \leq \lim_{j\to+\infty} \inf \int_{D_b} |\nabla w_j|^2 dx \leq \lim_{j\to+\infty} k^2 \int_{D_b} n|w_j|^2 dx = k^2 \int_{D_b} n|w|^2 dx, \tag{2.50}$$

which contradicts

$$k^2 < \inf_{w\in H^1_0(D_b), w\neq 0} \frac{\|\nabla w\|^2_{L^2(D_b)}}{\int_{D_b} n|w|^2 dx} = \eta_0(n, D_b). \tag{2.51}$$

□

We suggest another version of this proof.

Proof. Introduce two eigenvalue problems. Let $\alpha > 0$ be a fixed parameter and τ be the spectral parameter.

$$\begin{cases} w \in H^1_c(D_b), \\ \Delta w + \tau n w = 0 \text{ in } D_b, \\ \alpha|\partial D_b| w + \int_{\partial D_b} \partial_\nu w = 0 \text{ on } \partial D_b, \end{cases} \tag{2.52}$$

and

$$\begin{cases} w \in H^1_c(D_b), \\ \Delta w + \tau w = 0 \text{ in } D_b, \\ \alpha|\partial D_b| w + \int_{\partial D_b} \partial_\nu w = 0 \text{ on } \partial D_b, \end{cases} \tag{2.53}$$

Both problems have a similar structure as Robin problems. From classical results on self adjoint compact operators, it follows that the spectrum of both problems is a discrete set of non zero eigenvalues k^2 without finite accumulation point.
We denote by τ_n (respectively τ_1) the first eigenvalue of problem (2.52) (respectively (2.53)). The application of Courant-Fischer min-max Principle gives:

$$\tau_n(\alpha) = \inf_{w\in H^1_c(D_b),w\neq 0} \frac{\int_{D_b} |\nabla w|^2 dx + \alpha \int_{\partial D_b} |w|^2 ds}{\int_{D_b} n|w|^2 dx}, \tag{2.54}$$

$$\tau_1 = \inf_{w\in H^1_c(D_b),w\neq 0} \frac{\int_{D_b} |\nabla w|^2 dx + \alpha \int_{\partial D_b} |w|^2 ds}{\int_{D_b} |w|^2 dx}. \tag{2.55}$$

We wish to find a positive constant Λ such that (2.47) is true.
Using (2.54), one obtains for all $w \in H^1_c(D_b)$, $w \neq 0$:

$$\begin{aligned} \int_{D_b} |\nabla w|^2 dx - \; & k^2 \int_{D_b} n|w|^2 dx + \Lambda \int_{\partial D_b} |w|^2 \\ & \geq (1 - \tfrac{k^2}{\tau_n(\alpha)}) \int_{D_b} |\nabla w|^2 dx + (\Lambda - \tfrac{k^2\alpha}{\tau_n(\alpha)}) \int_{\partial D_b} |w|^2 \end{aligned} \tag{2.56}$$

Since

$$\alpha \int_{\partial D_b} |w|^2 \geq \tau_1 \int_{D_b} |w|^2 dx - \int_{D_b} |\nabla w|^2 dx, \tag{2.57}$$

one gets:

$$\begin{aligned} \int_{D_b} |\nabla w|^2 dx - \; & k^2 \int_{D_b} n|w|^2 dx + \Lambda \int_{\partial D_b} |w|^2 \\ & \geq (1 - \tfrac{\Lambda}{\alpha}) \int_{D_b} |\nabla w|^2 dx + \tau_1(\tfrac{\Lambda}{\alpha} - \tfrac{k^2}{\tau_n(\alpha)}) \int_{D_b} |w|^2. \end{aligned} \tag{2.58}$$

We can find such $\Lambda > 0$ that verifies (2.47) assuming that $(1 - \frac{\Lambda}{\alpha}) > 0$ and $(\frac{\Lambda}{\alpha} - \frac{k^2}{\tau_n(\alpha)}) > 0$ which is true if $\tau_n(\alpha) > k^2$. Since $\alpha > 0$ is a parameter we can play on, we need to determine the maximum of the sequence $(\tau_n(\alpha))_\alpha$.
The latter is an increasing sequence and is upper bounded by $\eta_0(n, D_b)$, whence $\lim_{\alpha\to+\infty} \tau_n(\alpha)$ exists.
Let $(\alpha_j)_{j\in\mathbb{N}}$ be an unbounded increasing sequence of positive number. Denote by τ_n^j the eigenvalue of (2.52) for $\alpha = \alpha_j$ and let w_j be the $H^1(D_b)$ normalized associated eigenvector. Problem (2.52) is equivalent to the variational formulation:

$$\int_{D_b} \nabla w_j \nabla w' dx - \tau_n^j \int_{D_b} n w_j w' dx = -\alpha_j \int_{\partial D_b} w_j w' ds, \tag{2.59}$$

for all $w' \in H^1_c(D_b)$. Because the sequence (w_j) is bounded, up to a subsequence, we can assume that w_j converges weakly in $H^1(D_b)$ to some w and strongly in $L^2(D_b)$. Taking $w' = \overline{w_j}$ shows that $\alpha_j \int_{\partial D_b} |w_j|^2 ds$ remains bounded. Therefore, w_j converges strongly to 0 in $L^2(\partial D_b)$. We then infer that $w \in H^1_0(D_b)$ and $\Delta w + \lim_{j\to\infty} \tau_n^j n w = 0$ in D_b. We

now prove by contradiction that w is not a trivial function. From equation (2.59), one can deduce with $w' = \overline{w_j}$ that:

$$\int_{D_b} |\nabla w_j|^2 dx \leq \tau_n^j \int_{D_b} n|w_j|^2 dx.$$

Assume that $w = 0$, then $\nabla w_j \to 0$ in $L^2(D_b)$ and consequently w_j strongly converges to 0 in $H^1(D_b)$, which is absurd since $\|w_j\|_{H^1(D_b)} = 1$. Therefore, w is not the null function.The fact that w is non trivial implies that $\lim_{j\to+\infty} \tau_n^j$ is a Dirichlet eigenvalue of (1.35) and therefore $\lim_{j\to+\infty} \tau_n^j \geq \eta_0(n, D_b)$. We then have $\eta_0(n, D_b) = \lim_{j\to+\infty} \tau_n^j$. □

Chapter 3

An indicator function for the refractive index

Contents

3.1 Introduction

We develop in this chapter a method to recover some macroscopic information on the refractive index n from the far field operator F. This method is inspired by the one introduced in [7] and exploit the monotonicity property of the modified transmission eigenvalue of the spectral problem (2.3) with respect to n (see Theorem 12). The first step is to explain how one can identify the modified transmission eigenvalue from F^μ [16, 4, 22]. We employ the framework of the Generalized Linear Sampling Method [8] (GLSM) to prove this result in a constructive way. The proposed algorithm for a quantitative indicator function associated with the refractive index is then as follows: 1) choose a disc of given radius that we shall sweep over some sampling positions in the probed domain; 2) for each sampling position, identify the eigenvalue from far field data using the GLSM approach; 3) assign to the sampling position the difference between this eigenvalue and the eigenvalue associated with an index of refraction equals to one. The obtained indicator function would then be monotonically dependent with respect to the values of the true refractive index

intersecting the disc. We shall explain the details of this procedure in the numerical section and discuss the choice of the disc radius in terms of the used frequency. We then show how the resulting indicator function gives superior results to those given by qualitative approaches such as the Linear Sampling Method [24]. Moreover, the sign of the indicator function would give an indication on how the mean value of the refractive index compares with respect to 1. This is also discussed and illustrated through some numerical tests in 2D.

In order to avoid unnecessarily technical complications, we shall restrict ourselves in sections 3.2 and 3.3 to the case where $\partial D_b \cap D = \emptyset$.

3.2 Factorization of $\mathcal{F}^\mu$

We introduce $\Omega_D := D \backslash D_b$ the component of Ω outside of D_b as illustrated in Figure 3.1.
Let $\mathcal{H}^\mu : L^2(\mathbb{S}) \to \mathbb{R} \times H^{-\frac{1}{2}}(\partial D_b) \times L^2(\Omega_D)$ be defined as:

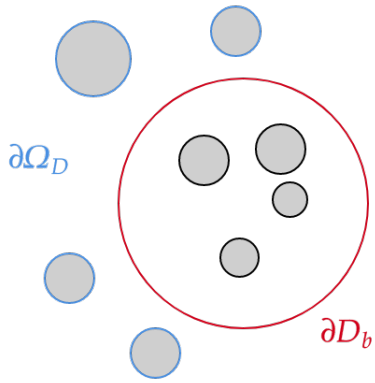

Figure 3.1: Visual representation of the set Ω_D.

$$\mathcal{H}^\mu g := (u_{b,g}|_{\partial D_b}, \partial_\nu u_{b,g}|_{\partial D_b}, u_{b,g}|_{\Omega_D}), \tag{3.1}$$

where $u_{b,g}$ is solution of (2.24) with $u^i = v_g$ and

$$V_{inc}(\Omega_D) = \{u \in L^2(\Omega_D) \text{ such that } \Delta u + k^2 u = 0 \text{ in } \Omega_D\}.$$

We define the operator $\mathcal{G}^\mu : \overline{\mathcal{R}(\mathcal{H}^\mu)} \to L^2(\mathbb{S})$ as. $\mathcal{G}^\mu(\varphi, \psi, u) := w^\infty$ where w^∞ is the far field of $w^s \in H^1_{loc}(\mathbb{R}^m \backslash D_b)$ solution to:

$$\begin{cases} \Delta w + k^2 n w = 0 \text{ in } D_b, \\ \Delta w^s + k^2 w^s = k^2(1-n)(u + w^s) \text{ in } \mathbb{R}^m \backslash D_b, \\ w - w^s = \varphi \text{ on } \partial D_b, \\ \partial_\nu w - \partial_\nu w^s = \psi \text{ on } \partial D_b, \\ \lim\limits_{r \to +\infty} \int_{|x|=r} |\frac{\partial w^s}{\partial r} - ikw^s|^2 = 0. \end{cases} \tag{3.2}$$

Observing that $w := u_g^s + v_g$ in D_b and $w^s = u_g^s - u_{b,g}^s$ in $\mathbb{R}^m \backslash D_b$ satisfy (3.2) with $u = u_{b,g}|_{\Omega_D}$, $\varphi = u_{b,g}|_{\partial D_b}$ and $\psi = \partial_\nu u_{b,g}|_{\partial D_b}$, we then deduce the following factorization:

$$\mathcal{F}^\mu = \mathcal{G}^\mu \mathcal{H}^\mu. \tag{3.3}$$

3.2.1 Properties of $\mathcal{H}^\mu$

Lemma 19. *We introduce the subspace V defined as:*

$$V = \{(\varphi, \psi, u) \in \mathbb{R} \times H^{-\frac{1}{2}}(\partial D_b) \times V_{inc}(\Omega_D) \text{ such that } \mu\varphi + \int_{\partial D_b} \psi ds = 0\}.$$

The closure of the range of $\mathcal{H}^\mu$, denoted $\mathcal{R}(\mathcal{H}^\mu)$, in $\mathbb{R} \times H^{-\frac{1}{2}}(\partial D_b) \times L^2(\Omega_D)$ satisfies:

$$\overline{\mathcal{R}(\mathcal{H}^\mu)} = V. \tag{3.4}$$

Proof. One can easily verify that $\overline{\mathcal{R}(\mathcal{H}^\mu)} \subset V$. To prove the reverse inclusion, it is sufficient to prove that the orthogonal complement of $\mathcal{R}(\mathcal{H}^\mu)$ in V is reduced to the trivial vector. Let $(\varphi, \psi, u) \in V$, such that $(\mathcal{H}^\mu g, (\varphi, \psi, u)) = 0$, for all $g \in L^2(\mathbb{S})$, which can be rewritten as follow:

$$\varphi u_{b,g} + (\psi, \partial_\nu \overline{u_{b,g}})_{H^{-\frac{1}{2}}(\partial D_b)} + (u, \overline{u_{b,g}}|_{\Omega_D})_{L^2(\Omega_D)} = 0. \tag{3.5}$$

Let $\widetilde{\psi} \in H^{\frac{1}{2}}(\partial D_b)$ be the unique vector such that for all $f \in H^{-\frac{1}{2}}(\partial D_b)$, we have

$$(\psi, f)_{H^{-\frac{1}{2}}(\partial D_b)} = \int_{\partial D_b} \widetilde{\psi} \overline{f} ds, \tag{3.6}$$

where the integral on the right hand side refers to the $\left\langle H^{-\frac{1}{2}}(\partial D_b), H^{\frac{1}{2}}(\partial D_b) \right\rangle$ duality pairing that can be replaced by the integral if $f \in L^2(\partial D_b)$ for instance. In particular, from equation (3.5), we get for all $g \in L^2(\mathbb{S})$:

$$\varphi u_{b,g} + \int_{\partial D_b} \widetilde{\psi} \partial_\nu u_{b,g} ds + \int_{\Omega_D} u u_{b,g} dx = 0. \tag{3.7}$$

Let $w \in H^1_{loc}(\mathbb{R}^m \backslash D_b)$ be a solution to

$$\begin{cases} \Delta w + k^2 w = u|_{\Omega_D} \text{ in } \mathbb{R}^m \backslash D_b, \\ \frac{1}{\mu} \int_{\partial D_b} \partial_\nu w + w = \frac{\varphi}{\mu} - \widetilde{\psi} \text{ on } \partial D_b, \\ \lim\limits_{r \to +\infty} \int_{|x|=r} |\frac{\partial w}{\partial r} - ikw|^2 = 0. \end{cases} \tag{3.8}$$

Thus, we can replace the last integral in (3.7) by an integral on a centered ball B_R for $R > 0$.

$$(u, \overline{u_{b,g}}|_{\Omega_D})_{L^2(\Omega_D)} = \int_{B_R \setminus D_b} (\Delta w + k^2 w) u^s_{b,g} dx + \int_{\Omega_D} u v_g dx. \tag{3.9}$$

Applying the Green formula twice and using the relation $u_{b,g} = v_g + u^s_{b,g}$ in $\mathbb{R}^m \setminus D_b$, one obtains:

$$\begin{aligned} \int_{B_R \setminus D_b} (\Delta w + k^2 w) u^s_{b,g} dx &= \int_{\partial B_R} (\partial_\nu w u^s_{b,g} - w \partial_\nu u^s_{b,g}) ds \\ &\quad - \int_{\partial D_b} (\partial_\nu w u_{b,g} - w \partial_\nu u_{b,g}) ds + \int_{\partial D_b} (\partial_\nu w v_g - w \partial_\nu v_g) ds. \end{aligned} \tag{3.10}$$

The first term on the right hand side goes to 0 as $R \to +\infty$ thanks to the radiation condition. Therefore, inserting the previous equality in (3.9) gives:

$$(u, \overline{u^s_{b,g}}|_{\Omega_D})_{L^2(\Omega_D)} = - \int_{\partial D_b} (\partial_\nu w u_{b,g} - w \partial_\nu u_{b,g}) ds + \int_{\partial D_b} (\partial_\nu w v_g - w \partial_\nu v_g) ds. \tag{3.11}$$

Inserting (3.11) in equation (3.7) and using the boundary condition of w, we obtain:

$$\int_{\partial D_b} (\partial_\nu w v_g - \partial_\nu v_g w) ds + \int_{\Omega_D} u v_g dx = 0. \tag{3.12}$$

Replacing v_g by its expression and reversing the order of integration shows:

$$\int_{\mathbb{S}} g(d) w^\infty(-d) ds(d) = 0, \tag{3.13}$$

where

$$w^\infty(d) = - \int_{\partial D_b} (\partial_{\nu(x)} w(x) e^{-ikx\cdot d} - \partial_{\nu(x)} e^{-ikx.d} w) ds(x) - \int_{\Omega_D} u(x) e^{-ikx\cdot d} dx,$$

is the far field pattern of w. By the Rellich lemma, we then get that $w = 0$ in $\mathbb{R}^m \setminus D_b$. Hence, $w \in H^2_0(\Omega_D)$ and $\frac{\varphi}{\mu} - \widetilde{\psi} = 0$ on ∂D_b. Since $u \in L^2(\Omega_D)$ and satisfies $\Delta \overline{u} + k^2 \overline{u} = 0$ in Ω_D, we have in particular:

$$\int_{\Omega_D} \overline{u} (\Delta w + k^2 w) dx = 0,$$

which gives $\|u\|^2_{L^2(\Omega_D)} = 0$ therefore $u = 0$. On the other hand, taking the duality product between $\frac{\varphi}{\mu} - \widetilde{\psi}$ and $f \in H^{-\frac{1}{2}}(\partial D_b)$, and using the definition of $\widetilde{\psi}$, we get

$$\frac{\varphi}{\mu} \int_{\partial D_b} \overline{f} ds - (\psi, f)_{H^{-\frac{1}{2}}(\partial D_b)} = 0, \tag{3.14}$$

for all $f \in H^{-\frac{1}{2}}(\partial D_b)$. Taking $f = \psi$ gives us $\frac{\varphi}{\mu} \int_{\partial D_b} \overline{\psi} ds - \|\psi\|^2_{H^{-\frac{1}{2}}(\partial D_b)} = 0$. Recalling that $\mu\varphi + \int_{\partial D_b} \psi dx = 0$, we end up with $\|\psi\|^2_{H^{-\frac{1}{2}}(\partial D_b)} + |\varphi|^2 = 0$, hence $\psi = 0$ and $\varphi = 0$. This concludes the proof. □

3.2.2 Properties of the range of $\mathcal{G}^\mu$

Lemma 20. *Assume μ is not an eigenvalue of problem (2.3). Then $\phi_z^\infty \in \mathcal{R}(\mathcal{G}^\mu)$, the range of $\mathcal{G}^\mu$, for all $z \in D_b$.*

Proof. Let $z \in D_b$. Let χ_z be a $C^\infty(\mathbb{R}^m)$ function such that $\chi_z = 1$ in $\mathbb{R}^m \backslash D_b$ and $\chi_z|_{\mathcal{V}} = 0$ where $\mathcal{V}$ is a neighbourhood of z. Consider $\Theta_z := \chi_z \phi(., z) \in H^2_{loc}(\mathbb{R}^m)$. Let $W_z \in H^1_c(D_b)$ be the unique solution of

$$\begin{cases} \Delta W_z + k^2 n W_z = -(\Delta + k^2 n)\Theta_z \text{ in } D_b, \\ \mu W_z + \int_{\partial D_b} \partial_\nu W_z ds = 0 \text{ on } \partial D_b. \end{cases} \tag{3.15}$$

We define $w_z = W_z + \Theta_z \in H^1(D_b)$. We notice that w_z is solution of

$$\begin{cases} \Delta w_z + k^2 n w_z = 0 \text{ in } D_b, \\ \mu w_z + \int_{\partial D_b} \partial_\nu w_z ds = \mu \phi(., z) + \int_{\partial D_b} \partial_\nu \phi(., z) ds \text{ on } \partial D_b. \end{cases} \tag{3.16}$$

Let us set $w := w_z$ in D_b and $w^s := \phi(., z)$ in $\mathbb{R}^m \backslash D_b$. We shall prove that w and w^s satisfy (3.2) with $\varphi = (u^s_{b,z} + v_z)|_{\partial D_b}$, $\psi = (\partial_\nu u^s_{b,z} + \partial_\nu v_z)|_{\partial D_b}$ and $u = -\phi(., z)|_{\Omega_D}$ where

$$v_z(x) := \int_{\partial D_b} (\partial_{\nu(y)} w_z(y) \phi(x, y) - \partial_{\nu(y)} \phi(x, y) w_z(y)) ds(y),$$

and $u^s_{b,z}$ the solution of problem (2.31) with $u^i = v_z$. Indeed, the first and second equations in (3.2) are clearly verified together with the radiation condition. It only remains to prove that the $w - w^s = \varphi$ and $\partial_\nu w - \partial_\nu w^s = \psi$ on ∂D_b.
From representation formula of solutions to the Helmholtz equation, we get the decomposition $w_z = w^s_z + v_z$ where

$$w^s_z(x) := -k^2 \int_{D_b} (1 - n) w_z(y) \phi(x, y) dy, \ x \in D_b. \tag{3.17}$$

We extend $w^s_z(x)$ for $x \in \mathbb{R}^m \backslash D_b$ using the same formula. Set $u^s_{b,z} := w^s_z - \phi(., z)$ in $\mathbb{R}^m \backslash D_b$. We notice that $u^s_{b,z}$ is solution to (2.31) with $u^i = v_z$. Thus we get on the boundary ∂D_b:

$$\begin{cases} w_z = w^s_z + v_z = u^s_{b,z} + \phi(., z) + v_z, \\ \partial_\nu w_z = \partial_\nu w^s_z + \partial_\nu v_z = \partial_\nu u^s_{b,z} + \partial_\nu \phi(., z) + \partial_\nu v_z, \end{cases} \tag{3.18}$$

which correspond to the desired transmission conditions since $w_s = \phi(., z)$. □

Lemma 21. *Assume μ is an eigenvalue of problem (2.3). Then the set of points z for which $\phi_z^\infty \in \mathcal{R}(\mathcal{G}^\mu)$ is nowhere dense in D_b.*

Proof. Let $w_0 \in H^1_c(D_b)$ be the eigenvector of (2.3) such that $\|w_0\|_{H^1(D_b)} = 1$. We will proceed by contradiction. Assume there exists $(\varphi, \psi, u) \in V$, such that,

$$\mathcal{G}^\mu(\varphi, \psi, u) = \ \phi_z^\infty,$$

for all $z \in \mathcal{Z}$, a dense set in D_b. From the definition of $\mathcal{G}^\mu$ and the Rellich lemma, we obtain that $w_z := w$, where w and w^s verify the scattering problem (3.2), is a solution of (3.16). Let $\Theta_z \in H^2(D_b)$ defined as in the previous lemma and consider $W_z := w_z - \Theta_z \in H^1_c(D_b)$ that satisfies (3.15).
Multiplying the first equation in (3.15) by $\overline{w_0}$ and using twice the Green formula, yields the compatibility condition

$$\int_{D_b} (\Delta\Theta_z + k^2 n\Theta_z)\overline{w_0}dx = 0, \tag{3.19}$$

which gives, by applying again twice the Green formula, that

$$v_\mu(z) := \int_{\partial D_b} (\partial_{\nu(x)}\phi(x,z)\overline{w_0}(x) - \partial_{\nu(x)}\overline{w_0}(x)\phi(x,z))ds(x) = 0, \tag{3.20}$$

for all $z \in \mathcal{Z}$. Since v_μ satisfies the Helmholtz equation in D_b and vanishes on a dense subset of D_b, we get $v_\mu = 0$ in D_b.
From representation formula of w_0, we have the following decomposition $\overline{w_0} = v_\mu + w_0^s$ in D_b, where

$$w_0^s(x) := -k^2 \int_{D_b} (1-n)\overline{w_0(y)}\phi(x,y)dy, \ x \in \mathbb{R}^m. \tag{3.21}$$

Hence, w_0^s defines a radiating solution of (1.6) with $D = D_b$ and $\psi = v_\mu$ in D_b. Since $v_\mu = 0$, we then conclude by uniqueness of solutions to (1.6) that $w_0^s = 0$ in $\mathbb{R}^m$ and then $\overline{w_0} = 0$, which gives a contradiction. □

Remark The choice of the lift Θ_z in the previous proof may be done differently. Assume k^2 is not a Dirichlet eigenvalue of (1.35), one can use Θ_z the unique solution of the equation $\Delta\Theta_z + k^2 n\Theta_z = 0$ in D_b and $\Theta_z = \phi_z$ on ∂D_b. Define $W_z := w_z - \Theta_z$ which satisfies:

$$\begin{cases} \Delta W_z + k^2 n W_z = 0 \text{ in } D_b, \\ \mu W_z + \int_{\partial D_b} \partial_\nu W_z ds = \int_{\partial D_b} (\partial_\nu \phi_z - \partial_\nu \Theta_z)ds \text{ on } \partial D_b. \end{cases} \tag{3.22}$$

Using Green's formula, the compatibility condition yields:

$$\int_{\partial D_b} \partial_\nu W_z \overline{w_0} ds = \int_{\partial D_b} \partial_\nu \overline{w_0} W_z ds, \tag{3.23}$$

which can be simplified as

$$\int_{\partial D_b} \partial_\nu \Theta_z = \int_{\partial D_b} \partial_\nu \phi_z. \tag{3.24}$$

Consequently, for $z \in D_b$, $\phi_z^\infty \in \mathcal{R}(\mathcal{G}^\mu)$ if and only if the following system

$$\begin{cases} \Delta\Theta_z + k^2 n\Theta_z = 0 \text{ in } D_b \\ \Theta_z = \phi_z \text{ on } \partial D_b \\ \int_{\partial D_b} \partial_\nu \Theta_z = \int_{\partial D_b} \partial_\nu \phi_z \text{ on } \partial D_b \end{cases} \tag{3.25}$$

has a solution.
In some analytical cases, equation (3.25) provides insights on the location of the points

$z \in D_b$ that allow $\phi_z^\infty \in \mathcal{R}(\mathcal{G})$ and therefore the set of point to avoid in Lemma 21. If D_b is a centered ball of radius $\rho > 0$ and n is a constant, Θ_z and ϕ_z assume the following analytical expression for all $x \in D_b$:

$$\begin{cases} \Theta_z(x) &= \sum_{q\in\mathbb{Z}} \alpha_q J_q(k\sqrt{n}|x|)e^{iq\frac{x}{|x|}}, \\ \phi_z(x) &= \frac{i}{4}\sum_{q\in\mathbb{Z}} J_q(k|z|)H_q^{(1)}(k|x|)e^{iq(\frac{x}{|x|}-\frac{z}{|z|})}, \end{cases} \tag{3.26}$$

where $\alpha_q \in \mathbb{C}$ for all $q \in \mathbb{Z}$. The two boundary conditions in (3.25) give two equations for α_0:

$$\alpha_0 = \begin{cases} \frac{i}{4}\frac{J_0(k|z|)H_0^{(1)}(k\rho)}{J_0(k\sqrt{n}\rho)}, \\ \frac{i}{4}\frac{J_0(k|z|)H_0^{(1)'}(k\rho)}{\sqrt{n}J_0'(k\sqrt{n}\rho)}. \end{cases} \tag{3.27}$$

A solution exists when $J_0(k|z|) = 0$. Therefore, $\phi_z^\infty \in \mathcal{R}(\mathcal{G})$ for all z lying on the spheres of radius $\frac{j_i}{k} < \rho$ where j_i denotes the i-th zero of J_0.

3.3 The GLSM Theorem for averaged Steklov eigenvalue

The previous lemmas allow us to apply Theorem 4 with $X = X^* = L^2(\mathbb{S})$ and $Y = \mathbb{R} \times H^{-\frac{1}{2}}(\partial D_b) \times L^2(\Omega_D)$ to the modified far field operator $\mathcal{F}^\mu$.
However, we need to construct an operator B that satisfies Assumption 3, with $H := \mathcal{H}^\mu$ defined in (3.1). Keeping an implementable inverse method in mind, the operator B must use computable quantities, such as Fg, $v_g|_{D_b}$ or $F_b^\mu g$.

Lemma 22. *If k is not a transmission eigenvalue associated with D and there exists $\beta > 0$ such that $n - 1 \geq \beta$ (or $1 - n \geq \beta$) in a neighborhood of ∂D, then*

$$B(g) = |(Fg, g)_{L^2(\mathbb{S})}| + \|v_g\|^2_{H^1(D_b)}, \tag{3.28}$$

satisfies Assumption 3.

Proof. We start our proof by mentioning that under the assumption on k^2, the operator T given by (1.10) is coercive on $V_{inc}(D)$(see [3]).
Let us start with the first implication. Assume that the quantity $|(Fg_n, g_n)_{L^2(\mathbb{S})}|+\|v_{g_n}\|^2_{H^1(D_b)}$ is bounded for a sequence $\{g_n\}$. The latter implies in particular (thanks to classical trace theorem) that $\|v_{g_n}\|_{H^{\frac{1}{2}}(\partial D_b)}$ and $\|\partial_\nu v_{g_n}\|_{H^{-\frac{1}{2}}(\partial D_b)}$ are bounded sequences. The well-posedness of (2.31) yields that the sequence u^s_{b,g_n} is bounded in $H^1(K\backslash D_b)$ for any compact set K containing D_b. Then, since $u_{b,g_n} = u^s_{b,g_n} + v_{g_n}$ in $\mathbb{R}^m\backslash D_b$, we also get that $\|u_{b,g_n}\|_{H^{\frac{1}{2}}(\partial D_b)}$ and $\|\partial_\nu u_{b,g_n}\|_{H^{-\frac{1}{2}}(\partial D_b)}$ are bounded sequences.
From the coercivity of T and the factorization $F = H^*TH$, we get:

$$\|v_g\|^2_{L^2(\Omega_D)} \leq C|(Fg, g)_{L^2(\mathbb{S})}|, \tag{3.29}$$

where C is a constant independent from g. This implies that $\|v_{g_n}\|_{L^2(\Omega_D)}$ is bounded and again from the identity $u_{b,g_n} = u^s_{b,g_n} + v_{g_n}$ in $\mathbb{R}^m \backslash D_b$ we also deduce that $\|u_{b,g_n}\|_{L^2(\Omega_D)}$. This proves that$\|\mathcal{H}^\mu g_n\|^2_Y$ is bounded.
Now, for the reverse implication, assume $\|\mathcal{H}^\mu g_n\|^2_Y$ bounded. From the representation formula on the scattered field and from the fact that v_g satisfies Helmholtz equation, we have for $x \in \mathbb{R}^m \backslash D_b$

$$u^s_{b,g}(x) = \int_{\partial D_b} (u_b(y)\partial_{\nu(y)}\phi(x,y) - \partial_\nu u_b(y)\phi(x,y))ds(y). \tag{3.30}$$

Hence, from continuity properties of single and double layers potentials,([52]) we infer that the scattered field u^s_{b,g_n} is bounded in $H^1(K\backslash D_b)$, for any compact set K containing D_b, and particularly $(u^s_{b,g_n}, \partial_\nu u^s_{b,g_n})$ are bounded in $H^{\frac{1}{2}}(\partial D_b) \times H^{-\frac{1}{2}}(\partial D_b)$. Therefore, $(v_{g_n}, \partial_\nu v_{g_n})|_{\partial D_b}$ is a bounded sequence in $H^{\frac{1}{2}}(\partial D_b) \times H^{-\frac{1}{2}}(\partial D_b)$. The representation formula for solution to the Helmholtz equation in D_b applied on v_{g_n} gives the boundedness of v_{g_n} in $H^1(D_b)$.
In addition, since u_{b,g_n} is bounded in $L^2(\Omega_D)$, we also get $\|v_{g_n}\|_{L^2(\Omega_D)}$ bounded. We then deduce that $\|v_{g_n}\|_{L^2(D)}$ is bounded. From the continuity of the operator T and the factorization (1.9), we finally conclude that $|(Fg_n, g_n)_{L^2(\mathbb{S})}|$ is bounded. □

We are ready to apply Theorem 4 to the operator $\mathcal{F}^\mu$. We observe that if μ is not an eigenvalue of (2.3), then $\mathcal{F}^\mu$ is injective and by reciprocity relations for far fields, we also obtain that it has dense range.
Combining Lemma 21, 20 and Theorem 4, we conclude with the main theorem of this section:

Theorem 23. *Assume that the hypothesis of Lemma 22 hold, with B defined by (3.28). Consider the functional*

$$J_\alpha(\phi^\infty_z, g) := \alpha B(g) + \|\mathcal{F}^\mu g - \phi^\infty_z\|^2_{L^2(\mathbb{S})} \quad \text{and set} \quad j_\alpha(\phi^\infty_z) := \inf_{g\in L^2(\mathbb{S})} J_\alpha(\phi^\infty_z, g). \tag{3.31}$$

Let g^z_α be a minimizing sequence defined by

$$J_\alpha(\phi^\infty_z, g^z_\alpha) \le j_\alpha(\phi^\infty_z) + C\alpha, \tag{3.32}$$

where $C > 0$ is a constant independent of α. Then a real number $\mu > 0$ is an eigenvalue of (2.3) if and only if the set of points z such that $B(g^z_\alpha)$ is bounded and $\|\mathcal{F}^\mu g^z_\alpha - \phi^\infty_z\|_{L^2(\mathbb{S})} \to 0$ as $\alpha \to 0$ is nowhere dense in D_b.

Remark 5. *In the case of noisy data, yielding a noisy operator F^δ satisfying $\|F^\delta - F\| \le \delta$, the theorem above also applies under the following modifications ([8]) : the functional J_α should be replaced by*

$$J^\delta_\alpha(\phi^\infty_z, g) = \alpha(B^\delta(g) + \delta\|g\|^2) + \|(F^\delta - F^\mu_b)g - \phi^\infty_z\|^2_{L^2(\mathbb{S})}, \tag{3.33}$$

with $B^\delta(g) := |(F^\delta g, g)_{L^2(\mathbb{S})}|^2 + \|v_g\|^2_{H^1(D_b)}$.

Theorem 24. *Assume that F^δ is compact with dense range and the hypothesis of Lemma 22 hold. The functional $J^\delta_\alpha(\phi^\infty_z, .)$ admits a minimizer $g^{z,\delta}_\alpha$. Moreover a real number $\mu > 0$ is not an eigenvalue of (2.3) if only if the set of points z such that*

$$\lim_{\alpha\to 0}\lim_{\delta\to 0}(B^\delta(g^{z,\delta}_\alpha) + \delta\|g^{z,\delta}_\alpha\|^2) < \infty \text{ and } \lim_{\alpha\to 0}\lim_{\delta\to 0}\|\mathcal{F}^\mu g^{z,\delta}_\alpha - \phi^\infty_z\|_{L^2(\mathbb{S})} = 0$$

is nowhere dense in D_b.

3.4 Numerical inversion algorithm and validation

3.4.1 The inversion algorithm

Motivated by the analysis above and inspired by the inversion algorithm suggested in [7], we propose the following scheme to build an indicator function for the refractive index n of the media from the knowledge of the far field operator F at a fixed frequency k. It can be formally synthesised by the following three steps:

1. Let $\rho > 0$ be a given parameter. Choose D_b to be the ball B^y_ρ of center $y \in \mathbb{R}^m$ and radius ρ satisfying the condition $k^2 < \eta_0(n, D_b)$, the first Dirichlet eigenvalue of (1.35).

2. Evaluate the eigenvalue $\mu(y, n)$ of problem (2.3) from the measurements F and the analytically computed F^μ_b using the GLSM method described by Theorem 4.

3. Plot the function $\mathcal{I} : y \to \mu(y, n) - \mu_{\text{ref}}(1)$ (defined in (2.6)) for y sampling the probed domain containing the inclusions.

We now describe how to numerically implement the steps 2 and 3 for 2D problems. We will discuss the choice of ρ and the influence of k in the numerical validation subsection.

Synthetic generation of the data

Our numerical validating examples (in $\mathbb{R}^2$) use synthetic data F that is numerically generated by solving the scattering problem (1.6) using a finite element method implemented using the Freefem++ [37] package. We use the Perfectly Matched Layer ([13]) technique to bound the computational domain and model the the Sommerfeld radiation condition.
The outcome of our numerical solver is the matrix $\mathbb{F}$ with entries

$$\mathbb{F}_{pq} = u^\infty(\hat{x}_p, d_q), \quad 1 \le p, q \le N, \tag{3.34}$$

where $\hat{x}_p = d_p = (\cos(\theta_p), \sin(\theta_p))$ with $\theta_p = \frac{p}{N}2\pi$ and where u^∞ is the numerically computed far field.

Evaluation of the background operator

In order to evaluate the far field pattern $u^\infty_{b,y}$ associated with the background domain $D_b = B^y_\rho$, we shall rely on the following transformation of the far field pattern under translation [26, eq (5.3)]:

$$u^\infty_{b,y}(\hat{x}, d) = e^{iky\cdot(d-\hat{x})} u^\infty_b(\hat{x}, d) \tag{3.35}$$

where u^∞_b is the far field associated with $D_b = B^0_\rho$ (i.e the ball of radius ρ centered at the origin). The numerical evaluation of u^∞_b can be done using the numerical solver as described above or also analytically using separation of variables. We chose to use the latter option. Indeed, for $D_b = B^0_\rho$, the solution of equation (2.24) can be analytically expressed as:

$$u_b(r\hat{x}, d) = \sum_{j\in\mathbb{Z}} (\alpha_j H^{(1)}_j(kr) + i^j J_j(kr)) e^{ij(\theta_{\hat{x}} - \theta_d)} \text{ for } r \geq \rho, \tag{3.36}$$

with

$$\begin{cases} \alpha_j = -i^j \frac{J_j(k\rho)}{H^{(1)}_j(k\rho)} \quad j \neq 0, \\ \alpha_0 = -\frac{\mu J_0(k\rho) + 2\pi\rho k J_0'(k\rho)}{\mu H^{(1)}_0(k\rho) + 2\pi\rho k H^{(1)'}_0(k\rho)}, \end{cases} \tag{3.37}$$

where $H^{(1)}_j$ denotes the Hankel function of the first kind of order j. Then the far field pattern assumes the following analytic expression:

$$u^\infty_{b,0}(\hat{x}, d) = \sqrt{\frac{2}{\pi k}} e^{-i\frac{\pi}{4}} \sum_{j\in\mathbb{Z}} \alpha_j e^{ij(\theta_{\hat{x}} - \theta_d - \frac{\pi}{2})}, \tag{3.38}$$

with $\hat{x} = (\cos(\theta_{\hat{x}}), \sin(\theta_{\hat{x}}))$ and $d = (\cos(\theta_d), \sin(\theta_d))$.
The numerical outcome of (3.38) and (3.35) is the background far field matrix $\mathbb{F}^\mu_{b,y}$ which entries are:

$$(\mathbb{F}^\mu_{b,y})_{pq} = u^\infty_{b,y}(\hat{x}_p, d_q), \quad 1 \leq p, q \leq N, \tag{3.39}$$

where $u^\infty_{b,y}$ is evaluated using (3.35) and where $u^\infty_{b,0}$ is approximated by truncating the sum in (3.38), keeping the indices $j \in \mathbb{Z}$ such that $|j| < M$.

Remark 6. *The solution of equation (2.43) for $f = e^{iq\theta}$, $q \in \mathbb{N}^*$ assumes the same analytical expression (3.36) with*

$$\begin{cases} \alpha_j = -i^j \frac{J_j(k\rho)}{H^{(1)}_j(k\rho)} \quad j \neq q, \\ \alpha_q = -\frac{\mu J_q(k\rho) + 2\pi\rho k J_q'(k\rho)}{\mu H^{(1)}_q(k\rho) + 2\pi\rho k H^{(1)'}_q(k\rho)}, \end{cases} \tag{3.40}$$

Implementation of the GLSM method to identify $\mu(y, n)$

For the implementation of the GLSM method, one needs to introduce a discretization of $\|v_g\|^2_{H^1(D_b)}$ where $D_b = B^y_\rho$ for some given y in $\mathbb{R}^2$. This norm can be computed using separation of variables. We first expand $g \in L^2(\mathbb{S})$ in Fourier series. More precisely, setting

$$g(\theta) := \sum_{m\in\mathbb{Z}} \hat{g}^y_m e^{im\theta} e^{-ik\hat{x}(\theta)\cdot y},$$

with $\hat{x}(\theta) = (\cos(\theta), \sin(\theta))$ and

$$\hat{g}_m^y := \frac{1}{2\pi} \int_0^{2\pi} g(\theta) e^{ik\hat{x}(\theta)\cdot y} e^{-im\theta} d\theta,$$

we have:

$$v_g(x+y) = 2\pi \sum_{m\in\mathbb{Z}} i^m \hat{g}_m^y J_m(kr) e^{im\theta}, \text{ for } x = r(\cos(\theta), \sin(\theta)). \tag{3.41}$$

Then we deduce:

$$\|v_g\|^2_{H^1(D_b)} = 8\pi^3 \sum_{m\in\mathbb{Z}} |\hat{g}_m^y|^2 \left((1+m^2) \int_0^R J_m(kr)^2 r dr + k^2 \int_0^R J_m'(kr)^2 r dr \right) \tag{3.42}$$

In order to simulate noise in the data, we change the values of the synthetic data $\mathbb{F}$ by adding random noise of level δ to construct the noisy far field matrix $\mathbb{F}^\delta = \mathbb{F} \cdot (1 + \delta(A + iB))$ where the entries of the matrices A and B are uniformly distributed real values in $[-1, 1]$ and where $\cdot$ denotes the element-wise product of matrices.
Since in our experiments, the refractive index n is real, when k^2 is not a classical transmission eigenvalue, it is proved in [2] that we can substitute the term $|(Fg, g)_{L^2(\mathbb{S})}|$ in $B(g)$ by $((F^*F)^{\frac{1}{2}} g, g)_{L^2(\mathbb{S})} = \|(F^*F)^{\frac{1}{4}} g\|^2_{L^2(\mathbb{S})}$. For $z \in D_b$, considering $\phi_z^\infty := (\phi_z^\infty(\theta_1), ..., \phi_z^\infty(\theta_N)) \in \mathbb{C}^N$, the cost function J_α can be approximated as

$$J_\alpha(\phi_z^\infty, g) := \alpha(\|\mathbb{H}_y g\|^2_{\mathbb{C}^{2M+1}} + \|((\mathbb{F}^\delta)^*\mathbb{F}^\delta)^{\frac{1}{4}} g\|^2_{\mathbb{C}^N} + \delta\|g\|^2_{\mathbb{C}^N}) + \|(\mathbb{F}^\delta - \mathbb{F}^\mu_{b,y})g - \phi_z^\infty\|^2_{\mathbb{C}^N}, \tag{3.43}$$

for $g \in \mathbb{C}^N$ where $\|.\|_{\mathbb{C}^N}$ denotes the euclidian norm in $\mathbb{C}^N$ and the matrix $\mathbb{H}_y$ in $\mathbb{C}^{(2M+1)\times N}$ defined by:

$$(\mathbb{H}_y g)_m = \hat{g}_m^y \sqrt{8\pi^3((1+(m-M)^2) \int_0^R J_{m-M}(kr)^2 r dr + k^2 \int_0^R J'_{m-M}(kr)^2 r dr)},$$

with:

$$\hat{g}_m^y := \frac{1}{2\pi N} \sum_{\ell=1}^N g_\ell e^{ik\hat{x}(\theta_\ell)\cdot y} e^{-i(m-M)\theta_\ell}, \tag{3.44}$$

for $m = 0, ..., 2M$.
For y fixed, the minimizing sequence of Theorem 24 is actually computed as the minimizer $g_y^*(\alpha, z, \mu)$ of the function $J_\alpha(\phi_z^\infty, .)$ which is also solution to the normal equation:

$$(\alpha(D_y^*\mathbb{H}_y + ((\mathbb{F}^\delta)^*\mathbb{F}^\delta)^{\frac{1}{2}} + \delta I) + (\mathbb{F}^\delta - \mathbb{F}^\mu_{b,y})^*(\mathbb{F}^\delta - \mathbb{F}^\mu_{b,y}))g_y^*(\alpha, z, \mu) = (\mathbb{F}^\delta - \mathbb{F}^\mu_{b,y})^*\phi_z^\infty. \tag{3.45}$$

The theoretical result of Theorem 24 does not indicate how to choose α in practice. Inspired by the classical Linear Sampling Method, we employ the Morozov principle ([32]) by seeking α that ensures the equality:

$$\|(\mathbb{F}^\delta - \mathbb{F}^\mu_{b,y})g_\alpha - \phi_z^\infty\|^2 = \delta\|g_\alpha\|^2, \tag{3.46}$$

for g_α being the solution to the normal equation:

$$\left(\alpha I + (\mathbb{F}^\delta - \mathbb{F}^\mu_{b,y})^*(\mathbb{F}^\delta - \mathbb{F}^\mu_{b,y})\right) g_\alpha = (\mathbb{F}^\delta - \mathbb{F}^\mu_{b,y})^*\phi_z^\infty. \tag{3.47}$$

Implementation of the inversion algorithm

Let $\mathcal{Y}$ be an uniform grid in the probed domain and Λ a uniform discretization of an interval of positive values μ that contains $\mu_{\text{ref}}(1)$ (see (2.6)), the reference eigenvalue (ie, the eigenvalue of problem (2.3) with $n|_{D_b} = 1$). Beforehand, we precompute a collection of far field matrices $\mathbb{F}^{\mu}_{b,y}$ for each $(y, \mu) \in \mathcal{Y} \times \Lambda$ (recall that, for fixed μ, $\mathbb{F}^{\mu}_{b,y}$ can be computed from $\mathbb{F}^{\mu}_{b,0}$ using the relation (3.35)).
For each $y \in \mathcal{Y}$, we compute the minimizer $g^*_y(\alpha, z)$ for $z \in Z$ a finite set of points in inside D_b of cardinal $|Z|$. We then set as an approximation of the eigenvalue $\mu(y, n)$ the value of μ where the function

$$\mathcal{P}_y(\mu) := \frac{1}{|Z|} \sum_{z \in Z} \|g^*_y(\alpha, z, \mu)\|^2_{\mathbb{C}^N}, \tag{3.48}$$

attains its maximum. To give an illustration of the behavior the function $\mu \to \mathcal{P}_y(\mu)$, we display in Figure 3.2 this function in the case where $D = D_b = B^0_\rho$ with $\rho = 0.5$, $n|_{D_b} = 1$ and $k = 2$. We observe that the function has a sharp peak at the expected eigenvalue $\mu_{\text{ref}}(1)$ for $k = 2$ and $\rho = 0.5$.

After obtaining the numerical approximation of $\mu(y, n)$, we plot the function $\mathcal{I}(y) :=$

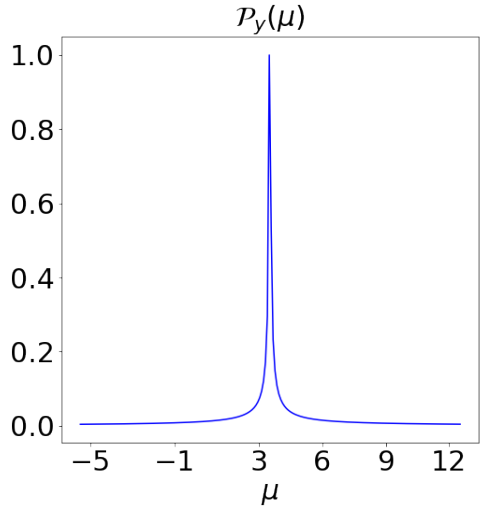

Figure 3.2: The indicator function $\mathcal{P}_y(\mu)$ given by (3.48) for $D = D_b = B^0_\rho$ with $\rho = 0.5$, $n|_{D_b} = 1$ and $k = 2$.

$\mu(y, n) - \mu_{\text{ref}}(1)$.
We recall that thanks to the monotonicity property of $\mu(y, n)$ with respect to n as stated in Theorem 12, $\mathcal{I}(y) > 0$ if $n|_{B^y_\rho} > 1$ and $\mathcal{I}(y) < 0$ if $n|_{B^y_\rho} < 1$. Furthermore, the larger is the value of $n|_{B^y_\rho}$, the larger is the value of $\mathcal{I}(y)$.

3.4.2 Numerical validation

The case of extended scatterers

Before treating the motivating example given in the Introduction, Figure 3, we first show that the new inverse method can also work in the case of extended scatterers. We consider in this example four circular inclusions of radii 0.3 and having four different constant refractive indices as presented in Figure 3.3 (right). The indicator function $\mathcal{I}$ is computed on an uniform grid $\mathcal{Y}$ of 50×50 sampling points of $[-2, 2] \times [-2, 2]$ and we take $\rho = 0.3$ for the artificial background (see Figure 3.3 (left)). The interval Λ for identifying $\mu(y, n)$ is set to be equal to $[0, \mu_{ref}(2)]$. Figure 3.4 (left) presents the values of the function $\mathcal{I} : \mathcal{Y} \to \mathbb{R}^+$ for $k = 4$. We indeed distinguish 4 scattering circular objects. We observe from the sign of the indicator function, that the objects on the left have indeed a refractive index smaller than 1 and greater than 1 on the right. Thanks to the monotonicity property of the eigenvalue (Theorem 12), it is then possible to sort the 4 different refractive indices from the values of the indicator function $\mathcal{I}$.

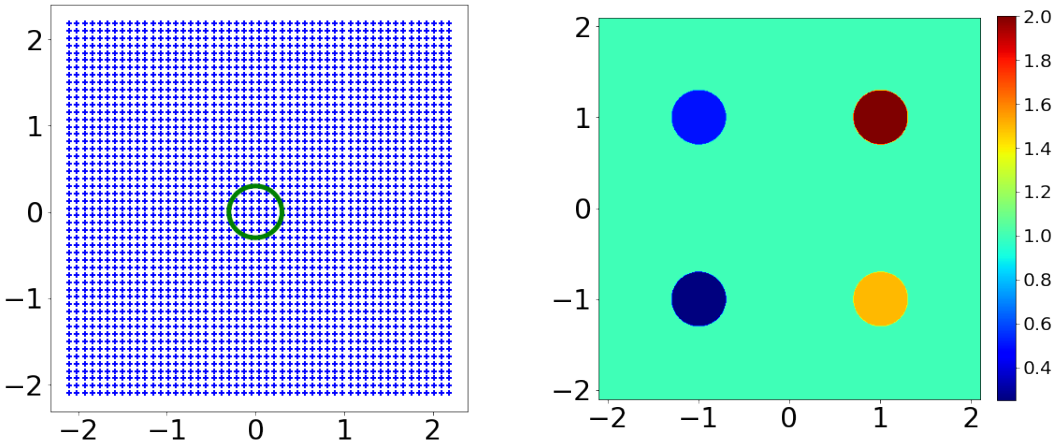

Figure 3.3: Left: Sampling grid $\mathcal{Y}$ formed by 50×50 points (blue points) and $D_b = B_\rho^0$ with $\rho = 0.3$ (green). Right: Four diffracting circles of radius 0.3 associated with four different values of the refractive index $n = 0.25$ (bottom left), $n = 0.5$ (top left), $n = 1.5$ (bottom right) and $n = 2$ (upper right).

Discussion on the choice of the parameters k and ρ: In the particular case of $D = D_b$ and constant n, the analytical expression of the eigenvalue (2.6) shows that its sensitivity with respect to the refractive index is correlated with the value of the product $k\rho$. The behavior of the eigenvalue (2.6) is directly linked to the function $x \to x\frac{J_1(x)}{J_0(x)}$, which derivative is an increasing function that goes to infinity as $x \to j_0$, the first zero of J_0. Therefore the product $k\rho$ must be chosen with 3 constraints in mind:

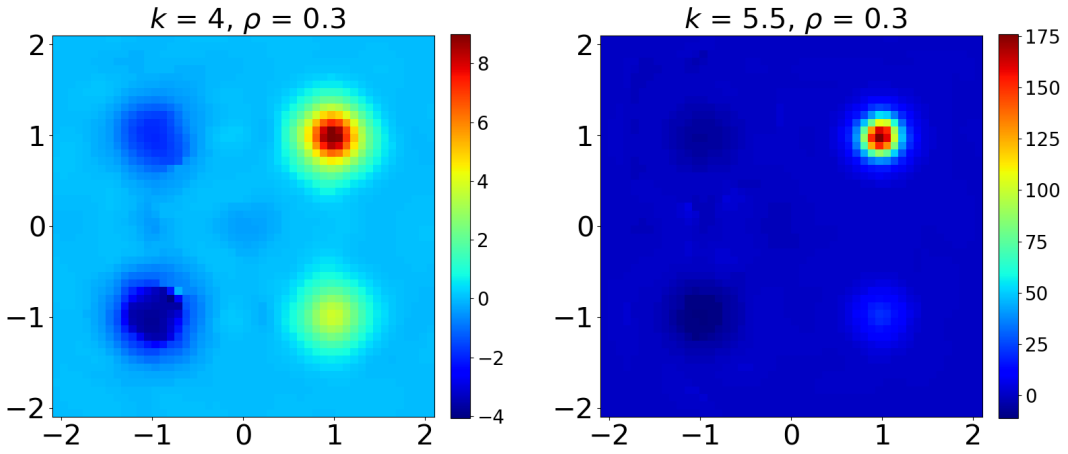

Figure 3.4: Indicator function $\mathcal{I}$ on the grid $\mathcal{Y}$ indicated in Figure 3.3 (left) for the scatterers shown in Figure 3.3 (right). We chose the parameter $\rho = 0.3$ and the noise level to be $\delta = 1\%$. Left: Reconstruction obtained for wavenumber $k = 4$. Right: Reconstruction obtained for wavenumber $k = 5.5$.

1) The condition $0 < k^2 < \eta_0(n, D_b)$ which can be rewritten as $k\rho\sqrt{n} < j_0$ must be satisfied.

2) If the product $k\rho\sqrt{n}$ is close to j_0, the sensitivity of $\mu(n, y)$ with respect to n would be very high, and only the regions with the largest values of n will be visible. Furthermore, a small error in the data can lead to a significant error in the computed eigenvalue.

3) If the product $k\rho\sqrt{n}$ is far from j_0, the sensitivity would be smaller. Different values of n may become more challenging to differentiate.

To illustrate this sensitivity, we compare the result of Figure 3.4 (left) with the indicator function $\mathcal{I}$ for $k = 5.5$ keeping the same radius $\rho = 0.3$ (i.e., a larger product $k\rho$) shown in Figure 3.4 (right). In this case, k^2 is close to the Dirichlet eigenvalue (1.35) for $D_b = B_\rho^0$ with constant $n = 2$. Although the values of $\mathcal{I}$ are coherent with the theory, it becomes challenging to visually discern the obstacles with $n < 1$ as some values of $\mathcal{I}$ get large inside the inclusion with refractive index $n = 2$.

The case of small scatterers locally densely distributed

We will use an uniform grid $\mathcal{Y}_2$ of 50×50 sampling points on $[-3.2, 3.2] \times [-3.2, 3.2]$ similarly to the one presented in Figure 3.3 (left). For the inverse algorithm, we keep the set Λ the same as in the previous example. Although the eigenvalue $\eta_0(n, D_b)$ is unknown, since it is monotonically decreasing with respect to n, using that $n|_{D_b} \leq 2$, one obtains that $\eta_0(2, D_b) = \frac{j_0^2}{2\rho^2}$ is a lower bound of $\eta_0(n, D_b)$. Selecting ρ such that $0 < k^2 < \eta_0(2, D_b)$

will ensure the hypothesis on the wavenumber needed in Theorem 12. We design in this settings four circular areas in the four corners of the domain that we fill with small circular scatterers of radius 0.02 as depicted in Figure 3.5 (left) with $n = 2$ inside. We compute the indicator function $\mathcal{I}$ on the grid $\mathcal{Y}_2$ for $k = 3$ and $\rho = \frac{1.3}{k}$ and we present the result in Figure 3.5 (right). In addition to localizing the four areas, the imaging result provides a more precise visual representation of the obstacle supports, in contrast to Figure 1.3.

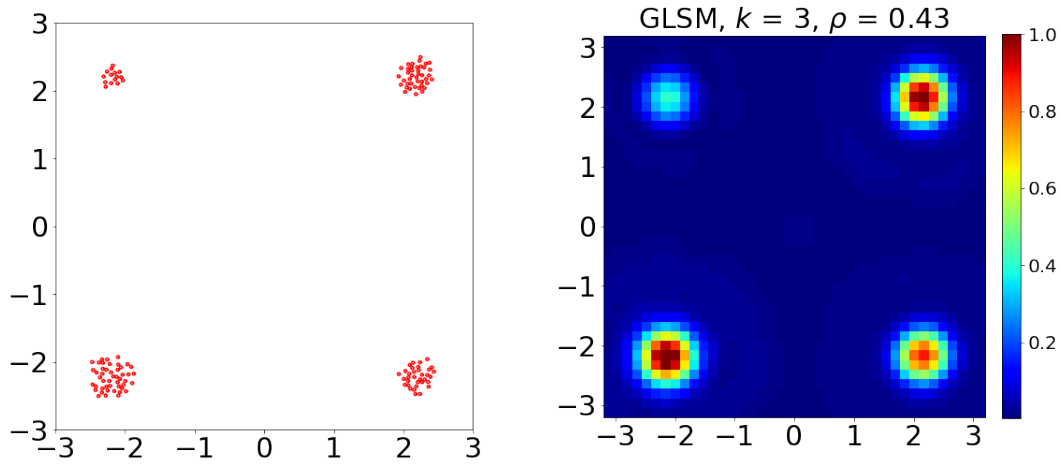

Figure 3.5: Left: the domain D constituted by small circles concentrated in the four corner. Right: Indicator function $\mathcal{I}$ on the grid $\mathcal{Y}_2$ with $\rho = 0.43$, $k = 3$ and the noise level to be $\delta = 1\%$.

The space in between the four corners of the domain is partially filled with some circular scatters (see Figure 3.6 (left)) and the indicator function $\mathcal{I}$ on this example is shown in Figure 3.6 (right).

To challenge the method, we add a circular obstacle D_o of radius 0.3 with a refractive index $n|_{D_o} = 0.5$ (see Figure 3.7 (left)). The presence of a the scatterer with refractive index smaller than 1 does not appear to affect the result for the ρ considered.

The case of densely distributed small scatterers

We consider in this example the configuration given in the introductory section shown in Figure 3 (left) where we have a large number of small scatterers densely distributed on the probed domain with a constant refractive index $n = 2$. We chose the radius ρ of the background D_b in order to have a high sensitivity of the eigenvalue to visually highlight the areas of higher concentration. Several numerical experimentations suggested that the choice $\rho = \sqrt{\frac{3\eta_0(2,D_b)}{k}}$ would give satisfactory results and this is the value of ρ that is used in the following results. Figure 3.8 presents the function $\mathcal{I}$ for two wavenumbers: $k = 3$ (left) and $k = 4$ (right). The indicator function manages in both cases to distinguish 5 main regions that correspond to the 5 areas of higher concentration. The obtained result have

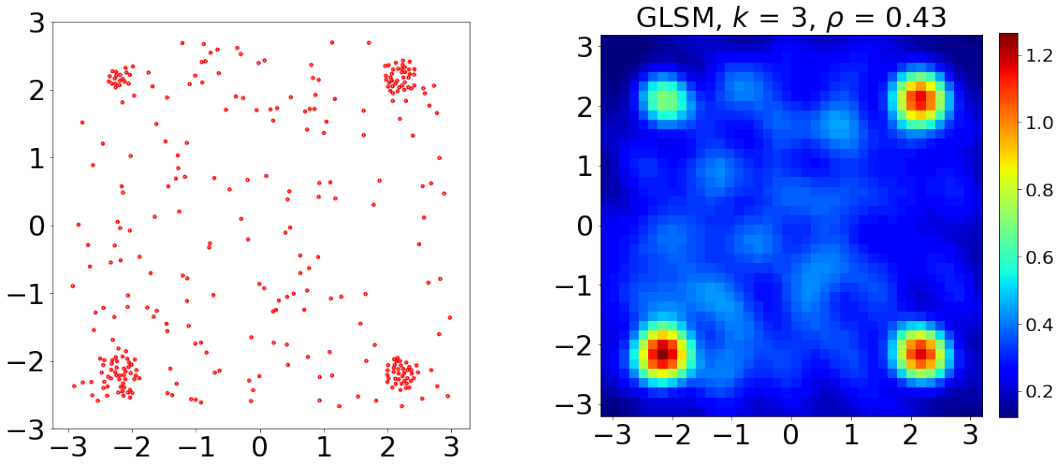

Figure 3.6: Left: the domain D constituted by small circles concentrated in the four corner with additional obstacles in between the corners. Right: Indicator function $\mathcal{I}$ on the grid $\mathcal{Y}_2$ with $\rho = 0.43$, $k = 3$ and the noise level to be $\delta = 1\%$.

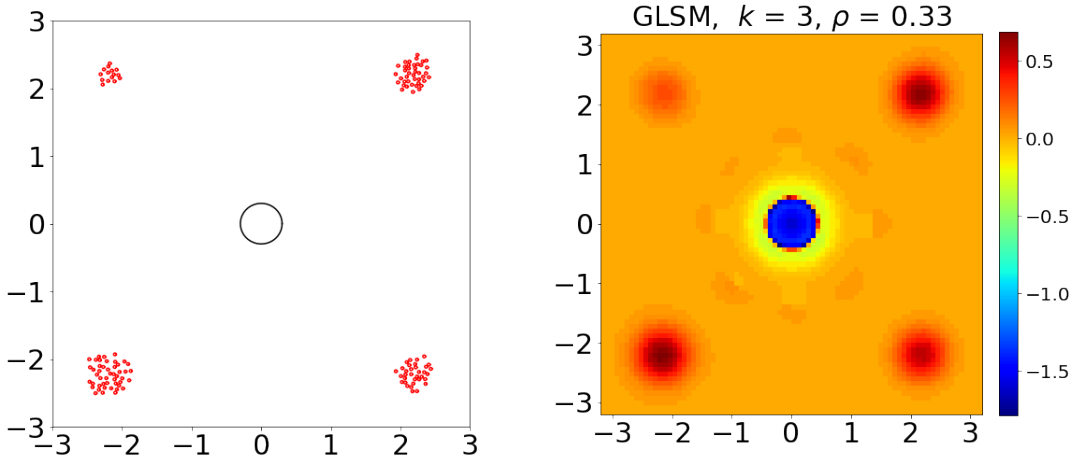

Figure 3.7: Left: the domain D constituted by small circles concentrated in the four corner with an additional centered ball of radius 0.5 with a refractive index $n = 0.5$ inside. Right: Indicator function $\mathcal{I}$ on the grid of 100×100 sampling points on $[-3.2, 3.2] \times [-3.2, 3.2]$ with $\rho = 0.33$, $k = 3$ and the noise level to be $\delta = 1\%$.

indeed better qualitative aspect in relation to the local density of the small scatterers than the one given by the Linear Sampling Method in Figure 3 (right).

A second example of densely distributed obstacles is shown in Figure 3.9 where we have a fewer number of scatterers. We observe that the indicator function works even better in this case, providing more accurate results than the LSM method shown in Figure 1.6.

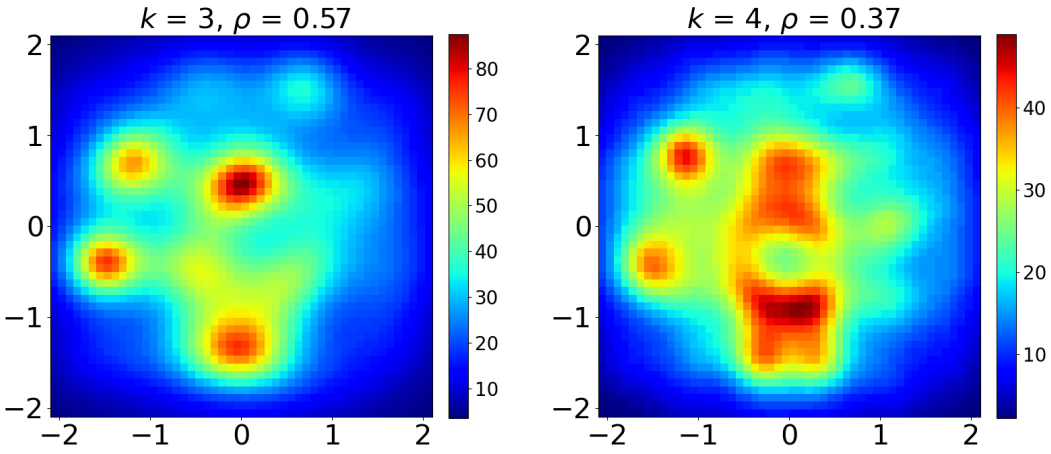

Figure 3.8: Indicator function $\mathcal{I}$ on the grid $\mathcal{Y}$ indicated in Figure 3.3 (left) for the scatterers shown in Figure 3 (left). We chose the parameter $\rho = \sqrt{\frac{3\eta_0(2,D_b)}{k}}$ and the noise level to be $\delta = 1\%$. Left: Reconstruction obtained for wavenumber $k = 3$ and $\rho = 0.57$. Right: Reconstruction obtained for wavenumber $k = 4$ and $\rho = 0.37$.

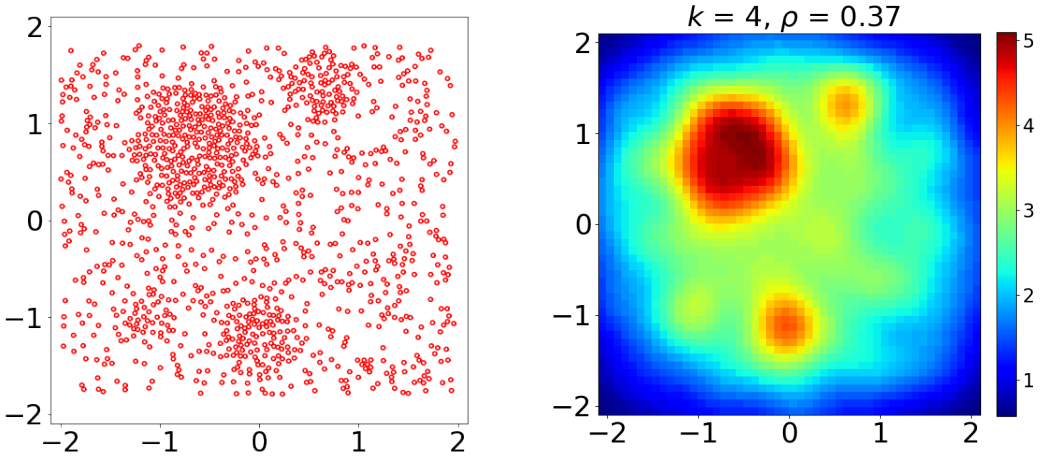

Figure 3.9: Left: the domain D constituted by 1257 small circles of radius 0.02 having a constant index of refraction $n = 2$. Right: Indicator function $\mathcal{I}$ on the grid $\mathcal{Y}$ indicated in Figure 3.3 (left). The noise level is $\delta = 1\%$ and we chose $\rho = \sqrt{\frac{3\eta_0(2,D_b)}{k}}$ for a wavenumber $k = 4$.

The case of $f \neq 1$

The previous imaging algorithm can be adapted for $f-$averaged Steklov eigenvalue with $f = e^{iq\theta}$ for $q \in \mathbb{N}^*$. The steps are outlined as follows:

1. Let $\rho > 0$ be a given parameter. Choose D_b to be the ball B_ρ^y of center $y \in \mathbb{R}^m$ and radius ρ satisfying the condition $k^2 < \eta_0(n, D_b)$, the first Dirichlet eigenvalue of (1.35).

2. For each sampling point y, make a change of coordinates for the measured data so that the center of coordinates becomes y. This means that the far field operator F becomes, in the new coordinate system,

$$(F_y g)(\hat{x}) := \int_S g(d) u^\infty(\hat{x}, d) e^{-ik(d-\hat{x})\cdot y} ds(d), \quad \hat{x} \in S. \tag{3.49}$$

   Evaluate the eigenvalue $\mu(y, n)$ of problem (2.35) from the measurements F_y and the analytically computed F_b^μ using the GLSM method described by Theorem 4.

3. Plot the function $\mathcal{I} : y \to \mu(y, n) - \mu_{\text{ref,q}}(1)$ (defined in (2.42)) for y sampling the probed domain containing the inclusions.

Figure 3.10 shows the indicator function $\mathcal{I}$ for the configuration depicted in Figure 3.5 (left) for $f = e^{i\theta}$. The expected lower sensibility is confirmed, and the result differs from the

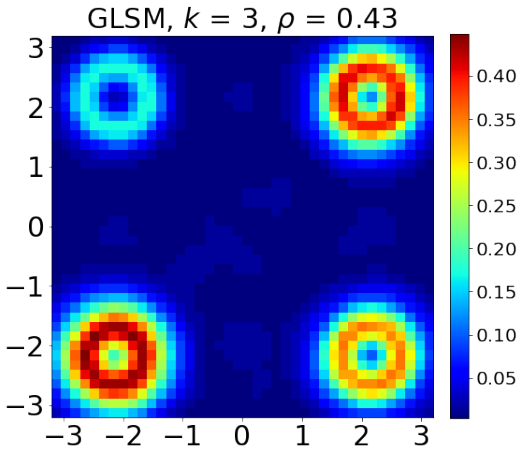

Figure 3.10: Indicator function $\mathcal{I}$ on the grid $\mathcal{Y}_2$ for the scatterers shown in Figure 3.5 (left) with $f = e^{i\theta}$, $\rho = 0.43$ and $k = 3$. The noise level is $\delta = 1\%$.

one of Figure 3.5 (right) as halos form around the areas with the highest concentration of scatters. Let $f = e^{i\theta}$ and let w_1 be the eigenvector of (2.35) associated with the eigenvalue $\mu(k, n, D_b, e^{i\theta})$. For all $w' \in H_f^1(D_b)$ (defined in section 2.4), Theorem 15, gives the following expression:

$$\mu(k, n, D_b, e^{i\theta}) = -\int_{\partial D_b} \partial_\nu w_1 \overline{f} = k^2 \int_{D_b} n w_1 \overline{w'} dx - \int_{D_b} \nabla w_1 \nabla \overline{w'} dx. \tag{3.50}$$

Set $v := \frac{J_1(kr)}{J_1(k\rho)} e^{i\theta}$ the solution of $\Delta v + k^2 v = 0$ in D_b and $v = e^{i\theta}$ on ∂D_b. By integration by parts, one obtains:

$$\mu(k, n, D_b, e^{i\theta}) - \mu(k, 1, D_b, e^{i\theta}) = k^2 \int_{D_b} (n-1) w_1 \overline{v} dx. \tag{3.51}$$

Thus, the difference $\mu(k, n, D_b, e^{i\theta}) - \mu(k, 1, D_b, e^{i\theta})$ can be interpreted as the $w_1\overline{v}$-mean of $n-1$ in D_b. Since the Bessel function of first kind of order 1 is an increasing function that vanishes at $r = 0$, the scatterers near the center of D_b have little to no impact on the eigenvalue, which explains the halos in Figure 3.10.

Remark 7. *We numerically observed that, for a fixed radius ρ, only the $f-$averaged Steklov eigenvalues in the form $e^{iq\theta}$ for $q = 0$ or $q = 1$ can provide meaningful numerical result. The function $\mathcal{P}_y$ used to determine the $f-$eigenvalues (defined for $f = 1$ in (3.48)) does not have a sharp peak for $q \geq 2$. Due to potential noise in the data, the eigenvalue can not be efficiently recovered. This is illustrated in Figure 3.11 where the function $\mathcal{P}_y$ is shown for four values of $q = 0, 1, 2, 3$ on a simple setting. To overcome this issue, one can consider a larger radius ρ.*

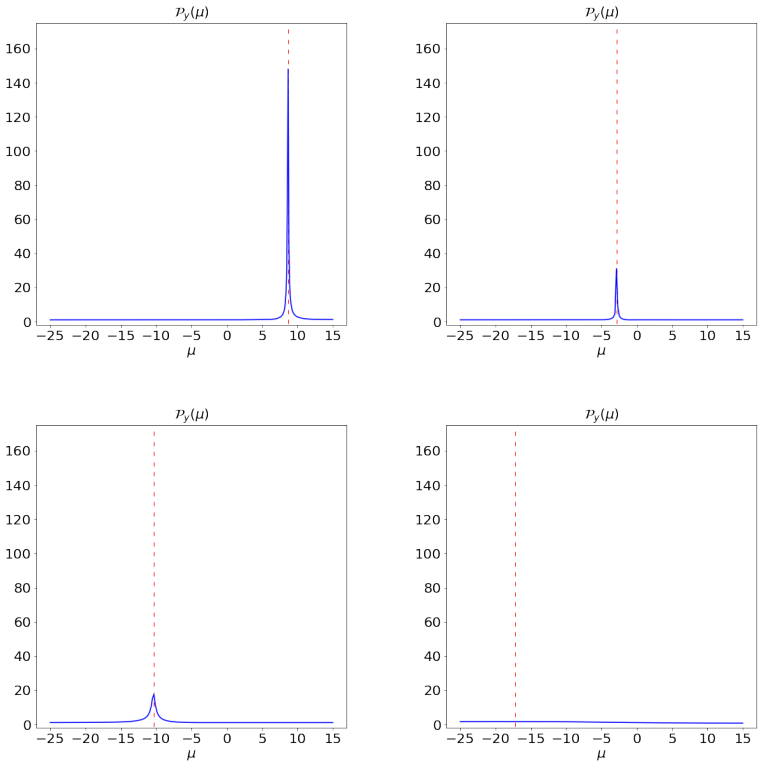

Figure 3.11: The indicator function $\mathcal{P}_y(\mu)$ given by (3.48) for $f = e^{iq\theta}$ and $D = D_b = B_\rho^0$ with $\rho = 0.5$, $n|_{D_b} = 2$ and $k = 2$ with 1% of added noise. From left to right and top to bottom: $q = 0, 1, 2, 3$. The $f-$averaged Steklov eigenvalue is represented with a red dashed line.

Chapter 4

Averaged Steklov Eigenvalues, Inside Outside Duality and Application to Inverse Scattering

Contents

4.1 Introduction

This chapter is motivated by the study of fixed-frequency inverse scattering problems using multistatic data. Specifically, our objective is to develop a new inversion algorithms that avoid the use of forward solvers, in the sense of linear sampling methods [41, 15], and that can be applied to the imaging of complex media. This new class of algorithms uses spectral signatures to infer either an indicator function for defects or averaged values of material properties [7, 12, 10].

An example of spectral signatures is the so-called transmission eigenvalues ([15, 24]). Their connection with the material properties of the scatterer [15] and the possibility to recover them from the far field data [14, 8] have led to an imaging method in [7] that provides a quantitative indicator of crack density. The latter inspired the development of analogous imaging algorithms at a fixed frequency. In these algorithms, transmission eigenvalues are replaced by artificial spectral parameters associated with artificial backgrounds [12, 10].

The utilization of artificial backgrounds for the construction of spectral signatures or for the design of imaging algorithms has been explored in various ways in the literature ([23, 22, 5, 34, 20, 1]). The objective of this chapter is to focus on the concept of averaged Steklov eigenvalues as introduced in Chapter 2 and in [12, 10]. The main advantage is that the spectrum is very simple, since it contains only one non-trivial eigenvalue. This has significant implications for the robustness and accuracy of the associated imaging algorithm.

The novel contributions are threefold. Firstly, we present a more general definition of averaged Steklov eigenvalues by formulating the underlying impedance boundary condition with an abstract boundary operator of finite rank $M \geq 1$. This results in a spectral problems with M non-zero eigenvalues (the parameter M can be chosen arbitrarily). In fact, the abstract model includes the explicit models used in [10] with $M = 1$. Further examples of such operators with $M > 1$ are provided in the numerical section.

The second new contribution is the analysis of the so-called Inside-Outside Duality Method (IODM) [31, 43] which is used to retrieve these spectral parameters. This is in contrast to the work in [7, 10], where a different method based on the Generalized Linear Sampling Method is employed. The IODM was initially proposed for Dirichlet eigenvalues [43]. It has since been extended to the identification of transmission eigenvalues in [43, 50] under some restrictive assumptions on the material parameters. For a special design of the background parameters in [35, 6] these restrictions were removed. In the present work we will show that the simple structure of the impedance boundary conditions allows a necessary and sufficient condition to characterize the spectral parameters in terms of the phase of the eigenvalues of a modified far-field operator.

Since there are only a few spectral parameters, the IODM allows a simple numerical implementation (compared to the cases in [50, 35]) and provides a faster and more reliable alternative to the method in [8]. This constitutes the core of our third novel contribution. The efficiency of this method is demonstrated by revisiting the imaging algorithm in [10] in which the IODM is employed to identify the spectral parameter and reconstruct the averaged values of the refractive index.

The chapter is structured as follows. Section 4.2 is dedicated to the definition of the artificial background with an abstract formulation of the associated impedance boundary

conditions. We then define the associated averaged Steklov eigenvalues (referred to as $\mathcal{B}-$eigenvalues). In Section 4.3 we introduce the inverse problem for inhomogeneous media and define a modified far field operator relative to the artificial background. A key factorization of this far field operator in then given. Section 4.4 contains the main theoretical result of this work, which is the characterization of the $\mathcal{B}-$eigenvalues using the IODM. In Section 4.5 we propose some validating numerical tests against analytical expressions obtained for circular domains. We then propose an algorithm implementing the IODM that can be used in the imaging algorithm proposed in [10]. We conclude with some validating numerical examples where we reconstruct the average value of refractive index of the probed medium from noisy far field data. Some technical results are given in an appendix.

4.2 $\mathcal{B}-$Averaged Steklov Eigenvalues

The motivation of the following developments is to infer some macroscopic properties of the refractive index n from measurements of the far fields associated with incident plane waves. To do so, we shall further develop the approach proposed in [7] by exploiting the notion of modified transmission eigenvalues relative to some artificial background media. In the context here, these eigenvalues correspond with Steklov-like eigenvalues since we shall use a background media that correspond with a generalization of the one introduced in [12, 10]. More precisely, we shall consider the following model for the background media: the total field for the artificial background media, denoted by $u_b \in H^1_{loc}(\mathbb{R}^m \backslash D_b)$ satisfies the following equations

$$\begin{cases} \Delta u_b + k^2 u_b = 0 \text{ in } \mathbb{R}^m \backslash D_b, \\ \mu u_b + \mathcal{B}(\partial_\nu u_b) = 0 \text{ on } \partial D_b \\ u_b = u_b^s + u^i \\ \lim\limits_{R \to +\infty} \int_{|x|=R} |\frac{\partial u_b^s}{\partial r} - iku_b^s|^2 ds = 0, \end{cases} \tag{4.1}$$

for some incident field u^i and for some parameter $\mu \in \mathbb{R}$. The domain $D_b \subset \mathbb{R}^m$ is supposed to be regular bounded and simply connected. For simplicity, we assume that $D \subset D_b$. This assumption can be weakened as we shall later explained in the numerical section (Section 4.5).
The operator $\mathcal{B} : H^{-\frac{1}{2}}(\partial D_b) \to H^{\frac{1}{2}}(\partial D_b)$ in the boundary condition in (4.1) is supposed to be of finite rank. More specifically, in all of the following, we assume that the following hypothesis holds true for the operator $\mathcal{B}$.

Assumption 25. *There exists a family of M vectors $\{e_1, ..., e_M\} \subset H^{\frac{1}{2}}(\partial D_b)$ which are orthonormal with respect to the $L^2(\partial D_b)$ scalar product and a positive real constant Λ such that:*

$$\mathcal{B}(\psi) = \kappa \sum_{i=1}^{M} \langle \psi, e_i \rangle_{H^{-\frac{1}{2}}(\partial D_b), H^{\frac{1}{2}}(\partial D_b)} e_i, \quad \forall \psi \in H^{-\frac{1}{2}}(\partial D_b). \tag{4.2}$$

This assumption implies in particular that the operator $\mathcal{B}$ satisfies:

$$\kappa(\mathcal{B}\psi, \mathcal{B}\phi)_{L^2(\partial D_b)} = \langle \psi, \mathcal{B}\phi \rangle_{H^{-\frac{1}{2}}(\partial D_b), H^{\frac{1}{2}}(\partial D_b)}, \tag{4.3}$$

for all $\psi, \phi \in H^{-\frac{1}{2}}(\partial D_b)$. In fact, this property (4.3) is also a sufficient condition for the operator $\mathcal{B}$ to be of the form (4.2) (see 4.6.1).

Using (4.3), one can prove, by standard variational techniques, that the direct problem (4.1) is well posed. The details are also given in 4.6.1.

Definition 5. *A non zero real μ is called a $\mathcal{B}-$averaged Steklov eigenvalue (in short $\mathcal{B}-$eigenvalue) if there exists $w_0 \in H^1(D_b)$ non trivial solution of*

$$\begin{cases} \Delta w_0 + k^2 n w_0 = 0 \text{ in } D_b, \\ \mu w_0 + \mathcal{B}(\partial_\nu w_0) = 0 \text{ on } \partial D_b. \end{cases} \tag{4.4}$$

Then one can construct M functions $w_i \in H^1(D_b)$, $i = 1, ..., M$ solution of:

$$\begin{cases} \Delta w_i + k^2 n w_i = 0 \text{ in } D_b, \\ w_i = e_i \text{ on } \partial D_b. \end{cases} \tag{4.5}$$

It is then easily verified that these functions are eigenvectors of $\mathcal{B}-$eigenvalues μ_i given by:

$$\mu_i := -\kappa \langle \partial_\nu w_i, e_i \rangle = \kappa(k^2 \int_{D_b} n|w_i|^2 dx - \int_{D_b} |\nabla w_i|^2 dx). \tag{4.6}$$

In fact, we prove that these are the only possible eigenvalues if k^2 is not a Dirichlet eigenvalue of (1.35) as stated in the following theorem.

Theorem 26. *Assume that k^2 is not an eigenvalue of (1.35), then there are only M non zeros real $\mathcal{B}-$eigenvalues (including multiplicity). These eigenvalues are given by (4.5).*

Proof. Let μ be an eigenvalue of (4.4) and denote by u its associated eigenvector. From the boundary condition, we deduce that $u|_{\partial D_b} \in span(e_1, ..., e_M)$. Since k^2 is not a Dirichlet eigenvalue, we deduce that there exists M complex numbers $\alpha_1, ..., \alpha_M$ such that $u = \sum_{i=1}^{M} \alpha_i w_i$ where the w_i are defined in (4.5). Inserting this expression in the boundary condition, one obtains

$$\alpha_i(\mu - \mu_i) = 0, \qquad i = 1, ..., M. \tag{4.7}$$

This shows that there exists $i \leq M$ such that $\mu = \mu_i$ (otherwise u would be trivial). □

These $\mathcal{B}-$eigenvalues corresponds to the values of μ for which one can construct an incident field $u^i \in H^1(D_b)$ solution of $\Delta u^i + k^2 u^i = 0$ in D_b for which $u_b^s = u^s$ in $\mathbb{R}^m \backslash D_b$ where u^s, u_b^s are respectively solutions of (1.1), (4.1). More explicitly, for $\mu = \mu_j$, this incident field is given by $u^i = w_j - u_j^s$ where $u_j^s \in H^1_{loc}(\mathbb{R}^m)$ is the solution of:

$$\begin{cases} \Delta u_j^s + k^2 u_j^s = k^2(1-n) w_j \text{ in } \mathbb{R}^m, \\ \lim\limits_{r \to +\infty} \int_{|x|=r} |\frac{\partial u_j^s}{\partial r} - iku_j^s|^2 = 0. \end{cases} \tag{4.8}$$

4.3 The far field operators and statement of the inverse problem

The algorithm we propose is based on retrieving the $\mathcal{B}-$eigenvalues from the operator F. This will be done by incorporating the far field operator associated with the artificial background defined by (4.1). We therefore similarly introduce the operator $F_b^\mu : L^2(\mathbb{S}) \to L^2(\mathbb{S})$ defined by

$$(F_b^\mu g)(\hat{x}) := \int_{\mathbb{S}} g(d) u_b^\infty(\hat{x}, d) ds(d), \quad \hat{x} \in \mathbb{S}, \tag{4.9}$$

where $u_b^\infty(., d)$ is the far field associated with $u_b^s(., d)$ the scattered field in (4.1) with $u^i = u^i(., d)$. This operator is computed numerically or analytically if D_b is a sphere. Then we define the modified far field operator

$$\mathcal{F}^\mu := F - F_b^\mu. \tag{4.10}$$

One of the main results of this chapter is to show that $B-$eigenvalues can be determined by applying the inside-outside algorithm to the operator

$$\mathbf{F}^\mu := \gamma S_b^* \mathcal{F}^\mu, \tag{4.11}$$

where $S_b := I + \frac{2ik}{\bar{\gamma}} F_b^\mu$ is the scattering operator associated with the background. This is done in the next section. As a preparatory material, we establish first some needed properties of these far field operators.

4.3.1 Properties of the far field operators

We introduce the operator $\mathcal{H}_\mathcal{B} : L^2(\mathbb{S}) \to H^{-\frac{1}{2}}(\partial D_b)$ defined as:

$$\mathcal{H}_\mathcal{B} g := \partial_\nu u_{b,g}|_{\partial D_b}, \tag{4.12}$$

where $u_{b,g}$ is solution of (4.1) with $u^i = v_g$, the Herglotz wave function defined in (1.5). For u_g solution of (1.1) with $u^i = v_g$, set

$$\begin{cases} w^s := u_g - u_{b,g} & \text{in } \mathbb{R}^m \backslash D_b, \\ w := u_g & \text{in } D_b, \end{cases} \tag{4.13}$$

so that $\mathcal{F}^\mu g = w^\infty$ the far field associated with w^s. By linearity, we obtain that the pair $(w, w^s) \in H^1(D_b) \times H^1_{loc}(\mathbb{R}^m \backslash D_b)$ is solution of:

$$\begin{cases} \Delta w + k^2 n w = 0 \text{ in } D_b, \\ \Delta w^s + k^2 w^s = 0 \text{ in } \mathbb{R}^m \backslash D_b, \\ w^s + \frac{1}{\mu}\mathcal{B}(\partial_\nu w^s) = w + \frac{1}{\mu}\mathcal{B}(\partial_\nu w) \text{ on } \partial D_b, \\ \partial_\nu w - \partial_\nu w^s = \psi \text{ on } \partial D_b, \\ \lim\limits_{r \to +\infty} \int_{|x|=r} |\frac{\partial w^s}{\partial r} - ikw^s|^2 = 0, \end{cases} \tag{4.14}$$

where $\psi = \partial_\nu u_{b,g}$.
The solution of this problem is linear with respect to $\frac{1}{\mu}$. In fact, one can write $w = w_D + \frac{1}{\mu} w_N$ (respectively $w^s = w_D^s + \frac{1}{\mu} w_N^s$) where (w_D, w_D^s) and (w_N, w_N^s) do not depend on μ and are solution of

$$\begin{cases} \Delta w_N + k^2 n w_N = 0 \text{ in } D_b, \\ \Delta w_N^s + k^2 w_N^s = 0 \text{ in } \mathbb{R}^m \backslash D_b, \\ w_N - w_N^s = -\mathcal{B}(\psi) \text{ on } \partial D_b, \\ \partial_\nu w_N - \partial_\nu w_N^s = 0 \text{ on } \partial D_b, \\ \lim\limits_{r \to +\infty} \int_{|x|=r} |\frac{\partial w_N^s}{\partial r} - ik w_N^s|^2 = 0, \end{cases} \quad \begin{cases} \Delta w_D + k^2 n w_D = 0 \text{ in } D_b, \\ \Delta w_D^s + k^2 w_D^s = 0 \text{ in } \mathbb{R}^m \backslash D_b, \\ w_D - w_D^s = 0 \text{ on } \partial D_b, \\ \partial_\nu w_D - \partial_\nu w_D^s = \psi \text{ on } \partial D_b, \\ \lim\limits_{r \to +\infty} \int_{|x|=r} |\frac{\partial w_D^s}{\partial r} - ik w_D^s|^2 = 0. \end{cases} \tag{4.15}$$

Lemma 27. *Problem (4.14) is well posed for all ψ in $H^{-\frac{1}{2}}(\partial D_b)$. Furthermore, the solution (w, w^s) of (4.14) with source term ψ satisfies the estimate for any compact set Ω that contains D_b:*

$$\|\Delta w\|^2_{L^2(D_b)} + \|\Delta w^s\|^2_{L^2(\Omega \backslash D_b)} + \|w^s\|^2_{H^1(K \backslash D_b)} + \|w\|^2_{H^1(D_b)} \leq (C_1 + \frac{1}{\mu} C_2) \|\psi\|^2_{H^{-\frac{1}{2}}(\partial D_b)}, \tag{4.16}$$

where $C_1, C_2 > 0$ do not depend on ψ and μ. In addition, by elliptic regularity, for any compact set $\Omega \subset \mathbb{R}^m \backslash \overline{D_b}$, there exists a constant $C_b > 0$ independant from ψ such that

$$\|w^s\|^2_{H^2(\Omega)} \leq C_b \|\psi\|^2_{H^{-\frac{1}{2}}(\partial D_b)}. \tag{4.17}$$

Proof. This result is a direct consequence on the well posedness of the problems (4.15) and the linearity of the solution of (4.14) with respect to $\frac{1}{\mu}$. □

Define the operator $\mathcal{G}_\mathcal{B} : H^{-\frac{1}{2}}(\partial D_b) \to L^2(\mathbb{S})$ such that: $\mathcal{G}_\mathcal{B}(\psi) := w^\infty$, with w^∞ being the far field of w^s the solution of (4.14). We then deduce the following factorization:

$$\mathcal{F}^\mu = \mathcal{G}_\mathcal{B} \mathcal{H}_\mathcal{B}. \tag{4.18}$$

In the following, we shall further expand the factorization of the operator $\mathcal{F}^\mu$ and write it in the form $S_b \mathcal{H}_\mathcal{B}^* T_\mathcal{B} \mathcal{H}_\mathcal{B}$, with a particular operator $T_\mathcal{B}$ whose injectivity is related to the $\mathcal{B}-$eigenvalues. We first state a lemma that characterizes the adjoint of $\mathcal{H}_\mathcal{B}$ denoted by $\mathcal{H}_\mathcal{B}^* : H^{\frac{1}{2}}(\partial D_b) \to L^2(\mathbb{S})$.

Lemma 28. *The operator $\mathcal{H}_\mathcal{B}$ is injective and its range is dense in $H^{-\frac{1}{2}}(\partial D_b)$. Moreover, the adjoint operator $\mathcal{H}_\mathcal{B}^*$ is defined by: $\mathcal{H}_\mathcal{B}^* \phi = \gamma S_b^* \widetilde{w}^\infty$ for all $\phi \in H^{\frac{1}{2}}(\partial D_b)$, where $\widetilde{w}^\infty$ is the far field pattern of $\widetilde{w} \in H^1_{loc}(\mathbb{R}^m \backslash D_b)$ solution of:*

$$\begin{cases} \Delta \widetilde{w} + k^2 \widetilde{w} = 0 \text{ in } \mathbb{R}^m \backslash D_b, \\ \widetilde{w} + \frac{1}{\mu} \mathcal{B}(\partial_\nu \widetilde{w}) = \phi \text{ on } \partial D_b, \\ \lim\limits_{r \to +\infty} \int_{|x|=r} |\frac{\partial \widetilde{w}}{\partial r} - ik \widetilde{w}|^2 = 0. \end{cases} \tag{4.19}$$

Proof. We first prove the last part of the lemma. Let $g \in L^2(\mathbb{S})$. Applying Green's formula twice, one obtains

$$\begin{aligned} 0 &= \int_{B_R \setminus D_b} (\Delta \overline{\widetilde{w}} + k^2 \overline{\widetilde{w}}) u^s_{b,g} dx \\ &= \int_{\partial B_R} (\partial_\nu \overline{\widetilde{w}} u^s_{b,g} - \overline{\widetilde{w}} \partial_\nu u^s_{b,g}) ds - \int_{\partial D_b} (\partial_\nu \overline{\widetilde{w}} u_{b,g} - \overline{\widetilde{w}} \partial_\nu u_{b,g}) ds \\ &+ \int_{\partial D_b} (\partial_\nu \overline{\widetilde{w}} v_g - \overline{\widetilde{w}} \partial_\nu v_g) ds. \end{aligned} \tag{4.20}$$

Using the Sommerfeld radiation condition, one gets

$$\lim_{R \to +\infty} \int_{\partial B_R} (\partial_\nu \overline{\widetilde{w}} u^s_{b,g} - \overline{\widetilde{w}} \partial_\nu u^s_{b,g}) ds = -2ik \int_{\mathbb{S}} \overline{\widetilde{w}^\infty}(d) u^\infty_{b,g}(d) ds(d). \tag{4.21}$$

We recall that the far field $\widetilde{w}^\infty$ admits the following expression:

$$\gamma \widetilde{w}^\infty(d) = -\int_{\partial D_b} (\partial_{\nu(x)} \widetilde{w}(x) e^{-ikx \cdot d} - \partial_{\nu(x)} e^{-ikx.d} \widetilde{w}) ds(x). \tag{4.22}$$

Thus, replacing v_g by its expression, one obtains:

$$-\overline{\gamma} \int_{\mathbb{S}} g(d) \overline{\widetilde{w}^\infty(d)} ds = \int_{\partial D_b} (\partial_\nu \overline{\widetilde{w}} v_g - \overline{\widetilde{w}} \partial_\nu v_g) ds. \tag{4.23}$$

Using the boundary condition of $\widetilde{w}$ and $u_{b,g}$, we deduce that

$$\begin{aligned} \int_{\partial D_b} (\partial_\nu \overline{\widetilde{w}} u_{b,g} - \overline{\widetilde{w}} \partial_\nu u_{b,g}) ds &= \int_{\partial D_b} (\partial_\nu \overline{\widetilde{w}} (-\tfrac{1}{\mu} \mathcal{B}(\partial_\nu u_{b,g})) - \overline{\widetilde{w}} \partial_\nu u_{b,g}) ds \\ &= -\int_{\partial D_b} \partial_\nu u_{b,g} \overline{\phi} ds, \end{aligned} \tag{4.24}$$

where, for the last equality we used the fact that $\mathcal{B}$ is self-adjoint. Equation (4.20), (4.21), (4.23) and (4.24) give

$$\int_{\partial D_b} \partial_\nu u_{b,g} \overline{\phi} ds = 2ik \int_{\mathbb{S}} \overline{\widetilde{w}^\infty}(d) u^\infty_{b,g}(d) ds(d) + \overline{\gamma} \int_{\mathbb{S}} g(d) \overline{\widetilde{w}^\infty(d)} ds. \tag{4.25}$$

Hence, using the definition of $\mathcal{H}_\mathcal{B}$, we get:

$$\begin{aligned} \langle \mathcal{H}_\mathcal{B} g, \phi \rangle_{H^{-\frac{1}{2}}(\partial D_b), H^{\frac{1}{2}}(\partial D_b)} &= \overline{\gamma} (g, \widetilde{w}^\infty)_{L^2(\mathbb{S})} + 2ik (F^b g, \widetilde{w}^\infty) \\ &= \overline{\gamma} (S_b g, \widetilde{w}^\infty)_{L^2(\mathbb{S})}. \end{aligned} \tag{4.26}$$

We then conclude that $\mathcal{H}_\mathcal{B}{}^* \phi = \gamma S_b^* \widetilde{w}^\infty$.
We now prove the injectivity of $\mathcal{H}_\mathcal{B}$. Assume that $\mathcal{H}_\mathcal{B} g = 0$ for some $g \in L^2(\mathbb{S})$. This implies in particular that $\partial_\nu u_{b,g}|_{\partial D_b} = 0$ and $u_{b,g}$ vanishes on ∂D_b by the boundary condition, which gives $u^s_{b,g} = -v_g$ in $\mathbb{R}^m \setminus D_b$. Therefore the Herglotz wave function v_g which satisfies the Helmhotz equation in $\mathbb{R}^m$ also satisfies the radiation condition. This proves that $v_g = 0$ and then $g = 0$ ([26, Theorem 3.19]).
We know prove that $\mathcal{H}_\mathcal{B}$ has dense range by showing that $\mathcal{H}^*_\mathcal{B}$ is injective. If $H^*_\mathcal{B} \phi = 0$ then $\gamma S_b^* \widetilde{w}^\infty = 0$ for some $\phi \in H^{\frac{1}{2}}(\partial D_b)$. Using Rellich's lemma and the fact that S_b^* is unitary (see Proposition 40) and therefore injective, we infer that only $\phi = 0$ satisfies the equality. □

The previous lemma implies in particular that $S_b\mathcal{H}_{\mathcal{B}}{}^* = \gamma\widetilde{w}^\infty$. Let us introduce the operator $T_{\mathcal{B}} : H^{-\frac{1}{2}}(\partial D_b) \to H^{\frac{1}{2}}(\partial D_b)$ defined by

$$T_{\mathcal{B}}(\psi) = w + \frac{1}{\mu}\mathcal{B}(\partial_\nu w) = w^s + \frac{1}{\mu}\mathcal{B}(\partial_\nu w^s) \tag{4.27}$$

where (w, w^s) is the unique solution of (4.14). We then have $\mathcal{G}_{\mathcal{B}}\psi = S_b\mathcal{H}_{\mathcal{B}}{}^* T_{\mathcal{B}}\psi$. We deduce from (4.18) that $\mathcal{F}^\mu$ assumes the following factorization:

$$\gamma\mathcal{F}^\mu = S_b\mathcal{H}^*_{\mathcal{B}} T_{\mathcal{B}}\mathcal{H}_{\mathcal{B}}. \tag{4.28}$$

Using the fact that S_b is unitary (see Proposition 40 in section 4.6.2), we infer that

$$\mathbf{F} = H^*_{\mathcal{B}} T_{\mathcal{B}} H_{\mathcal{B}}. \tag{4.29}$$

In addition, let us also observe that the operator $\mathbf{S} := I + \frac{2ik}{|\gamma|^2}\mathbf{F}$ is unitary due to the fact that S and S_b are unitary. This also implies in particular that $\mathbf{F}$ is a normal operator.

4.4 The inside-outside duality applied to F

Consider the case where $\mu \neq 0$ is not a $\mathcal{B}-$eigenvalue. Since $\mathbf{F}$ is a compact normal operator, there exists an orthonormal complete basis $(g_j)_{j\in\mathbb{N}}$ of $L^2(\mathbb{S})$ such that $\mathbf{F}g_j = \lambda_j g_j$ where $(\lambda_j)_{j\in\mathbb{N}}$ are the eigenvalues of $\mathbf{F}$ that accumulate at 0.
Exploiting the fact that $\mathbf{S}$ is unitary, we deduce that the eigenvalues of $\mathbf{F}$ lie on the circle of radius $\frac{|\gamma|^2}{2k}$ and center $\frac{|\gamma|^2}{2ik}$. We set $\lambda_j := \frac{|\gamma|^2}{2ik}(e^{i\delta_j} - 1)$ with $e^{i\delta_j}$ being an eigenvalue of $\mathbf{S}$, $\delta_j \in [0, 2\pi)$ and define

$$\begin{cases} \delta_*(\mu) & := \max_{j\geq 1}\delta_j, \\ \lambda_* & := \frac{|\gamma|^2}{2ik}(e^{i\delta_*} - 1). \end{cases} \tag{4.30}$$

We then can state the main theorem of this section:

Theorem 29. *Assume that k^2 is not an eigenvalue of (1.35). μ_0 is a $\mathcal{B}-$eigenvalue if and only if $\delta_*(\mu) \to 2\pi$ as $\mu \to \mu_0$ with $\mu > \mu_0$.*

This theorem is a straightforward corollary of Proposition 34 (sufficient condition) and Proposition 36 (necessary condition). In order to prove these propositions, we first establish some properties of the operator $T_{\mathcal{B}}$ in the factorization (4.29).

4.4.1 Some key properties of the operator $T_{\mathcal{B}}$

One of the important ingredients of the inside-outside duality is the link between the kernel of the operator $T_{\mathcal{B}}$ and the $\mathcal{B}-$eigenvalues. The latter is proved in the following lemmas.

To shorten the notations, the duality product $\langle ., . \rangle_{H^{\frac{1}{2}}(\partial D_b), H^{-\frac{1}{2}}(\partial D_b)}$ will be denoted $\langle ., . \rangle$ or in an abuse of notation as an integral over ∂D_b.

Lemma 30. *The operator $T_{\mathcal{B}}$ satisfies the energy identity:*

$$\Im m\,\langle T_{\mathcal{B}}\psi,\psi\rangle = k\int_{\mathbb{S}}|w^{\infty}|^2 ds,\quad \forall\psi\in H^{-\frac{1}{2}}(\partial D_b), \tag{4.31}$$

where w^{∞} is the far field pattern of w^s, with (w,w^s) being the solution of (4.14) with source term ψ.

Proof. Let $\psi\in H^{-\frac{1}{2}}(\partial D_b)$, using that $\psi=\partial_\nu w-\partial_\nu w^s$, we get

$$\langle T_{\mathcal{B}}\psi,\psi\rangle = \int_{\partial D_b}\partial_\nu\overline{w}(w+\frac{1}{\mu}\mathcal{B}(\partial_\nu w))ds - \int_{\partial D_b}\partial_\nu\overline{w^s}(w^s+\frac{1}{\mu}\mathcal{B}(\partial_\nu w^s))ds. \tag{4.32}$$

Let us focus on the last term of the previous equality. Using Green's formula on a ball B_R of radius $R>0$ large enough, one obtains:

$$\begin{aligned} 0 &= -\textstyle\int_{B_R\setminus D_b} w^s(\Delta\overline{w^s}+k^2n\overline{w^s})dx\\ &= \textstyle\int_{B_R\setminus D_b}|\nabla w^s|^2dx - k^2\int_{B_R\setminus D_b} n|w^s|^2dx\\ &+ik\textstyle\int_{\partial B_R}|w^s|^2ds - \int_{\partial B_R}(\partial_\nu\overline{w^s}+ik\overline{w^s})w^s ds\\ &+\textstyle\int_{\partial D_b}\partial_\nu\overline{w^s}w^s ds. \end{aligned} \tag{4.33}$$

Substituting the expression of $\int_{\partial D_b}\partial_\nu\overline{w^s}w^s ds$ in (4.32) gives

$$\begin{aligned} \langle T_{\mathcal{B}}\psi,\psi\rangle &= \textstyle\int_{\partial D_b}\partial_\nu\overline{w}w ds\\ &+\textstyle\int_{B_R\setminus D_b}|\nabla w^s|^2dx - k^2\int_{B_R\setminus D_b} n|w^s|^2dx\\ &+ik\textstyle\int_{\partial B_R}|w^s|^2ds - \int_{\partial B_R}(\partial_\nu\overline{w^s}+ik\overline{w^s})w^s ds\\ &+\textstyle\frac{1}{\mu}\int_{\partial D_b}\mathcal{B}(\partial_\nu w)\partial_\nu\overline{w} - \frac{1}{\mu}\int_{\partial D_b}\mathcal{B}(\partial_\nu w^s)\partial_\nu\overline{w^s}. \end{aligned} \tag{4.34}$$

Taking the imaginary part of this equality while letting $R\to+\infty$, we obtain

$$\begin{aligned} \Im m\,\langle T_{\mathcal{B}}\psi,\psi\rangle &= k\textstyle\int_{\mathbb{S}}|w^{\infty}|^2ds + \Im m\int_{\partial D_b}\partial_\nu\overline{w}w ds,\\ &= k\textstyle\int_{\mathbb{S}}|w^{\infty}|^2ds - k^2\int_{D_b}\Im m(n)|w|^2dx, \end{aligned} \tag{4.35}$$

where for the last equality, we used that $\Delta w+k^2nw=0$ in D_b. □

Proposition 31. *Let $\mu\in\mathbb{R}^*$. μ is a $\mathcal{B}-$eigenvalue if and only if there exists a non trivial $\psi\in H^{-\frac{1}{2}}(\partial D_b)$ such that $\Im m\,\langle T_{\mathcal{B}}\psi,\psi\rangle=0$.*

Proof. Assume that μ is a $\mathcal{B}-$eigenvalue. We denote by $w_0\in H^1(D_b)$ its associated eigenvector. Set $\psi=\partial_\nu w_0|_{\partial D_b}$ which is necessarily non trivial. Consider (w,w^s) the associated solution of (4.14). We then get thanks to Green's theorem:

$$\begin{aligned} \langle T_{\mathcal{B}}\psi,\psi\rangle &= \textstyle\int_{\partial D_b} w\partial_\nu\overline{w_0}ds + \frac{1}{\mu}\int_{\partial D_b}\partial_\nu\overline{w_0}\mathcal{B}(\partial_\nu w)ds\\ &= \textstyle\int_{\partial D_b}\overline{w_0}\partial_\nu w ds + \frac{1}{\mu}\int_{\partial D_b}\partial_\nu w\mathcal{B}(\partial_\nu\overline{w_0})ds = 0, \end{aligned} \tag{4.36}$$

where we used the fact that $\mathcal{B}$ is self-adjoint and the fact w, w_0 verify the same inhomogeneous Helmholtz equation in D_b. Conversely, assume there exists $\psi \in H^{-\frac{1}{2}}(\partial D_b)$ non trivial such that $\Im m \langle T_{\mathcal{B}}\psi, \psi\rangle = 0$. By Rellich lemma, this implies $w^s = 0$ in $\mathbb{R}^m \backslash D_b$ where (w, w^s) is the solution of (4.14) with source term ψ. In particular, we get $w^s|_{\partial D_b} = 0$ and $\partial_\nu w^s|_{\partial D_b} = 0$. Thus, μ is a $\mathcal{B}-$eigenvalue associated with the non trivial eigenvector w. □

We conclude this section by showing that $T_{\mathcal{B}}$ is a Fredholm operator of index 0.

Lemma 32. *$T_{\mathcal{B}}$ admits the following decomposition*

$$T_{\mathcal{B}} = T_0 + K, \tag{4.37}$$

where K is compact and T_0 is coercive. More precisely, there exists a $\alpha > 0$ such that

$$\langle T_0\psi, \psi\rangle \geq \alpha \|\psi\|^2_{H^{-\frac{1}{2}}(\partial D_b)}. \tag{4.38}$$

Proof. Let $\psi, \psi' \in H^{-\frac{1}{2}}(\partial D_b)$ and (w, w^s) (respectively (w', w'^s)) the solution of (4.14) with source term ψ (respectively ψ'). Exploiting the definition of $T_{\mathcal{B}}$, one can deduce:

$$\begin{aligned}\langle T_{\mathcal{B}}\psi, \psi'\rangle &= \int_{\partial D_b} \overline{\psi'}(w + \tfrac{1}{\mu}\mathcal{B}(\partial_\nu w))ds = \int_{\partial D_b} \overline{\psi'}(w^s + \tfrac{1}{\mu}\mathcal{B}(\partial_\nu w^s))ds,\\ &= \int_{\partial D_b} \partial_\nu \overline{w'} w ds - \int_{\partial D_b} \partial_\nu \overline{w'^s} w^s ds\\ &+\tfrac{1}{\mu}\int_{\partial D_b} \partial_\nu \overline{w'}\mathcal{B}(\partial_\nu w)ds - \tfrac{1}{\mu}\int_{\partial D_b} \partial_\nu \overline{w'^s}\mathcal{B}(\partial_\nu w^s)ds.\end{aligned} \tag{4.39}$$

Let B_R be a ball containing D_b for R large enough. We define the operator $T_0 : H^{-\frac{1}{2}}(\partial D_b) \to H^{\frac{1}{2}}(\partial D_b)$ as:

$$\begin{aligned}\langle T_0\psi, \psi'\rangle = &\int_{B_R\backslash D_b} \nabla w^s \nabla \overline{w'^s} dx + \int_{B_R\backslash D_b} w^s \overline{w'^s} dx\\ &+ \int_{D_b} \nabla w \nabla \overline{w'} dx + \int_{D_b} w\overline{w'} dx,\end{aligned} \tag{4.40}$$

and $K : H^{-\frac{1}{2}}(\partial D_b) \to H^{\frac{1}{2}}(\partial D_b)$ as:

$$\begin{aligned}\langle K\psi, \psi'\rangle = &-(1+k^2)\int_{B_R\backslash D_b} w^s \overline{w'^s} dx\\ &-(1+k^2)\int_{D_b} nw\overline{w'} dx\\ &-\int_{\partial B_R} \partial_\nu \overline{w'^s} w^s ds\\ &+\tfrac{1}{\mu}\int_{\partial D_b} \partial_\nu \overline{w'}\mathcal{B}(\partial_\nu w)ds - \tfrac{1}{\mu}\int_{\partial D_b} \partial_\nu \overline{w'^s}\mathcal{B}(\partial_\nu w^s)ds.\end{aligned} \tag{4.41}$$

Thus, one can write $T_{\mathcal{B}} = T_0 + K$.
Since $\psi = \partial_\nu w - \partial_\nu w^s$, we deduce that

$$\begin{aligned}\|\psi\|^2_{H^{-\frac{1}{2}}(\partial D_b)} &\leq 2(\|\partial_\nu w\|^2_{H^{-\frac{1}{2}}(\partial D_b)} + \|\partial_\nu w^s\|^2_{H^{-\frac{1}{2}}(\partial D_b)}),\\ &\leq 2(\|\nabla w\|^2_{L^2(D_b)} + \|\Delta w\|^2_{L^2(D_b)} + \|\nabla w^s\|^2_{L^2(B_R\backslash D_b)} + \|\Delta w^s\|^2_{L^2(B_R\backslash D_b)}).\end{aligned} \tag{4.42}$$

Using the fact that w and w^s satisfy the Helmholtz equation, one can therefore deduce the existence of some $\alpha > 0$ such that

$$\begin{aligned} \alpha \|\psi\|^2_{H^{-\frac{1}{2}}(\partial D_b)} &\leq (\|w\|^2_{H^1(D_b)} + \|w^s\|^2_{H^1(B_R \setminus D_b)}), \\ &= \langle T_0 \psi, \psi \rangle . \end{aligned} \tag{4.43}$$

The compactness of the operator K is a direct consequence of a priori estimates in Lemma 27, trace theorems, Rellich's compact embedding theorems and the compactness of the operator $\mathcal{B}$. □

One of the consequences of the previous decomposition of $T_{\mathcal{B}}$ in Lemma 32 is that if μ is not a $\mathcal{B}-$eigenvalue, the eigenvalues λ_j of the operator $\mathbf{F}$ accumulate at 0 from the right, that is $\Re e(\lambda_j) > 0$ for j large enough ([41, 43]). This is equivalent to say that δ_j (the argument of λ_j) converges to 0 as j goes to $+\infty$. In contrast, Theorem 29 states that when μ approaches a $\mathcal{B}-$eigenvalue, the eigenvalue $\lambda_*(\mu)$ approaches 0 from the left as illustrated in Figure 4.1. In addition, if μ is not a $\mathcal{B}-$eigenvalue, Lemma 6 and 8 imply $T_{\mathcal{B}}$ is coercive [41], that is there exists a constant $\alpha > 0$ such that for all $\psi \in H^{-\frac{1}{2}}(\partial D_b)$

$$| \langle T_{\mathcal{B}} \psi, \psi \rangle | \geq \alpha \|\psi\|^2_{H^{-\frac{1}{2}}(\partial D_b)}. \tag{4.44}$$

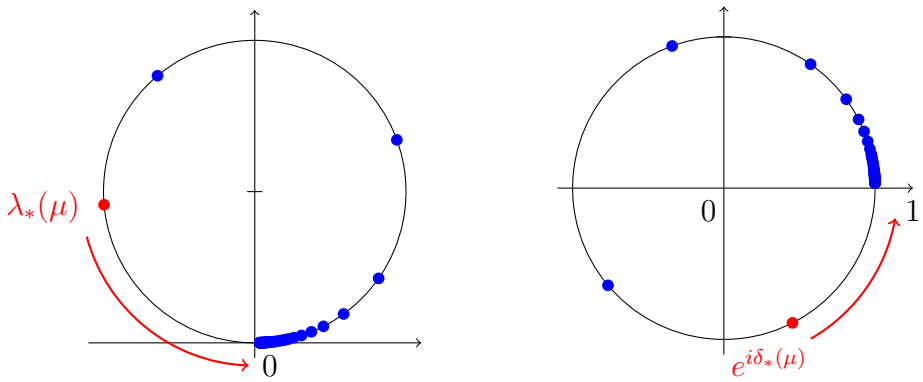

Figure 4.1: Illustration of Theorem 29. Left: The eigenvalues of $\mathbf{F}$ accumulates at 0 from the right (in blue) while $\lambda_*(\mu)$ (in red) approaches 0 from the left as μ approaches the $\mathcal{B}-$eigenvalue. Right: The argument of the eigenvalues of $\mathbf{S}$ accumulates at 0 (in blue) while $\delta_*(\mu)$ (in red) approaches 2π as μ approaches the $\mathcal{B}-$eigenvalue.

We dedicate the two next subsections to the proof of Theorem 29.

4.4.2 Proof of the sufficient condition in Theorem 29

Since we will be dealing with convergence of sequences that depend on μ, we shall explicitly indicate the dependence on μ in the notation for the operators (in particular, the operator $\mathbf{F}(\mu)$ is factorized as $\mathcal{H}^*_{\mathcal{B}}(\mu) T_{\mathcal{B}}(\mu) \mathcal{H}_{\mathcal{B}}(\mu)$).

Proposition 33. *The mapping $\mu \to T_{\mathcal{B}}(\mu)$ is continuous from $\mathbb{R}^*$ to the space of linear bounded operators from $H^{-\frac{1}{2}}(\partial D_b)$ to $H^{\frac{1}{2}}(\partial D_b)$ endowed with the usual operator norm.*

Proof. The proof is a direct consequence of the linear dependence with respect to $\frac{1}{\mu}$ of the solution (w, w^s) of problem (4.14) (see (4.15)) and the expression of $T_{\mathcal{B}}(\mu)$. □

Proposition 34. *Let $\mu_0 \in \mathbb{R}^*$ and $I = (\mu_0 - \varepsilon, \mu_0 + \varepsilon)\backslash\{\mu_0\}$ for some $\varepsilon > 0$ sufficient small such that no $\mu \in I$ is a $\mathcal{B}-$eigenvalue and such that $0 \notin I$. Assume there is a sequence $(\mu_j)_j$ of elements of I such that*

$$\mu_j \longrightarrow \mu_0 \qquad \text{and} \qquad \delta_*(\mu_j) \longrightarrow 2\pi. \tag{4.45}$$

Then μ_0 is a $\mathcal{B}-$eigenvalue.

Proof. Consider the sequence $\varphi_j = \frac{1}{\sqrt{|\lambda_*|}}\mathcal{H}_{\mathcal{B}}(\mu_j)g_j$, where g_j is the normalized eigenvector of $\mathbf{F}(\mu_j)$ associated with $\lambda_*(\mu_j)$. We then have by assumptions

$$\langle T_{\mathcal{B}}(\mu_j)\varphi_i, \varphi_i\rangle = \frac{\lambda_*(\mu_j)}{|\lambda_*(\mu_j)|} \longrightarrow_{j\to+\infty} -1. \tag{4.46}$$

Assume by contradiction that μ_0 is not a $\mathcal{B}-$eigenvalue.
In that case, the operator $T_{\mathcal{B}}(\mu_j)$ is coercive for every $\mu_j \in I$. Using that $\mu \to T_{\mathcal{B}}(\mu)$ is continuous in the operator norm, we infer that the coercivity constant can be chosen independent from $\mu \in \overline{I}$ (see Lemma 41). The coercivity of $T_{\mathcal{B}}(\mu_j)$ and identity (4.46) show that $(\varphi_j)_j$ is bounded and therefore weakly converges (up to a subsequence) to some φ_0 in $H^{-\frac{1}{2}}(\partial D_b)$. Denote by (w_j, w_j^s) (respectively (w_0, w_0^s)) the solution of (4.14) with $\psi = \varphi_j$ (respectively $\psi = \varphi_0$). From Lemma 30, one gets:

$$\Im m\, \langle T_{\mathcal{B}}(\mu_j)\varphi_j, \varphi_j\rangle = k \int_{\mathbb{S}} |w_j^\infty|^2 ds. \tag{4.47}$$

Since the application $\psi \in H^{-\frac{1}{2}}(\partial D_b) \to w^\infty(\psi) \in L^2(\mathbb{S})$ (where $w^\infty(\psi)$ is the far field pattern of w^s solution of (4.14) with source term ψ) is compact, then $\Im m\, \langle T_{\mathcal{B}}(\mu_j)\varphi_j, \varphi_j\rangle$ converges to $\Im m\, \langle T_{\mathcal{B}}(\mu_0)\varphi_0, \varphi_0\rangle$. Identity (4.46) implies that $\lim_{j\to+\infty} \Im m\, \langle T_{\mathcal{B}}(\mu_j)\varphi_j, \varphi_j\rangle = 0$ and therefore $\varphi_0 = 0$ by Proposition 31.
Recall that $T_{\mathcal{B}}(\mu_j)$ assumes the decomposition $T_{\mathcal{B}}(\mu_j) = T_0(\mu_j) + K(\mu_j)$, where $T_0(\mu_j)$ is real coercive and $K(\mu_j)$ is compact. Let us show that $\lim_{j\to+\infty} \langle K(\mu_j)\varphi_j, \varphi_j\rangle = 0$. From the decomposition shown in Lemma 32, we get that

$$\begin{aligned}
\langle K(\mu_j)\varphi_j, \varphi_j\rangle = \; & -(1+k^2)\|w_j^s\|^2_{H^1(B_R\backslash D_b)} \\
& -(1+k^2)(nw_j, w_j)_{H^1(D_b)} \\
& -\textstyle\int_{\partial B_R} \partial_\nu \overline{w_j^s} w_j^s ds \\
& +\tfrac{1}{\mu_j}\textstyle\int_{\partial D_b} \partial_\nu \overline{w_j}\mathcal{B}(\partial_\nu w_j) ds - \tfrac{1}{\mu_j}\textstyle\int_{\partial D_b} \partial_\nu \overline{w_j^s}\mathcal{B}(\partial_\nu w_j^s) ds.
\end{aligned} \tag{4.48}$$

The first three terms converge to 0 by the same arguments as in the proof of the compactness of $K(\mu_j)$ for μ_j fixed in Lemma 32. We conclude in the same way for the last two terms using that the sequence $\frac{1}{\mu_j}$ converges to $\frac{1}{\mu_0}$. This shows that $\lim_{j\to+\infty}\langle K(\mu_j)\varphi_j,\varphi_j\rangle = 0$. We deduce that (up to a subsequence) $\langle T_0(\mu_j)\varphi_j,\varphi_j\rangle$ converges to -1 which is a contradiction since $\langle T_0(\mu_j)\varphi_j,\varphi_j\rangle \geq 0$ for all $j\in\mathbb{N}$ (Lemma 32). □

4.4.3 Proof of the necessary condition in Theorem 29

For the proof of the necessary condition, we use the Cayley transform associated with $\mathbf{S}$ ([43]).
Assume that μ is not a $\mathcal{B}-$eigenvalue. Then 1 is not an eigenvalue of $\mathbf{S}$ because $\mathbf{F}$ is injective and we can define the Cayley transform:

$$\mathcal{T} := i(Id+\mathbf{S})(Id-\mathbf{S})^{-1}.$$

$\mathcal{T}$ is self-adjoint and has a discrete spectrum. We have the equivalence $e^{i\delta_*}$ is an eigenvalue of $\mathbf{S}$ if and only if $\cot(\delta_*/2)\in\mathbb{R}$ is an eigenvalue of $\mathcal{T}$. Applying Courant Fischer min max principle to $\mathcal{T}$, we get:

$$\cot(\delta_*/2) = \inf_{\psi\in H^{-\frac{1}{2}}(\partial D_b)} \frac{\Re e\,\langle T\psi,\psi\rangle}{\Im m\,\langle T\psi,\psi\rangle}. \tag{4.49}$$

Let μ_0 be a $\mathcal{B}-$eigenvalue associated with the eigenvector w_0. For $\mu\in\mathbb{R}^*$, define $(w(\mu),w^s(\mu))$ the solution of (4.14) with source term $\psi=\partial_\nu w_0$. From the linearity of those solutions with respect to $\frac{1}{\mu}$ (see decomposition (4.15)), one can obtain the following expansion:

$$w(\mu)-w_0 = (\frac{1}{\mu}-\frac{1}{\mu_0})w_N^0, \tag{4.50}$$

where w_N^0 does not depend on μ and is solution of (4.15) with $\psi=\partial_\nu w_0$.

Proposition 35. *Let μ_0 be a $\mathcal{B}-$eigenvalue associated with w_0. For $\mu\in\mathbb{R}^*$, define $(w(\mu),w^s(\mu))$ the solution of (4.14) with source term $\psi=\partial_\nu w_0$ and parameter μ. Then :*

$$\langle T_{\mathcal{B}}(\mu)\partial_\nu w_0,\partial_\nu w_0\rangle = (\frac{1}{\mu}-\frac{1}{\mu_0})\langle\mathcal{B}(\partial_\nu w_0),\partial_\nu w_0\rangle + (\frac{1}{\mu}-\frac{1}{\mu_0})^2\langle\mathcal{B}(\partial_\nu w_N^0),\partial_\nu w_0\rangle. \tag{4.51}$$

Proof. According to the definition of $T_{\mathcal{B}}(\mu)$, we get:

$$\langle T_{\mathcal{B}}(\mu)\partial_\nu w_0,\partial_\nu w_0\rangle = \left\langle w(\mu)+\frac{1}{\mu}\mathcal{B}(\partial_\nu w(\mu)),\partial_\nu w_0\right\rangle. \tag{4.52}$$

Since $-\langle T_{\mathcal{B}}(\mu_0)\partial_\nu w_0,\partial_\nu w_0\rangle = 0$, we can add it to the previous equality and by rearranging the terms, one has

$$\langle T_{\mathcal{B}}(\mu)\partial_\nu w_0,\partial_\nu w_0\rangle = \left\langle (w(\mu)-w_0)+\frac{1}{\mu}\mathcal{B}(\partial_\nu w(\mu)-\partial_\nu w_0),\partial_\nu w_0\right\rangle + (\frac{1}{\mu}-\frac{1}{\mu_0})\langle\mathcal{B}(\partial_\nu w_0),\partial_\nu w_0\rangle. \tag{4.53}$$

The previous equality can be rewritten using (4.50) as:

$$\langle T_{\mathcal{B}}(\mu)\partial_\nu w_0, \partial_\nu w_0\rangle = (\frac{1}{\mu} - \frac{1}{\mu_0})\left(\left\langle w_N^0 + \frac{1}{\mu}\mathcal{B}(\partial_\nu w_N^0), \partial_\nu w_0\right\rangle + \langle \mathcal{B}(\partial_\nu w_0), \partial_\nu w_0\rangle\right). \tag{4.54}$$

Using Green's theorem, we have:

$$\begin{aligned} 0 &= -\int_{D_b}(\Delta w_N^0 + k^2 n w_N^0)\overline{w_0}dx = \int_{\partial D_b}(\partial_\nu \overline{w_0} w_N^0 - \partial_\nu w_N^0 \overline{w_0})ds \\ &= \left\langle w_N^0 + \tfrac{1}{\mu_0}\mathcal{B}(\partial_\nu w_N^0), \partial_\nu w_0\right\rangle. \end{aligned} \tag{4.55}$$

Expression (4.51) is obtained by substituting $\langle w_N^0, \partial_\nu w_0\rangle$ in (4.54). □

We possess all the ingredients to prove the following necessary condition.

Proposition 36. *Assume that μ_0 is a $\mathcal{B}-$eigenvalue and k^2 is not an eigenvalue of (1.35). Then $\delta_*(\mu) \to 2\pi$ as $\mu \to \mu_0$ with $\mu > \mu_0$.*

Proof. The proof uses the positiveness of the $\mathcal{B}$ operator. Let us first show that the first term in the decomposition (4.51) is non zero. Assume by contradiction that $\langle \mathcal{B}(\partial_\nu w_0), \partial_\nu w_0\rangle = 0$. Using the form of $\mathcal{B}$ in (4.2), one has that $\langle \partial_\nu w_0, e_i\rangle = 0$ for all $i \leq M$ which implies $\mathcal{B}(\partial_\nu w_0) = 0$. Using that $\mu_0 \neq 0$, one obtains thanks to the boundary condition that $w_0|_{\partial D_b} = 0$ which contradicts the assumption on k^2. Hence, we have $\langle \mathcal{B}(\partial_\nu w_0), \partial_\nu w_0\rangle > 0$. Let μ_0 be a $\mathcal{B}-$eigenvalue associated with the eigenvector w_0. Then we have for μ in a neighbourhood of μ_0:

$$\cot(\delta_*(\mu)/2) = \inf_{\psi \in H^{-\frac{1}{2}}(\partial D_b)} \frac{\Re\langle T_{\mathcal{B}}(\mu)\psi, \psi\rangle}{\Im m\langle T_{\mathcal{B}}(\mu)\psi, \psi\rangle} \leq \frac{\Re\langle T_{\mathcal{B}}(\mu)\partial_\nu w_0, \partial_\nu w_0\rangle}{\Im m\langle T_{\mathcal{B}}(\mu)\partial_\nu w_0, \partial_\nu w_0\rangle}, \tag{4.56}$$

with $\Im m\langle T_{\mathcal{B}}(\mu)\partial_\nu w_0, \partial_\nu w_0\rangle > 0$ thanks to Lemma 30. From the previous Lemma, we conclude that:

$$\frac{\Re\langle T_{\mathcal{B}}(\mu)\partial_\nu w_0, \partial_\nu w_0\rangle}{\Im m\langle T_{\mathcal{B}}(\mu)\partial_\nu w_0, \partial_\nu w_0\rangle} = \frac{\langle \mathcal{B}(\partial_\nu w_0), \partial_\nu w_0\rangle + (\frac{1}{\mu} - \frac{1}{\mu_0})\Re e(\langle \mathcal{B}(\partial_\nu w_N^0), \partial_\nu w_0\rangle)}{(\frac{1}{\mu} - \frac{1}{\mu_0})\Im m\langle T_{\mathcal{B}}(\mu)\partial_\nu w_0, \partial_\nu w_0\rangle} \to -\infty, \tag{4.57}$$

as $\mu \to \mu_0$ with $\mu > \mu_0$. Combined with 4.56, this proves the claim of the proposition. □

We end this section by a result that indicates how one can also recover an eigenvector w_0 associated with μ. The proof is similar to the one in [6].

Proposition 37. *Let μ_0 be a $\mathcal{B}-$eigenvalue. Take the sequence*

$$\psi_j = \frac{H(\mu_j)g_j}{\|H(\mu_j)g_j\|_{H^{-\frac{1}{2}}(\partial D_b)}}, \tag{4.58}$$

and (w_j, w_j^s) the associated solution of (4.14) with source term ψ_j. Then, ψ_j admits a subsequence which converges strongly in $H^{-\frac{1}{2}}(\partial D_b)$ to $\partial_\nu w_0$, the normal trace of an eigenvector w_0 of (4.4). Here, g_j is the normalised eigenvector of $\mathbf{F}(\mu_j)$ associated with $\lambda_*(\mu_j)$.

Proof. Since the sequence $(\psi_j)_j$ is bounded, it weakly converges (up to a subsequence) in $H^{-\frac{1}{2}}(\partial D_b)$ to some ψ_0 (and w_j, w_j^s converge weakly to some w_0, w_0^s in $H^1(D_b) \times H^1(B_R \backslash D_b)$. Observe that:

$$\langle T_{\mathcal{B}}(\mu_j)\psi_j, \psi_j \rangle = \theta_j \frac{\lambda_*(\mu_j)}{|\lambda_*(\mu_j)|}, \tag{4.59}$$

where $\theta_j := |\lambda_*(\mu_j)|/\|H(\mu_j)g_j\|^2_{H^{-\frac{1}{2}}(\partial D_b)}$ is real and $\frac{\lambda_*(\mu_j)}{|\lambda_*(\mu_j)|}$ converges to -1 by Theorem 29. Using similar arguments as in Proposition 34, one can prove from equation (4.59) that $\Im m \langle T_{\mathcal{B}}(\mu_0)\psi_0, \psi_0 \rangle = 0$ and therefore w_0 satisfies (4.4). Let us show that $(\psi_j)_j$ converges strongly to ψ_0 and that ψ_0 is non trivial.
Using the fact that $\mu \to T_{\mathcal{B}}(\mu)$ is continuous, up to a subsequence, one can show that the sequence $(\theta_j)_j$ converges to some $\theta_0 \geq 0$. From the decomposition in Lemma 32, we have:

$$\langle T_0(\mu_j)\psi_j, \psi_j \rangle = \langle T_{\mathcal{B}}(\mu_j)\psi_j, \psi_j \rangle - \langle K(\mu_j)\psi_j, \psi_j \rangle , \tag{4.60}$$

where $\langle T_{\mathcal{B}}(\mu_j)\psi_j, \psi_j \rangle$ converges to some negative number and $\langle K(\mu_j)\psi_j, \psi_j \rangle$ converges to $\langle K(\mu_0)\psi_0, \psi_0 \rangle$ (see the proof of Proposition 34). Therefore, we deduce that $\lim_{j\to+\infty} \langle T_0(\mu_j)\psi_j, \psi_j \rangle$ exists and that

$$\lim_{j\to+\infty} \langle T_0(\mu_j)\psi_j, \psi_j \rangle \leq - \langle K(\mu_0)\psi_0, \psi_0 \rangle . \tag{4.61}$$

One can observe using the definition of $K(\mu_0)$ that $\langle K(\mu_0)\psi_0, \psi_0 \rangle = -\|w_0\|^2_{H^1(D_b)}$ and, using the coercivity of T_0, show that

$$\lim_{j\to+\infty} \left(\|w_j\|^2_{H^1(D_b)} + \|w_j^s\|^2_{H^1(B_R\backslash D_b)} \right) \leq \|w_0\|^2_{H^1(D_b)}, \tag{4.62}$$

which is enough to prove the strong convergence of w_j toward w_0 in $H^1(D_b)$ and the strong convergence of w_j^s in $H^1(B_R\backslash D_b)$ toward 0. Those convergences are sufficient to demonstrate that $\psi_j = \partial_\nu w_j - \partial_\nu w_j^s$ strongly converges to $\psi_0 = \partial_\nu w_0$. Since for all $j \in \mathbb{N}$, $\|\psi_j\|_{H^{-\frac{1}{2}}(\partial D_b)} = 1$, we have $\psi_0 \neq 0$. □

Remark 8. *In the context of imaging algorithms, the assumption $D \subset D_b$, while practical for the presentation of results, is both restrictive and inappropriate, as obstacles may exist outside the region D_b. To properly formalize this scenario while maintaining the structure of the proofs, particularly to keep an eigenvalue problem within D_b, we exclude the cases where D intersects ∂D_b (as depicted in Figure 1.7) and the transmission eigenvalues ([15]) k^2 associated with the operator F.*
The contribution of the obstacles $\Omega_D := D\backslash D_b$ (the component of D outside of D_b) leads to the following modifications of the operators $\mathcal{H}_{\mathcal{B}} : L^2(\mathbb{S}) \to H^{-\frac{1}{2}}(\partial D_b) \times L^2(\Omega_D)$ and $T_{\mathcal{B}} : H^{-\frac{1}{2}}(\partial D_b) \times \overline{\mathcal{R}(\mathcal{H}_{\mathcal{B}})} \to H^{\frac{1}{2}}(\partial D_b) \times L^2(\Omega_D)$:

$$\begin{cases} \mathcal{H}_{\mathcal{B}} g = (\partial_\nu u_{b,g}|_{\partial D_b}, u_{b,g}|_{\Omega_D}), \\ T_{\mathcal{B}}(\psi, u) = (w + \frac{1}{\mu}\mathcal{B}(\partial_\nu w), -k^2(1-n)(u+w^s)|_{\Omega_D}), \end{cases} \tag{4.63}$$

where (w, w^s) *are solution of:*

$$\begin{cases} \Delta w + k^2 n w = 0 \text{ in } D_b, \\ \Delta w^s + k^2 w^s = k^2(1-n)(u+w^s)|_{\Omega_D} \text{ in } \mathbb{R}^m \backslash D_b, \\ w^s + \frac{1}{\mu}\mathcal{B}(\partial_\nu w^s) = w + \frac{1}{\mu}\mathcal{B}(\partial_\nu w) \text{ on } \partial D_b, \\ \partial_\nu w - \partial_\nu w^s = \psi \text{ on } \partial D_b, \\ \lim\limits_{r\to+\infty} \int_{|x|=r} |\frac{\partial w^s}{\partial r} - ikw^s|^2 = 0, \end{cases} \tag{4.64}$$

and $\overline{\mathcal{R}(\mathcal{H}_\mathcal{B})}$ *denotes the closure of the range of* $\mathcal{H}_\mathcal{B}$ *in* $L^2(\Omega_D)$*. The decomposition in Lemma 32 still holds provided that* $n > 1$ *in* Ω_D*.*

4.5 Numerical validation of the inside-outside duality method

The goal of this section is to provide a numerical validation for the inside-outside duality method inspired by Theorem 29. Our numerical experiments will be conducted in dimension 2, meaning for $m = 2$.

4.5.1 The case of a disc

Consider the simple situation where $D = D_b = B_\rho$ is a disk of radius $\rho > 0$ centered at the origin. We assume that n is constant inside B_ρ and $n = 1$ outside. For $\mathcal{Q}$ a subset of $\mathbb{N}$, we use as operator $\mathcal{B}$ in the background problem (4.1) the one defined by

$$\mathcal{B}\psi = \sum_{q\in\mathcal{Q}} \langle \psi, e_q \rangle \, e_q, \tag{4.65}$$

where $e_q(\theta) := e^{iq\theta}$, $\theta \in [0, 2\pi)$. In that case, the $\mathcal{B}-$eigenvalues, denoted $\mu_{\text{ref,q}}$ assume the analytical expression (16) for $q \in \mathcal{Q}$.
The far field pattern Fg due to a Herglotz wave function of the form (1.5) as an incident field with density

$$g(\theta) = \sum_{m\in\mathbb{Z}} g_m e^{im\theta}, \tag{4.66}$$

takes the form

$$Fg(\theta) = \sum_{m\in\mathbb{Z}} \alpha_m g_m e^{im\theta}, \tag{4.67}$$

where

$$\alpha_m = i^m \sqrt{\frac{8\pi}{k}} e^{-i\frac{\pi}{4}} \frac{J_m'(k\rho)J_m(k\rho\sqrt{n}) - \sqrt{n}J_m(k\rho)J_m'(k\rho\sqrt{n})}{-J_m(k\rho\sqrt{n})H_m'^1(k\rho) + \sqrt{n}J_m'(k\sqrt{n}\rho)H_m^1(k\rho)}. \tag{4.68}$$

Similarly, one can derive an expression of the background far field as:

$$F_b^\mu g(\theta) = \sum_{m\in\mathbb{Z}} \beta_m g_m e^{im\theta}, \tag{4.69}$$

where

$$\begin{cases} \beta_m = -i^m \sqrt{\frac{8\pi}{k}} e^{-i\frac{\pi}{4}} \frac{\mu J_m(k\rho)+2\pi\rho k J'_m(k\rho)}{\mu H_m^{(1)}(k\rho)+2\pi\rho k H_m'^{(1)}(k\rho)}, & m \in \mathcal{Q} \\ \beta_m = -i^m \sqrt{\frac{8\pi}{k}} e^{-i\frac{\pi}{4}} \frac{J_m(k\rho)}{H_m^{(1)}(k\rho)} \quad \text{otherwise} , \end{cases} \tag{4.70}$$

We clearly observe that the eigenvalues of $\mathcal{F}^\mu$ are $(\alpha_m - \beta_m)$, $m \in \mathbb{Z}$ and they are respectively associated with the eigenvector e_m. Consequently, the eigenvalues of the scattering operator $\mathbf{S}$ are

$$e^{i\delta_m} := 1 + \frac{2ik}{\overline{\gamma}}(1 - \frac{2ik}{\gamma}\overline{\beta_m})(\alpha_m - \beta_m)$$

where $\delta_m \in [0, 2\pi)$ denote their corresponding phases. Observe that only the eigenvalues for $m \in \mathcal{Q}$ depend on μ.

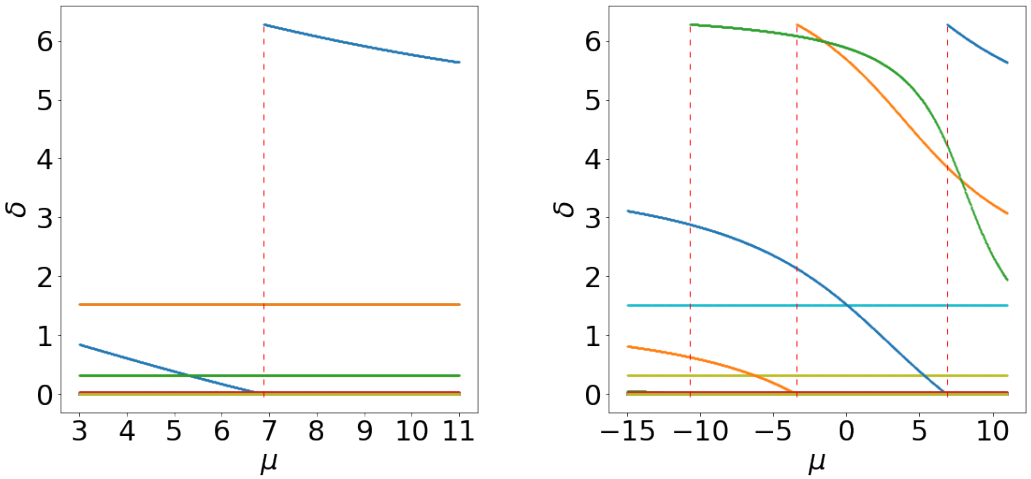

Figure 4.2: For $m \in \{-10, ...10\}$, we plot the curves $\mu \to \delta_m(\mu)$ where $D = D_b = B_\rho$ for $\rho = 0.4333$, $k = 3$ and $n = 1$. Each color (other than red) corresponds to a value of m. The red dashed line indicates the $\mathcal{B}-$eigenvalue (16) for $\mathcal{Q} = \{0\}$ (left) and $\mathcal{Q} = \{0, 1, 2\}$ (right).

In Figure 4.2 (left), we display the curves $\mu \to \delta_m(\mu)$ for $m \in \{-10, ...10\}$ and $\mathcal{Q} = \{0\}$. We clearly see that the curves for $m \neq 0$ are horizontal lines, meaning that they do not depend on μ. The only non constant curve $\delta_0(\mu)$ has a discontinuity at the expected $\mathcal{B}-$eigenvalue $\mu_{\text{ref},0}(2)$. In addition, we observe that $\delta_0(\mu) \to 2\pi$ as $\mu \to \mu_{\text{ref},0}(2)$ and $\mu > \mu_{\text{ref},0}(2)$, which coincides with Theorem 29. In Figure 4.2 (right), one can draw similar conclusions with $\mathcal{Q} = \{0, 1, 2\}$ and the presence of 3 distinct $\mathcal{B}-$eigenvalues.

4.5.2 The case of other geometries using synthetic simulated data

We consider a domain D_b shown in Figure 4.3 is composed of small circular scatterers with $n = 2$ that occupy four different regions in the space (see Figure 4.3). The operator F cannot

be computed analytically in this case. It is numerically generated by solving the scattering problem (1.1) using a finite element method implemented with the Freefem++ [37] package. We use the Perfectly Matched Layer ([13]) technique to bound the computational domain and model the Sommerfeld radiation condition.

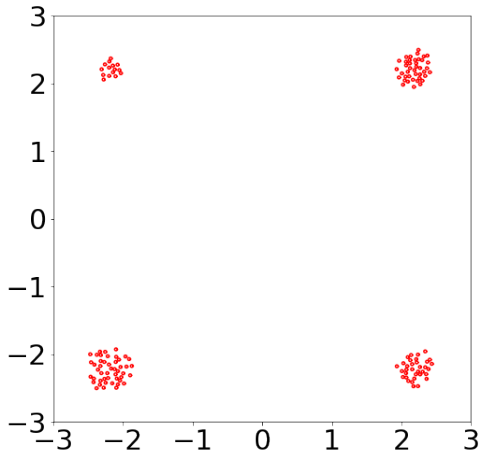

Figure 4.3: Left: The domain D (in red) composed of four areas in the four corners that we fill with small circular scatterers of radius 0.02 with $n = 2$ inside

The outcome of our numerical solver is the matrix $\mathbb{F}$ (that plays the role of an numerical approximation of F) with entries

$$\mathbb{F}_{pq} = u^\infty(\hat{x}_p, d_q), \quad 1 \leq p, q \leq N, \tag{4.71}$$

where $\hat{x}_p = d_p = (\cos(\theta_p), \sin(\theta_p))$ with $\theta_p = \frac{p}{N} 2\pi$ and where u^∞ is the numerically computed far field. In this following, we take $N = 40$ and $k = 3$.
We shall test the inside-outside duality for the case where the domain D_b will occupy two different regions as illustrated in Figure 4.4 (left) and Figure 4.6 (left). The first one does not contain any inclusion and the second one contains one the packs of small circles.

Since in the following examples and in the imaging algorithm introduced later, we need to compute the background far field operator for different positions of the circular domain D_b. We therefore briefly explain how one quickly evaluate this far field operator.
Denote by B_ρ^y the disk of center $y \in \mathbb{R}^2$ and radius $\rho > 0$. The far field pattern $u_{b,y}^\infty$ associated with the background problem (4.1) with $D_b = B_\rho^y$ can be expressed as

$$u_{b,y}^\infty(\hat{x}, d) = e^{iky.(d-\hat{x})} u_b^\infty(\hat{x}, d), \tag{4.72}$$

where u_b^∞ is the far field associated with $D_b = B_\rho^0$ (i.e the disk of radius ρ centered at the origin). The far field pattern assumes the following analytic expression:

$$u_{b,0}^\infty(\hat{x}, d) = \sum_{m \in \mathbb{Z}} \beta_m e^{im(\theta_{\hat{x}} - \theta_d)}, \tag{4.73}$$

with $\hat{x} = (\cos(\theta_{\hat{x}}), \sin(\theta_{\hat{x}}))$, $d = (\cos(\theta_d), \sin(\theta_d))$ and β_m are given by (4.70).
The numerical approximation of the background far field operator $F^{\mu}_{b,y}$ is the background far field matrix $\mathbb{F}^{\mu}_{b,y}$ which entries are:

$$(\mathbb{F}^{\mu}_{b,y})_{pq} = u^{\infty}_{b,y}(\hat{x}_p, d_q), \quad 1 \leq p, q \leq N, \tag{4.74}$$

where $u^{\infty}_{b,y}$ is evaluated using (4.72) and where u^{∞}_{b} is approximated by a truncation of the sum in (4.73), keeping the indices $j \in \mathbb{Z}$ such that $|j| < J$. In the following, we use $J = 10$.

We shall illustrate how the B eigenvalues depends on the position of the domain D_b on the synthetic configuration depicted in Figure 4.3.

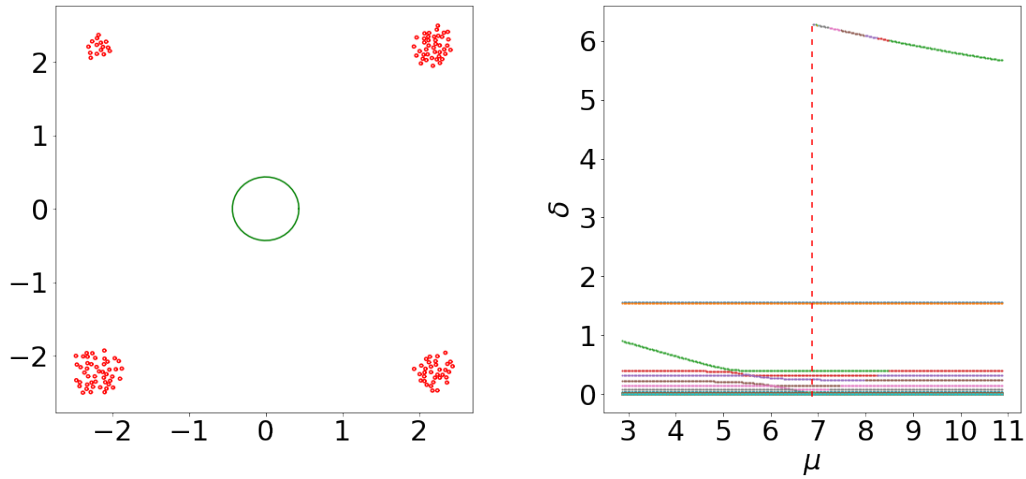

Figure 4.4: Left: The domain D (in red) and D_b, the disk of radius $\rho = 0.433$ (in green). Right: Plot of the curves $\mu \to \delta_m(\mu)$ for $k = 3$ and $n = 2$ inside the defects. The red dashed line indicates the analytical $\mathcal{B}-$eigenvalue (16) for constant $n = 1$ and $\mathcal{Q} = \{0\}$.

In Figure 4.4 (right), we display (for $\mathcal{Q} = \{0\}$), the curves $\mu \to \delta_m(\mu)$ associated with the configuration in Figure 4.4 (left) where D_b is a disk of radius $\rho = \frac{1.3}{k}$ centered at the origin with $k = 3$. Since there are no scatterers inside D_b, we expect the $\mathcal{B}-$eigenvalue to be equal to $\mu_{\text{ref,q}}(1)$ for $q \in \mathcal{Q}$. In line with the theory, we observe that the discontinuity for one of the curves occurs at the predicted eigenvalue (represented by the red dashed line) and a behavior similar to Figure 4.2 (left). In the case $\mathcal{Q} = \{0, 1, 2\}$, we have the same conclusions as we obtain results represented in Figure 4.5 (right) that are similar to the one in Figure 4.2 (right). The only difference between the analytical case and this one is that the curves not associated with $\mathcal{B}-$eigenvalues are no longer independent from μ.

In Figure 4.6 and 4.7, the domain D_b is the same disk as before but centered at the point $(2.2, 2.2)$. The reference $\mathcal{B}-$eigenvalues cannot be analytically computed for this configuration. We numerically evaluate them by solving (4.5) using the finite element methods implemented in Freefem++. The expression of these eigenvalues is given by (4.6).

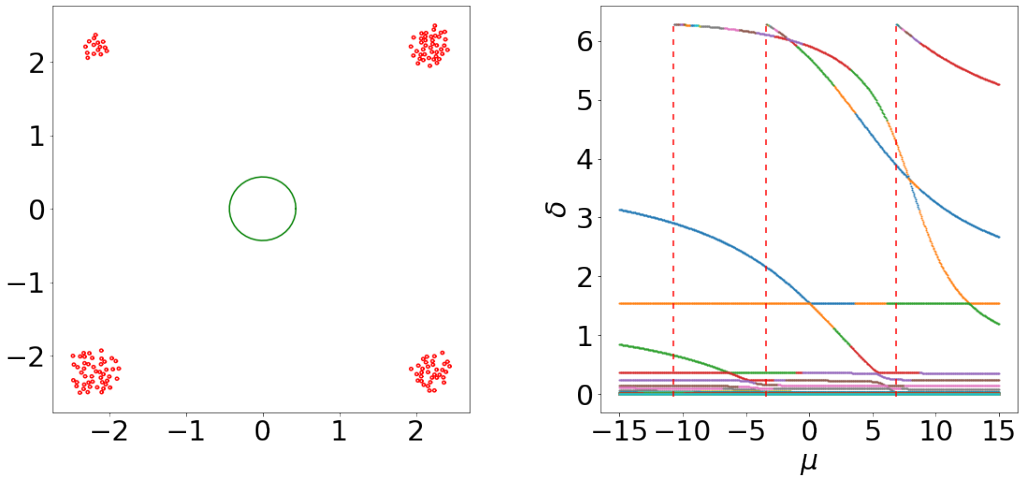

Figure 4.5: Left: The domain D (in red) and D_b, the disk of radius $\rho = 0.433$ (in green). Right: Plot of the curves $\mu \to \delta_m(\mu)$ for $k = 3$ and $n = 2$ inside the defects. The red dashed line indicates the analytical $\mathcal{B}-$eigenvalue (16) for constant $n = 1$ and $\mathcal{Q} = \{0, 1, 2\}$.

These computed values are indicated in the figures by a red straight dashed vertical line. The results for $\mathcal{Q} = \{0\}$ in Figure 4.6 and $\mathcal{Q} = \{0, 1, 2\}$ in Figure 4.7 show that the inside-outside duality is capable of correctly identifying the $\mathcal{B}-$eigenvalues for this configuration.

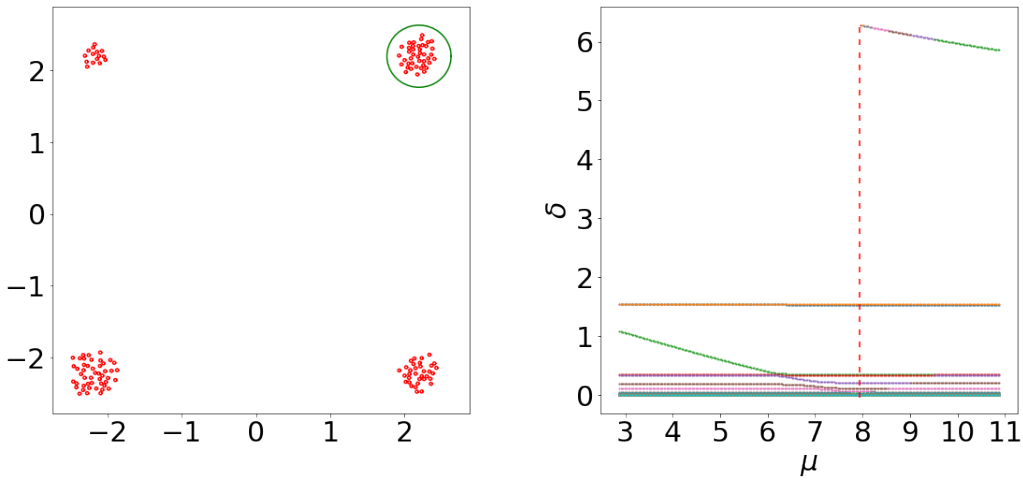

Figure 4.6: Left: The domain D (in red) and D_b, the ball of radius $\rho = 0.433$ centered at $(2.2, 2.2)$ (in green). Right: Plot of the curves $\mu \to \delta_m(\mu)$ for $k = 3$ and $n = 2$ inside the defects. The red dashed line indicates the approximated $\mathcal{B}-$eigenvalue computed with the relation (4.6) for $\mathcal{Q} = \{0\}$.

In the imaging algorithm introduced below, we shall use $\mathcal{Q} = \{0\}$ to minimize the

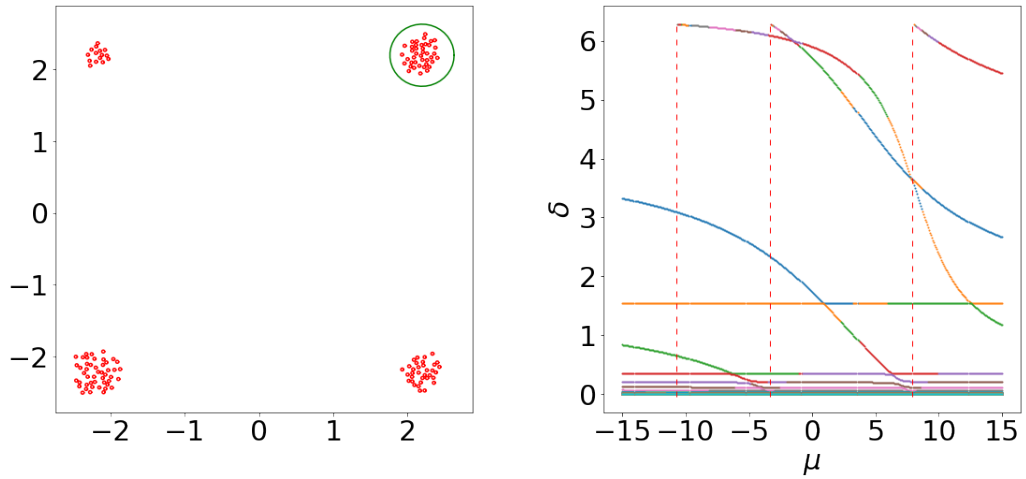

Figure 4.7: Left: The domain D (in red) and D_b, the ball of radius $\rho = 0.433$ centered at $(2.2, 2.2)$ (in green). Right: Plot of the curves $\mu \to \delta_m(\mu)$ for $k = 3$ and $n = 2$ inside the defects. The red dashed line indicates the approximated $\mathcal{B}-$eigenvalue computed with the relation (4.6) for $\mathcal{Q} = \{0, 1, 2\}$.

number of $\mathcal{B}-$eigenvalues that has to be determined. Figure 4.8 indicates the dependence of the inside-outside duality outcome with respect to noise in the data F. In order to simulate noise in the data, we change the values of the synthetic data $\mathbb{F}$ by adding random noise of level δ to construct the noisy far field matrix $\mathbb{F}^\delta = \mathbb{F} \cdot (1 + \delta(A + iB))$ where the entries of the matrices A and B are uniformly distributed real values in $[-1, 1]$ and where $\cdot$ denotes the element-wise product of matrices. Figure 7 clearly shows that the location of the eigenvalues is very robust with respect to the noise level. This is one of the main motivations for using these $\mathcal{B}-$eigenvalues in the.

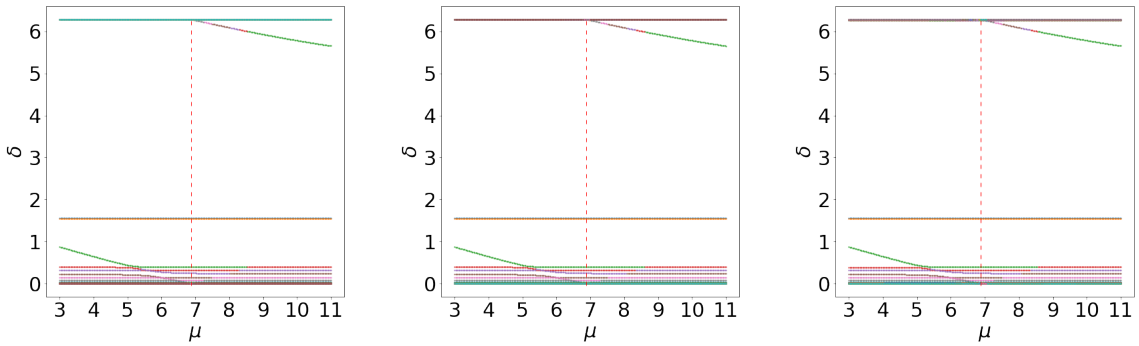

Figure 4.8: Plot of the curves $\mu \to \delta_m(\mu)$ for $k = 3$ and $n = 2$ inside the defects for the configuration shown in Figure 4.6 (left), D_b being a ball of radius $\rho = 0.4333$ centered at the origin and $\mathcal{Q} = \{0\}$ Left: $\delta = 1\%$, Middle: $\delta = 10\%$, Right: $\delta = 50\%$. The red dashed line indicates the analytical $\mathcal{B}-$eigenvalue (16) for constant $n = 1$ and $\mathcal{Q} = \{0\}$.

4.5.3 Application to the reconstruction of averaged values of the refractive index n

Several works in the literature have proposed inversion algorithms that exploit special forms of $\mathcal{B}-$eigenvalues or so-called transmissions eigenvalues [12, 7, 10]. In order to determine the $\mathcal{B}-$eigenvalues, these contributions employ a method based on the GLSM method ([8]). We here revisit the method proposed in [10] for reconstructing the averaged values of the refractive index by replacing the GLSM with the inside-outside duality method. Let us first outline this imaging algorithm. The method uses the operator $\mathcal{B}$ in (4.65) with $\mathcal{Q} = \{0\}$. In this case, the boundary condition on ∂D_b is of the form:

$$\mu u + \int_{\partial D_b} \partial_\nu u ds = 0 \text{ on } \partial D_b. \tag{4.75}$$

In this case, there is only one $\mathcal{B}-$eigenvalue and the reference eigenvalue for constant index n is given by $\mu_{\text{ref},0}(n)$ in (12). The function $\mu_{\text{ref},0}$ is a bijection between $[0, j_0/(k\rho)[$ and $\mathbb{R}^+$, where j_0 is the first zero of J_0.

The algorithm can be described with the following steps:

1. Let $\rho > 0$ be a given parameter. Choose D_b to be the ball B_ρ^y of radius ρ and center $y \in \mathcal{Y}$, a grid of points sampling the region of interest.

2. Evaluate the $\mathcal{B}-$eigenvalue $\mu(y, n)$ from the measurements $\mathbb{F}$ and the analytically computed $\mathbb{F}_{b,y}^{\mu}$ using the inside-outside method (see *Method 1* and *Method 2* below).

3. Compute $n^*(y) \in [0, j_0/(k\rho)[$ such that $\mu(y, n) = \mu_{\text{ref},0}(n^*(y))$.

4. Plot the function $y \to n^*(y)$

The key step in this algorithm is (ii), that is how to automatically recover $\mu(y, n)$ from graphics as in Figure 4.6 (right). We indicate two possible methods.

Method 1: Let Λ be the interval of values where $\mu(y, n)$ is supposed to belong. This interval should contains $\mu_{\text{ref},0}(1)$. Fix a parameter small $\varepsilon > 0$ and a threshold $\sigma \in [0, 2\pi - \varepsilon)$ not too close to 0. For each μ in Λ, we compute the eigenvalues $e^{i\delta_m}$ of the operator $\mathbf{S}(\mu)$. Then we count the number of phases δ_m that belong to $[\sigma, 2\pi - \varepsilon)$. For carefully chosen ε and σ, this number is constant for $\mu < \mu(y, n)$ in Λ and increases by 1 for the first value in Λ that exceeds $\mu(y, n)$. This allows us to identify $\mu(y, n)$.

Method 2: This method exploits the observation that all the eigenvalues $e^{i\delta_m}$ slowly vary with respect to μ expect one. Denote by $\widehat{\delta}_m \in [-\pi, \pi)$ such that $e^{i\delta_m} = e^{i\widehat{\delta}_m}$. We then expect the function $\mathcal{I}(\mu) = \sum_m |\widehat{\delta}_m|$ to have a minimum at $\mu(y, n)$ (see illustration in Figure 4.9).

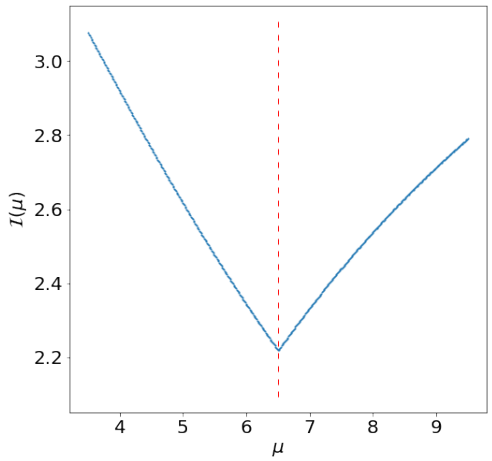

Figure 4.9: Plot of the curve $\mu \to \mathcal{I}(\mu)$ for $D = D_b = B_\rho$ the ball centered at the origin for $\rho = 0.3$, $k = 3$ and $n = 2$ in D. The red dashed line indicates $\mu_{\text{ref},0}(2)$.

In the following, we use method 1 with $\varepsilon = 10^{-2}$ and $\sigma = 2\pi - 1$. The second method also works fine and gives similar results. Before commenting the numerical tests, we briefly explain why $n^*(y)$ is expected to be an approximation of the averaged value:

$$\overline{n}(y) = \frac{1}{|B_\rho^y|} \int_{B_\rho^y} n(x)dx.$$

Consider a sequence of refractive index $(n_\varepsilon)_\varepsilon$ that converges weakly$-*$ in $L^\infty(D_b)$ to some $\widehat{n}$ as $\varepsilon \to 0$ (and denote by μ_ε its associated $\mathcal{B}-$eigenvalue). One can show from (4.6) that μ_ε converges to $\mu(\widehat{n})$ as ε goes to 0. For highly oscillating medium, $\widehat{n}$ can be seen as an approximation of the mean value $\overline{n}$ of n as defined above.
We shall test the algorithms described above for two configurations of the media as indicated in Figure 4.10. The configuration on the left indicates clustering of small disks with refractive index $n = 2$ and radius 0.02 with different densities in five distinct regions. The second configuration on the right is formed by 4 circular inhomogeneities with different refractive index $n = 0.25$ (bottom left), $n = 0.5$ (top left), $n = 1.5$ (bottom right) and $n = 2$ (upper right). The reconstruction associated with configuration in Figure 4.10 (left) is shown in Figure 4.11. In Figure 4.11 (left), we display the function $y \to \overline{n}(y)$ and in Figure 9 (right), we display the function $y \to n^*(y)$ resulting from the inside-outside duality with $k = 4$, $\rho = 0.33$ and the noise level $\delta = 1\%$. We clearly observe very good agreement between the two functions. Similar conclusions can be drawn from the results associated with the configuration in Figure 4.10 (right). These results are indicated in Figure 4.12, where again the function $y \to \overline{n}(y)$ (left) and $y \to n^*(y)$ (right) are displayed. In this case, we used $k = 4$, $\rho = 0.3$ and the noise level $\delta = 1\%$. Observe that we chose $\rho = 0.3$ to ensure that D_b is not strictly included inside D. In fact, in this case, $\mu(y, n)$ may not be a positive value. We conclude this numerical illustration with examples from Chapter 3. The left side of Figure 4.13, 4.14 and 4.15 shows the true averaged values of the refractive index $y \to \overline{n}(y)$

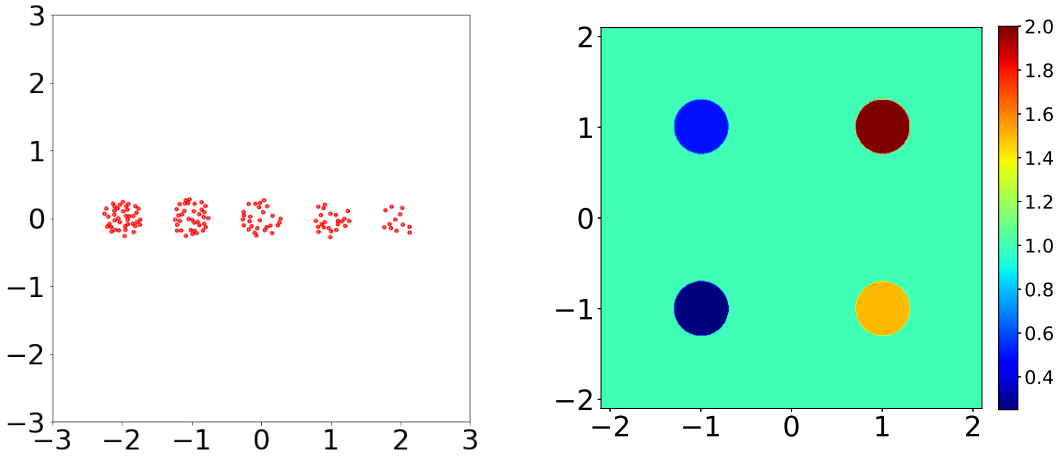

Figure 4.10: Left: the domain D constituted by small circles concentrated in five aligned areas. The scatterers have a radius 0.02 and a constant index refraction $n = 2$ inside. Right: Four diffracting circles of radius 0.3 associated with four different values of the refractive index $n = 0.25$ (bottom left), $n = 0.5$ (top left), $n = 1.5$ (bottom right) and $n = 2$ (upper right).

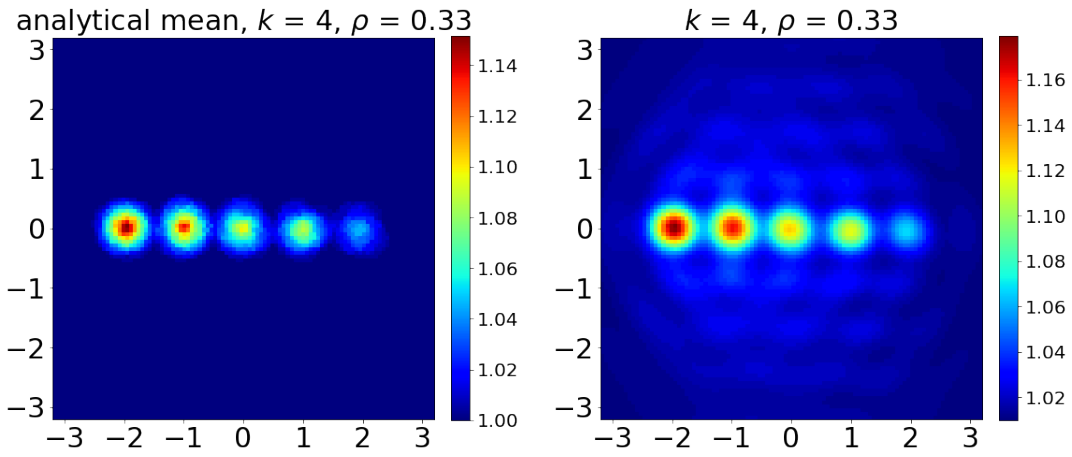

Figure 4.11: Results associated with configuration of the domain D in Figure 4.10 (left). Left: $y \to \overline{n}(y)$ representing the true averaged values of the refractive index. Right: $y \to n^*(y)$ representing the outcome of the inversion algorithm plotted on the 100×100 uniformed grid $\mathcal{Y}$ for $k = 4$, $\rho = \frac{1.3}{k}$ and the noise level $\delta = 1\%$.

while the right side presents $y \to n^*(y)$ for the corresponding configurations displayed on the left of Figures 3.5, 3.6 and 3.7.

Remark 9. *Unfortunately, the good agreement observed in the* 5 *last examples appears to*

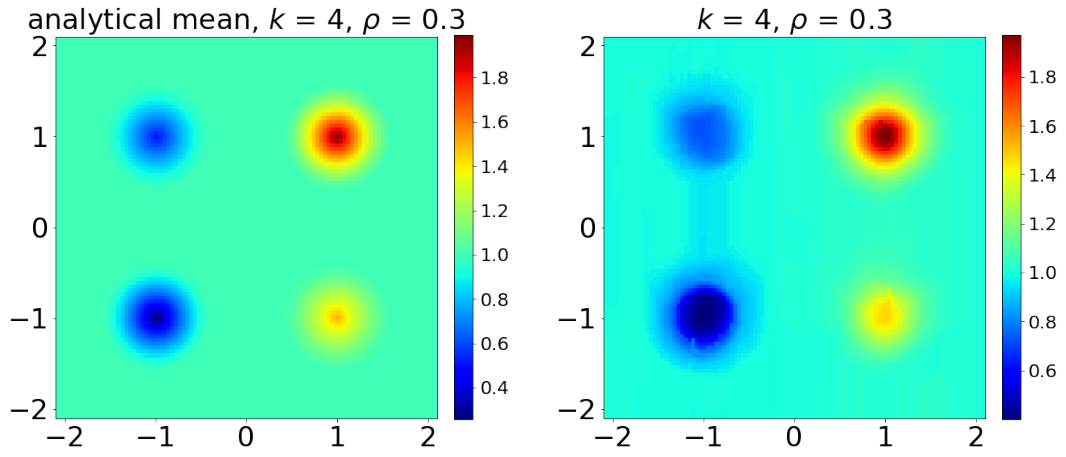

Figure 4.12: Results associated with configuration of the domain D in Figure 4.10 (right). Left: $y \to \overline{n}(y)$ representing the true averaged values of the refractive index. Right: $y \to n^*(y)$ representing the outcome of the inversion algorithm plotted on the 100×100 uniformed grid $\mathcal{Y}$ for $k = 4$, $\rho = 0.3$ and the noise level $\delta = 1\%$.

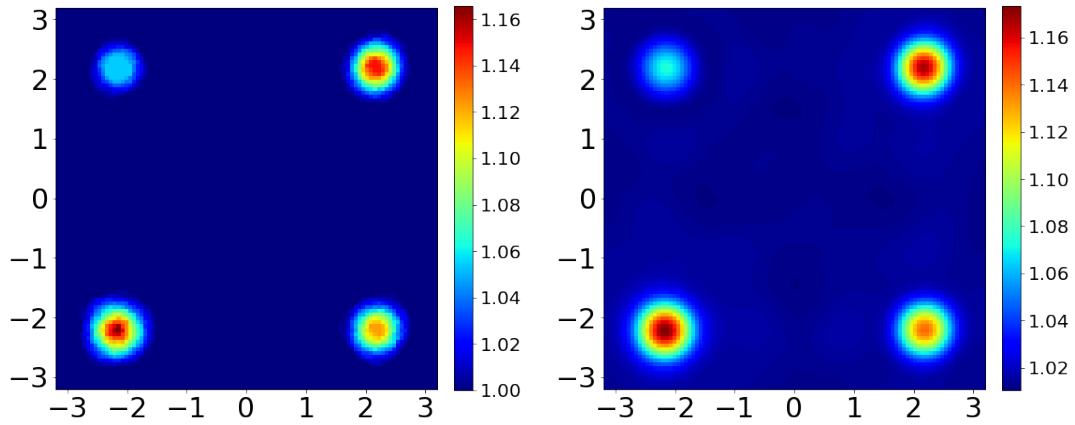

Figure 4.13: Results associated with configuration of the domain D in Figure 3.5 (left). Left: $y \to \overline{n}(y)$ representing the true averaged values of the refractive index. Right: $y \to n^*(y)$ representing the outcome of the inversion algorithm plotted on the 100×100 uniformed grid $\mathcal{Y}$ for $k = 3$, $\rho = \frac{1}{k}$ and the noise level $\delta = 1\%$.

be lost in the case of a medium saturated with small obstacles. Once again, we present the two indicator functions $y \to \overline{n}(y)$ and $y \to n^*(y)$ on the configuration shown in Figure 3 (left) in Figure 4.16. There are three possible explanations for this result:

1. *The assumption that D does not intersect ∂D_b, as illustrated in Figure 1.7, is not*

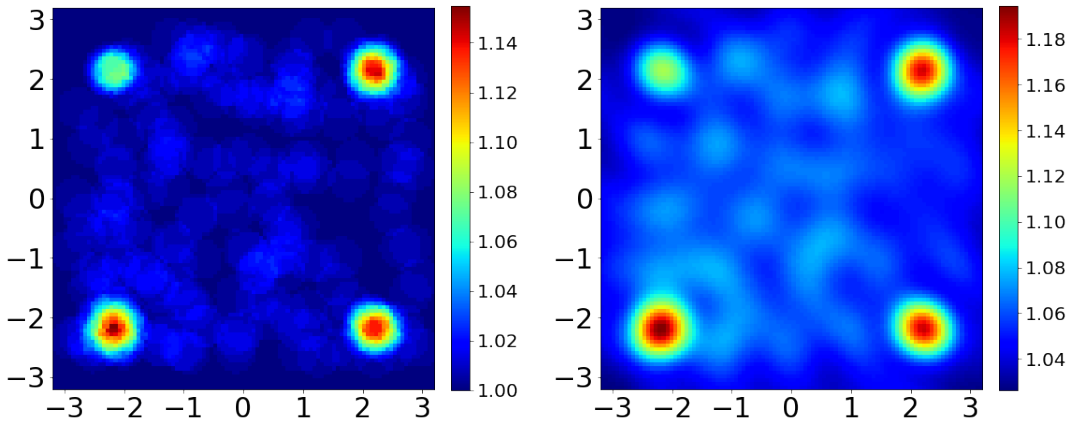

Figure 4.14: Results associated with configuration of the domain D in Figure 3.6 (left). Left: $y \to \overline{n}(y)$ representing the true averaged values of the refractive index. Right: $y \to n^*(y)$ representing the outcome of the inversion algorithm plotted on the 100×100 uniformed grid $\mathcal{Y}$ for $k = 3$, $\rho = \frac{1}{k}$ and the noise level $\delta = 1\%$.

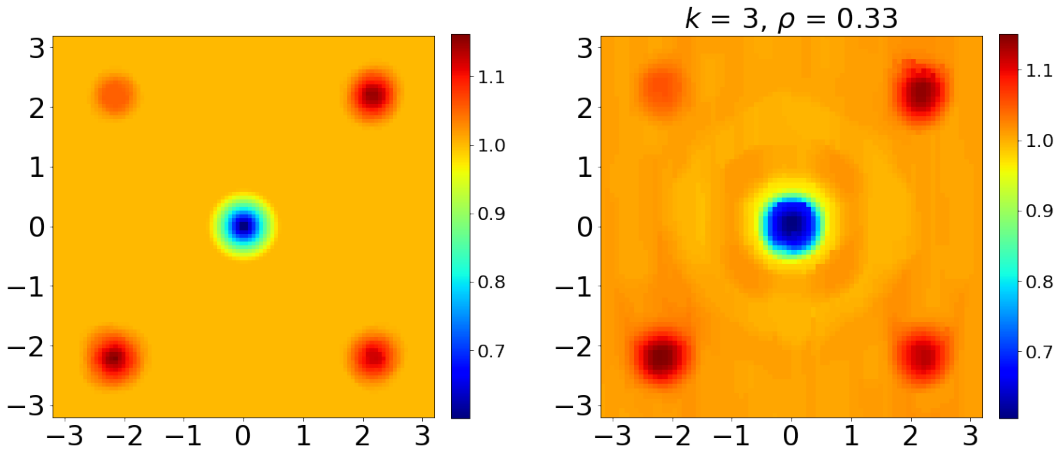

Figure 4.15: Results associated with configuration of the domain D in Figure 3.7 (left). Left: $y \to \overline{n}(y)$ representing the true averaged values of the refractive index. Right: $y \to n^*(y)$ representing the outcome of the inversion algorithm plotted on the 100×100 uniformed grid $\mathcal{Y}$ for $k = 3$, $\rho = \frac{1}{k}$ and the noise level $\delta = 1\%$.

verified because of the high number of scatterers.

2. *Theorem 11 provides an expression of the averaged Steklov eigenvalue as* $\mu = k^2 \int_{D_b} n w_1 dx$, *where* $w_1 \in H^1(D_b)$ *is the unique solution of* $\Delta w_1 + k^2 n w_1 = 0$ *in* D_b *and* $w_1 = 1$

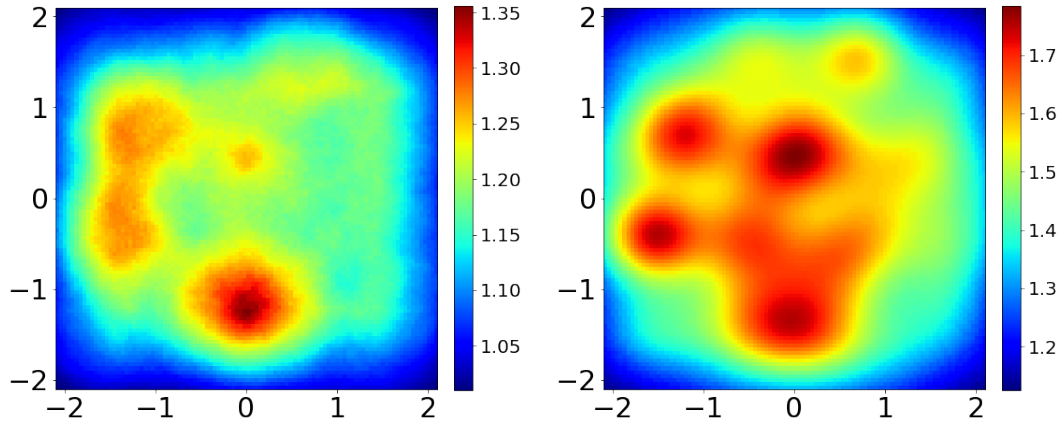

Figure 4.16: Results associated with configuration of the domain D in Figure 3.6 (left). Left: $y \to \overline{n}(y)$ representing the true averaged values of the refractive index. Right: $y \to n^*(y)$ representing the outcome of the inversion algorithm plotted on the 100×100 uniformed grid $\mathcal{Y}$ for $k = 3$, $\rho = \sqrt{\frac{3\eta_0(2,D_b)}{k}}$ and the noise level $\delta = 1\%$.

on ∂D_b. When D_b is a centered ball, w_1 behaves similarly to J_0, the Bessel funtion of first kind of order 0. In particular, it reaches its maximum at the center of D_b and decreases toward the boundary ∂D_b. In that situation, the w_1-weighted mean of n differs from the true mean of n as it emphasises the effects of the scatterers near the center of D_b.

3. *While in theory, the averaged Steklov eigenvalue is solely dependent on $n|_{D_b}$. However, in practice, we can only compute an approximation of the eigenvalue. This approximation is derived from the data, which is generated taking into account all the scatterers present. As a result, the eigenvalue does not solely reflect the characteristics of $n|_{D_b}$, but also incorporates the influence of other obstacles.*

4.6 Complementary technical results

4.6.1 Structure of the $\mathcal{B}$ operator

Theorem 38. *Consider a bounded linear positive, self-adjoint and compact operator $\mathcal{B} : H^{-\frac{1}{2}}(\partial D_b) \to H^{\frac{1}{2}}(\partial D_b)$. For κ a positive constant, the two following assertions are equivalent.*

1. *For all $\psi, \phi \in H^{-\frac{1}{2}}(\partial D_b)$,*

$$\kappa(\mathcal{B}\psi, \mathcal{B}\phi)_{L^2(\partial D_b)} = \langle \psi, \mathcal{B}\phi \rangle_{H^{-\frac{1}{2}}(\partial D_b), H^{\frac{1}{2}}(\partial D_b)}. \tag{4.76}$$

2. *There exists a family of M vectors $\{e_1, ..., e_M\} \subset H^{\frac{1}{2}}(\partial D_b)$ which are orthonormal with respect to the $L^2(\partial D_b)$ scalar product such that:*

$$\mathcal{B}(\psi) = \kappa \sum_{i=1}^{M} \langle \psi, e_i \rangle_{H^{-\frac{1}{2}}(\partial D_b), H^{\frac{1}{2}}(\partial D_b)} e_i, \quad \forall \psi \in H^{-\frac{1}{2}}(\partial D_b). \tag{4.77}$$

Proof. Assume item *(i)* holds. Let $\mathcal{I} : H^{\frac{1}{2}}(\partial D_b) \to L^2(\partial D_b)$ denote a bijective operator. Applying the spectral theorem to $\mathcal{I}\mathcal{B}\mathcal{I}^* : L^2(\partial D_b) \to L^2(\partial D_b)$, we deduce the existence of a sequence of positive real number $(\lambda_i)_i$ that converges toward 0 and $(b_i)_{i\in\mathbb{N}^*}$ an orthonormal basis of $L^2(\partial D_b)$ such that:

$$\mathcal{I}\mathcal{B}\mathcal{I}^* b_i = \lambda_i b_i, \tag{4.78}$$

which can be rewritten as

$$\mathcal{B}\mathcal{I}^* b_i = \lambda_i \mathcal{I}^{-1} b_i. \tag{4.79}$$

Every $\psi \in H^{-\frac{1}{2}}(\partial D_b)$ (respectively $\phi \in H^{\frac{1}{2}}(\partial D_b)$) admits an unique element $\widetilde{\psi} \in L^2(\partial D_b)$ such that $\psi = \mathcal{I}^*\widetilde{\psi}$ (respectively $\widetilde{\phi} \in L^2(\partial D_b)$ such that $\phi = \mathcal{I}^{-1}\widetilde{\phi}$).
Setting $a_i := (\widetilde{a}, b_i)_{L^2(\partial D_b)}$, $a \in L^2(\partial D_b)$, one has:

$$\begin{aligned} (\mathcal{B}\psi, \mathcal{B}\phi)_{L^2(\partial D_b)} &= \textstyle\sum_{i,j\in\mathbb{N}^*} \phi_j \psi_i (\mathcal{B}\mathcal{I}^* b_i, \mathcal{B}\mathcal{I}^* b_j)_{L^2(\partial D_b)}, \\ &= \textstyle\sum_{i,j\in\mathbb{N}^*} \phi_j \psi_i \lambda_i \lambda_j (\mathcal{I}^{-1} b_i, \mathcal{I}^{-1} b_j)_{L^2(\partial D_b)}. \end{aligned} \tag{4.80}$$

On the other hand:

$$\kappa \langle \psi, \mathcal{B}\phi \rangle_{H^{-\frac{1}{2}}(\partial D_b), H^{\frac{1}{2}}(\partial D_b)} = \kappa \sum_{i\in\mathbb{N}^*} \phi_i \psi_i \lambda_i. \tag{4.81}$$

Since (4.80) and (4.81) should be equal for every square summable sequences $(\phi_i)_i, (\psi_i)_i$, taking $\phi_k \psi_l = \delta_{ik}\delta_{li}$, we obtain that λ_i is equal to 0 or $\kappa \|\mathcal{I}^{-1} b_i\|^{-2}_{L^2(\partial D_b)}$. Since $\mathcal{I}$ is bounded, the sequence $(\|\mathcal{I}^{-1} b_i\|^2)_i$ remains also bounded. We deduce by compactness of the operator $\mathcal{B}$ that (up to a renumbering) the sequence $(\lambda_i)_i$ is equal to $\kappa \|e_i\|^{-2}_{L^2(\partial D_b)}$ up to a certain rank M $\lambda_i = 0$ for $i > M$.

For $k,l \leq M$, setting $\phi_k \psi_l = \delta_{ik}\delta_{lj}$ enforces $(\mathcal{I}^{-1}b_k, \mathcal{I}^{-1}b_l)_{L^2(\partial D_b)} = 0$ for $k \neq l$ and $k,l \leq M$. Hence, for all $\psi \in H^{-\frac{1}{2}}(\partial D_b)$, the operator $\mathcal{B}$ can be written as:

$$\begin{aligned} \mathcal{B}\psi &= \mathcal{B}\mathcal{I}^*\mathcal{I}^{*-1}\psi \\ &= \kappa \textstyle\sum_{i=0}^{M} (\mathcal{I}^{*-1}\psi, b_i)_{L^2(\partial D_b)} \mathcal{I}^{-1} b_i \\ &= \kappa \textstyle\sum_{i=0}^{M} \langle \psi, e_i \rangle_{H^{-\frac{1}{2}}(\partial D_b), H^{\frac{1}{2}}(\partial D_b)} e_i, \end{aligned} \tag{4.82}$$

where $e_i = \frac{\mathcal{I}^{-1}b_i}{\|\mathcal{I}^{-1}b_i\|_{L^2(\partial D_b)}}$. This proves that *(i)* implies *(ii)*. The reciprocal is straightforward. □

4.6.2 Study of the background problem (4.1)

The well posedness of problem (4.1) is established by variational approach. Let B_R be a ball containing D_b for R large enough. We define the Dirichlet to Neumann map $\Lambda : H^{\frac{1}{2}}(\partial B_R) \to H^{-\frac{1}{2}}(\partial B_R)$ by $\Lambda\phi := \partial_\nu v|_{\partial B_R}$, where v is the radiating solution to the Helmholtz equation in $\mathbb{R}^m \backslash B_R$ with $v = \phi$ on ∂B_R, and where ν is the outward unit normal to S_R. Define the closed subspace of $H^1(B_R \backslash D_b)$:

$$H^1_{\mathcal{B}}(B_R \backslash D_b) := \{w \in H^1(B_R \backslash D_b), w|_{\partial D_b} \in \mathcal{B}(H^{-\frac{1}{2}}(\partial D_b))\}. \tag{4.83}$$

Then, by Green's formula and using property (4.3), one can prove that solving the scattering problem (4.1) is equivalent to solving the following variational problem: $u \in H^1_{\mathcal{B}}(B_R \backslash D_b)$,

$$\int_{B_R \backslash D_b} (\nabla u \nabla v - k^2 uv) dx - \int_{\partial B_R} \Lambda uv ds - \mu\kappa \int_{\partial D_b} uv ds = \ell(v) \tag{4.84}$$

for all $v \in H^1_{\mathcal{B}}(B_R \backslash D_b)$, where

$$\ell(v) := \textstyle\int_{\partial B_R} (\partial_\nu u^i - \Lambda u^i) v ds, \tag{4.85}$$

The study of the well-posedness of this problem follows classical schemes based on proving that the problem is of Fredholm type and the uniqueness is a consequence of Rellish's lemma. We then can state the following lemma.

Lemma 39. *Problem (4.84) is well posed for $\mu \in \mathbb{R}^*$ if $(\partial_\nu u^i - \Lambda u^i) \in H^{-\frac{1}{2}}(\partial B_R)$.*

We prove in the following lemma the normality of the operator F_b^μ.

Proposition 40. *For $\mu \in \mathbb{R}^*$, F_b^μ is normal and $S_b = I + \frac{2ik}{\overline{\gamma}} F_b^\mu$ is unitary.*

Proof. This proof is similar to the one in [41, Theorem 1.8].
We first show that for all $g, h \in L^2(\mathbb{S})$,

$$2ik(F_b^\mu g, F_b^\mu h)_{L^2(\mathbb{S})} = \gamma(F_b^\mu g, h)_{L^2(\mathbb{S})} - \overline{\gamma}(g, F_b^\mu h)_{L^2(\mathbb{S})}. \tag{4.86}$$

Let us deal with the three terms independently.

1. Let w_g^s and w_h^s radiating solution of problem (4.1) with u^i an Herglotz wave of kernel g and h respectively with far field pattern w_g^∞, w_h^∞. We denote by w_g^t, w_h^t the total fields. Let B_R all disk centered at the origin containing D_b. Applying Green second theorem, we get

$$0 = \int_{\partial B_R} (\partial_\nu w_g^s \overline{w_h^s} - \partial_\nu \overline{w_h^s} w_g^s) ds - \int_{\partial D_b} (\partial_\nu w_g^s \overline{w_h^s} - \partial_\nu \overline{w_h^s} w_g^s) ds. \tag{4.87}$$

Letting $R \to +\infty$ and using the radiation condition, one obtains

$$2ik(F_b^\mu g, F_b^\mu h)_{L^2(\mathbb{S})} = 2ik \int_{\mathbb{S}} w_g^\infty \overline{w_h^\infty} ds = \int_{\partial D_b} (\partial_\nu w_g^s \overline{w_h^s} - \partial_\nu \overline{w_h^s} w_g^s) ds. \tag{4.88}$$

2. If $u^i = v_h$ an Herglotz wave of kernel $h \in L^2(\mathbb{S})$, then we have

$$\begin{aligned} \int_{\partial D_b} (\partial_\nu w_g^s \overline{v_h} - \partial_\nu \overline{v_h} w_g^s) ds &= \int_{\mathbb{S}} \overline{h}(d) \int_{\partial D_b} (\partial_\nu w_g^s(y) e^{-iky\cdot d} - \partial_\nu e^{-iky\cdot d} w_g^s(y)) ds(y) ds(d) \\ &= -\gamma \int_{\mathbb{S}} w_g^\infty(d) \overline{h}(d) ds(d) \\ &= -\gamma (F_b^\mu g, h)_{L^2(\mathbb{S})}. \end{aligned} \tag{4.89}$$

Similarly, one gets

$$\int_{\partial D_b} (\partial_\nu v_g \overline{w_h^s} - \partial_\nu \overline{w_h^s} v_g) ds = \overline{\gamma} (g, F_b^\mu h)_{L^2(\mathbb{S})} \tag{4.90}$$

3. We then compute $-2ik(F_b g, F_b h) + \gamma(F_b g, h) - \overline{\gamma}(g, F_b h)$:

$$\begin{aligned} &= -2ik \int_{\mathbb{S}} w_g^\infty \overline{w_g^\infty} ds + \gamma \int_{\mathbb{S}} w_g^\infty(d) \overline{h}(d) ds(d) - \overline{\gamma} \int_{\mathbb{S}} \overline{w_h^\infty}(d) g(d) ds(d) \\ &= \int_{\partial D_b} (w_g^t(y) \partial_{\nu(y)} \overline{w_h^t}(y) - \overline{w_h^t}(y) \partial_{\nu(y)} w_g^t(y)) ds(y) \\ &= -\tfrac{1}{\mu} \int_{\partial D_b} (\mathcal{B}(\partial_{\nu(y)} w_g^t(y)) \partial_{\nu(y)} \overline{w_h^t}(y) + \tfrac{1}{\overline{\mu}} \mathcal{B}(\partial_{\nu(y)} \overline{w_h^t}(y)) \partial_{\nu(y)} w_g^t(y)) ds(y) \\ &= (\tfrac{1}{\overline{\mu}} - \tfrac{1}{\mu}) \int_{\partial D_b} (\mathcal{B}(\partial_{\nu(y)} w_g^t(y)) \partial_{\nu(y)} \overline{w_h^t}(y) ds(y) \\ &= 0, \end{aligned} \tag{4.91}$$

Therefore, one has:

$$F_b^{\mu *} F_b^\mu = \frac{1}{2ik} (\gamma F_b^\mu - \overline{\gamma} F_b^{\mu *}). \tag{4.92}$$

From this equality, one can easily show that $S_b^* S_b = I$ and, because S_b is a compact perturbation of I, conclude that S_b is unitary. This is enough to prove that F_b^μ is normal. □

4.6.3 Uniform coercivity

Lemma 41. *The operator $T_{\mathcal{B}}(\mu)$ is uniformly coercive on any compact set $I \subset \mathbb{R}^*$. In other words, there exists $M_I > 0$ such that:*

$$| \langle T_{\mathcal{B}}(\mu)\psi, \psi \rangle | \geq M_I \|\psi\|^2_{H^{-\frac{1}{2}}(\partial D_b)}, \quad \forall \psi \in H^{-\frac{1}{2}}(\partial D_b), \tag{4.93}$$

for all $\mu \in I$.

Proof. Let $I \subset \mathbb{R}^*$ be a compact set and set $\mu_0 \in I$. We denote by M_{μ_0} the coercivity constant associated with $T_{\mathcal{B}}(\mu_0)$. For all $\mu \in I$ such that $|||T_{\mathcal{B}}(\mu) - T_{\mathcal{B}}(\mu_0)||| \leq \frac{1}{2} M_{\mu_0}$, one can write

$$\begin{aligned} | \langle T_{\mathcal{B}}(\mu)\psi, \psi \rangle | &\geq | \langle T_{\mathcal{B}}(\mu_0)\psi, \psi \rangle | - | \langle (T_{\mathcal{B}}(\mu) - T_{\mathcal{B}}(\mu_0))\psi, \psi \rangle | \\ &\geq M_{\mu_0} \|\psi\|^2_{H^{-\frac{1}{2}}(\partial D_b)} - |||T_{\mathcal{B}}(\mu) - T_{\mathcal{B}}(\mu_0)|||\|\psi\|^2_{H^{-\frac{1}{2}}(\partial D_b)} \\ &\geq \tfrac{1}{2} M_{\mu_0} \|\psi\|^2_{H^{-\frac{1}{2}}(\partial D_b)}. \end{aligned} \tag{4.94}$$

Since I is compact, it admits a finite cover

$$I \subset \bigcup_{i=1}^{N} B(\mu_i, M_{\mu_i}) \tag{4.95}$$

where $N > 0$, $\mu_i \in I$ and $B(\mu_i, M_{\mu_i})$ denotes the ball of center μ_i and radius M_{μ_i}. Therefore, for every μ in I, there exists a μ_i such that $|||T_{\mathcal{B}}(\mu) - T_{\mathcal{B}}(\mu_i)||| \leq \frac{1}{2} M_{\mu_i}$, which implies

$$| \langle T_{\mathcal{B}}(\mu)\psi, \psi \rangle | \geq \frac{1}{2} \left(\inf_{i=1,..,N} M_{\mu_i} \right) \|\psi\|^2_{H^{-\frac{1}{2}}(\partial D_b)}. \tag{4.96}$$

□

Chapter 5

The Inside-outside duality with artificial background with a non penetrable resonator

Contents

5.1 Introduction

In the context of inverse scattering, the notion of modified transmission eigenvalues gained significance over the years. For an unknown complex media, we assemble an artificial background media that can be analyzed and computed independently. This background media possesses a resonator (often denoted D_b or Ω_b) in which intervenes a specific parameter (in its interior problem or boundary condition). Those modified transmission eigenvalues are special values of this parameter for which there exists an incident field so that the scattered field of the unknown complex media matches the scattered field of the artificial background media everywhere outside the scatterers and the resonator.
For a well chosen background media, those eigenvalues can be studied from the theory of compact self-adjoint operators. The parameter in question can be the frequency (in that case we refer to the Transmission eigenvalues ([15])) or an element in the interior equation (see [6, 35, 4]), a component in the boundary condition of the resonator (we refer to the Averaged Steklov eigenvalues in Chapter 2 and in [12, 10]). Those previously mentioned eigenvalues have a monotonicity property (derived from a Courant-Fischer min-max principle) with respect to: 1) the numbers of components of the defects inside the resonator, 2) the values of the physical parameters inside the resonator. The crucial point of this property is the link between the eigenvalue and the local properties of the complex media. This has lead to the development of a new imaging algorithm consisting in plotting the said eigenvalues for various positions of the resonator D_b. The monotonicity provides an image which provides an initial approach to the distribution of obstacles, their density.
This result can only be achieved by recovering these modified transmission eigenvalues from the data, in this case the far field operator. Over the last decades, two main methods have emerged:

1) The first one is based on the Generalized Linear Sampling Method. by varying the parameter in the background medium, we compute an indicator function. This function remains bounded if and only if the parameter is a modified transmission eigenvalue. In the literature, this approach has been employed to recover transmission eigenvalues as demonstrated in [15], Averaged Steklov eigenvalues as shown in [12], and modified Steklov eigenvalues, as discussed in [4].

2) The second one, barely ten years old, is known as the inside-outside duality. It relies on the behavior of the spectrum of the data operators. Utilizing compactness results and an appropriately chosen decomposition, the spectrum accumulates at zero from one side only, with a single eigenvalue crossing zero from the opposite side. This crossing occurs precisely when the parameter is a modified transmission eigenvalue. We refer to [43] for an introduction to this method.

The utilization of artificial backgrounds for the construction of spectral signature thanks to the inside-outside duality has been well studied in the case of penetrable resonator D_b ([35, 6]). [11] introduces the formalism the structure of the objects and the proofs of the inside-outside duality with non penetrable obstacle D_b in the background medium. It focuses in particular on the so-called $\mathcal{B}-$eigenvalues, a family that includes the Averaged

Steklov eigenvalues. In this chapter, we extend this work by proving the inside-outside duality for various modified transmission eigenvalues based on the introduction of an artificial background for non penetrable resonator D_b.

This chapter addresses two key aspects in the first two sections:

1) Section 5.2 is based on the artificial background introduced in Chapter 4. It develops the inside-outside duality method, where the resonator has a boundary condition in the form
$$\mu w + \mathcal{B}(\partial_\nu w) = 0$$
withthe frequency k acting as the spectral parameter for a fixed μ.

2) Section 5.3 introduces, for a fixed wavenumber k, a new boundary condition for the resonator in the form
$$\mu \mathcal{D}(w) + \partial_\nu w = 0$$
and a new class of eigenvalues called the $\mathcal{D}-$eigenvalues. After presenting the properties of the operator $\mathcal{D}$ and proving the existence of the eigenvalues μ, we present the inside-outside duality method to recover this spectrum.

Although these two sections are independent, they are closely related by the nature of the mathematical objects and the similarity of the proofs. The third and final section provides numerical illustration of both approaches and concludes with an imaging algorithm, similar to the one in Chapter 3 exploiting the $\mathcal{B}-$Dirichlet eigenvalues. The different settings discussed in this chapter are summarized in the following table.

Section	Boundary condition	Fixed parameter	Spectral parameter	Name of the eigenvalues
5.2	$\mu w + \mathcal{B}(\partial_\nu w) = 0$	μ	wavenumber k	$\mathcal{B}-$Dirichlet eigenvalues
5.3	$\mu \mathcal{D}(w) + \partial_\nu w = 0$	wavenumber k	μ	$\mathcal{D}-$eigenvalues

5.2 The $\mathcal{B}-$Dirichlet eigenvalues

Boundary condition	Fixed parameter	Spectral parameter	Name of the eigenvalues
$\mu w + \mathcal{B}(\partial_\nu w) = 0$	μ	wavenumber k	$\mathcal{B}-$Dirichlet eigenvalues

While the previous chapter was centered around the $\mathcal{B}-$eigenvalues for a fixed wavenumber k^2, this section focuses for a fixed parameter μ on the $\mathcal{B}-$Dirichlet eigenvalues whose definition is given below. The domain D_b is regular bounded and simply connected.

Definition 6. *For a fixed $\mu \neq 0$, a non zero wavenumber k^2 is called a $\mathcal{B}-$Dirichlet eigenvalue if there exists $w_0 \in H^1(D_b)$ non trivial solution of*

$$\begin{cases} \Delta w_0 + k^2 n w_0 = 0 \text{ in } D_b, \\ \mu w_0 + \mathcal{B}(\partial_\nu w_0) = 0 \text{ on } \partial D_b, \end{cases} \tag{5.1}$$

where the operator $\mathcal{B}$ is introduced in Assumption 25.

The determination of the $\mathcal{B}-$Dirichlet eigenvalues requires the same artificial background media (4.1). Consequently, the structure of the operators and the proofs are similar and can also be used . This section will follow the same key steps as for the identification of the $\mathcal{B}-$eigenvalues, the main difference being that the wavenumber plays the role of the spectral parameter. For $\mathcal{B} = 0$, it corresponds to the Dirichlet eigenvalues of (1.35). This slightly generalizes the method presented in [49] because it does not require a Dirichlet scattering object and allow to determine the Dirichlet eigenvalues for any real valued $n \in L^\infty(D_b)$.
The operators are identical to the one in Chapter 4 section 4.3 but to emphasize their dependence on k, they will be denoted as $F_b(k), \mathcal{F}(k), S_b(k), \mathbf{F}(k), \mathcal{H}_\mathcal{B}(k), T_\mathcal{B}(k)$ and $\mathbf{S}(k)$. Once again, we assume that $D \subset D_b$.‘
Thank to property (4.3) and Green's formula, problem (5.1) is equivalent to the variational formulation: $w_0 \in H^1_\mathcal{B}(D_b)$,

$$\int_{D_b} (\nabla w_0 \nabla w' - k^2 w_0 w') dx + \mu\kappa \int_{\partial D_b} w_0 w' ds = 0 \tag{5.2}$$

for all $w' \in H^1_\mathcal{B}(D_b) := \{w' \in H^1(D_b), w'|_{\partial D_b} \in \mathcal{B}(H^{-\frac{1}{2}}(\partial D_b))\}$.
The eigenvalue problem (5.1) has a similar structure as Dirichlet or Neumann eigenvalue problems, and from standard results on the spectrum of self-adjoint compact operator, it is discrete and formed by a real sequence that accumulates at $+\infty$. In addition, the first $\mathcal{B}-$Dirichlet denoted $\eta_\mathcal{B}(n, D_b)$ eigenvalue satisfies:

$$\eta_\mathcal{B}(n, D_b) = \inf_{w \in H^1_\mathcal{B}(D_b), w \neq 0} \frac{\int_{D_b} |\nabla w|^2 dx + \kappa\mu \int_{\partial D_b} |w|^2 ds}{\int_{D_b} n|w|^2 dx}. \tag{5.3}$$

This shows in particular that $\eta_\mathcal{B}(n, D_b)$ is monotonically decreasing with respect to the refractive index n.
The next subsection is dedicated to the proof of the inside-outside duality applied on the operator $\mathbf{S}(k)$, where one again, the behavior of its eigenvalues around the unitary circle provides information about the localization of the $\mathcal{B}-$Dirichlet eigenvalues.

5.2.1 The inside-outside duality applied to $\mathbf{F}(k)$

Assume that k^2 is not a $\mathcal{B}-$Dirichlet eigenvalue. Since $\mathbf{F}(k)$ is a compact normal operator, there exists an orthonormal complete basis $(g_j)_{j\in\mathbb{N}}$ of $L^2(\mathbb{S})$ such that $\mathbf{F}(k)g_j = \lambda_j g_j$ where $(\lambda_j)_{j\in\mathbb{N}}$ are the eigenvalues of $\mathbf{F}(k)$ that accumulate at 0.

Exploiting the fact that $\mathbf{S}(k)$ is unitary, we deduce that the eigenvalues of $\mathbf{F}(k)$ lie on the circle of radius $\frac{|\gamma|^2}{2k}$ and center $\frac{|\gamma|^2}{2ik}$. We define $\lambda_j := \frac{|\gamma|^2}{2ik}(e^{i\delta_j}-1)$ with $e^{i\delta_j}$ being an eigenvalue of $\mathbf{S}(k)$, $\delta_j \in [0, 2\pi)$ and introduce the following quantities

$$\begin{cases} \delta_*(k) & := \max_{j\geq 1} \delta_j, \\ \lambda_* & := \frac{|\gamma|^2}{2ik}(e^{i\delta_*}-1). \end{cases} \tag{5.4}$$

We then can state the main theorem:

Theorem 42. *k_0^2 is a $\mathcal{B}-$Dirichlet eigenvalue if and only if $\delta_*(k) \to 2\pi$ as $k \to k_0$ with $k < k_0$.*

The absence of the absolute value in the coercivity relation of the operator T_0 leads to an accumulation of the eigenvalues λ_j of the operator $\mathbf{S}(k)$ to 0 from right. Theorem 42 indicates that when the wavenumber k approaches a $\mathcal{B}-$Dirichlet eigenvalue from below, there is one eigenvalue that converges to 0 from the left. This theorem is a straightforward corollary of Proposition 44 (sufficient condition) and Proposition 47 (necessary condition).

5.2.2 Proof of the sufficient condition in Theorem 42

For U, V two Banach spaces, we denote by $\mathcal{L}(U, V)$ the the space of linear bounded operators from U to V. This space is endowed with the following operator norm:

$$||L|| := \sup_{\psi\in X} \frac{||L\psi||_V}{||\psi||_U}, \quad \forall L \in \mathcal{L}(U, V). \tag{5.5}$$

The next proposition is a technical result whose demonstration (in section 5.5) relies on variational approach.

Proposition 43. *The mapping $k \to T_{\mathcal{B}}(k)$ is continuous from any compact set $I \subset \mathbb{R}^+$ to $\mathcal{L}(H^{-\frac{1}{2}}(\partial D_b), H^{\frac{1}{2}}(\partial D_b))$.*

Proposition 44. *Let $k_0 \in \mathbb{R}^+$ and $I = (k_0-\varepsilon, k_0+\varepsilon)\backslash\{k_0\}$ for some $\varepsilon > 0$ sufficient small such that no $k \in I$ is negative. Assume there is a sequence $(k_j)_j$ of elements of I such that*

$$k_j \longrightarrow k_0 \qquad \text{and} \qquad \delta_*(k_j) \longrightarrow 2\pi. \tag{5.6}$$

Then k_0 is a $\mathcal{B}-$Dirichlet eigenvalue.

By replacing the dependence on μ with the wavenumber, the proof of this proposition is identical to the proof of Proposition 34.

5.2.3 Proof of the necessary condition in Theorem 42

Assume that k is not a $\mathcal{B}-$Dirichlet eigenvalue. Then 1 is not an eigenvalue of $\mathbf{S}(k)$ because $\mathbf{F}(k)$ is injective and we can define the Cayley transform:

$$\mathcal{T} := i(Id + \mathbf{S}(k))(Id - \mathbf{S}(k))^{-1}.$$

$\mathcal{T}$ is self-adjoint and has a discrete spectrum. We have the equivalence $e^{i\delta_*}$ is an eigenvalue of $\mathbf{S}$ if and only if $\cot(\delta_*/2) \in \mathbb{R}$ is an eigenvalue of $\mathcal{T}$. Applying Courant Fischer min max principle to $\mathcal{T}$, we get:

$$\cot(\delta_*/2) = \inf_{\psi \in H^{-\frac{1}{2}}(\partial D_b)} \frac{\Re e \langle T_{\mathcal{B}}(k)\psi, \psi\rangle}{\Im m \langle T_{\mathcal{B}}(k)\psi, \psi\rangle}. \tag{5.7}$$

Lemma 45. *Let k_0 be a $\mathcal{B}-$Dirichlet eigenvalue associated with an eigenvector w_0. For $k \in \mathbb{R}^+$, define $(w(k), w^s(k))$ the solution of (4.14) with source term $\psi = \partial_\nu w_0$. We have the following expansion as $k \to k_0$:*

$$w(k) - w_0 = (k - k_0)w' + (k - k_0)^2 \widetilde{w}(k), \tag{5.8}$$

where w' is independent from k and $\widetilde{w}(k)$ have a bounded norm as $k \to k_0$.

Proof. Set $v = w(k) - w_0$ and $v^s = w^s(k)$. From the linearity of the equations, one obtains that (v, v^s) is solution of:

$$\begin{cases} \Delta v + k_0^2 n v = (k_0^2 - k^2) n w(k) \text{ in } D_b, \\ \Delta v^s + k_0^2 v^s = (k_0^2 - k^2) w^s(k) \text{ in } \mathbb{R}^m \backslash D_b, \\ v - v^s = 0 \text{ on } \partial D_b, \\ \partial_\nu v - \partial_\nu v^s = 0 \text{ on } \partial D_b, \\ \lim_{r \to +\infty} \int_{|x|=r} |\frac{\partial v^s}{\partial r} - ikv^s|^2 = 0, \end{cases} \tag{5.9}$$

Dividing the previous equations by $k - k_0$ and using the continuity of the application $k \to w(k)$, we deduce that (w', w'^s) is solution of:

$$\begin{cases} \Delta w' + k_0^2 n w' = -2k_0 n w_0 \text{ in } D_b, \\ \Delta w'^s + k_0^2 w'^s = 0 \text{ in } \mathbb{R}^m \backslash D_b, \\ w' - w'^s = 0 \text{ on } \partial D_b, \\ \partial_\nu w' - \partial_\nu w'^s = 0 \text{ on } \partial D_b, \\ \lim_{r \to +\infty} \int_{|x|=r} |\frac{\partial w'^s}{\partial r} - ikw'^s|^2 = 0. \end{cases} \tag{5.10}$$

We then conclude from the decomposition (5.8) that $(\widetilde{w}, \widetilde{w}^s)$ solves:

$$\begin{cases} \Delta \widetilde{w} + k^2 n \widetilde{w} = -(k + k_0) n (w' + w_0) \text{ in } D_b, \\ \Delta \widetilde{w}^s + k^2 \widetilde{w}^s = -(k + k_0) w'^s \text{ in } \mathbb{R}^m \backslash D_b, \\ \widetilde{w} - \widetilde{w}^s = 0 \text{ on } \partial D_b, \\ \partial_\nu \widetilde{w} - \partial_\nu \widetilde{w}^s = 0 \text{ on } \partial D_b, \\ \lim_{r \to +\infty} \int_{|x|=r} |\frac{\partial \widetilde{w}^s}{\partial r} - ik\widetilde{w}^s|^2 = 0, \end{cases} \tag{5.11}$$

which is bounded as $k \to k_0$. □

Proposition 46. *Let k_0 be a $\mathcal{B}-$Dirichlet eigenvalue associated with w_0. For $k \in \mathbb{R}^+$, define $(w(k), w^s(k))$ the solution of (4.14) with source term $\psi = \partial_\nu w_0$. Then there exists a quantity $E(k)$ such that :*

$$\langle T_{\mathcal{B}}(k)\partial_\nu w_0, \partial_\nu w_0\rangle = (k-k_0)2k_0 \int_{D_b} n|w_0|^2 s dx + (k-k_0)^2 E(k), \tag{5.12}$$

where $E(k)$ has a bounded norm as $k \to k_0$.

Proof. According to the definition of $T_{\mathcal{B}}(k)$, the decomposition introduced in Lemma 45 and the boundary relation of w_0, one can show:

$$\begin{aligned} \langle T_{\mathcal{B}}(k)\partial_\nu w_0, \partial_\nu w_0\rangle = \; & (k-k_0)\left\langle w' + \tfrac{1}{\mu}\mathcal{B}(\partial_\nu w'), \partial_\nu w_0 \right\rangle \\ & +(k-k_0)^2 \left\langle \widetilde{w} + \tfrac{1}{\mu}\mathcal{B}(\partial_\nu \widetilde{w}), \partial_\nu w_0 \right\rangle. \end{aligned} \tag{5.13}$$

By applying Green's theorem, we obtain:

$$\begin{aligned} 2k_0 \textstyle\int_{D_b} n|w_0|^2 &= -\textstyle\int_{D_b} (\Delta w' + k^2 n w')\overline{w_0} dx \\ &= \left\langle w' + \tfrac{1}{\mu}\mathcal{B}(\partial_\nu w'), \partial_\nu w_0 \right\rangle. \end{aligned} \tag{5.14}$$

Setting $E(k) := \left\langle \widetilde{w} + \frac{1}{\mu}\mathcal{B}(\partial_\nu \widetilde{w}), \partial_\nu w_0 \right\rangle$ concludes the proof. □

We have all the elements required to prove the necessary condition.

Proposition 47. *Assume that k_0 is a $\mathcal{B}-$Dirichlet eigenvalue. Then $\delta_*(k) \to 2\pi$ as $k \to k_0$ with $k < k_0$.*

Proof. Let k_0 be a $\mathcal{B}-$Dirichlet eigenvalue associated with the eigenvector w_0. Then we have for k in a neighbourhood of k_0:

$$\cot(\delta_*(k)/2) = \inf_{\psi \in H^{-\frac{1}{2}}(\partial D_b)} \frac{\Re\langle T_{\mathcal{B}}(k)\psi, \psi\rangle}{\Im m\langle T_{\mathcal{B}}(k)\psi, \psi\rangle} \leq \frac{\Re\langle T_{\mathcal{B}}(k)\partial_\nu w_0, \partial_\nu w_0\rangle}{\Im m\langle T_{\mathcal{B}}(k)\partial_\nu w_0, \partial_\nu w_0\rangle}, \tag{5.15}$$

with $\Im m\langle T_{\mathcal{B}}(k)\partial_\nu w_0, \partial_\nu w_0\rangle > 0$ thanks to Lemma 31. From Proposition 46, we conclude:

$$\frac{\Re\langle T_{\mathcal{B}}(k)\partial_\nu w_0, \partial_\nu w_0\rangle}{\Im m\langle T_{\mathcal{B}}(k)\partial_\nu w_0, \partial_\nu w_0\rangle} = \frac{2k_0 \int_{D_b} n|w_0|^2 s dx + (k-k_0)\Re e(E(k))}{(k-k_0)\Im m(E(k))} \to -\infty, \tag{5.16}$$

as $k \to k_0$ with $k < k_0$, thus, proving the stated proposition. □

5.3 The $\mathcal{D}-$eigenvalue

Boundary condition	Fixed parameter	Spectral parameter	Name of the eigenvalues
$\mu\mathcal{D}(w)+\partial_\nu w=0$	wavenumber k	μ	$\mathcal{D}-$eigenvalues

In [11], the inside-outside duality is proved for the $\mathcal{B}-$eigenvalues μ which are associated with an eigenvalue problem defined within D_b under a specific boundary condition:

$$\mu w+\mathcal{B}(\partial_\nu w)=0 \text{ on } \partial D_b. \tag{5.17}$$

The operator $\mathcal{B}$, characterized in Assumption 25, does not include the identity operator. Consequently, the analysis presented in Chapter 4 does not allow the determination of the Steklov eigenvalues ([16]). Indeed, those Steklov eigenvalues belong to another kind of spectral problem characterized by a boundary condition of the form:

$$\mu\mathcal{D}(w)+\partial_\nu w=0 \text{ on } \partial D_b, \tag{5.18}$$

where $\mathcal{D}$ is an operator to be specified. Although the operators and properties involved are similar to those discussed in the preceding section, there are some significant technical differences.

5.3.1 Existence and discreteness of the eigenvalues

Definition 7. *μ is a $\mathcal{D}-$eigenvalue if there exists $w_0\in H^1(D_b)$ non trivial solution of*

$$\begin{cases} \Delta w_0+k^2 n w_0=0 \text{ in } D_b, \\ \mu\mathcal{D}(w_0)+\partial_\nu w_0=0 \text{ on } \partial D_b. \end{cases} \tag{5.19}$$

The study of the inside-outside duality requires the operator $\mathcal{D}$ to satisfy some properties. They are summarized in the following assumption:

Assumption 48. *The operator $\mathcal{D}: L^2(\partial D_b)\to L^2(\partial D_b)$ is*

1) linear bounded,

2) definite positive and self-adjoint.

3) $\mathcal{D}(H^{\frac{1}{2}}(\partial D_b)))\subset H^{\frac{1}{2}}(\partial D_b)$.

The last item ensures that for a given bounded sequence $(w_n)_{n\in\mathbb{N}}$ in $H^{\frac{1}{2}}(\partial D_b)$, $(\mathcal{D}(w_n))_{n\in\mathbb{N}}$ converges up to a subsequence in $L^2(\partial D_b)$.

Remark 10. *Alternatively, item 2) can be replaced with self-adjoint positive and of finite rank. In that case, the existence of a discrete set of eigenvalues is straightforward.*

Since $\mathcal{D}$ is definite positive and self adjoint, we introduce the definite positive self adjoint operator $\mathcal{D}^{\frac{1}{2}}$ such that $\mathcal{D}^{\frac{1}{2}}\mathcal{D}^{\frac{1}{2}}=\mathcal{D}$.

Proposition 49. *Assume k^2 is not a Dirichlet eigenvalue of (1.35). Then, the set of $\mathcal{D}-$eigenvalue is discrete.*

Proof. Multiplying the previous equation by a test function $w' \in H^1(D_b)$, integrating over the domain D_b and using Green formula, we obtain the equivalent variational formulation of (5.19): find $w_0 \in H^1(D_b)$ such that:

$$\int_{D_b} (\nabla w_0 \nabla \overline{w'} - k^2 n w_0 \overline{w'}) dx + \mu \int_{\partial D_b} \mathcal{D}(w_0) \overline{w'} ds = 0. \tag{5.20}$$

Thanks to the Riesz representation theorem, we introduce the following operator $\mathbb{A}_{\mathcal{D}}(\mu) : H^1(D_b) \to H^1(D_b)$:

$$(\mathbb{A}_{\mathcal{D}}(\mu) w_0, w')_{H^1(D_b)} = \int_{D_b} (\nabla w_0 \nabla \overline{w'} - k^2 n w_0 \overline{w'}) dx + \mu \int_{\partial D_b} \mathcal{D}(w_0) \overline{w'} ds, \tag{5.21}$$

for all $w' \in H^1(D_b)$.
One notices that $\mathbb{A}_{\mathcal{D}}(\mu)$ is a Fredholm operator by compact embedding of $H^1(D_b)$ (resp $H^{\frac{1}{2}}(\partial D_b)$) into $L^2(D_b)$ (resp into $L^2(\partial D_b)$) and analytic with respect to μ. Because n is real valued and k^2 is not a Dirichlet eigenvalue of (1.35), for every complex value μ with non zero imaginary part, $\mathbb{A}_{\mathcal{D}}(\mu)$ is injective. The proof is completed by applying the Analytic Fredholm Theorem. □

Introduce the compact self-adjoint operator $R_\alpha : L^2(\partial D_b) \to L^2(\partial D_b)$ such that $R_\alpha \theta = w_\theta$ where w_θ is the unique solution of

$$\begin{cases} \Delta w_\theta + k^2 n w_\theta = 0 \text{ in } D_b, \\ \alpha \mathcal{D}(w_\theta) + \partial_\nu w_\theta = \theta \text{ on } \partial D_b. \end{cases} \tag{5.22}$$

for $\alpha \in \mathbb{R}$ not a $\mathcal{D}-$eigenvalue.

Theorem 50. *Assume k^2 is not a Dirichlet eigenvalue of (1.35). Then μ is a $\mathcal{D}-$eigenvalue if and only if $\frac{1}{\alpha-\mu}$ is an eigenvalue of the compact self-adjoint operator $\mathcal{D}^{\frac{1}{2}} R_\alpha \mathcal{D}^{\frac{1}{2}}$.*

Proof. This proof draws inspiration from the work in [21].
We begin the proof by mentioning the existence of a discrete set of eigenvalues of the operator $\mathcal{D}^{\frac{1}{2}} R_\alpha \mathcal{D}^{\frac{1}{2}}$ without finite accumulation points.
Assume μ is a $\mathcal{D}-$eigenvalue associated with w_0. We can rewrite the variational formulation (5.20) as:

$$\begin{aligned} \int_{D_b} (\nabla w_0 \nabla \overline{w'} - k^2 w_0 \overline{w'}) dx + \alpha \int_{\partial D_b} \mathcal{D}(w_0) \overline{w'} d &= (\alpha - \mu) \int_{\partial D_b} \mathcal{D}(w_0) \overline{w'} ds, \\ &= \int_{\partial D_b} \mathcal{D}^{\frac{1}{2}}(\phi) \overline{w'} ds, \end{aligned} \tag{5.23}$$

where $\phi = (\alpha - \mu) \mathcal{D}^{\frac{1}{2}} w_0$. Hence, w_0 is solution of (5.22) with source term $\theta = \mathcal{D}^{\frac{1}{2}} \phi$ which gives us $R_\alpha \mathcal{D}^{\frac{1}{2}} \phi = w_0$. By definition of ϕ, we obtain $(\alpha - \mu) \mathcal{D}^{\frac{1}{2}} R_\alpha \mathcal{D}^{\frac{1}{2}} \phi = \phi$, proving the first implication ($\phi \neq 0$ because $w_0 \neq 0$ and $\mathcal{D}^{\frac{1}{2}}$ is definite).

Let $(\alpha-\mu)^{-1}$ be an eigenvalue of $\mathcal{D}^{\frac{1}{2}}R_\alpha\mathcal{D}^{\frac{1}{2}}$ associated with the eigenvector ϕ. Denote by $\varphi = R_\alpha\mathcal{D}^{\frac{1}{2}}\phi$ where φ is by definition the trace of $w_\theta \in H^1(D_b)$ the unique solution of (5.22) with $\theta = \mathcal{D}^{\frac{1}{2}}\phi = (\alpha-\mu)\mathcal{D}(w_\theta)$. $(w_\theta)|_{\partial D_b}$ is non trivial because $\mathcal{D}^{\frac{1}{2}}$ is definite positive and k^2 is not a Dirichlet eigenvalue. Inserting these equations in (5.22) gives the wanted result. □

Following the steps of proof of Theorem 2.15, assuming that $k^2 < \eta_0(n, D_b)$ (the smallest eigenvalue of (1.35)), one can show that the first $\mathcal{D}$-eigenvalue, denoted $\mu_{\mathcal{D}}$, satisfies:

$$\mu_{\mathcal{D}} = \sup_{w\in H^1(D_b), w|_{\partial D_b}\neq 0} \frac{\int_{D_b} n|w|^2dx - \int_{D_b}|\nabla w|^2dx}{\int_{\partial D_b}\mathcal{D}(w)\overline{w}ds}, \tag{5.24}$$

yielding once again a monotonicity property with respect to n.

5.3.2 Background media and operators

In this subsection, we introduce the background media associated to the $\mathcal{D}-$eigenvalues. We will revisit the steps outlined in section 4.2. Let $u_b \in H^1_{loc}(\mathbb{R}^m\backslash D_b)$ be the total field solution of:

$$\begin{cases} \Delta u_b + k^2 u_b = 0 \text{ in } \mathbb{R}^m\backslash D_b, \\ \mu\mathcal{D}(u_b) + \partial_\nu u_b = 0 \\ u_b = u_b^s + u^i \\ \lim\limits_{r\to+\infty}\int_{|x|=r}|\frac{\partial u_b^s}{\partial r} - iku_b^s|^2 = 0, \end{cases} \tag{5.25}$$

for some incident field u^i and for some parameter $\mu \in \mathbb{R}$. The domain $D_b \subset \mathbb{R}^m$ has the same properties as in the previous section. For simplicity, we assume that $D \subset D_b$. The well-posedness of this problem for $\mu \in \mathbb{R}$ is similar to the one for problem (4.1) proved in section 4.6.2. In addition, (5.25) is equivalent to the following variational problem: find $u \in H^1(B_R\backslash D_b)$ such that

$$\int_{B_R\backslash D_b}(\nabla u\nabla v - k^2uv)dx - \int_{\partial B_R}\Lambda uvds - \mu\int_{\partial D_b}\mathcal{D}(u)vds = \ell(v) \tag{5.26}$$

where

$$\ell(v) := \int_{\partial B_R}(\partial_\nu u^i - \Lambda u^i)vds, \tag{5.27}$$

for all $v \in H^1(B_R\backslash D_b)$. B_R is a ball of radius R containing D_b and Λ is the Dirichlet to Neumann map defined in section 4.6.2.
In line with the background problem associated with the $\mathcal{B}-$eigenvalues, we introduce the operator $F^\mu_{\mathcal{D}} : L^2(\mathbb{S}) \to L^2(\mathbb{S})$ defined by

$$(F^\mu_{\mathcal{D}}g)(\hat{x}) := \int_{\mathbb{S}} g(d)u_b^\infty(\hat{x}, d)ds(d), \quad \hat{x} \in \mathbb{S}, \tag{5.28}$$

where $u_b^\infty(., d)$ is the far field associated with u_b^s the scattered field in (5.25) with $u^i(x) = e^{ikx\cdot d}$, for $d \in \mathbb{S} := \{x \in \mathbb{R}^m, |x| = 1\}$.
The inside-outside duality method is based on the behavior of the operator

$$\mathbf{F}^\mu := -\gamma S_b^*\mathcal{F}^\mu, \tag{5.29}$$

where $\mathcal{F}^\mu := F - F_{\mathcal{D}}^\mu$ and $S_b := I + \frac{2ik}{\overline{\gamma}} F_b^\mu$ is the scattering operator associated with the background. This scattering operator is unitary, this can be demonstrated similarly to the proof in Proposition 40. We highlight the negative sign in this definition that contrasts with the previous chapter. We shall now review the steps of the inside-outside duality that will be developed in the following sections:

1) Factorize the operator $\mathbf{F}^\mu$ in the form $\mathbf{F}^\mu = \mathcal{H}_{\mathcal{D}}{}^* T_{\mathcal{D}} \mathcal{H}_{\mathcal{D}}$.

2) Show that the operator $T_{\mathcal{D}}$ can be decomposed as the sum of a compact and a real coercive operator.

3) Link the imaginary part of the operator $T_{\mathcal{D}}$ to the $\mathcal{D}-$eigenvalue.

4) Prove the sufficient condition of the inside-outside duality theorem relying on the real coercive operator in the decomposition of $T_{\mathcal{D}}$.

5) Prove the necessary condition.

5.3.3 Factorization of $\mathbf{F}^\mu$

The operator $\mathbf{F}^\mu$ can be factorized as follow:

$$\mathbf{F}^\mu = \mathcal{H}_{\mathcal{D}}^* T_{\mathcal{D}} \mathcal{H}_{\mathcal{D}}. \tag{5.30}$$

The steps to obtain this factorization are close to those in section 4.3, as the operators share similar properties with those presented in that section.
Let $\mathcal{H}_{\mathcal{D}} : L^2(\mathbb{S}) \to H^{\frac{1}{2}}(\partial D_b)$ be defined as:

$$\mathcal{H}_{\mathcal{D}} g := u_{b,g}|_{\partial D_b}, \tag{5.31}$$

where $u_{b,g}$ is solution of (5.25) with $u^i = v_g$, the Herglotz wave function defined in (1.5). The following lemma characterizes its range and adjoint.

Lemma 51. *The operator $\mathcal{H}_{\mathcal{D}}$ is injective and its range is dense in $H^{\frac{1}{2}}(\partial D_b)$. Moreover, the adjoint operator $\mathcal{H}_{\mathcal{D}}^*$ is defined by: $\mathcal{H}_{\mathcal{D}}^* \psi = -\gamma S_b^* \widetilde{w}^\infty$ for all $\psi \in H^{-\frac{1}{2}}(\partial D_b)$, where $\widetilde{w}^\infty$ is the far field pattern of $\widetilde{w} \in H^1_{loc}(\mathbb{R}^m \backslash D_b)$ solution of:*

$$\begin{cases} \Delta \widetilde{w} + k^2 \widetilde{w} = 0 \text{ in } \mathbb{R}^m \backslash D_b, \\ \mu \mathcal{D}(\widetilde{w}) + \partial_\nu \widetilde{w} = \psi \text{ on } \partial D_b, \\ \lim\limits_{r \to +\infty} \int_{|x|=r} |\frac{\partial \widetilde{w}}{\partial r} - ik\widetilde{w}|^2 = 0. \end{cases} \tag{5.32}$$

Proof. The injectivity of $\mathcal{H}_{\mathcal{D}}$ can be prove by contradiction with the same arguments used to prove the injectivity of $\mathcal{H}_{\mathcal{B}}$. We now prove the last part of the lemma. Let $g \in L^2(\mathbb{S})$. Equations (4.20), (4.21) and (4.23) can also be obtained for $\widetilde{w}$ solution of (5.32).
Using the boundary condition of $\widetilde{w}$ and $u_{b,g}$, we deduce that

$$\begin{aligned} \int_{\partial D_b} (\partial_\nu \overline{\widetilde{w}} u_{b,g} - \overline{\widetilde{w}} \partial_\nu u_{b,g}) ds &= \int_{\partial D_b} \partial_\nu \overline{\widetilde{w}} u_{b,g} - \mu \overline{\widetilde{w}} \mathcal{D}(u_{b,g}) ds \\ &= \int_{\partial D_b} u_{b,g} \overline{\psi} ds, \end{aligned} \tag{5.33}$$

where, for the last equality we used the fact that $\mathcal{D}$ is self-adjoint. Equation (4.20), (4.21), (4.23) and (5.33) give

$$\int_{\partial D_b} u_{b,g}\overline{\psi}ds = -2ik\int_{\mathbb{S}}\overline{\widetilde{w}^{\infty}}(d)u^{\infty}_{b,g}(d)ds(d) - \overline{\gamma}\int_{\mathbb{S}} g(d)\overline{\widetilde{w}^{\infty}(d)}ds. \tag{5.34}$$

Hence, using the definition of $\mathcal{H}_{\mathcal{D}}$, we get:

$$\begin{aligned}\langle \mathcal{H}_{\mathcal{D}}g,\psi\rangle_{H^{\frac{1}{2}}(\partial D_b),H^{-\frac{1}{2}}(\partial D_b)} &= -\overline{\gamma}(g,\widetilde{w}^{\infty})_{L^2(\mathbb{S})} - 2ik(F^b g,\widetilde{w}^{\infty})\\ &= -\overline{\gamma}(S_b g,\widetilde{w}^{\infty})_{L^2(\mathbb{S})}.\end{aligned} \tag{5.35}$$

We then conclude that $\mathcal{H}_{\mathcal{D}}{}^*\psi = -\gamma S_b^*\widetilde{w}^{\infty}$. The densessness of the range of $\mathcal{H}_{\mathcal{D}}$ is a direct consequence of the injectivity of $\mathcal{H}_{\mathcal{D}}{}^*$ which can be proved using Rellich's lemma and the fact that S_b^* is unitary. □

The operator $T_{\mathcal{D}} : H^{\frac{1}{2}}(\partial D_b) \to H^{-\frac{1}{2}}(\partial D_b)$ is defined as follow:

$$T_{\mathcal{D}}(\phi) = \mu\mathcal{D}(w) + \partial_\nu w = \mu\mathcal{D}(w^s) + \partial_\nu w^s, \tag{5.36}$$

where $(w, w^s) \in H^1(D_b) \times H^1_{loc}(\mathbb{R}^m\backslash D_b)$ is the unique solution of:

$$\begin{cases} \Delta w + k^2 n w = 0 \text{ in } D_b,\\ \Delta w^s + k^2 w^s = 0 \text{ in } \mathbb{R}^m\backslash D_b,\\ \mu\mathcal{D}(w^s) + \partial_\nu w^s = \mu\mathcal{D}(w) + \partial_\nu w \text{ on } \partial D_b,\\ w - w^s = \phi \text{ on } \partial D_b,\\ \lim\limits_{r\to+\infty}\int_{|x|=r}|\frac{\partial w^s}{\partial r} - ikw^s|^2 = 0. \end{cases} \tag{5.37}$$

Therefore, one can show the equality $\gamma\mathcal{F}^{\mu} = -S_b\mathcal{H}_{\mathcal{D}}{}^*T_{\mathcal{D}}\mathcal{H}_{\mathcal{D}}$ and deduce the factorization (5.30).
We remark that the solution (w, w^s) of (5.37) are linear with respect to μ. Indeed, we have $w = \mu w_D + w_N$ (respectively $w^s = \mu w_D^s + w_N^s$) where (w_D, w_D^s) and (w_N, w_N^s) do not depend on μ and are solution of

$$\begin{cases} \Delta w_N + k^2 n w_N = 0 \text{ in } D_b,\\ \Delta w_N^s + k^2 w_N^s = 0 \text{ in } \mathbb{R}^m\backslash D_b,\\ w_N - w_N^s = \phi \text{ on } \partial D_b,\\ \partial_\nu w_N - \partial_\nu w_N^s = 0 \text{ on } \partial D_b,\\ \lim\limits_{r\to+\infty}\int_{|x|=r}|\frac{\partial w_N^s}{\partial r} - ikw_N^s|^2 = 0, \end{cases} \qquad \begin{cases} \Delta w_D + k^2 n w_D = 0 \text{ in } D_b,\\ \Delta w_D^s + k^2 w_D^s = 0 \text{ in } \mathbb{R}^m\backslash D_b,\\ w_D - w_D^s = 0 \text{ on } \partial D_b,\\ \partial_\nu w_D - \partial_\nu w_D^s = -\mathcal{D}(\phi) \text{ on } \partial D_b,\\ \lim\limits_{r\to+\infty}\int_{|x|=r}|\frac{\partial w_D^s}{\partial r} - ikw_D^s|^2 = 0. \end{cases} \tag{5.38}$$

Lemma 52. *Problem (5.37) is well posed for all ϕ in $H^{\frac{1}{2}}(\partial D_b)$. Furthermore, the solution (w, w^s) of (5.37) with source term ϕ satisfies the estimate for any compact set Ω that contains D_b:*

$$\|w^s\|^2_{H^1(K\backslash D_b)} + \|w\|^2_{H^1(D_b)} \leq (\mu C_1 + C_2)\|\phi\|^2_{H^{\frac{1}{2}}(\partial D_b)}, \tag{5.39}$$

where $C_1, C_2 > 0$ do not depend on ϕ and μ. In addition, by elliptic regularity, for any compact set $\Omega \subset \mathbb{R}^m \backslash \overline{D_b}$, there exists a constant $C_b > 0$ independent from ϕ such that

$$\|w^s\|^2_{H^2(\Omega)} \leq C_b \|\phi\|^2_{H^{\frac{1}{2}}(\partial D_b)}. \tag{5.40}$$

Proof. This result is a direct consequence of the well posedness of the problems (5.38) and the linearity of the solution of (5.37) with respect to μ. □

5.3.4 Key properties of the operator $T_{\mathcal{D}}$

To shorten the notations, the duality product $\langle ., . \rangle_{H^{-\frac{1}{2}}(\partial D_b), H^{\frac{1}{2}}(\partial D_b)}$ will be denoted $\langle ., . \rangle$ or in an abuse of notation as an integral over ∂D_b.

Lemma 53. *The operator $T_{\mathcal{D}}$ satisfies the energy identity:*

$$\Im m \, \langle T_{\mathcal{D}} \phi, \phi \rangle = -k \int_{\mathbb{S}} |w^\infty|^2 ds, \quad \forall \phi \in H^{-\frac{1}{2}}(\partial D_b), \tag{5.41}$$

where w^∞ is the far field pattern of w^s, with (w, w^s) being the solution of (5.37) with source term ϕ.

Proof. Let $\phi \in H^{\frac{1}{2}}(\partial D_b)$, using that $\phi = w - w^s$, we get

$$\langle T_{\mathcal{D}} \phi, \phi \rangle = \int_{\partial D_b} \overline{w}(\mu \mathcal{D}(w) + \partial_\nu w) ds - \int_{\partial D_b} \partial_\nu \overline{w^s}(\mu \mathcal{D}(w^s) + \partial_\nu w^s) ds. \tag{5.42}$$

Let us focus on the last term of the previous equality. Using Green's formula on a ball B_R of radius $R > 0$ large enough, one obtains:

$$\begin{aligned} 0 \; &= - \textstyle\int_{B_R \backslash D_b} \overline{w^s}(\Delta w^s + k^2 w^s) dx \\ &= \textstyle\int_{B_R \backslash D_b} |\nabla w^s|^2 dx - k^2 \int_{B_R \backslash D_b} |w^s|^2 dx \\ &-ik \textstyle\int_{\partial B_R} |w^s|^2 ds - \int_{\partial B_R} (\partial_\nu w^s - ik w^s) \overline{w^s} ds \\ &+ \textstyle\int_{\partial D_b} \partial_\nu w^s \overline{w^s} ds. \end{aligned} \tag{5.43}$$

Substituting the expression of $\int_{\partial D_b} \partial_\nu w^s \overline{w^s} ds$ in (5.42) gives

$$\begin{aligned} \langle T_{\mathcal{D}} \phi, \phi \rangle \; &= \textstyle\int_{\partial D_b} \partial_\nu w \overline{w} ds \\ &+ \textstyle\int_{B_R \backslash D_b} |\nabla w^s|^2 dx - k^2 \int_{B_R \backslash D_b} |w^s|^2 dx \\ &-ik \textstyle\int_{\partial B_R} |w^s|^2 ds - \int_{\partial B_R} (\partial_\nu w^s - ik w^s) \overline{w^s} ds \\ &+\mu \textstyle\int_{\partial D_b} \mathcal{D}(w) \overline{w} - \mu \int_{\partial D_b} \mathcal{D}(w^s) \overline{w^s}, \end{aligned} \tag{5.44}$$

Taking the imaginary part of this equality while letting $R \to +\infty$, we obtain

$$\begin{aligned} \Im m \langle T_{\mathcal{D}}\phi, \phi\rangle &= -k \int_S |w^\infty|^2 ds + \Im m \int_{\partial D_b} \partial_\nu w \overline{w} ds, \\ &= -k \int_S |w^\infty|^2 ds, \end{aligned} \tag{5.45}$$

where for the last equality, we used that $\Delta w + k^2 n w = 0$ in D_b. □

Proposition 54. *Let $\mu \in \mathbb{R}$. μ is a $\mathcal{D}-$eigenvalue if and only if there exists a non trivial $\phi \in H^{\frac{1}{2}}(\partial D_b)$ such that $\Im m \langle T_{\mathcal{D}}\phi, \phi\rangle = 0$.*

Proof. Assume that μ is a $\mathcal{D}-$eigenvalue. We denote by $w_0 \in H^1(D_b)$ its associated eigenvector. Set $\phi = w_0|_{\partial D_b}$ which is necessarily non trivial. Consider (w, w^s) the associated solution of (5.37). We then get thanks to Green's theorem:

$$\begin{aligned} \langle T_{\mathcal{D}}\phi, \phi\rangle &= \int_{\partial D_b} \partial_\nu w \overline{w_0} ds + \mu \int_{\partial D_b} \overline{w_0} \mathcal{D}(w) ds \\ &= \int_{\partial D_b} \partial_\nu \overline{w_0} w ds + \mu \int_{\partial D_b} w \mathcal{D}(\overline{w_0}) ds = 0, \end{aligned} \tag{5.46}$$

where we used the fact that $\mathcal{D}$ is self-adjoint and the fact w, w_0 verify the same inhomogeneous Helmholtz equation in D_b.
Conversely, assume there exists $\phi \in H^{\frac{1}{2}}(\partial D_b)$ non trivial such that $\Im m \langle T_{\mathcal{D}}\phi, \phi\rangle = 0$. By Rellich lemma, this implies $w^s = 0$ in $\mathbb{R}^m \backslash D_b$ where (w, w^s) is the solution of (5.37) with source term ϕ. In particular, we get $w^s|_{\partial D_b} = 0$ and $\partial_\nu w^s|_{\partial D_b} = 0$. Thus, μ is a $\mathcal{D}-$eigenvalue associated with the non trivial eigenvector w. □

We conclude this section by showing that $T_{\mathcal{D}}$ is a Fredholm operator of index 0.

Lemma 55. *$T_{\mathcal{D}}$ admits the following decomposition*

$$T_{\mathcal{D}} = T_0 + K, \tag{5.47}$$

where K is compact and T_0 is coercive. More precisely, there exists a $\alpha > 0$ such that

$$\langle T_0\phi, \phi\rangle \geq \alpha \|\phi\|^2_{H^{\frac{1}{2}}(\partial D_b)}. \tag{5.48}$$

Proof. The proof follows the approach used in the proof of Lemma 32. Let B_R be a ball containing D_b for R large enough. For $\phi, \phi' \in H^{\frac{1}{2}}(\partial D_b)$, we define the operator $T_0 : H^{\frac{1}{2}}(\partial D_b) \to H^{-\frac{1}{2}}(\partial D_b)$ as:

$$\begin{aligned} \langle T_0\phi, \phi'\rangle = &\int_{B_R \backslash D_b} \nabla w^s \nabla \overline{w'^s} dx + \int_{B_R \backslash D_b} w^s \overline{w'^s} dx \\ &+ \int_{D_b} \nabla w \nabla \overline{w'} dx + \int_{D_b} w \overline{w'} dx, \end{aligned} \tag{5.49}$$

and $K : H^{\frac{1}{2}}(\partial D_b) \to H^{-\frac{1}{2}}(\partial D_b)$ as:

$$\begin{aligned}\langle K\phi, \phi' \rangle = \quad & -(1+k^2)\int_{B_R \setminus D_b} w^s \overline{w'^s} dx \\ & -(1+k^2)\int_{D_b} n w \overline{w'} dx \\ & -\int_{\partial B_R} \partial_\nu w^s \overline{w'^s} ds \\ & +\mu \int_{\partial D_b} \overline{w'} \mathcal{D}(w) ds - \mu \int_{\partial D_b} \overline{w'^s} \mathcal{D}(w^s) ds.\end{aligned} \tag{5.50}$$

Thus, one can write $T_{\mathcal{B}} = T_0 + K$.
Since $\phi = w - w^s$, we deduce that

$$\begin{aligned}\|\phi\|^2_{H^{\frac{1}{2}}(\partial D_b)} & \leq 2(\|w\|^2_{H^{\frac{1}{2}}(\partial D_b)} + \|w^s\|^2_{H^{\frac{1}{2}}(\partial D_b)}), \\ & \leq 2(\|w\|^2_{H^1(D_b)} + \|w^s\|^2_{H^1(B_R \setminus D_b)}), \\ & = 2\langle T_0 \phi, \phi \rangle .\end{aligned} \tag{5.51}$$

The compactness of the operator K is a direct consequence of a priori estimates in Lemma 52, trace theorems, Rellich's compact embedding theorems and the fact that $\mathcal{D}(H^{\frac{1}{2}}(\partial D_b))) \subset H^{\frac{1}{2}}(\partial D_b)$. □

5.3.5 The inside-outside duality applied to $\mathbf{F}^\mu$

Consider the case where μ is not a $\mathcal{D}-$eigenvalue. Since $\mathbf{F}^\mu$ is a compact normal operator, there exists an orthonormal complete basis $(g_j)_{j\in\mathbb{N}}$ of $L^2(\mathbb{S})$ such that $\mathbf{F}^\mu g_j = \lambda_j g_j$ where $(\lambda_j)_{j\in\mathbb{N}}$ are the eigenvalues of $\mathbf{F}^\lambda$ that accumulate at 0.
Exploiting the fact that $\mathbf{S} := I - \frac{2ik}{|\gamma|^2}\mathbf{F}^\mu$ is unitary, we deduce that the eigenvalues of $\mathbf{F}^\mu$ lie on the circle of radius $\frac{|\gamma|^2}{2k}$ and center $-\frac{|\gamma|^2}{2ik}$. We set $\lambda_j := \frac{|\gamma|^2}{2ik}(1 - e^{i\delta_j})$ with $e^{i\delta_j}$ being an eigenvalue of $\mathbf{S}$, $\delta_j \in [0, 2\pi)$ and define

$$\begin{cases} \delta_*(\mu) & := \max_{j\geq 1} \delta_j, \\ \lambda_* & := \frac{|\gamma|^2}{2ik}(1 - e^{i\delta_*}). \end{cases} \tag{5.52}$$

We then can state the main theorem of this section:

Theorem 56. *Assume that k^2 is not an eigenvalue of (1.35). μ_0 is a $\mathcal{D}-$eigenvalue if and only if $\delta_*(\mu) \to 2\pi$ as $\mu \to \mu_0$ with $\mu > \mu_0$.*

5.3.6 Proof of the sufficient condition in Theorem 56

Since we will be dealing with convergence of sequences that depend on μ, we shall explicitly indicate the dependence on μ in the notation for the operators (in particular, the operator $\mathbf{F}^\mu$ is factorized as $\mathcal{H}^*_{\mathcal{D}}(\mu) T_{\mathcal{D}}(\mu) \mathcal{H}_{\mathcal{D}}(\mu)$).

Proposition 57. *The mapping $\mu \to T_{\mathcal{D}}(\mu)$ is continuous from $\mathbb{R}$ to the space of linear bounded operators from $H^{\frac{1}{2}}(\partial D_b)$ to $H^{-\frac{1}{2}}(\partial D_b)$ endowed with the usual operator norm.*

Proof. The proof is a direct consequence of the linear dependence with respect to μ of the solution (w, w^s) of problem (5.37) (see (5.38)) and the expression of $T_{\mathcal{D}}(\lambda)$. □

Proposition 58. *Let $\lambda_0 \in \mathbb{R}$ and $I = (\lambda_0 - \varepsilon, \lambda_0 + \varepsilon)\backslash\{\lambda_0\}$ for some $\varepsilon > 0$ sufficient small such that no $\lambda \in I$ is a $\mathcal{D}-$eigenvalue. Assume there is a sequence $(\lambda_j)_j$ of elements of I such that*

$$\lambda_j \longrightarrow \lambda_0 \qquad \text{and} \qquad \delta_*(\lambda_j) \longrightarrow 2\pi. \tag{5.53}$$

Then λ_0 is a $\mathcal{D}-$eigenvalue.

Proof. This can be proved by contradiction using the same steps as in the proof of Proposition 34. We use this time the sequence $\varphi_j = \frac{1}{\sqrt{|\lambda_*|}}\mathcal{H}_{\mathcal{D}}(\lambda_j)g_j$. The argument using the compactness of the operator $\mathcal{B}$ is replaced by the fact that $\mathcal{D}(H^{\frac{1}{2}}(\partial D_b))) \subset H^{\frac{1}{2}}(\partial D_b)$.

Consider the sequence $\varphi_j = \frac{1}{\sqrt{|\lambda_*|}}\mathcal{H}_{\mathcal{D}}(\mu_j)g_j$, where g_j is the normalized eigenvector of $\mathbf{F}^{\mu_j}$ associated with $\lambda_*(\mu_j)$. We then have by assumptions

$$\langle T_{\mathcal{D}}(\mu_j)\varphi_i, \varphi_i\rangle = \frac{\lambda_*(\mu_j)}{|\lambda_*(\mu_j)|} \longrightarrow_{j\to+\infty} -1. \tag{5.54}$$

Assume by contradiction that μ_0 is not a $\mathcal{D}-$eigenvalue.
In that case, the operator $T_{\mathcal{D}}(\mu_j)$ is coercive for every $\mu_j \in I$. Using that $\mu \to T_{\mathcal{D}}(\mu)$ is continuous in the operator norm, we infer that the coercivity constant can be chosen independent from $\mu \in \overline{I}$ (see Lemma 41). The coercivity of $T_{\mathcal{D}}(\mu_j)$ and identity (5.54) show that $(\varphi_j)_j$ is bounded and therefore weakly converges (up to a subsequence) to some φ_0 in $H^{\frac{1}{2}}(\partial D_b)$. Denote by (w_j, w_j^s) (respectively (w_0, w_0^s)) the solution of (5.37) with $\phi = \varphi_j$ (respectively $\phi = \varphi_0$). From Lemma 53, one gets:

$$\Im m\,\langle T_{\mathcal{D}}(\mu_j)\varphi_j, \varphi_j\rangle = -k\int_{\mathbb{S}} |w_j^\infty|^2 ds. \tag{5.55}$$

Since the application $\phi \in H^{\frac{1}{2}}(\partial D_b) \to w^\infty(\phi) \in L^2(\mathbb{S})$ (where $w^\infty(\phi)$ is the far field pattern of w^s solution of (5.37) with source term ϕ) is compact, then $\Im m\,\langle T_{\mathcal{D}}(\mu_j)\varphi_j, \varphi_j\rangle$ converges to $\Im m\,\langle T_{\mathcal{D}}(\mu_0)\varphi_0, \varphi_0\rangle$. Identity (5.54) implies that $\lim_{j\to+\infty} \Im m\,\langle T_{\mathcal{D}}(\mu_j)\varphi_j, \varphi_j\rangle = 0$ and therefore $\varphi_0 = 0$ by Proposition 54.
Recall that $T_{\mathcal{D}}(\mu_j)$ assumes the decomposition $T_{\mathcal{D}}(\mu_j) = T_0(\mu_j) + K(\mu_j)$, where $T_0(\mu_j)$ is real coercive and $K(\mu_j)$ is compact. Let us show that $\lim_{j\to+\infty} \langle K(\mu_j)\varphi_j, \varphi_j\rangle = 0$. From the decomposition shown in Lemma 55, we get that

$$\begin{aligned}\langle K(\mu_j)\varphi_j, \varphi_j\rangle = \; & -(1+k^2)\|w_j^s\|^2_{H^1(B_R\backslash D_b)} \\ & -(1+k^2)(nw_j, w_j)_{H^1(D_b)} \\ & -\textstyle\int_{\partial B_R} \partial_\nu w_j^s \overline{w_j^s} ds \\ & +\mu_j \textstyle\int_{\partial D_b} \overline{w_j}\mathcal{D}(w_j)ds - \mu_j \int_{\partial D_b} \overline{w_j^s}\mathcal{D}(w_j^s)ds.\end{aligned} \tag{5.56}$$

All the terms converge to 0 by the same arguments as in the proof of the compactness of $K(\mu_j)$ for μ_j fixed in Lemma 55 and the fact that μ_j converges to μ_0. This shows that $\lim_{j\to+\infty}\langle K(\mu_j)\varphi_j,\varphi_j\rangle = 0$.
We deduce that (up to a subsequence) $\langle T_0(\mu_j)\varphi_j,\varphi_j\rangle$ converges to -1 which is a contradiction since $\langle T_0(\mu_j)\varphi_j,\varphi_j\rangle \geq 0$ for all $j\in\mathbb{N}$ (Lemma 55).

□

5.3.7 Proof of the necessary condition in Theorem 56

For the proof of the necessary condition, we use the Cayley transform associated with $\mathbf{S}$ ([43]).
Assume that μ is not a $\mathcal{D}-$eigenvalue. Then 1 is not an eigenvalue of $\mathbf{S}$ because $\mathbf{F}$ is injective and we can define the Cayley transform:

$$\mathcal{T} := i(Id+\mathbf{S})(Id-\mathbf{S})^{-1}.$$

$\mathcal{T}$ is self-adjoint and has a discrete spectrum. We have the equivalence $e^{i\delta_*}$ is an eigenvalue of $\mathbf{S}$ if and only if $\cot(\delta_*/2)\in\mathbb{R}$ is an eigenvalue of $\mathcal{T}$. Applying Courant Fischer min max principle to $\mathcal{T}$, we get:

$$\cot(\delta_*/2) = \inf_{\phi\in H^{\frac{1}{2}}(\partial D_b)} \frac{\Re e\,\langle T\phi,\phi\rangle}{\Im m\,\langle T\phi,\phi\rangle}. \tag{5.57}$$

Let μ_0 be a $\mathcal{D}-$eigenvalue associated with the eigenvector w_0. For $\mu\in\mathbb{R}$, define $(w(\mu),w^s(\mu))$ the solution of (5.37) with source term $\phi = w_0$. From the linearity of those solutions with respect to μ (see decomposition (5.38)), one can obtain the following expansion:

$$w(\mu) - w_0 = (\mu-\mu_0)w_D^0, \tag{5.58}$$

where w_D^0 does not depend on μ and is solution of (5.38) with $\phi = w_0$.

Proposition 59. *Let μ_0 be a $\mathcal{D}-$eigenvalue associated with w_0. For $\mu\in\mathbb{R}$, define $(w(\mu),w^s(\mu))$ the solution of (5.37) with source term $\phi = w_0$ and parameter μ. Then :*

$$\langle T_{\mathcal{D}}(\mu)w_0,\partial_\nu w_0\rangle = (\mu-\mu_0)\langle\mathcal{D}(w_0),w_0\rangle + (\mu-\mu_0)^2\langle\partial_\nu w_D^0,w_0\rangle. \tag{5.59}$$

Proof. According to the definition of $T_{\mathcal{D}}(\mu)$, we get:

$$\langle T_{\mathcal{D}}(\mu)w_0,w_0\rangle = \langle\mu\mathcal{D}(w(\mu)) + \partial_\nu w(\mu),w_0\rangle. \tag{5.60}$$

Since $-\langle T_{\mathcal{D}}(\mu_0)w_0,w_0\rangle = 0$, we can add it to the previous equality and by rearranging the terms, one has

$$\langle T_{\mathcal{D}}(\mu)w_0,w_0\rangle = \langle\mu\mathcal{D}(w(\mu)-w_0) + (\partial_\nu w(\mu)-\partial_\nu w_0),w_0\rangle + (\mu-\mu_0)\langle\mathcal{D}(w_0),w_0\rangle. \tag{5.61}$$

The previous equality can be rewritten using (5.58) as:

$$\langle T_{\mathcal{D}}(\mu)w_0,w_0\rangle = (\mu-\mu_0)\left(\langle\mu\mathcal{D}(w_D^0)+\partial_\nu w_D^0,w_0\rangle + \langle\mathcal{D}(w_0),w_0\rangle\right). \tag{5.62}$$

Using Green's theorem, we have:

$$\begin{aligned} 0 &= -\int_{D_b}(\Delta w_D^0 + k^2 n w_D^0)\overline{w_0}dx = \int_{\partial D_b}(\partial_\nu \overline{w_0} w_D^0 - \partial_\nu w_D^0 \overline{w_0})ds \\ &= \langle \mu_0 \mathcal{D}(w_D^0) + \partial_\nu w_D^0, w_0 \rangle . \end{aligned} \tag{5.63}$$

Expression (5.59) is obtained by substituting $\langle w_D^0, w_0 \rangle$ in (5.62). □

We possess all the ingredients to prove the following necessary condition.

Proposition 60. *Assume that μ_0 is a $\mathcal{D}-$eigenvalue. Then $\delta_*(\mu) \to 2\pi$ as $\mu \to \mu_0$ with $\mu > \mu_0$.*

Proof. Since $\mathcal{D}$ is definite positive, $\langle \mathcal{D}(w_0), w_0 \rangle$ is non zero.
Let μ_0 be a $\mathcal{D}-$eigenvalue associated with the eigenvector w_0. Then we have for μ in a neighbourhood of μ_0:

$$\cot(\delta_*(\mu)/2) = \inf_{\phi \in H^{\frac{1}{2}}(\partial D_b)} \frac{\Re \langle T_{\mathcal{D}}(\mu)\phi, \phi \rangle}{\Im m \langle T_{\mathcal{D}}(\mu)\phi, \phi \rangle} \leq \frac{\Re \langle T_{\mathcal{D}}(\mu) w_0, w_0 \rangle}{\Im m \langle T_{\mathcal{D}}(\mu) w_0, w_0 \rangle}, \tag{5.64}$$

with $\Im m \langle T_{\mathcal{D}}(\mu) w_0, w_0 \rangle < 0$ thanks to Lemma 53. From the previous Lemma, we conclude that:

$$\frac{\Re \langle T_{\mathcal{D}}(\mu) w_0, w_0 \rangle}{\Im m \langle T_{\mathcal{D}}(\mu) w_0, w_0 \rangle} = \frac{\langle \mathcal{D}(w_0), w_0 \rangle + (\mu - \mu_0)\Re e(\langle \partial_\nu w_D^0, w_0 \rangle)}{(\mu - \mu_0)\Im m \langle T_{\mathcal{D}}(\mu) w_0, w_0 \rangle} \to -\infty, \tag{5.65}$$

as $\mu \to \mu_0$ with $\mu > \mu_0$. Combined with 5.64, this proves the claim of the proposition. □

5.4 Numerical validation and indicator function of the refractive index

The purpose of this section is twofold. The first objective is to numerically validate Theorem 42 and 56. To achieve this, we will work on a simple circular case in dimension 2. The other objective is to enhance the indicator function introduced in Chapter 3 with the $\mathcal{B}-$Dirichlet eigenvalues.

5.4.1 Case of a disc

We begin this section with the same configuration as in Section 4.5. Consider the situation where $D = D_b = B_\rho$ is a disk of radius $\rho > 0$ centered at the origin. We assume that n is constant inside B_ρ and $n = 1$ outside.

The $\mathcal{B}-$Dirichlet eigenvalues

For $\mathcal{Q}$ a subset of $\mathbb{N}$, we use as operator $\mathcal{B}$ in the background problem (4.1) the one defined by

$$\mathcal{B}\psi = \sum_{q \in \mathcal{Q}} \langle \psi, e_q \rangle e_q, \tag{5.66}$$

where $e_q(\theta) := e^{iq\theta}$, $\theta \in [0, 2\pi)$. In that case, for a fixed parameter $\mu > 0$, the $\mathcal{B}-$Dirichlet eigenvalues are solution of the following equations:

$$\begin{cases} \mu J_q(k\rho\sqrt{n}) + 2\pi k\rho\sqrt{n} J_q'(k\rho\sqrt{n}) = 0, \text{ for } q \in \mathcal{Q}, \\ J_q(k\rho\sqrt{n}) = 0, \text{ for } q \notin \mathcal{Q}, \end{cases} \tag{5.67}$$

where J_j denotes the Bessel function of the first kind of order j.
With a Herglotz wave function of the form (1.5) as an incident field with density

$$g(\theta) = \sum_{m\in\mathbb{Z}} g_m e^{im\theta}, \tag{5.68}$$

the far field patterns F and F_b^μ takes the form (4.67) and (4.69).
In that situation, the eigenvalues of the scattering operator $\mathbf{S}$ are

$$e^{i\delta_m} := 1 + \frac{2ik}{\overline{\gamma}}(1 - \frac{2ik}{\gamma}\overline{\beta_m})(\alpha_m - \beta_m)$$

where $\delta_m \in [0, 2\pi)$ denote their corresponding phases and the α_m are defined in (4.68).

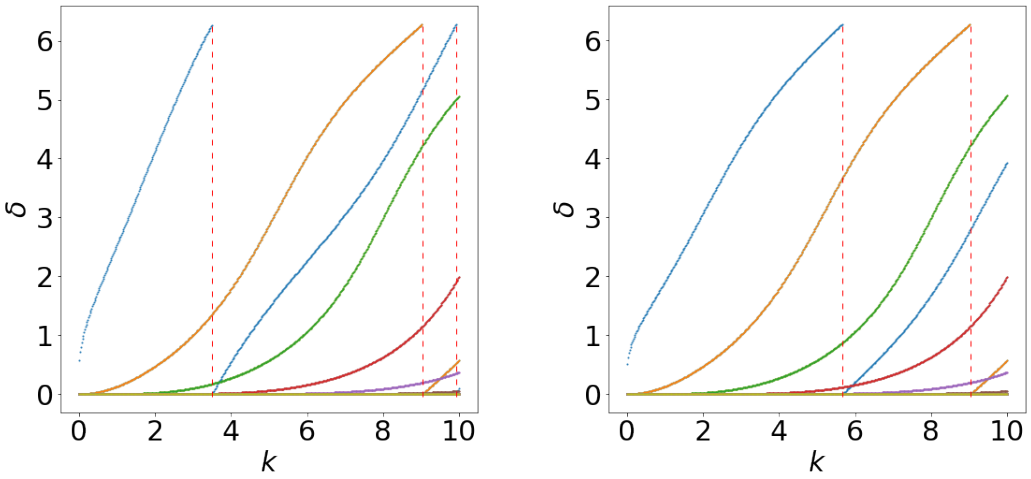

Figure 5.1: For $m \in \{-10, ...10\}$, we plot the curves $k \to \delta_m(k)$ where $D = D_b = B_\rho$ for $\rho = 0.3$ and $n = 1$. Each color corresponds to a value of m. The red dashed lines indicate the $\mathcal{B}-$Dirichlet eigenvalues. Left: $\mu = 10$ and $\mathcal{Q} = \{0\}$. Right: $\mathcal{B} = 0$ and $\mathcal{Q} = \varnothing$.

In Figure 5.1 (left), we plot the curves $k \to \delta_m(k)$ for $m \in \{-10, ...10\}$ and $\mathcal{Q} = \{0\}$. The vertical red dashed indicate the $\mathcal{B}-$Dirichlet eigenvalues, computed by solving equations (5.67). The one in the middle corresponds to the first non trivial zero of the function $x \to J_1(\rho\sqrt{n}x)$ while the other two are solution to the first equations in (5.67). In line with Theorem 42, the curves $k \to \delta_m(k)$ converge to 2π from the left as k approaches a $\mathcal{B}-$Dirichlet eigenvalue. Figure 5.1 (right) shows the same curves for a trivial operator $\mathcal{B}$, leading to similar conclusion that validate the theorem. The specific case of $\mathcal{Q} = \varnothing$ corresponds to finding the Dirichlet eigenvalues of (1.35).

The $\mathcal{D}-$eigenvalues

Take $\mathcal{D} = I$ the identity operator to verify Assumption 48. In that situation, the $\mathcal{D}-$eigenvalues, called the Steklov eigenvalues, denoted $\lambda_{\text{ref,q}}(n)$ assume the following analytical expression for $q \in \mathbb{Z}$:

$$\lambda_{\text{ref,q}}(n) = -k\sqrt{n}\frac{J_q'(k\rho\sqrt{n})}{J_q(k\rho\sqrt{n})}. \tag{5.69}$$

With a Herglotz wave function as an incident field with density g (5.68), the background far field pattern $F_{\mathcal{D}}^{\mu}$ takes the form

$$F_{\mathcal{D}}^{\mu}g(\theta) = \sum_{m\in\mathbb{Z}} \gamma_m g_m e^{im\theta}, \tag{5.70}$$

where

$$\gamma_m = -i^m\sqrt{\frac{8\pi}{k}}e^{-i\frac{\pi}{4}}\frac{\mu J_m(k\rho) + kJ_m'(k\rho)}{\mu H_m^{(1)}(k\rho) + kH_m'^{(1)}(k\rho)}, \quad m \in \mathbb{Z}. \tag{5.71}$$

We deduce that the eigenvalues of the scattering operators are:

$$e^{i\delta_m} := 1 + \frac{2ik}{\overline{\gamma}}(1 - \frac{2ik}{\gamma}\overline{\gamma_m})(\alpha_m - \gamma_m)$$

where $\delta_m \in [0, 2\pi)$ denote their corresponding phases and the α_m are defined in (4.68).

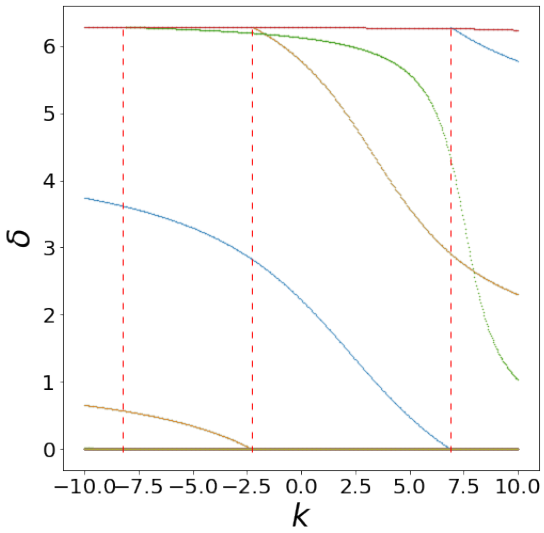

Figure 5.2: For $m \in \{-10, ...10\}$, we plot the curves $\mu \to \delta_m(\mu)$ where $D = D_b = B_\rho$ for $k = 5$, $\rho = 0.2$ and $n = 1$. Each color corresponds to a value of m. The red dashed lines indicate the Steklov eigenvalues (5.69).

Figure 5.2 (left) shows the curves $\mu \to \delta_m(\mu)$ for $m \in \{-10, ...10\}$. The results confirms Theorem 56, with the curves $\mu \to \delta_m(\mu)$ converging from the right as μ approaches a Steklov eigenvalue.

5.4.2 An indicator function of the refractive index

We propose to conclude this chapter by introducing an indicator function of the refractive index based on the one presented in Chapter 3. Indeed, the latter utilizes the monotonicity of the averaged Steklov eigenvalue at a fixed wavenumber. In this section, we aim to exploit the same monotonicity property of $\eta_{\mathcal{B}}(n, D_b)$ (5.3). This value can be determined using the far field patterns $F(k)$ for various wavenumbers k by applying the inside-outside duality method derived from Theorem 42. In the examples considered here, the assumption that $D \subset D_b$ no longer holds. However, we assume that the signatures of the components of D outside of D_b are weak, or that the associated transmission eigenvalues lie outside the frequency range we are considering.

Recovering $\eta_{\mathcal{B}}(n, D_b)$: We detail in this paragraph how to recover the first $\mathcal{B}-$Dirichlet eigenvalue from graphics as in Figure 5.1. Unlike the averaged Steklov eigenvalues, the set of eigenvalues of (5.1) is infinite. There is a need to be cautious to recover exactly $\eta_{\mathcal{B}}(n, D_b)$ and not to confuse it with the another Dirichlet eigenvalue. Let H be the interval of values where $\eta_{\mathcal{B}}(n, D_b)$ is supposed to belong, denoted $H = \{k_0, k_1, ..., k_{max}\}$ with $0 < k_0 < k_1 < ... < k_{max}$. Fix a small parameter $\varepsilon > 0$ and a threshold $\sigma \in [0, 2\pi - \varepsilon)$ not too close to 0. For k_0 in H, we compute the eigenvalues $e^{i\delta_m}$ of the operator $\mathbf{S}(k_0)$ and then we count the number of phases δ_m that belong to $[\sigma, 2\pi - \varepsilon)$. While this number is constant, repeat the process for the next element in H. For a carefully chosen ε and σ, this number increases by 1 when the values k in H approach $\eta_{\mathcal{B}}(n, D_b)$ with $k < \eta_{\mathcal{B}}(n, D_b)$. This allows us to identify an approximation of the first Dirichlet eigenvalue.

Indicator function: We refer to section 4.5.2 for the notation and presentation of the synthetic simulated data. The imaging algorithm can be described with the following steps:

1) Let $\rho > 0$ be a given parameter. Choose D_b to be the ball B_ρ^y of radius ρ and center $y \in \mathcal{Y}$, a grid of points sampling the region of interest.

2) Evaluate the $\mathcal{B}-$eigenvalue $\eta_{\mathcal{B}}(n, D_b, y)$ of problem (5.1) from the measurements $\mathbb{F}(k)$ and the analytically computed $\mathbb{F}_{b,y}^{\mu}(k)$ using the inside-outside method (see **Recovering $\eta_{\mathcal{B}}(n, D_b)$**).

3) Plot the function $y \to \eta_{\mathcal{B}}(n, D_b, y)$.

We illustrate this algorithm with one simple configuration. Figure 5.3 (left) shows a clustering of small disks with refractive index $n = 2$ and radius 0.02 with varying densities across five distinct regions. The indicator function, for $\mathcal{B} = 0$, displayed in Figure 5.3 (right), with parameter $\rho = 0.5$ and 1% of added noise, successfully distinguishes the five aligned areas with scatterers. Furthermore, the monotonicity of the eigenvalue allows us to sort the density of scatterers in each area.

Next, we consider the example given in the introductory chapter that we recall in Figure 5.4 (left). Using the same parameter as in the previous example, Figure 5.4 (left) presents the indicator function $y \to \eta_0(n, D_b, y)$ on a 100×100 uniformed grid of $[-2.1, 2.1] \times$

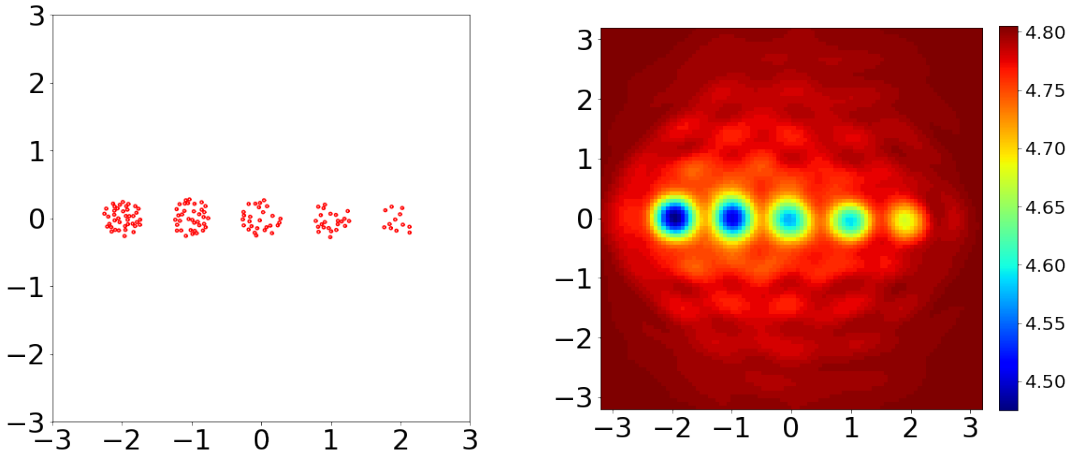

Figure 5.3: Left: the domain D constituted by small circles concentrated in five aligned areas. The scatterers have a radius 0.02 and a constant index refraction $n = 2$ inside. Right: Indicator function plotted on the 100×100 uniformed grid of $[-3.2, 3.2] \times [-3.2, 3.2]$ for $\mathcal{B} = 0$, $\rho = 0.5$ and the noise level $\delta = 1\%$.

$[-2.1, 2.1]$. While it manages to identify the five high-density regions, the eigenvalue $\eta_0(n, D_b)$ appears to be less sensitive to the variations of the refractive index compared to the indicator function presented in Figure 3.8.

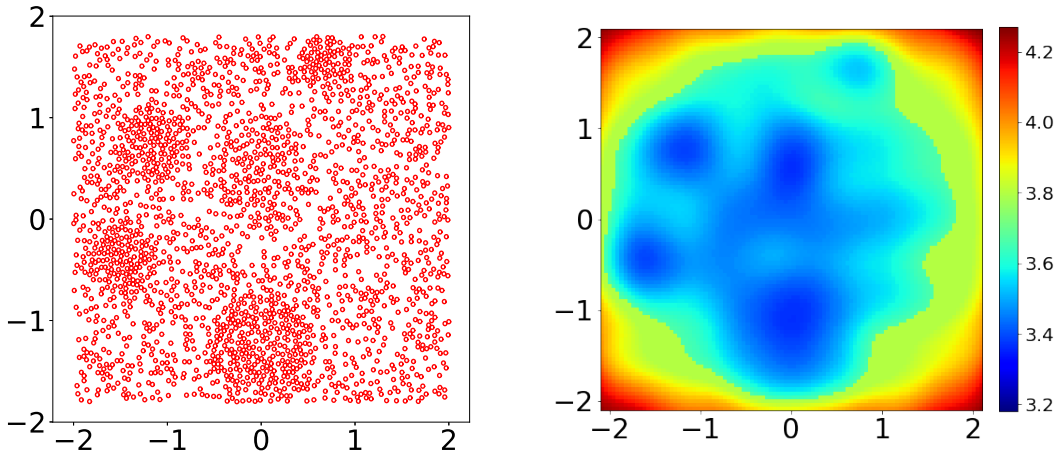

Figure 5.4: Left: the domain D constituted by 2250 small circles of radius 0.02 having a constant index of refraction $n = 2$. Right: Indicator function plotted on the 100×100 uniformed grid of $[-2.1, 2.1] \times [-2.1, 2.1]$ for $\mathcal{B} = 0$, $\rho = 0.5$ and the noise level $\delta = 1\%$.

5.5 Proof of Proposition 43

To clarify the lecture of this proof, we decompose the operator $T_{\mathcal{B}}(k) = T_D(k) + \frac{1}{\mu}T_N(k)$ where:

$$\begin{cases} T_D(k)\psi = w_D(k) + \frac{1}{\mu}\mathcal{B}(\partial_\nu w_D(k)), \\ T_N(k)\psi = w_N(k) + \frac{1}{\mu}\mathcal{B}(\partial_\nu w_N(k)), \end{cases} \tag{5.72}$$

(w_D, w_D^s) and (w_N, w_N^s) being the solution of (4.15) with source term ψ. We focus on the continuity of $k \to T_D(k)$.
Consider two wavenumbers $k > 0$ and $k' > 0$ in some given bounded interval I. For any $\psi \in H^{-\frac{1}{2}}(\partial D_b)$, we denote by $(w_D(k), w_D^s(k))$ (respectively $(w_D(k'), w_D^s(k'))$) the solution of (4.14) with source term ψ and wavenumber k (respectively k'). Using the linearity of the equations, there exists (w'_D, w'^s_D) such that $w_D(k) - w_D(k') = (k-k')w'_D$ and $w_D^s(k) - w_D^s(k') = (k-k')w'^s_D$. The pair (w'_D, w'^s_D) satisfies the variational equality:

$$(I(k)w'_D, u)_{H^1(D_b)} + (J(k)w'^s_D, v)_{H^1(B_R\backslash D_b)} = (k+k')(F,(u,v))_{H^1(D_b)\times H^1(B_R\backslash D_b)}, \tag{5.73}$$

for all $(u,v) \in H^1(D_b) \times H^1(B_R\backslash D_b)$. With the Riesz representation theorem, we define the linear bounded operators $I(k) : H^1(D_b) \to H^1(D_b)$, $J(k) : H^1(B_R\backslash D_b) \to H^1(B_R\backslash D_b)$ and $F \in H^1(D_b) \times H^1(B_R\backslash D_b)$ as:

$$\begin{cases} (I(k)u, u')_{H^1(D_b)} & = \displaystyle\int_{D_b} \nabla u \nabla \overline{u'}\, dx - k^2 \int_{D_b} nu\overline{u'}\, dx, \quad \forall u, u' \in H^1(D_b), \\ (J(k)v, v')_{H^1(B_R\backslash D_b)} & = \displaystyle\int_{B_R\backslash D_b} \nabla v \nabla \overline{v'}\, dx - k^2 \int_{B_R\backslash D_b} nv\overline{v'}\, dx \\ & \quad - \langle \Lambda(k)v, v' \rangle_{H^{-\frac{1}{2}}(\partial B_R), H^{\frac{1}{2}}(\partial B_R)}, \quad \forall v, v' \in H^1(B_R\backslash D_b), \\ (F,(u',v'))_{H^1(D_b)\times H^1(B_R\backslash D_b)} & = \displaystyle\int_{D_b} nw_D(k')\overline{u'}\, dx \\ & \quad + \int_{B_R\backslash D_b} w_D^s(k')\overline{v'}\, dx, \quad \forall (u',v') \in H^1(D_b) \times H^1(B_R\backslash D_b), \end{cases} \tag{5.74}$$

where B_R be a disk of radius $R > 0$ centered at the origin containing D_b. Here, $\Lambda(k) : H^{-\frac{1}{2}}(\partial B_R) \to H^{\frac{1}{2}}(\partial B_R)$ denotes the Dirichlet to Neumann map where $\Lambda(k)\phi := \partial_\nu v|_{\partial B_R}$, v being the radiating solution to the Helmholtz equation with wavenumber k in $\mathbb{R}^m\backslash B_R$ with $v = \phi$ on ∂B_R. Therefore, the pair (w', w'^s) is solution of (5.73) if and only if it satisfies:

$$A(k)(w', w'^s) = (k+k')F, \tag{5.75}$$

where the operator $A(k)$ is defined by

$$(A(k)(u,v),(u'v'))_{H^1(D_b)\times H^1(B_R\backslash D_b)} = (I(k)u, u')_{H^1(D_b)} + (J(k)v, v')_{H^1(B_R\backslash D_b)},$$

for all $u, u' \in H^1(D_b), v, v' \in H^1(B_R\backslash D_b)$.
From the definition of $\Lambda(k)$ ([15, Chapter 1]), one can show that the map $k \to \Lambda(k)$ is continuous from $\mathbb{R}^+$ to $\mathcal{L}(H^{-\frac{1}{2}}(\partial B_R), H^{\frac{1}{2}}(\partial B_R))$. The operator $A(k)$ is invertible by Fredholm

theory for any $k \in \mathbb{R}^+$. Rewriting $A(k) = A(k') + (A(k) - A(k'))$, we take k sufficiently close to k' to ensure convergence of the Neumann series. This leads to the continuity of the map $k \to A(k)^{-1}$ from $\mathbb{R}^+$ to $\mathcal{L}(H^1(D_b) \times H^1(B_R \backslash D_b), H^1(D_b) \times H^1(B_R \backslash D_b))$. Heine–Cantor theorem ensures that this map is uniformly bounded in I. Hence, we conclude that there exists a constant $C > 0$ independent from $k \in I$ such that $||w'_D||_{H^1(D_b)} \leq C||\psi||_{H^{-\frac{1}{2}}(\partial D_b)}$. Using the continuity of the normal trace application and the application $\mathcal{B}$, this is enough to prove that the map $k \to T_D(k)$ is continuous. The continuity of the map $k \to T_N(k)$ can be demonstrated in a similar manner. Consequently, the map $k \to T_{\mathcal{B}}(k)$ is also continuous.

Chapter 6

Conclusion and perspectives

Our objective was to develop an imaging algorithm capable of recovering the **local distribution** of small inhomogeneities in an unknown medium. To address this challenge in any dimension, inspiration was drawn from the monotonicity property of the Transmission eigenvalues (Theorem 2). This lead to the introduction of a **new class of eigenvalues called the $f-$averaged Steklov eigenvalues**. Each of these eigenvalues is associated with an artificial background problem that contains a resonator and is solution to a simple spectral problem inside the resonator. The problem is simple because **its spectrum has only one element** and its analysis falls within the framework of eigenvalue problems for self-adjoint operators. In addition, according to the Courant-Fischer principle, each $f-$averaged Steklov eigenvalue is **monotonically increasing with respect to refractive index** and the number of inhomogeneities inside the resonator.
The next step was to **recover these spectral signatures from the far field pattern**. Chapter 3 rigorously justifies a first method based on the Generalized Linear Sampling Method, while Chapter 4 explores the inside-outside duality method which, although more mathematically restrictive, requires less computation time.
The specific case of the $1-$averaged Steklov eigenvalue is particularly suited for an imaging algorithm for several reasons: 1) it is the easiest to reconstruct, 2) it appears to be the most sensitive to variations of the refractive index, and 3) in the case of a circular resonator, the artificial background can be analytically computed. **By computing this eigenvalue for various positions of the resonator**, we can estimate the variation of the local density of the inhomogeneities in an unknown medium. This approach provides more relevant results than classical methods, such as the Linear Sampling Method, particularly due to the mathematically interpretable nature of the indicator function. Figure 6.1 compares the indicator function given by the Linear Sampling Method with the one given by the computation of the $1-$averaged Steklov eigenvalue for various configurations of scatterers. Unlike the Linear Sampling Method, the $1-$averaged Steklov eigenvalue **effectively localizes the regions with higher concentrations of scatterers** in each case and distinguishes them from the surrounding background of scatterers. In addition to these promising results, we investigated which constant refractive index would give the same $1-$averaged Steklov eigenvalue. The outcome offers an **accurate approximation of the mean value** of the refractive index (under a smallness assumption on the frequency).

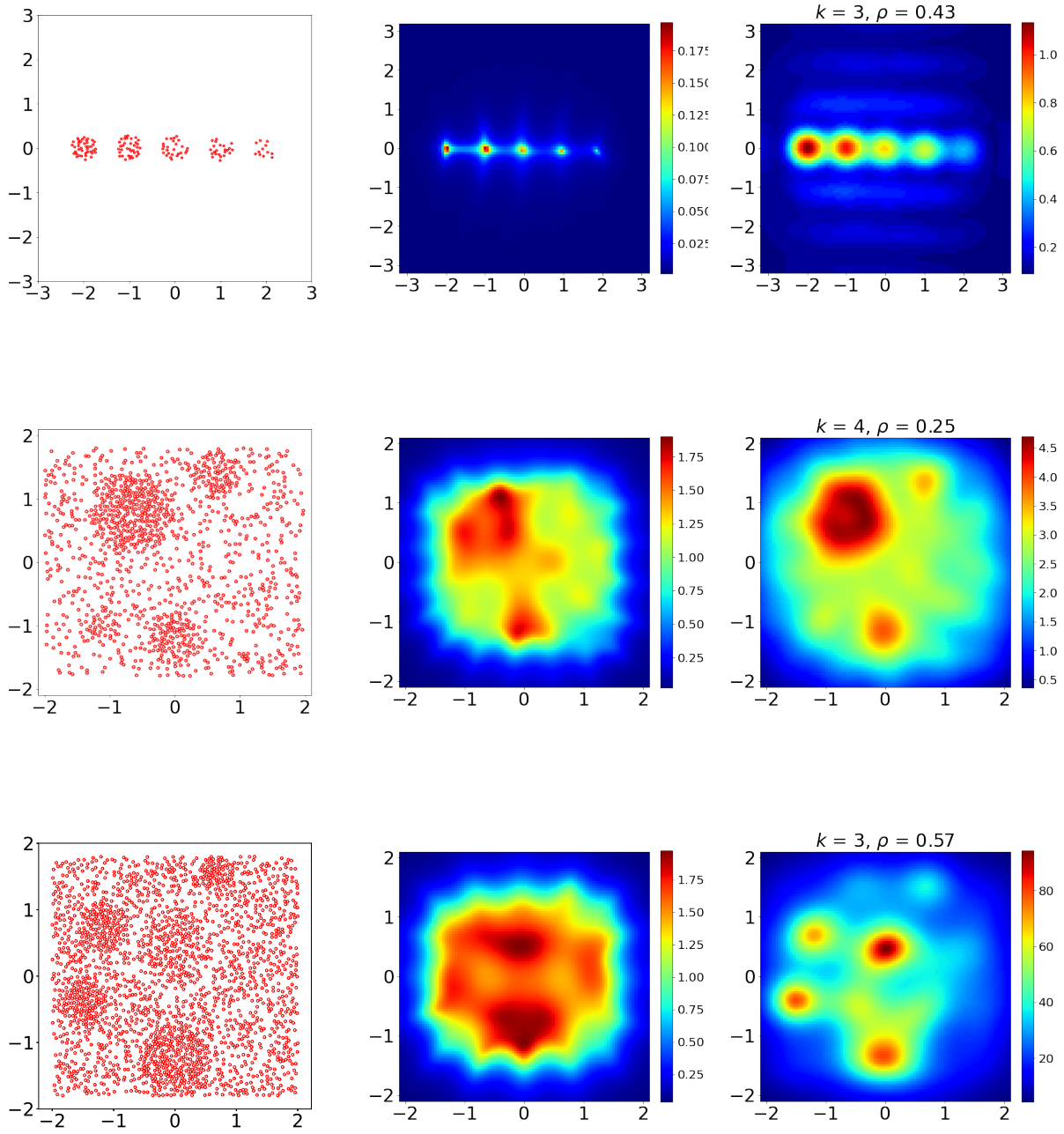

Figure 6.1: Comparison of the Linear Sampling Methods and the Indicator function given in Chapter 3 at the same wavenumber with 1% of added noise. Left column: Configuration of scatterers. Middle column: Linear Sampling Method imaging result. Right column: New indicator function

This investigation demonstrated that the set of f-averaged Steklov eigenvalues can be utilized to refine the understanding of the refractive index beyond its mean value. We list a few examples to further exploit this family of eigenvalues and some future applications.

Homogenization Under classical hypotheses of stochastic homogenization [57, 44], this set may provide an alternative method for recovering the homogenized parameters. The indicator function introduced in Chapter 4 supports this approach, particularly in the case of highly oscillating media. We further illustrate this possibility with a simple example. Consider the scenario discussed in Remark 3 with a constant refractive index $n = 1$ and $A = \alpha^2 I$ for $\alpha > 0$. For D_b a centered at the origin ball of radius ρ, the $1-$averaged Steklov eigenvalue assumes the following analytical expression:

$$\mu(k, 1, A, D_b) := 2\pi\rho k\alpha \frac{J_1(k\rho\frac{1}{\alpha})}{J_0(k\rho\frac{1}{\alpha})}. \tag{6.1}$$

Since the function $x \to 2\pi\rho k\frac{1}{x}J_1(k\rho x)/J_0(k\rho x)$ is a bijection from $(0, \frac{j_0}{k\rho})$ to $(0, +\infty)$ (where j_0 is the first zero of J_0), it is possible to recover the parameter α from the knowledge of the eigenvalue.
Next, consider D_ε, a collection small circular scatterers of radius $\varepsilon > 0$ such that

$$A = \begin{cases} \frac{1}{2}I \text{ in } D_\varepsilon, \\ I \text{ in } D_b \backslash D_\varepsilon. \end{cases} \tag{6.2}$$

The area of D_ε constitutes 10% of D_b and the number of scatterers is adjusted for each value of ε as shown in Figure 6.2 (left). For various values of ε, at a fixed wavenumber $k = 3$ and $\rho = 0.4$, we generated 30 set of random positions of these scatterers and computed the $1-$averaged Steklov eigenvalue for each configuration. Figure 6.2 displays the associated α from equation (6.1) for each random configuration and for each value ε. Figure 6.2 suggests a convergence toward a constant, approximately 0.938, which differs from the mean value $\frac{1}{|D_b|}\int_{D_b} A dx \sim 0.95$. We conjecture that this new constant is the one given by homogenization theory.

An optimization approach An optimization method that minimizes the difference between the far field pattern from the simulations and real data measurements can be computationally expensive. Indeed, simulating the direct problem requires a detailed mesh of all the scatterers and the domain. However, the family of $f-$averaged Steklov eigenvalues are theoretically solely determined by the refractive index inside the resonator D_b thanks to the relation given in Theorem 15, item 1). The refractive index within D_b can be reconstructed at a fixed wavenumber k by minimizing the cost function

$$J(n_{guess}) = \sum_{f\in\Lambda} |\mu(k, n_{guess}, D_b, f) - \mu_{meas}(f)|^2,$$

where Λ is a finite subset of $H^{\frac{1}{2}}(\partial D_b)$ and $(\mu_{meas}(f))_{f\in\Lambda}$ represents the $f-$averaged Steklov eigenvalues given by the far field data. By sweeping the position of D_b, it is possible

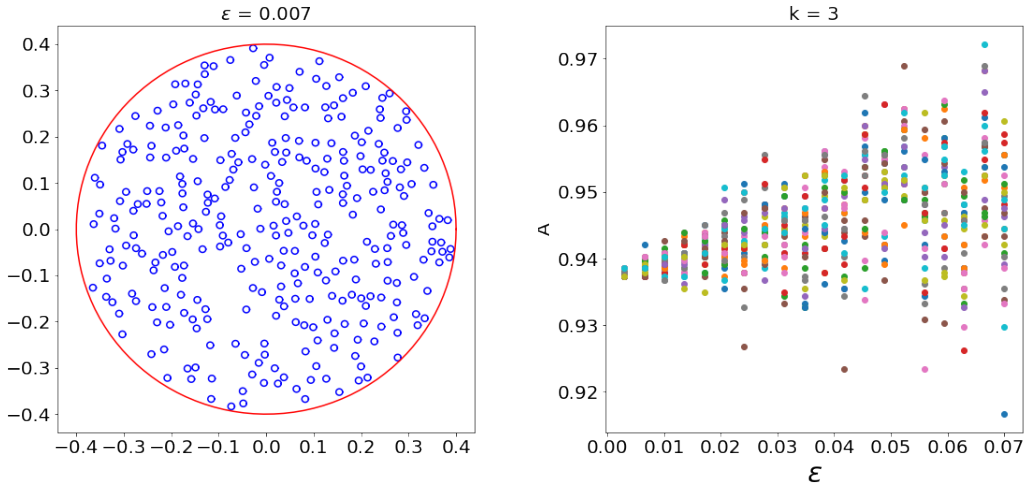

Figure 6.2: Left: 326 small circular scatters (in blue) of radius $\varepsilon = 0.007$ in D_b a disk of radius 0.4 (in red). Right: Plot of the value of the corresponding parameter α in equation (6.1) reconstructed from the 1−averaged Steklov eigenvalue for 30 configurations for various ε, with $k = 3$.

to approximate the true refractive index n in the whole domain. Rather than one large optimization problem, this approach offers several smaller optimizations problems.

The Dirichlet to Neumann operator Fix $n > 0$, D_b and k and let μ_f be the associated $f-$averaged Steklov eigenvalue. For each $f \in H^{\frac{1}{2}}(\partial D_b)$, let $w_f \in H^1(D_b)$ be the unique solution of:

$$\begin{cases} \Delta w_f + k^2 n w_f = 0 \text{ in } D_b, \\ w_f = f \text{ on } \partial D_b. \end{cases} \tag{6.3}$$

Let $\Lambda : H^{\frac{1}{2}}(\partial D_b) \to H^{-\frac{1}{2}}(\partial D_b)$ denote the Dirichlet to Neumann operator defined by $\Lambda f = \partial_\nu w_f$. This enables us to express the eigenvalue μ_f as follows:

$$\mu_f = - \langle \Lambda f, f \rangle_{H^{-\frac{1}{2}}(\partial D_b), H^{\frac{1}{2}}(\partial D_b)}.$$

For any real valued $f, g \in H^{\frac{1}{2}}(\partial D_b)$, the following identity holds:

$$-4 \langle \Lambda f, g \rangle_{H^{-\frac{1}{2}}(\partial D_b), H^{\frac{1}{2}}(\partial D_b)} = \mu_{f+g} - \mu_{f-g}. \tag{6.4}$$

Consequently, one can reconstruct numerically the self-adjoint Dirichlet to Neumann operator Λ from the knowledge of the set of $f-$averaged Steklov eigenvalues. This establish another connection between the inverse problem using far field data and those that exploit the local Dirichlet to Neumann operator.

Linearization The set of $f-$averaged Steklov eigenvalue can be used to recover more information about the refractive index beyond its mean value. In this paragraph, we provide

some insights in that direction.
For $\varepsilon > 0$, we decompose the refractive index as $n = n_0 + \varepsilon n_1 + O(\varepsilon^2)$, where $n_0 = \frac{1}{|D_b|}\int_{D_b} n dx$, $n_1 \in L^\infty(D_b)$ and $O(\varepsilon^2)$ represents a higher order term that we do not specify. Similarly, we assume that w_f, the solution of (6.3), can be expanded as $w_f = w_f^0 + \varepsilon w_f^1 + O(\varepsilon^2)$ where $w_f^0, w_f^1 \in H^1(D_b)$ solve:

$$\begin{cases} \Delta w_f^0 + k^2 n_0 w_f^0 = 0 \text{ in } D_b, \\ w_f^0 = f \text{ on } \partial D_b, \end{cases} \quad \begin{cases} \Delta w_f^1 + k^2 n_0 w_f^1 = -k^2 n_1 w_f^0 \text{ in } D_b, \\ w_f^1 = 0 \text{ on } \partial D_b. \end{cases} \tag{6.5}$$

For real valued $f, g \in H^{\frac{1}{2}}(\partial D_b)$, by integrating by part $(\Delta w_f^1 + k^2 n_0 w_f^1) w_g^0$ and using (6.4), we obtain:

$$\begin{aligned} \varepsilon k^2 \int_{D_b} n_1 w_f^0 w_g^0 dx &= \varepsilon \int_{\partial D_b} \partial_\nu w_f^1 g ds \\ &= \int_{\partial D_b} \partial_\nu w_f g ds - \int_{\partial D_b} \partial_\nu w_f^0 g ds + O(\varepsilon^2) \\ &= -\tfrac{1}{4}(\mu_{f+g} - \mu_{f-g}) - \int_{\partial D_b} \partial_\nu w_f^0 g ds + O(\varepsilon^2). \end{aligned} \tag{6.6}$$

This establishes a relation between the $f-$averaged Steklov eigenvalues and the components of the refractive index.
In dimension 2, we assume that n_1 takes the form:

$$n_1(r,\theta) = \sum_{i \in \mathbb{N}^*} n_c^i \cos(i\theta) + n_s^i \sin(i\theta). \tag{6.7}$$

with $(n_c^i)_i, (n_s^i)_i \in \mathbb{R}^{\mathbb{N}}$. For $m \in \mathbb{N}^*$, consider $f = 1$ and $g = cos(m\theta)$, and let $D_b = B_\rho$ be the centered at the origin ball of radius ρ. This leads to the system:

$$\begin{cases} \varepsilon \pi k^2 A(n_0, \rho, 0, m) n_c^m = -\frac{1}{4}(\mu_{1+\cos(m\theta)} - \mu_{1-\cos(m\theta)}) + O(\varepsilon^2) \\ \\ \varepsilon \pi k^2 A(n_0, \rho, 0, m) n_s^m = -\frac{1}{4}(\mu_{1+\sin(m\theta)} - \mu_{1-\sin(m\theta)}) + O(\varepsilon^2) \end{cases} \tag{6.8}$$

where $A(n_0, \rho, q, m)$ is defined as

$$A(n_0, \rho, q, m) = \int_0^\rho \frac{J_q(kr\sqrt{n_0})}{J_q(k\rho\sqrt{n_0})} \frac{J_m(kr\sqrt{n_0})}{J_m(k\rho\sqrt{n_0})} r dr.$$

Assuming that $n_0 \in \mathbb{R}$ is known, this system allows to approximate the coefficients n_c^i and n_s^i using the family of eigenvalues $(\mu_{1+\cos(m\theta)})_m$ and $(\mu_{1+\sin(m\theta)})_m$.
Although this example is simplistic and has many numerical limitations, it demonstrates the potential of the $f-$averaged Steklov eigenvalues to recover more information about the refractive index beyond its mean value.

Complex refractive indexes Our analysis and algorithm in Chapter 2 and Chapter 3 can apply to real refractive indices. The extension to refractive index with non zero imaginary part does not appear to be straightforward. The existence of eigenvalues for the limiting problem can be established using similar arguments. However, the monotonicity property given by equation (2.41) may be lost in this case. Furthermore, there are some numerical complications that arise in the inversion algorithm as the eigenvalue lies in the complex plane. To be efficient, some prior information on the location of this eigenvalue in the complex plane is needed.

Extension to other problems The construction of spectral signatures discussed in the thesis, along with the inversion methods and the imaging algorithms, is based on a mathematical framework that is not limited to the Helmholtz equation. This framework is flexible enough to be extended to other wave propagation problems such as linear elasticity and Maxwell equations. It is reasonable to believe that a similar spectral problem, with a unique eigenvalue that exhibits a monotonic dependence with respect to the unknown parameter, could be developed.

Application in an experimental setting The ultimate objective is to detect, within concrete material, ai filled voids (called gravel honeycomb) among the many aggregates. For example, on synthetic and far field data, we model the air as non penetrable Neumann obstacles. We consider the configuration presented in Figure 6.3 (left) and display on the same figure the indicator function from Chapter 3 for two cases : 1) when all scatterers are penetrable with the same refractive index (Figure 6.3 middle), 2) when the blue scatters are non-penetrable Neumann obstacles (Figure 6.3 right). The monotonic decreasing nature of the $f-$averaged Steklov eigenvalue with respect to the number of Neumann obstacles (which can be demonstrated using a Courant-Fischer identity as in equation (2.41)) allows us to localize region of the gravel honeycomb. The inversion algorithm, developed in Chapter 3

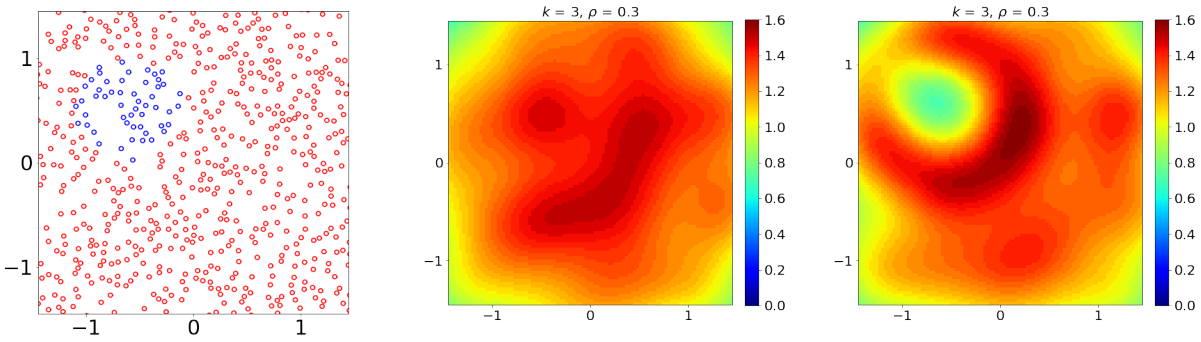

Figure 6.3: Left: the domain D constituted by uniformly distributed small circles of radius 0.02. Middle: Indicator function presented in Chapter 3 when all the scatters have a constant refractive index $n = 2$ inside. Right: Indicator function presented in Chapter 3 when the red scatters have a constant refractive index $n = 2$ inside and the blue scatterers are non penetrable Neumann obstacles.

and Chapter 4 relies on far field data. However, this far field data may be replaced by near field data, provided that similar factorization operators are maintained. This adjustment will generalize the method and will better reflect the realistic physical situations encountered. The final step would be to apply the proposed imaging algorithm to an experimental setting, particularly on concrete.

Bibliography

[1] T. Arens, R. Griesmaier, and R. Zhang, *Monotonicity-based shape reconstruction for an inverse scattering problem in a waveguide*, Inverse Problems, 39 (2023), p. 075009.

[2] L. Audibert, *Qualitative methods for heterogeneous media*, theses, Ecole polytechnique X, Sept. 2015.

[3] ——, *The generalized linear sampling and factorization methods only depends on the sign of contrast on the boundary.*, Inverse Problems & Imaging, 11 (2017).

[4] L. Audibert, F. Cakoni, and H. Haddar, *New sets of eigenvalues in inverse scattering for inhomogeneous media and their determination from scattering data*, Inverse Problems, 33 (2017), pp. 1–30.

[5] L. Audibert, L. Chesnel, and H. Haddar, *Transmission eigenvalues with artificial background for explicit material index identification*, Comptes Rendus Mathematique, 356 (2018), pp. 626–631.

[6] L. Audibert, L. Chesnel, and H. Haddar, *Inside-outside duality with artificial backgrounds*, Inverse Problems, 35 (2019), p. 104008.

[7] L. Audibert, L. Chesnel, H. Haddar, and K. Napal, *Qualitative indicator functions for imaging crack networks using acoustic waves*, 2020.

[8] L. Audibert and H. Haddar, *A generalized formulation of the linear sampling method with exact characterization of targets in terms of farfield measurements*, Inverse Problems, 30 (2014), p. 035011.

[9] L. Audibert, H. Haddar, and X. Liu, *An accelerated level-set method for inverse scattering problems*, SIAM Journal on Imaging Sciences, 15 (2022), pp. 1576–1600.

[10] L. Audibert, H. Haddar, and F. Pourre, *Imaging highly heterogeneous media using transmission eigenvalues*, in 2023 IEEE Conference on Antenna Measurements and Applications (CAMA), 2023, pp. 597–600.

[11] L. Audibert, H. Haddar, and F. Pourre, *Averaged steklov eigenvalues, inside outside duality and application to inverse scattering*, In soumission, (2024).

[12] ——, *Reconstruction of averaging indicators for highly heterogeneous media*, Inverse Problems, 40 (2024), p. 045028.

[13] E. Bécache, S. Fauqueux, and P. Joly, *Stability of perfectly matched layers, group velocities and anisotropic waves.*, Journal of Computational Physics, 188 (2003), pp. 399–433.

[14] F. Cakoni, D. Colton, and H. Haddar, *On the determination of Dirichlet or transmission eigenvalues from far field data*, Comptes rendus de l'Académie des sciences. Série I, Mathématique, 348 (2010), pp. 379–383.

[15] ——, *Inverse Scattering Theory and Transmission Eigenvalues*, vol. 98, CBMS-NSF, Dec. 2022.

[16] F. Cakoni, D. Colton, S. Meng, and P. Monk, *Stekloff eigenvalues in inverse scattering*, SIAM journal on applied mathematics, 76 (2016), pp. 1737–1763.

[17] F. Cakoni, D. Gintides, and H. Haddar, *The existence of an infinite discrete set of transmission eigenvalues*, SIAM J. Math. Anal., 42 (2010), pp. 237–255.

[18] F. Cakoni and M. S. Vogelius, *Singularities almost always scatter: regularity results for non-scattering inhomogeneities*, Commun. Pure Appl. Math., 76 (2023), pp. 4022–4047.

[19] ——, *Singularities almost always scatter: regularity results for non-scattering inhomogeneities*, Commun. Pure Appl. Math., 76 (2023), pp. 4022–4047.

[20] S. Cogar, *A modified transmission eigenvalue problem for scattering by a partially coated crack*, Inverse Problems, 34 (2018), p. 115003.

[21] ——, *Analysis of a trace class Stekloff eigenvalue problem arising in inverse scattering*, SIAM J. Appl. Math., 80 (2020), pp. 881–905.

[22] S. Cogar, D. Colton, S. Meng, and P. Monk, *Modified transmission eigenvalues in inverse scattering theory*, Inverse Problems, 33 (2017), p. 125002.

[23] D. Colton, F. Cakoni, and P. Monk, *Nondestructive testing and target identification*, (2016).

[24] D. Colton and A. Kirsch, *A simple method for solving inverse scattering problems in the resonance region*, Inverse Problems, 12 (1996), pp. 383–393.

[25] D. Colton, A. Kirsch, and L. Päivärinta, *Far-field patterns for acoustic waves in an inhomogeneous medium*, SIAM J. Math. Anal., 20 (1989), pp. 1472–1483.

[26] D. Colton and R. Kress, *Inverse Acoustic and Electromagnetic Scattering Theory*, Applied Mathematical Sciences, Springer Berlin Heidelberg, 2013.

[27] D. Colton and R. Kress, *Looking back on inverse scattering theory*, SIAM Rev., 60 (2018), pp. 779–807.

[28] D. Colton and P. Monk, *The inverse scattering problem for time-harmonic acoustic waves in an inhomogeneous medium*, Q. J. Mech. Appl. Math., 41 (1988), pp. 97–125.

[29] D. Colton and B. D. Sleeman, *Uniqueness theorems for the inverse problem of acoustic scattering*, IMA J. Appl. Math., 31 (1983), pp. 253–259.

[30] O. Dorn and D. Lesselier, *Level set methods for inverse scattering*, Inverse Problems, 22 (2006), p. R67.

[31] J. Eckmann and C. Pillet, *Spectral duality for planar billiards*, Comm. Math. Phys., 170 (1995), pp. 283–313.

[32] H. Engl, M. Hanke, and A. Neubauer, *Regularization of Inverse Problems*, Mathematics and Its Applications, Springer Netherlands, 2000.

[33] C. Farhat, R. Tezaur, and R. Djellouli, *On the solution of three-dimensional inverse obstacle acoustic scattering problems by a regularized newton method*, Inverse Problems, 18 (2002), p. 1229.

[34] R. Griesmaier and B. Harrach, *Monotonicity in inverse medium scattering on unbounded domains*, SIAM Journal on Applied Mathematics, 78 (2018), pp. 2533–2557.

[35] H. Haddar, M. Khenissi, and M. Mansouri, *Inside-Outside Duality for Modified Transmission Eigenvalues*, Inverse Problems and Imaging , 17 (2022), pp. 798–816.

[36] H. Harbrecht and T. Hohage, *Fast methods for three-dimensional inverse obstacle scattering problems*, Journal of Integral Equations and Applications, 19 (2007).

[37] F. Hecht, *New development in freefem++*, Journal of Numerical Mathematics, 20 (2012).

[38] M. Ikehata, *Reconstruction of an obstacle from the scattering amplitude at a fixed frequency*, Inverse Problems, 14 (1998), p. 949.

[39] W. Imbriale and R. Mittra, *The two-dimensional inverse scattering problem*, IEEE Transactions on Antennas and Propagation, 18 (1970), pp. 633–642.

[40] T. Johansson and B. Sleeman, *Reconstruction of an acoustically sound-soft obstacle from one incident field and the far-field pattern*, IMA Journal of Applied Mathematics, 72 (2007).

[41] A. Kirsch and N. Grinberg, *The Factorization Method for Inverse Problems*, Oxford University Press, 12 2007.

[42] A. Kirsch and R. Kress, *On an integral equation of the first kind in inverse acoustic scattering.* Inverse problems, Proc. Conf., Oberwolfach/Ger. 1986, ISNM 77, 93-102 (1986)., 1986.

[43] A. Kirsch and A. Lechleiter, *The inside–outside duality for scattering problems by inhomogeneous media*, Inverse Problems, 29 (2013), p. 104011.

[44] S. M. Kozlov, *Averaging of random operators*, Mathematics of The Ussr-sbornik, 37 (1980), pp. 167–180.

[45] R. Kress, *Newton's method for inverse obstacle scattering meets the method of least squares*, Inverse Problems, 19 (2003), p. S91.

[46] R. Kress and W. Rundell, *Nonlinear integral equations and the iterative solution for an inverse boundary value problem*, Inverse Problems, 21 (2005), p. 1207.

[47] P. D. Lax and R. S. Phillips, *Scattering theory*, vol. 26 of Pure Appl. Math., Academic Press, Academic Press, New York, NY, 1967.

[48] F. Le Louër and O. Ivanyshyn Yaman, *Material derivatives of boundary integral operators in electromagnetism and application to inverse scattering problems*, Inverse Problems, 32 (2016).

[49] A. Lechleiter and S. Peters, *Analytical characterization and numerical approximation of interior eigenvalues for impenetrable scatterers from far fields*, Inverse Probl., 30 (2014), p. 22. Id/No 045006.

[50] ——, *The inside–outside duality for inverse scattering problems with near field data*, Inverse Problems, 31 (2015), p. 085004.

[51] C. Liu, *Inverse obstacle problem: Local uniqueness for rougher obstacles and the identification of a ball*, Inverse Probl., 13 (1997), pp. 1063–1069.

[52] W. C. McLean, *Strongly Elliptic Systems and Boundary Integral Equations*, Cambridge University Press, 2000.

[53] V. Morozov, *On the solution of functional equations by the method of regularization.*, (1966), p. 414–417 (English translation).

[54] ——, *Choice of parameter for the solution of functional equations by the regularization method.*, (1967), p. 1000–1003 (English translation).

[55] L. Mönch, *On the inverse acoustic scattering problem by an open arc: the sound-hard case*, Inverse Problems, 13 (1997), p. 1379.

[56] A. I. Nachman, *Reconstructions from boundary measurements*, Ann. Math. (2), 128 (1988), pp. 531–576.

[57] G. C. Papanicolaou and S. R. S. Varadhan, *Boundary value problems with rapidly oscillating random coefficients*, in Random fields, Vol. I, II (Esztergom, 1979), vol. 27 of Colloq. Math. Soc. János Bolyai, North-Holland, Amsterdam-New York, 1981, pp. 835–873.

[58] R. Potthast, *A fast new method to solve inverse scattering problems*, Inverse Probl., 12 (1996), pp. 731–742.

[59] ——, *Stability estimates and reconstructions in inverse acoustic scattering using singular sources*, J. Comput. Appl. Math., 114 (2000), pp. 247–274.

[60] F. Rellich, *Über das asymptotische Verhalten der Lösungen von* $\Delta u + \lambda u = 0$ *in unendlichen Gebieten*, Jahresber. Dtsch. Math.-Ver., 53 (1943), pp. 57–65.

[61] A. Roger, *Newton-kantorovitch algorithm applied to an electromagnetic inverse problem*, IEEE Transactions on Antennas and Propagation, 29 (1981), pp. 232–238.

[62] B. P. Rynne and B. D. Sleeman, *The interior transmission problem and inverse scattering from inhomogeneous media*, SIAM J. Math. Anal., 22 (1991), pp. 1755–1762.

[63] F. Santosa, *A level-set approach for inverse problems involving obstacles fadil santosa*, ESAIM: Control, Optimisation and Calculus of Variations, 1 (1996), p. 17–33.

[64] A. Sommerfeld, *Die greensche funktion der schwingungsgleichung*, Jber. Deutsch. Math. Verein., (1912), p. 309–353.

[65] A. Tikhonov, *On the solution of incorrectly formulated problems and the regularization method.*, (1963), p. 1035–1038 (English translation).

[66] ——, *Regularization of incorrectly posed problems.*, (1963), p. 1624–1627 (English translation).

[67] I. N. Vekua, *On metaharmonic functions*, Tr. Tbilis. Mat. Inst. 12, 105-174 (1943)., (1943).

[68] M. Vogelius and J. Xiao, *Finiteness results concerning nonscattering wave numbers for incident plane and Herglotz waves*, SIAM J. Math. Anal., 53 (2021), pp. 5436–5464.

[69] H. Weyl, *Kapazität von Strahlungsfeldern*, Math. Z., 55 (1952), pp. 187–198.

ECOLE
DOCTORALE
DE MATHEMATIQUES
HADAMARD

Titre : Construction et analyse des signatures spectrales pour des défauts dans des milieux complexes

Mots clés : Equation aux dérivées partielles, Analyse numérique, Problèmes inverses, Diffraction, Analyse spectrale

Résumé : Le béton est largement employé dans le secteur de la construction, notamment dans les bâtiments réacteurs des centrales nucléaires. La surveillance de son évolution et la détection des défauts susceptibles de compromettre son bon fonctionnement peuvent être effectuées grâce à des tests non destructifs. Le béton est constitué d'agrégats. Ces derniers présentent des défis en raison de leur concentration élevée et de leur proximité. Ces caractéristiques rendent les méthodes classiques, telles que la Linear Sampling Method, inefficaces pour fournir des résultats quantitatifs ou des images exploitables.
Cette thèse a pour objectif de développer un algorithme d'imagerie capable d'estimer la densité des agrégats et de retrouver la distribution locale de ces petites hétérogénéités.
Pour résoudre ce problème, l'inspiration provient d'une propriété de monotonie des valeurs propres de transmission. Ces valeurs correspondent aux fréquences pour lesquelles il existe une onde incidente générant un champ diffracté trivial à l'extérieur des obstacles.
Plutôt que de comparer le champ diffracté à celui du vide, cette thèse propose une nouvelle approche consistant à le comparer, à un nombre d'onde fixé, à un problème de diffraction numérique. Cela a conduit à l'introduction d'une nouvelle classe de valeurs propres, appelées $f-$averaged Steklov eigenvalues. Chacune de ces valeurs est associée à un problème artificiel contenant un résonateur et est la solution d'un problème spectral simple à l'intérieur de ce résonateur. En outre, chaque $f-$averaged Steklov eigenvalue croît de manière monotone en fonction du nombre d'hétérogénéités présentes dans le résonateur. Ces signatures spectrales peuvent être extraites des données. En calculant ces valeurs propres pour différentes positions du résonateur, il devient possible d'estimer les variations de densité locale des hétérogénéités dans un milieu inconnu.

Title : Construction and analysis of spectral signatures for defects in complex media

Keywords : Inverse problems, Partial differential equations, Spectral Analysis, Scattering, Numerical analysis

Abstract : Concrete is widely used in construction, particularly in the reactor building of nuclear power plants. Monitoring its evolution and identifying any defects that could compromise its proper functioning can be achieved through non-destructive testing. Concrete is composed of aggregates, but their high concentration and proximity pose challenges for classical methods, such as the Linear Sampling Method, which fail to produce quantitative results or exploitable images.
The objective of this thesis is to build an imaging algorithm that can estimate the density of the aggregates and recover the local distribution of those small inhomogeneities.
To address this challenge, inspiration was drawn from a monotonicity property of the Transmission eigenvalues. They correspond to the frequencies for which an incident wave exists such that the scattered field is trivial outside the scatterers.
Instead of comparing the scattered field to the vacuum, this thesis introduces a new approach: comparing it, at a fixed wavenumber, to a numerical scattering problem, referred to as the background. This led to the introduction of a new class of eigenvalues known as the $f-$averaged Steklov eigenvalues. Each of these eigenvalues is associated with an artificial background problem that contains a resonator and is solution to a simple spectral problem inside the resonator. In addition, each $f-$averaged Steklov eigenvalue is monotonically increasing with respect to the number of inhomogeneities inside that resonator. These spectral signatures can be recovered from the data. By computing these eigenvalues for various positions of the resonator, we can estimate the variation of the local density of the inhomogeneities in an unknown medium.

Institut Polytechnique de Paris
91120 Palaiseau, France